


Summer 7-15-2017

# CHARACTERIZATION OF UNKNOWN BRIDGE FOUNDATIONS

Saman Rashidyan

Follow this and additional works at: [https://digitalrepository.unm.edu/ce\\_etds](https://digitalrepository.unm.edu/ce_etds)

 Part of the [Civil Engineering Commons](#), [Geotechnical Engineering Commons](#), and the [Structural Engineering Commons](#)

---

## Recommended Citation

Rashidyan, Saman. "CHARACTERIZATION OF UNKNOWN BRIDGE FOUNDATIONS." (2017).  
[https://digitalrepository.unm.edu/ce\\_etds/177](https://digitalrepository.unm.edu/ce_etds/177)

This Dissertation is brought to you for free and open access by the Engineering ETDs at UNM Digital Repository. It has been accepted for inclusion in Civil Engineering ETDs by an authorized administrator of UNM Digital Repository. For more information, please contact [disc@unm.edu](mailto:disc@unm.edu).

**Saman Rashidyan**

*Candidate*

---

**Civil Engineering**

*Department*

---

This dissertation is approved, and it is acceptable in quality and form for publication:

*Approved by the Dissertation Committee:*

**Dr. Tang-Tat Ng, Chairperson**

---

**Dr. Mahmoud Reda Taha**

---

**Dr. Arup Maji**

---

**Dr. Yu-Lin Shen**

---

# **CHARACTERIZATION OF UNKNOWN BRIDGE FOUNDATIONS**

**BY**

**SAMAN RASHIDYAN**

B.S., Civil Engineering, Tabriz University, 2000

M.S., Structural Engineering, Urmia University, 2005

DISSERTATION

Submitted in Partial Fulfillment of the  
Requirements for the Degree of

**Doctor of Philosophy  
Engineering**

The University of New Mexico  
Albuquerque, New Mexico

**July 2017**

## **DEDICATION**

This dissertation is dedicated to my mom and dad, who have been a constant source of support and encouragement throughout my life. I am deeply thankful for having you in my life. You have always loved me unconditionally and taught me to work hard for the things that I aspire to achieve.

## ACKNOWLEDGMENTS

I heartily acknowledge Dr. Tang-Tat Ng, my advisor and dissertation chair, for continuing to encourage me through the years of classroom teachings and the long number of months writing and rewriting these chapters. His guidance and professional style will remain with me as I continue my career.

I thank Dr Arup Maji, my co-advisor, for his kind advises during my research. I also thank my committee members, Dr. Mahmoud Reda Taha, and Dr Yu-Lin Shen, for their valuable recommendations pertaining to this study and assistance in my professional development.

I would like to thank Dr. Thiet Nguyen, Mr. James Castillo, Ms. Michelle Mann, Mr. Jeff Vigil, Dr. David Hadwiger, Ms. Keli Daniell, Ms. Dana Garcia and Mr. Mark Strzelczyk for their valuable suggestions and service during the technical meetings with NMDOT. Thanks to the help of Mr. Ali Jwary and Ms. April Eckhardt especially in conducting field experiments. To my best friend, Siavash Nikraves, thank you for the many years of support.

# **CHARACTERIZATION OF UNKNOWN BRIDGE FOUNDATIONS**

**BY**

**SAMAN RASHIDYAN**

B.S., Civil Engineering, Tabriz University, 2000

M.S., Structural Engineering, Urmia University, 2005

Ph.D., Civil Engineering, The University of New Mexico, 2017

## **ABSTRACT**

The National Bridge Inventory (NBI) recognized 86,133 bridges in the United States have no foundation data on record in 2003. It is evident that an unknown percentage of the 86,133 bridges identified by NBI with missing foundation data could also be highly vulnerable to scouring induced by water flow coupled with erodible soils. Conventional excavation, coring and boring excavations to identify unknown bridge foundation depths and types are deemed to be expensive, destructive, and limited in their application to the unknown foundation problem. Many surface and borehole nondestructive testing (NDT) technologies have been developed for this purpose. Three economical proven technique (Sonic Echo/Impulse Response (SE/IR), Parallel Seismic (PS) methods, and Induction Field (IF)) were selected for this study. The study focuses more on SE/IR method since it is the most inexpensive and quick method.

Studies on the applicability and methodology improvement of SE/IR and PS tests have been reported. However, the literature has been mainly focusing on individual pile without the pile cap. This study attempts to reveal practical aspects of the tests, for real bridge foundations including piles underneath pile caps and pier walls.

Equipment for conducting these three NDT tests was available. Preliminary tests under controlled environmental conditions were performed to study the applicability and limitations of these NDT methods. Then, numerous NDT tests were performed on six

bridges and one partially dismantled bridge. The foundation depths of two bridges are known in order to validate the NDT results.

A range of factors that affect the success of SE/IR tests were also investigated by finite element simulations. Finite element simulations of 1D wave propagation in square-section timber piles and 3D wave propagation in concrete pier walls and complicated foundations were carried out using ABAQUS/EXPLICIT. The full-waveform inversion method was carried out and the results have been compared against the observed field records. The comparison provides a means of better understanding and conducting the SE/IR tests and interpreting the results.

Finally, the selection of appropriate NDT methods and the guidelines for conducting these nondestructive tests were given in the Procedures Manual attached to this study.

# TABLE OF CONTENTS

<b>LIST OF FIGURES .....</b>	<b>xi</b>
<b>LIST OF TABLES .....</b>	<b>xxi</b>
<b>CHAPTER 1 INTRODUCTION.....</b>	<b>1</b>
<b>CHAPTER 2 LITERATURE REVIEW AND RESEARCH METHODOLOGY .....</b>	<b>5</b>
2.1 Deep Foundations and Common Nondestructive Techniques .....	5
2.1.1 Deep Foundations .....	5
2.1.2 Common Nondestructive Techniques .....	6
2.2 Drilling Equipment.....	10
2.3 Nondestructive Testing Implementation in Different States.....	11
2.4 Selection of the Three NDT Methods .....	17
2.5 Sonic Echo/Impulse Response Method.....	19
2.6 Parallel Seismic Method.....	25
2.7 Induction Field Method.....	26
2.8 Research Methodology.....	27
<b>CHAPTER 3 PHYSICAL TESTS.....</b>	<b>32</b>
3.1 Sonic Echo/Impulse Response Tests.....	32
3.1.1 Introduction to SE/IR Test Setup.....	32
3.1.1.1 Striking Setup.....	32
3.1.1.2 Sensor Setup.....	37
3.1.2 SE/IR Test Procedure .....	39
3.1.2.1 Method of Striking.....	39
3.1.2.2 Location of Receivers .....	43
3.1.2.3 Hardware Assembly.....	43
3.1.2.4 SE/IR Data Acquisition.....	44
3.1.2.5 SE/IR Data Processing and Length Determination.....	45
3.1.3 Preliminary SE Tests .....	47
3.1.3.1 SE Tests on A Wood Column.....	47
3.1.3.2 SE tests on A Concrete Column.....	49
3.1.3.3 SE Tests on A 3-story Concrete Column.....	52



3.1.3.4 SE Tests on a Reinforced Concrete Wall.....	57
3.1.3.5 Conclusions of Preliminary SE Tests .....	60
3.1.4 Field SE/IR Tests.....	62
3.1.4.1 Santo-Domingo Bridge .....	62
3.1.4.2 Bridge No. 6922.....	68
3.1.4.3 Bridge No. 1190.....	90
3.1.4.4 Bridge No. 1676.....	110
3.1.4.5 Partially Dismantled Bridge near Route 419 (Bridge No. 6253).....	124
3.1.4.6 Bridge No. 7480.....	126
3.1.4.7 Bridge No. 5899.....	128
3.2 Parallel Seismic Tests.....	141
3.2.1 PS Test Procedure.....	142
3.2.1.1 Hardware Assemblage .....	142
3.2.1.2 PS Data Acquisition.....	143
3.2.1.3 Data Processing.....	143
3.2.2 Preliminary PS Tests .....	144
3.2.3 Field PS Tests .....	147
3.2.3.1 PS tests on Bridge No. 7480 .....	147
3.2.3.2 PS tests on Bridge No. 1676 .....	162
3.3 Induction Field Method.....	172
3.3.1 IF Test Procedure.....	172
3.3.1.1 IF Hardware Setup .....	173
3.3.1.2 IF Data Acquisition.....	173
3.3.2 IF Testing: Testbed at UNM.....	175
3.3.2.1 IF Results in Air.....	176
3.3.2.2 IF Results in Sand .....	178
3.3.2.3 IF Results in Clay.....	179
3.3.3 IF testing: Testbed off Campus .....	179
3.4.1 SE/IR Tests .....	182
3.4.2 PS Tests .....	189
3.4.3 IF Tests .....	190

<b>CHAPTER 4 FINITE ELEMENT SIMULATIONS.....</b>	<b>191</b>
4.1 Wave Propagation in Piles and Columns .....	191
4.2. Wave Propagation in Pier Walls .....	206
4.2.1 Wave Propagation in Pier Walls without Damping .....	206
4.2.1.3 Effect of Deck Reflection .....	211
4.2.1.5 Summary of FEM Study of Pier Walls without Damping.....	214
4.2.2 Wave Propagation in Pier Walls with Damping .....	215
4.2.2.1 Effect of Pier Wall Width.....	215
4.2.2.2 Effect of Hammer Tip.....	218
4.2.2.3 Effect of Deck Reflection .....	218
4.2.2.4 Effect of Upward Striking .....	221
4.3 Complicated Foundations Comprising Pier Walls and Piles.....	224
4.5 Conclusions of Fem Simulations.....	235
4.5.1 Wood Columns .....	235
4.5.2 Concrete Pier Walls .....	236
<b>CHAPTER 5 CONCLUSIONS.....</b>	<b>238</b>
<b>APPENDIX A NDT PROCEDURAL MANUAL .....</b>	<b>246</b>
INTRODUCTION.....	247
BASIC PROCEDURES .....	250
Bridge Deck.....	250
Automotive Traffic .....	251
Season.....	251
Subsurface Conditions.....	252
SELECT THE APPROPRIATE NDT METHOD .....	252
Timber Piles.....	254
Concrete Piles .....	254
Steel Piles .....	254
SONIC ECHO/IMPULSE ECHO (SE/IR) METHOD .....	255
SE/IR Test Procedure .....	257
Appropriate Source Application Methods .....	258
Piles with Accessible Top .....	258

Piles without Accessible Top .....	259
Placement of Sensors .....	264
Locations of Sensors .....	264
Summary of Source Application and Sensor Placement .....	267
Assemble Equipment .....	268
Acquire Data .....	269
Interpretation of Velocity Graphs .....	276
Determining Pile Length with SE Analysis .....	277
Determining Pile Length with IR Analysis.....	279
<b>PARALLEL SEISMIC METHOD .....</b>	<b>281</b>
Parallel Seismic Overview .....	281
PS Test Procedure .....	282
Source Application .....	283
PS Data Acquisition.....	284
PS Data Processing and Determining the Pile Depth .....	284
<b>INDUCTION FIELD METHOD .....</b>	<b>287</b>
Hardware Components .....	288
IF Data Acquisition .....	288
Data Processing .....	289
Unsuccessful IF Tests .....	290
<b>REFERENCES.....</b>	<b>291</b>

## LIST OF FIGURES

Figure 1. A Bridge over the Gila River.....	1
Figure 2. Complete Loss of Support under a Bridge Pier (3) .....	2
Figure 3. Flowchart for North Carolina Unknown Bridge Foundation Process (17) .....	13
Figure 4. Various NDT Methods and Their Appropriate Use (1).....	14
Figure 5. SE/IR Test Setup for Piles Underneath a Bridge.....	20
Figure 6. A Typical Velocity Amplitude-time Graph.....	21
Figure 7. Resonant Frequencies on a Typical Mobility Graph.....	21
Figure 8. Effect of Accessible and Inaccessible Heads on Velocity Graph.....	23
Figure 9. Velocity Graph of a Defective Pile with a Bulge and a Neck .....	24
Figure 10. An Example of a Mobility Graph with Impedance Change in the Pile.....	25
Figure 11. Typical Setup and Test Data of PS Test (12) .....	26
Figure 12. The IF Result and a Typical IF Setup.....	27
Figure 13. Vertical Striking on Piles with Accessible Top.....	33
Figure 14. Vertical Striking on the Top Surface of Pile Cap.....	34
Figure 15. Eccentric Vertical Striking on the Top Surface of Pile Cap.....	35
Figure 16. Upward Vertical Striking on the Bottom Surface of Pile Cap .....	35
Figure 17. Vertical Striking on a Block Attached to the Side of a Pile .....	36
Figure 18. Inclined Striking on a Wedge Block Attached to the Side of a Pile.....	36
Figure 19. Horizontal Striking on the Side of a Pile.....	37
Figure 20. Accelerometer Setup for Piles with Accessible Top .....	37
Figure 21. Accelerometer Setup for Piles with Inaccessible Top.....	38
Figure 22. Wooden Blocks Used for Accelerometers Attachments .....	39
Figure 23. Proper Practical Source Locations, (a) Striking on top of the test pile (b), Downward striking on Point B (top of the pile cap directly above the test pile), C (top of the pile cap next to the test pile) and upward striking on Point A (bottom of the pile cap next to the test pile), (c) Striking on top surface of a block tightly attached onto the test pile .....	41

Figure 24. Dimentions of Wood and Aluminum Striking Blocks .....	42
Figure 25. Attachment of a Wooden Striking Block onto the Test Pile .....	42
Figure 26. Accelerometers Mounted on a Pile by Wooden Blocks.....	43
Figure 27. SE/IR Test Equipment.....	43
Figure 28. A Hammer and Four Different Tips .....	44
Figure 29. An Example of Acquired SE Data Including Raw Data (Top Graph) and Velocity Trace (Middle Graph) .....	44
Figure 30. Flowchart for Conducting SE/IR Tests .....	45
Figure 31. Produced Graphs from IR Analysis, Tme domain IR data (top), Coherence (middle) and Average Mobility (bottom) .....	46
Figure 32. Source and Receiver Locations on Investigated Wooden Column .....	48
Figure 33. A Velocity Graph Obtained from Horizontal Striking on Investigated Wood Column.....	49
Figure 34. A Velocity Graph Obtained from Vertical Upward Striking on Investigated Wood Column.....	49
Figure 35. Picture and Details of Centennial Engineering Concrete Column .....	50
Figure 36. An Example of Poor Velocity Signal Produced by Horizontal Striking.....	51
Figure 37. The Reinforced Concrete Column of Centennial Library on UNM Campus..	52
Figure 38. Source and Receiver Locations on the Concrete Column of Centennial Library on UNM Campus .....	54
Figure 39. Velocity Graphs for Tests 1 and 2 on the Concrete Column of Centennial Library on UNM Campus .....	55
Figure 40. Velocity Graphs for Tests 3 and 4 on the Concrete Column of Centennial Library on UNM Campus .....	56
Figure 41. Velocity Graphs for Tests 5 and 6 on the Concrete Column of Centennial Library on UNM Campus .....	56
Figure 42. Velocity Graph for Horizontal Hammer Striking with Hard Hammer Tip on the Concrete Column of Centennial Library on UNM Campus .....	57
Figure 43. The Reinforced Concrete Wall in the Structural Lab.....	58
Figure 44. Locations of Striking Points (A to D) and Accelerometers (E, F and G) on the Reinforced Concrete Wall.....	58

Figure 45. An SE Setup on the Reinforced Concrete Wall.....	59
Figure 46. Velocity Trace of the Accelerometer at Point D with Hard Tip.....	60
Figure 47. A Poor Velocity Graph Produced by Horizontal Striking.....	60
Figure 48. Location of the Santo Domingo Bridge.....	62
Figure 49. Street View of the Santo Domingo Bridge.....	62
Figure 50. Foundation Plan and Investigated Piles of Santo Domingo Bridge .....	63
Figure 51. SE Tests Setup for the Santo Doming Bridge Piles (Not to Scale).....	64
Figure 52. Velocity Graph from the Accelerometer (Pile 7-F).....	65
Figure 53. Velocity Graph of Test 7 .....	65
Figure 54. Velocity Graph of Test 8 .....	66
Figure 55. Velocity Graph of Test 9 .....	66
Figure 56. Velocity Graph of Test 10 .....	66
Figure 57. Velocity Graph of Test 11 .....	67
Figure 58. Velocity Graph of Test 12 .....	67
Figure 59. Velocity Graph of Test 13 .....	67
Figure 60. Location of Bridge No. 6922.....	69
Figure 61. Street View of Bridge No. 6922 .....	69
Figure 62. Foundation Plan and the Investigated Piles of Bridge No. 6922.....	70
Figure 63. Typical SE Test Setup for Piles of Bridge No. 6922.....	71
Figure 64. Location of Source and Accelerometers on Pile 1 .....	71
Figure 65. Location of Source and Accelerometers on Pile 2 .....	72
Figure 66. Location of Source and Accelerometers on Pile 3 .....	72
Figure 67. Location of Source and Accelerometers on Pile 14 .....	73
Figure 68. Location of Source and Accelerometers on Pile 15 .....	73
Figure 69 Velocity Graphs of Accelerometers 1 and 2.....	74
Figure 70. Velocity Graphs of Test 3.....	76
Figure 71. Mobility Graph Obtained from Accelerometer 1 (Test 1).....	77

Figure 72. Impulse Signals of Striking on an Aluminum Block.....	78
Figure 73. Impulse Signal of Striking on a Solid Surface .....	78
Figure 74. Velocity Graph Obtained from Accelerometer 1 (Test 4).....	79
Figure 75. Mobility Graph of Test 6.....	79
Figure 76. Velocity Graph of Accelerometer 1 (Test 7).....	80
Figure 77. Velocity Graph of Accelerometer 1 (Test 9).....	80
Figure 78. Initial Impulse from the Hammer’s Force Sensor (Wooden block, Hard-tip) 81	
Figure 79. Velocity Graphs of Test 11.....	81
Figure 80. Velocity Graphs of Test 12.....	82
Figure 81. Velocity Graphs of Test 13.....	82
Figure 82. Initial Hammer Impulses (Wooden blocks, Medium-hard-tip).....	83
Figure 83. Velocity Graphs of Test 14.....	84
Figure 84. Velocity Graphs of Test 15.....	84
Figure 85. Velocity Graphs of Test 16.....	84
Figure 86. Impulse Signals Generated by Striking the Aluminum Block with Hard Hammer Tips (Tests 17 to 19) .....	86
Figure 87. Examples of Poor Velocity Graphs Obtained by Striking the Aluminum Block .....	86
Figure 88. Velocity Graph Obtained from Striking the Aluminum Block (Test 18, Accelerometer 2).....	87
Figure 89. Velocity Graph Obtained from Accelerometer 1 (Tests 20 to 22) .....	88
Figure 90. Picture of a Crack along Pile 14 .....	88
Figure 91. Mobility Graph of Accelerometer 1 (Test 23).....	89
Figure 92. Location of Bridge No. 1190.....	90
Figure 93. Street View of Bridge No. 1190 Showing Running Water Surrounding Intermediate Bent during the First Visit .....	91
Figure 94. Photo of Bridge No. 1190 during the Second Visit.....	91
Figure 95. Foundation Plan and Investigated Piles of Bridge No. 1190.....	92
Figure 96. Mobile Scaffold from NMDOT District 4.....	92

Figure 97. Performing SE tests with the Aid of Mobile Scaffold.....	92
Figure 98. Velocity Graphs Obtained by Striking with Different Hammer Tips (Pile B)	93
Figure 99. Velocity Graphs of Pile E with Different Hammer Tips (Tests 4 to 6).....	94
Figure 100. Locations of Source and Receiver for Pile 1 .....	95
Figure 101. Velocity Graphs of Different Hammer Tips (Tests 7 to 9) .....	96
Figure 102. Velocity Graphs of Pile E with Different Hammer Tips (Tests 10 to 12).....	97
Figure 103. A Steel Plate Attached to Pile 10 .....	98
Figure 104. Velocity Graphs of Vertical Striking on the Pile Top and on the Steel Plate	98
Figure 105. Photo of Pile M-5 and the Pile Cap.....	99
Figure 106. Locations of Source and Receivers Blocks for Pile M-5 .....	99
Figure 107. Impact Signal and Velocity Graphs using a Hard Tip.....	102
Figure 108. Impact Signal and Velocity Graphs Using a Medium-soft Tip.....	103
Figure 109. Velocity Graphs for Various Hammer Tips Conducted on Pile M-5.....	104
Figure 110. Locations of the Receivers Blocks on Pile M-7 .....	105
Figure 111. Exterior Pile M-7 and the Pile Cap.....	107
Figure 112. Locations of Source and Receivers blocks for Pile M-1 .....	107
Figure 113. Velocity Graphs Obtained from Accelerometers 1 and 2 (Test 19).....	108
Figure 114. Velocity Graphs Obtained from Accelerometers 1 and 2 (Test 20).....	108
Figure 115. Location of Bridge No. 1676.....	111
Figure 116. Street View of Bridge No. 1676.....	111
Figure 117. Foundation Plan and Investigated Piles of Bridge No. 1676.....	112
Figure 118. Accelerometers Attached onto a Pile .....	112
Figure 119. SE Setup for Pile C-1 .....	113
Figure 120. Velocity Graph of Test 4 Conducted on Pile C-1.....	115
Figure 121. SE/IR Setup for Pile C-2 .....	117
Figure 122. SE Setup for Pile D-4 .....	121
Figure 123. Location of the Partially Dismantled Bridge near Route 419 .....	124



Figure 124. Photo of the Partially Dismantled Bridge near Route 419 .....	124
Figure 125. Investigated Piles of the Partially Dismantled Bridge near Route 419 .....	125
Figure 126. Location of Bridge No. 7480.....	126
Figure 127. Street View of Bridge No. 7480.....	126
Figure 128. SE Test Setup for a H-pile of Bridge No. 7480.....	127
Figure 129. Velocity Time History Signal Obtained from Vertical Striking on a Metal Block Attached to a H-pile .....	128
Figure 130. Location of Bridge No. 5899.....	129
Figure 131. Street and Aerial Views of Bridge No. 5899.....	129
Figure 132. Side View of One of the Piers .....	129
Figure 133. Schematic SE Test Setup for Each Pier.....	130
Figure 134. Attached Accelerometers on the Pier Side .....	131
Figure 135. Upward Striking on the Pile Cap and on the Bridge Deck.....	135
Figure 136. Typical Velocity Graph of Downward Striking at Point E .....	138
Figure 137. Typical Velocity Graph of Upward Vertically Striking at Point C.....	138
Figure 138. PS Equipment .....	142
Figure 139. Screen Shot of Software WinGEO-T .....	143
Figure 140. A Screen Shot of the Stack Plot with Four Consecutive Depths.....	144
Figure 141. Configuration of the PS Testbed .....	145
Figure 142. Duration and Amplitude of the Source Generated by a Hammer .....	145
Figure 143. PS Data at Ground Level and at a Depth of 4 Feet .....	146
Figure 144. Foundation Configuration and Locations of Boreholes of Bridge No. 7480 .....	148
Figure 145. An Aligned PVC Pipe and the Adjacent Pile .....	148
Figure 146. PS Test Result in a Dry Hole.....	150
Figure 147. Destroyed Pipe (B-06).....	150
Figure 148. An Acceleration Time History Obtained from the Hydrophone .....	152
Figure 149. First Peak Versus Depth for Test PS1 .....	152

Figure 150. First Arrival Time Versus Depth (PS2).....	153
Figure 151. First Arrival Time Versus Depth (PS3).....	153
Figure 152. First Arrival Time Versus Depth (PS4).....	154
Figure 153. Result of Test PS5 on Pile 2.....	155
Figure 154. Stacked Graph of Test PS6.....	155
Figure 155. Result of Three PS Tests on Pile 10.....	156
Figure 156. First Arrival Time Versus Depth (PS10).....	157
Figure 157. First Arrival Time Versus Depth (PS11).....	157
Figure 158. Stacked Graphs of PS Tests for Piles 16 and 19.....	158
Figure 159. Result for Test PS16.....	159
Figure 160. Results of Tests PS17, PS18, and PS19 (a) Vertical Striking, (b) Horizontal Striking on the Flange, (c) Horizontal Striking on the Web.....	160
Figure 161. Result of Test PS20.....	161
Figure 162. Plan View of Boreholes Locations.....	163
Figure 163. Geoprobe Model 7822DT- Low Headroom Drill Rig.....	163
Figure 164. Stacked Graphs for Steel H-piles and for Wood Piles.....	165
Figure 165. Examples of (a) Original View and (b) Enlarged View Showing the Initial Noise and First Arrival.....	165
Figure 166. First Arrival Time Versus Depth (Test 1).....	166
Figure 167. First Arrival Time Versus Depth (Test 2).....	166
Figure 168. First Arrival Time Versus Depth (Test 3).....	166
Figure 169. First Arrival Time Versus Depth (Test 4).....	167
Figure 170. First Arrival Time Versus Depth (Test 5).....	167
Figure 171. First Arrival Time Versus Depth (Test 6).....	167
Figure 172. First Arrival Time Versus Depth (Test 7).....	168
Figure 173. First Arrival Time Versus Depth (Test 8).....	168
Figure 174. First Arrival Time Versus Depth (Test 9).....	168
Figure 175. Reverse PS Setup for Piles C-1 and C-2 of Bridge No. 1676.....	171

Figure 176. Stacked Graphs for Piles C-1 and C-2.....	171
Figure 177. Length Inductive Test Equipment (LITE) for IF tests.....	173
Figure 178. Details of Signal Conditioning Box .....	173
Figure 179. A Successful IF Test Result .....	175
Figure 180. Test Configuration with Steel Beam and Wooden Box .....	176
Figure 181. Test Locations with Beam in the 1 <sup>st</sup> Configuration.....	177
Figure 182. Test Locations with Beam in the 2 <sup>nd</sup> Configuration.....	177
Figure 183. The 1-ft Reinforced Concrete Pier .....	180
Figure 184. Layout of the Concrete Pier and Boreholes.....	180
Figure 185. Schematics of the Reinforced Concrete Pier and the IF Test .....	181
Figure 186. Proper Source Locations.....	183
Figure 187. An FEM Model of a Wood Column.....	192
Figure 188. A Snap Shot of the Distribution of Stresses along the Column .....	192
Figure 189. Acceleration and Velocity Time Histories .....	193
Figure 190. Acceleration and Velocity Time Histories for Different Input Signals.....	194
Figure 191. Input Signal is Applied on Limited Area .....	194
Figure 192. Result of Input on a Limited Area.....	195
Figure 193. A FEM Model of a Wood Column with Foundation .....	195
Figure 194. Distribution of Stresses along the Column with Foundation at a Moment .	196
Figure 195. Results of Rectangular and Triangular Input Signals.....	196
Figure 196. Snap Shot of the Distribution of Stresses of a Model of the Santo Domingo's Pile .....	197
Figure 197. Results of Input Signals of Different Shapes .....	198
Figure 198. FEM Model of Foundation Located at Bent C in Bridge No.1676 showing striking points (a) B, C and (b) A .....	200
Figure 199. Velocity Signal Obtained at Node 1 and Produced by Striking on Point C	201
Figure 200. Velocity Signal Obtained at Node 1 And Produced by Upward Striking on Point A .....	201

Figure 201. Velocity Signal Obtained at Node 1 and Produced by Striking on Point B	202
Figure 202. FEM Mesh of Wood Column .....	203
Figure 203. Acceleration at a Node Close to the End of the Column.....	204
Figure 204. Acceleration at Node Close to the End with Rayleigh Damping .....	205
Figure 205. Acceleration at a Node 1/3 Length of the Pile from the Right End .....	205
Figure 206. Cross Section and Side View of the Pier Wall .....	207
Figure 207. Velocity Graphs Obtained at Node A ( $b = 5.2$ m).....	208
Figure 208. Impulses and the First Echoes of Models M1 to M6 .....	209
Figure 209. Dimensions of the Numerical Model and the Locations of the Source and Receiver .....	209
Figure 210. Velocity Graphs of Models M7 to M9 Obtained at Node A .....	211
Figure 211. Velocity Graphs of Models M7 to M9 Obtained at Node B .....	211
Figure 212. Cross Section and Side View of a Model with Deck .....	212
Figure 213. Velocity Graph Obtained in Node A ( $d = 10$ m).....	213
Figure 214. Velocity Graphs Obtained at Node A (M10 to M12).....	213
Figure 215. Velocity Graphs Obtained from Upward Striking at the Pile Cap .....	214
Figure 216. Velocity Graphs Obtained from Upward Striking at the Bridge Deck .....	214
Figure 217. Velocity Graph of Undamped and Damped Model M2 at Node A.....	216
Figure 218. Velocity Graph of Undamped and Damped Model M9 at Node A.....	216
Figure 219. Cross Section and Side View of the Models with Bridge Deck.....	219
Figure 220. Velocity Graphs Obtained at Node A (Models M10 to M12) (a) Undamped Models (b) Damped Models .....	220
Figure 221. Velocity Graphs Obtained at Node B (Models M10 to M12) (a) Undamped Models (b) Damped Models .....	221
Figure 222. Velocity Graphs of Undamped and Damped Models Obtained at (a) Node A and (b) Node B from Upward Striking on the Pier Cap (M13) .....	222
Figure 223. Velocity Graphs of Undamped and Damped Models Obtained at (a) Node A and (b) Node B from Upward Striking on the Pier Cap (M14) .....	223
Figure 224. Bridge Foundation Comprising a Pier Wall and Multiple Piles.....	225

Figure 225. An FEM model of a Pier Wall Supported by a Pile .....	226
Figure 226. Velocity Signal Obtained at Node B for FEM Model with Height of (a) 0.4m, (b) 0.6m, (c) 0.8m, (d) 1m, (e) 1.2m, (f) 1.4m.....	229
Figure 227. Velocity Graphs Obtained at Node B for Damped Models with Pier Wall Widths (B) of 3, 5 And 7m .....	230
Figure 228. Velocity Graphs Obtained at Node B for Damped Models with Pier Wall Widths (B) of 12, 14, 16 and 30m .....	231
Figure 229. FEM Model Utilized to Investigate the SE Tests in Pier Walls with Off-Center Piles.....	231
Figure 230. Velocity signal obtained at Node B for FEM model with a = 3, 5 and 7 m.	232
Figure 231. Velocity Time-amplitude Signal Recorded at Node A for different Pier Heights = 10 ft.....	234
Figure 232. Velocity signals obtained from nodes located 0.2, 0.4, 0.6, 0.8 and 1m above the pile and pier wall junction.....	235

## LIST OF TABLES

Table 1. Inventory of Bridges with Unknown Foundations in New Mexico.....	17
Table 2. Superstructure Materials of Bridges with Unknown Foundations in New Mexico. .....	18
Table 3. Factors Affecting SE/IR Testing (22).....	22
Table 4. Specifications of Preliminary and Field NDT Tests.....	29
Table 5. Direction and Location of Strikes on a Concrete Column at the Centennial Engineering Center. ....	51
Table 6. Calculated Lengths of Centennial Engineering Concrete Column.....	52
Table 7. Characteristics of SE Tests on the Concrete Column of Centennial Library on UNM Campus. ....	53
Table 8. Specifications of SE Tests Performed on the Santo Domingo Bridge Piles.....	64
Table 9. Calculated Pile Lengths of Pile 8-E.....	68
Table 10. Estimated Lengths of Piles of Santo Domingo Bridge. ....	68
Table 11. SE Tests Conducted on Pile 1.....	76
Table 12. Estimated Length of Pile 1 from SE Analysis. ....	76
Table 13. Estimated Length of Pile 1 from IR Analysis.....	77
Table 14. Estimated Length of Pile 1 from SE Analysis (Tests 4 to 6).....	79
Table 15. Estimated Length of Pile 1 from IR Analysis (Tests 4 to 6).....	79
Table 16. Estimated Length of Pile 3 (Tests 11 to 13) .....	83
Table 17. Estimated Length of Pile 3 (Tests 14 to 16). ....	85
Table 18. IR Results for Accelerometer 2 (Tests 14 to 16). ....	85
Table 19. Specification of Tests Conducted on Pile 14.....	87
Table 20. Specification of Tests Conducted on Pile 15.....	89
Table 21. Estimated Length of Pile 15 from Mobility Graphs (Tests 23 to 28). ....	89
Table 22. Estimated Average Length of Piles of Bridge No. 6922. ....	90
Table 23. Calculated Length of Pile B.....	93
Table 24. Calculated Length of Pile E.....	94

Table 25. Calculated Length of Pile 1. ....	96
Table 26. Calculated Length of Pile 8. ....	97
Table 27. Specifications of SE Tests Conducted on Pile M-5. ....	100
Table 28. Results of SE Tests Conducted on Pile M-5. ....	101
Table 29. Specifications and Results of SE Tests Conducted on Pile M-7. ....	106
Table 30. Specifications of SE Tests Conducted on Pile M-1. ....	109
Table 31. SE Tests Results for Piles of Bridge No. 1190. ....	110
Table 32. Location and Direction of Hammer Strikes for Pile C-1. ....	114
Table 33. Calculated Pile Lengths of Pile C-1. ....	115
Table 34. First Resonant Frequencies of IR Analysis for Pile C-1. ....	116
Table 35. Average First Resonant Frequencies and Calculated Lengths of Pile C-1. ....	117
Table 36. Location and Direction of Hammer Strikes for Pile C-2. ....	118
Table 37. Calculated Pile Lengths of Pile C-2. ....	119
Table 38. Average Calculated Pile Lengths of Pile C-2. ....	119
Table 39. First Resonant Frequencies (Hz) for Pile C-2. ....	120
Table 40. Location and Direction of Hammer Strikes for Pile D-4. ....	121
Table 41. Calculated Pile Lengths of Pile D-4. ....	122
Table 42. First Resonant Frequencies (Hz) for Pile D-4. ....	123
Table 43. SE Tests Results of Piles at Bridge No. 1676. ....	123
Table 44. SE Tests Results of the Partially Dismantled Bridge near Route 419. ....	125
Table 45. Distances $d_1$ and $d_2$ for Sensor Placement on Each Pier Wall. ....	130
Table 46. Estimated Wave Velocities of the Concrete Pier. ....	131
Table 47. Hammer Tips and Striking Locations and Directions for Testing at the North Side of Pier 1. ....	132
Table 48. Results of SE Tests Conducted at the North Side of Pier 1. ....	133
Table 49. Hammer Tips, Location, and Direction of Hammer Strikes at the South Side of Pier 2. ....	134
Table 50. Results of SE Tests Conducted at the South Side of Pier 2. ....	135

Table 51. Resonant Frequencies and Calculated Pier Lengths at the South Side of Pier 2. .....	136
Table 52. Hammer Tips, Location, and Direction of Hammer Strikes at the North Side of Pier 2. ....	137
Table 53. Results of SE Tests Conducted at the North Side of Pier 2. ....	138
Table 54. Average Buried Depths at the South and North Sides of Pier 2. ....	139
Table 55. Direction and Location of Hammer Strike at the North Side of Pier 3. ....	139
Table 56. Results of SE Tests Conducted at the North Side of Pier 3. ....	140
Table 57. Average Buried Lengths at the North Side of Pier 3. ....	140
Table 58. SE Tests Results for Piles of Bridge No. 5899. ....	141
Table 59. Boring Depths of the Holes. ....	149
Table 60. Subsurface Condition at the Site. ....	149
Table 61. Specifications of PS Tests. ....	151
Table 62. PS Tests Results of Bridge No. 7480. ....	161
Table 63. Specifications of PS Tests. ....	164
Table 64. Depths of the Inflection Points for Pile B-1. ....	169
Table 65. Depths of the Inflection Points for Pile C-1. ....	169
Table 66. The Range of Estimated Pile Length, Average and Known Pile Lengths. ....	170
Table 67. Test Results (Locations Correspond to Figure 182). ....	177
Table 68. Test Results (Locations Correspond to Figure 183). ....	178
Table 69. IF Test Results for Sand with 4% Moisture Content. ....	178
Table 70. IF Test Results for Saturated Sand. ....	178
Table 71. Measurements at Points on Axes B and C with the Presence of Clay. ....	179
Table 72. Voltage Readings Recorded at Each Borehole Location. ....	181
Table 73. Success Rate of SE Tests for Different Striking Blocks. ....	184
Table 74. Success Rate of SE Tests for Different Striking Methods. ....	185
Table 75. Success Rate of SE Tests Performed by Different Hammer Tip Types ....	186
Table 76. Success Rate of SE tests for tests performed by hard hammer tips ....	187



Table 77. Success Rate of SE tests for tests performed by Medium-hard hammer tips .	187
Table 78. Success Rate of SE tests for tests performed by Medium-soft hammer tips ..	187
Table 79. Success Rate of SE tests for tests performed by Medium-soft hammer tips ..	187
Table 80. Specifications of Foundation Models in Bridge No.1676 .....	199
Table 81. Lengths Calculation Results for Different Striking Methods on Foundation of Bridge No.1676.....	202
Table 82. Amplitudes of the source signals for Different Striking Methods on Foundation of Bridge No.1676 .....	203
Table 83. Input Parameters of the Finite Element Simulations. ....	206
Table 84. Widths of the Pier in Models M2 to M6.....	207
Table 85. Impulse Time Durations and Corresponding Hammer Tips (M7~M9).....	210
Table 86. Calculated Nodes A and B Heights for Different Hammer Tips.....	210
Table 87. Deck Widths for FEM Models M10 to M12. ....	212
Table 88. Calculated Heights for Upward Striking. ....	214
Table 89. Measured and Actual Heights of Node A in Models M2 to M9.....	217
Table 90. Measured and Actual Heights of Node B in Models M2 to M9.....	217
Table 91. Hammer Tips and the Corresponding Impulse Contact Durations of Three Models.....	218
Table 92. Calculated Heights of Nodes A and B for Damped Models.....	218
Table 93. FEM Models of Various Deck Widths. ....	219
Table 94. Calculated Heights Corresponding to Nodes A and B in Models M10 to M12. ....	221
Table 95. Calculated Heights for Upward Striking at Node A in Models M13 and M14. ....	223
Table 96. Calculated Heights for Upward Striking at Node B in Models M13 and M14. ....	224
Table 97. Specifications of Complicated Foundation FEM Models.....	225
Table 98. Length Calculation for Models with Different Pier Wall Height .....	229

## CHAPTER 1 INTRODUCTION

According to the Federal Highway Administration (*1*), there are about 85,000 bridges nationwide that do not have any design or as-built plans identifying the type, depth, geometry and materials of their foundations. The National Bridge Inventory (NBI) has identified 86,133 bridges in the United States that have no foundation data on record. It is evident that an unknown percentage of these 86,133 bridges, identified by NBI as missing foundation data, could also be highly vulnerable to scouring that is induced by water flow coupled with erodible soils. Currently, NMDOT has identified about 266 bridges with unknown foundations. Figure 1 shows a bridge over the Gila River. Unknown bridge foundations potentially give rise to scour safety risks (see Figure 2). Therefore, it is crucial to identify the bridge foundation characteristics of bridges for which the information is missing, particularly the type and depth of foundations, in order to determine the susceptibility to scour for each of these. Characterization of unknown foundations is also necessary for planning and retrofitting of each bridge's substructure.



**Figure 1. A Bridge over the Gila River**

Conventional excavation, coring and boring excavations to determine unknown bridge foundation depths and types are deemed to be expensive, destructive and limited in their application to the unknown foundation problem (2). There is therefore a real need to research and develop lower cost nondestructive testing (NDT) methods to provide foundation depth and type data on unknown bridge foundations to aid in evaluating scour safety.



**Figure 2. Complete Loss of Support under a Bridge Pier (3)**

Several NDT methods to evaluate unknown foundations have been developed and extended recently. The selection of the method depends on its specific utility and the type of the foundation to be tested. Due to numerous advantages, the Induction Field and dynamic low-strain methods are desirable non-destructive testing methods for evaluating concrete driven piles, cast-in-place piles, concrete filled steel pipe piles, steel H-piles and timber piles. The following three methods will be focused in this proposed research to study the characterization of the unknown bridge foundations.

- Sonic Echo/Impulse Response (SE/IR) Method
- Parallel Seismic (PS) Method
- Induction Field (IF) Method

Studies on the applicability and methodology improvement of SE/IR and PS tests have been reported. However, the literature has been mainly focusing on individual pile without the pile cap. Only some limited studies have been reported on piles underneath pile caps. Although those studies revealed various theoretical and practical aspects of the tests, more studies are required on more complicated foundations. In some bridges, the deck is supported by foundations comprising pier wall and piles. Sometimes only a part of the pier wall is exposed and the buried part of the foundation is unknown. There is no study on this kind of foundation in the literature. Thus, it could be revealed if NDT testing is able to detect this type of foundation.

In addition to the aforementioned complex foundations, individual piles underneath the regular pile caps supporting the bridges' decks have not yet been completely elaborated. Since a major part of the applicability of the SE/IR tests have been in the context of quality control of the drilled shafts, only individual piles without a real superstructure have been investigated in the literature. In real bridges comprising piles, pile cap, girders and bridge deck the top of the pile is not accessible for placing the source and sensors, proper methods of conducting the tests should be investigated.

Based on the above-mentioned discussions, this study attempts to investigate the characterizing of the unknown bridge foundations including two following main goals:

1. *Investigating* the applicability of SE method on complex foundations comprising pier walls and piles.
2. *Developing* a specific NDT methodology to determine the depth of the individual piles with a regular pile cap.

To achieve the goals of this study, extensive literature review on various NDT methods and collected DOT's experience of applying NDT methods in other states has implemented. Preliminary and field tests and numerical simulations were carried out. The results of the field data and numerical simulations are compared to identify the best practice of conducting NDT tests. Finally, based on the findings of this study, NDT tests procedural manuals for DOT engineers are developed to identify and characterize unknown bridge foundations. The procedural manuals include guidelines for use by engineers to characterize the type, depth, and geometry of unknown bridge foundations. The NDT procedural manual is attached to this dissertation in Appendix A. It should be noted that

the findings of this study are mainly based on the results of a research project conducted by the author and two faculty members of the Civil Engineering Department, UNM. The project was sponsored by the New Mexico Department of Transportation (NMDOT) in cooperation with Federal Highway Administration (FHWA).

## CHAPTER 2 LITERATURE REVIEW AND RESEARCH METHODOLOGY

### 2.1 Deep Foundations and Common Nondestructive Techniques

#### 2.1.1 Deep Foundations

Highway bridges are commonly supported on deep foundations. Shallow foundations are used occasionally. The deep foundations are structural members that are made of timber, concrete, steel, composite (combination of two materials out of timber, steel, and concrete). There are four common basic deep foundation construction methods. Deep foundations are based on one of the following techniques:

- Driven piles - Piles are driven into the ground by mechanical force. The prefabricated timber, steel, or concrete piles are banged into the ground by a hammer, pushed by shear brute force, or vibrated by a shaker.
- Driven cast-in-place piles – a hollow steel casing is driven into the ground first. The cavity is subsequently filled with concrete.
- Drilled shafts – a cylindrical hole of the required depth is excavated. Reinforcement cage is placed in the excavated hole and subsequently filled with concrete.
- Augercast (Continuous-flight auger) piles – a hollow stem auger is drilled into the ground. Concrete is pumped through the hollow stem of the auger while the auger is pulled up. Reinforcement, if necessary, is pushed into the concrete manually.

Preliminary information on the type of unknown foundation is essential to the selection of NDT methods and to the interpretation of the experimental results. The site characteristics and access limitation need to be considered. NDT testing methods have varying degrees of site access requirements. Surface NDT will generally require access to the substructure of a bridge. On larger bridges or in difficult terrain access may require some form of crane or scaffold from the superstructure. Borehole NDT methods will require a soil boring or probe and therefore will be more limited at each site. The access requirements should be reviewed prior to the selection of the NDT method.

**Bridge Deck** A bridge deck may have several variables that may impact the quality of the test data. The clearance below the bridge deck is very important especially for borehole methods. Special drilling equipment may be required for low clearance bridges.

Connections between the superstructure and the substructure determine the extent of traffic noise that is transmitted through the structure itself to the foundation, affecting the NDT tests that use wave transmission principles.

**Automotive Traffic** Traffic on bridges may pose a substantial problem for some NDT methods. One factor to consider is the number of traffic lanes on the bridge relative to the volume of traffic and time of day. This relationship between traffic flow and existing lanes will greatly influence maintenance of traffic (MOT) plans and schedule. For most of the NDT methods, testing during non-peak hours (i.e. at night) may be preferable (i.e. less noise and vibrations at night). If daytime lane closure is required on a highly traveled bridge, then some lane capacity analysis may be necessary to ensure minimal impact to traffic flow.

**Season** Seasonal weather fluctuations may affect the access of substructure. These impacts could be associated with variations in the water levels and flow velocities under a bridge.

**Subsurface Conditions** Highly variable soil strata may be reflected in the data resulting from NDT testing and should be considered while making predictions about foundation depth. Many of the NDT methods utilize wave transmission principles based on wave velocities through soil strata. Wave velocities vary differently from one material to the next; therefore, some basic understanding of the subsurface conditions is helpful. The data interpretation from the NDT methods should be analyzed in conjunction with known or estimated rock depths as they apply to the area.

### **2.1.2 Common Nondestructive Techniques**

Surface methods such as Sonic Echo/Impulse Response, Bending Wave, Ultra-seismic, and Spectral Analysis of Surface Wave require accelerometers or geophones that are mounted on the top or the side of the bridge substructure. These methods require access to the top and the side of bridge substructures. Parallel Seismic, Borehole Radar, Borehole Sonic, Cross-hole sonic and Induction Field methods are common borehole NDT methods. A brief overview of these nine common NDT methods and their capabilities and limitations is described here. (4).

The cost and the time delay of borehole installation before testing are the major disadvantage of the borehole methods. If testing of every pile is desired, a borehole may be needed for each pile which can be very expensive. In addition, an estimated pile length is required to determine the boring depth. However, borehole methods are more versatile and reliable than surface methods.

**Sonic Echo/Impulse Response (SE/IR)** The source and a receiver are typically placed on the top and/or sides of an exposed foundation. A longitudinal wave is generated by a hammer and the depth of the foundation is calculated by the time difference between the source (impulse) and the echo for SE analysis, or from the resonant peaks for IR analysis. The Sonic Echo and Impulse Response methods are similar to Low Strain Pulse Echo and Low Strain Transient Response methods in Pile Integrity Testing respectively.

*Capabilities* The method is quick and inexpensive. The method has shown good performance for determining the depths of timber piles, concrete piles, and drilled shafts that extend up above the ground or water surface. The method can be used to determine the depths of pier walls.

*Limitations* The echoes from pile bottom will likely not be measured for embedded length to diameter ratios much greater than 30:1 due to attenuation of waves. This limitation may decrease to 10:1 in stiff soils (high elastic modulus). No echo can be detected if the impedance of foundation soils (rock) is similar to that of the pile. Also, piles cannot be detected below a buried pile cap. Furthermore, the method does not work on steel piles (H-piles and pipe-piles) due to energy dissipation.

**Bending Wave** The Bending Wave method is based on the dispersion characteristics and echoes of bending waves traveling along very slender member like piles. The method has been applied to timber and concrete piles. The method involves mounting a minimum of two horizontal receivers a few feet apart on one side of an exposed pile, and then impacting the pile horizontally on the opposite side of the pile a few feet above the topmost receiver. The raw data is filtered based on the selected frequencies. For each selected frequency, the depth is calculated by identifying the initial wave arrival and subsequent reflection (echo).



*Capabilities* It does not require access to a pile's top surface since bending (flexural) waves are generated by striking horizontally on the side of a pile. Successful testing of timber piles of up to 60 ft in length has been reported.

*Limitations.* An accessible vertical surface of at least 4-5 ft or more in length is needed. Layers of stiff soils can result in apparent short pile lengths. There are difficulties in identifying flexural wave reflections from more massive, deep foundations. Data processing is more complicated than SE/IR tests. Piles cannot be detected below a buried pile cap. Also, the method will not work on steel piles (H-piles and pipe-piles) due to energy dissipation.

**Ultra-Seismic (US)** The Ultra-Seismic method is a sonic reflection technique that uses three or more sensors. The principle is similar to that of SE/IR method.

*Capabilities* Data reliability is typically increased since it does not require the knowledge of the wave velocity of the pile. The method was found to be less affected by the presence of large beams on top of columnar substructure than the SE/IR method. The data of multiple sensors are processed to distinguish waves travelling down and up and to minimize the noise from attached substructure reflections.

*Limitations.* An accessible vertical surface of at least 4-5 ft or more in length is needed. Piles cannot be detected below a buried pile cap. Other limitations are similar to those of SE/IR method.

**Spectral Analysis of Surface Waves (SASW)** The SASW test involves determining the variation of surface wave velocity versus depth in layered systems. The bottom depths of exposed substructures or footings are indicated by slower velocities of surface wave travel in underlying soils.

*Capabilities* Capable of determining the depths of shallow abutments, pier walls, and other solid substructures with a flat surface.

*Limitations* Requirement of a flat surface for generating surface waves. Not suitable for deep foundation since the maximum foundation depth that can be determined is limited by the longest horizontal dimension of tested foundation.

**Parallel Seismic (PS)** A Parallel Seismic test consists of impacting an exposed foundation substructure either vertically or horizontally with a hammer to generate either compressional or flexural waves which travel down the foundation and are transmitted to

the surrounding soil. The arrival of transmitted compressional wave is tracked at regular intervals by either hydrophone receiver suspended in a water-filled cased borehole or by a clamped three-component geophone receiver in a cased or uncased borehole (if it stands open without caving).

*Capabilities* The method has the widest range of application of any of the methods for determining unknown foundation bottom depths regardless of depth, substructure type, geology, and materials. Both compressional and shear waves can be used with the method as generated by vertical and horizontal impacts. The data interpretation is simple.

*Limitations* The method is more expensive than surface methods since a borehole must be drilled. Highly variable soil velocity conditions complicate the data interpretation. Larger impact force must be generated for long piles.

**Borehole Radar** The Borehole Radar test uses a transmitter/receiver radar antenna to measure the reflection of radar echoes from the side of the bridge substructure foundation. It works well with soils with low conductivity (sands). The use of a directional, focused radar antenna could potentially improve the results; however, it is quite expensive.

*Capabilities* The test is quick. Radar also works well at detecting steel and reinforced concrete because the steel reflects the signal strongly. It can be used to estimate the thicknesses of toes and heels of footings, as well as to indicate depths of unknown foundations.

*Limitations* Cost is higher than surface methods since a borehole must be drilled and cased with a 4-in. diameter PVC casing. The result is significantly affected by soil conditions and moisture in the ground since radar is severely attenuated in conductive soils (clays).

**Borehole Sonic** The Borehole Sonic test involves lowering a source and a receiver unit in a borehole and measuring the reflections of compressional or shear waves from the side of the bridge substructure foundation using essentially horizontal ray paths.

*Capabilities* Fair potential reflections have been reported in the process of determining the piles' lengths.

*Limitations* More expensive than surface methods since a borehole must be drilled. It may be difficult to obtain reflections of small targets without generating higher frequency waves in soils.

**Cross-Hole Sonic** Similar to the standard Cross-Hole Sonic Logging test for checking the integrity of drilled shafts, the Cross-Hole Sonic test involves lowering a source and a receiver unit in two separate boreholes simultaneously and measuring the wave transmitted time between the source and the receiver.

*Capabilities* The interpretation is simple. The method is applicable for any foundation type and material and NMDOT engineers have experience.

*Limitations* It is more expensive than single borehole methods. Well-aligned tube installation may be difficult.

**Induction Field (IF)** In Induction Field method an electro-magnetic field is induced through a soil-foundation system and the change of the field due to the nearby metal objects is detected. The testing is implemented by passing a DC current through a polarized magnetic field sensor which is lowered into a PVC cased borehole adjacent to the test pile. A magnetic field is consequently induced in the pile's metal which can be detected by the probe. The depth of the foundation is determined by measuring the magnetic field strength at various depths, and noting the changes in magnetic field strength.

*Capabilities* The IF is a proven technology for the determination of the depth of steel piles and reinforced concrete piles. IF is not affected by background vibration noise. The method could be performed in conjunction with the PS method or the Borehole Sonic method to improve reliability with minimal additional cost.

*Limitations* The method does not work on timber piles or unreinforced concrete piles. The boring must be drilled within 0.5 m (18 in) of the foundation. Interpretation of data from the IF method may be complicated by the existence of ferrous materials in soils.

## **2.2 Drilling Equipment**

All the borehole methods mentioned above require the drilling of a borehole (or two boreholes) parallel to the existing foundation. In order to be successful in determining the existing bridge pier depth the borehole must be located within 18 inches of the existing pier's location for the IF method and within six feet for the PS method. In either case a borehole of at least 3-in diameter needs to be drilled ten to fifteen feet below the estimated foundation bottom elevation. In some cases, the bridge superstructure might not provide enough clearance for the drilling rig to be located underneath the bridge deck. Specialized

low headroom drilling equipment may be needed. The service can be contracted out to a drilling company that has the capability. However, scheduling and the accumulative cost to complete the testing of all required bridges can be a concern.

### **2.3 Nondestructive Testing Implementation in Different States**

A comprehensive literature search was conducted on information available from national organizations (Transportation Research Board and American Association of State Highway and Transportation Officials), State DOTs (Alabama, Arizona, Colorado, Florida, Illinois, Indiana, Louisiana, and North Carolina), journal and conference publications. A search of the International Transport Research Document database did not provide information pertinent to NDT of unknown bridge foundations (UBF); all other sources provided valuable insights into both the technologies involved and the field applications. No information was found on application of NDT on UBF in Arizona. It may be due to the low number of UBF in Arizona. Also, these bridges are located on local and minor roads (5). The Federal Highway Administration (FHWA) presented guidelines on the methods of evaluation of bridges with unknown foundations, including a method of determining the embedment (1). A series of FHWA Webinars (6-9) outlined a road map on how to tackle the issue of unknown bridge foundations.

The policies implemented by the FHWA regarding how to reduce the number of bridges with unknown foundations led state DOTs to explore various methods to determine the foundation characteristics for these bridges, either directly through field testing or indirectly by implementing other methods. Risk-based approaches have been implemented by several states to establish priorities for their investigations, based on the results of National Cooperative Highway Research Program (NCHRP) Project 24-25 (5). Artificial Neural Networks (ANN) methods have been used in Florida, North Carolina, and Texas to predict foundation depths of bridges with unknown foundations. ANN consist of applying a mathematical model with capabilities similar to biological neural networks (e.g. central nervous system). The model creates a series of interconnected nodes, each capable of processing information in parallel with the other nodes. The network is trained with data examples from which to “learn” the complex relationships relating the inputs and outputs

of a system. McLemore et al. (1) describes the development of ANN for bridges in Florida. Two models were developed to predict the length of concrete and steel piles.

A comprehensive evaluation was made of potential NDT technologies that could be relevant to this problem in the NCHRP 21-5 project, as outlined in 'Determination of Unknown Subsurface Bridge Foundations' (2). This report presents the test results of a research study on the applicability of using borehole-based nondestructive testing techniques to disclose the characteristics of unknown subsurface bridge foundations. The results included in this report are from the three borehole-based NDT techniques of PS test, borehole sonic test, and borehole radar test. The field testing was performed at multiple bridges with known foundations in Alabama, Colorado, and Texas, using all methods that were considered state-of-the-practice at the time. Phase 2 consisted of multiple “blind” field tests at 21 bridge sites in Colorado, Massachusetts, Michigan, Minnesota, New Jersey, and Oregon. While this research did not create new NDT methods or technologies, it greatly enhanced the understanding of the nuances relevant for field applications and the successful transfer of various NDT technologies to the field engineer. The PS method has the broadest application to the investigations of concrete, timber and steel bridge substructures.

Nondestructive methods are increasingly being used in the determination of conditions of unknown bridge foundations. As per Olson et al. (2), the foremost need is to determine the foundation depth, followed by foundation type, geometry and subsurface conditions.

FHWA/Florida DOT (1) conducted a detailed evaluation of bridge foundation, including NDT, scour evaluation, and risk analyses. This investigation included summaries of activities in the DOTs of various states. Several surface and borehole NDT technologies were implemented in investigating unknown foundations (10-13). Both SE/IR and PS methods were found to work best in Louisiana (14). US and PS tests were carried out in Alabama (15). The finding indicated that the US method worked well to assess “short” pile and PS method was recommended for use when the result was inconclusive.

Successful IF tests were reported on determination of the embedment depth of H-piles in North Carolina and Pennsylvania (16).

Figure 3 shows the unknown foundation process developed at North Carolina DOT for UBF in their bridge management system in 2005. The use of the risk-based management guidelines for scour was suggested in 2010 to evaluate remaining low-risk bridges with unknown foundation in North Carolina. The review of all unknown foundation bridges was completed in 2012.

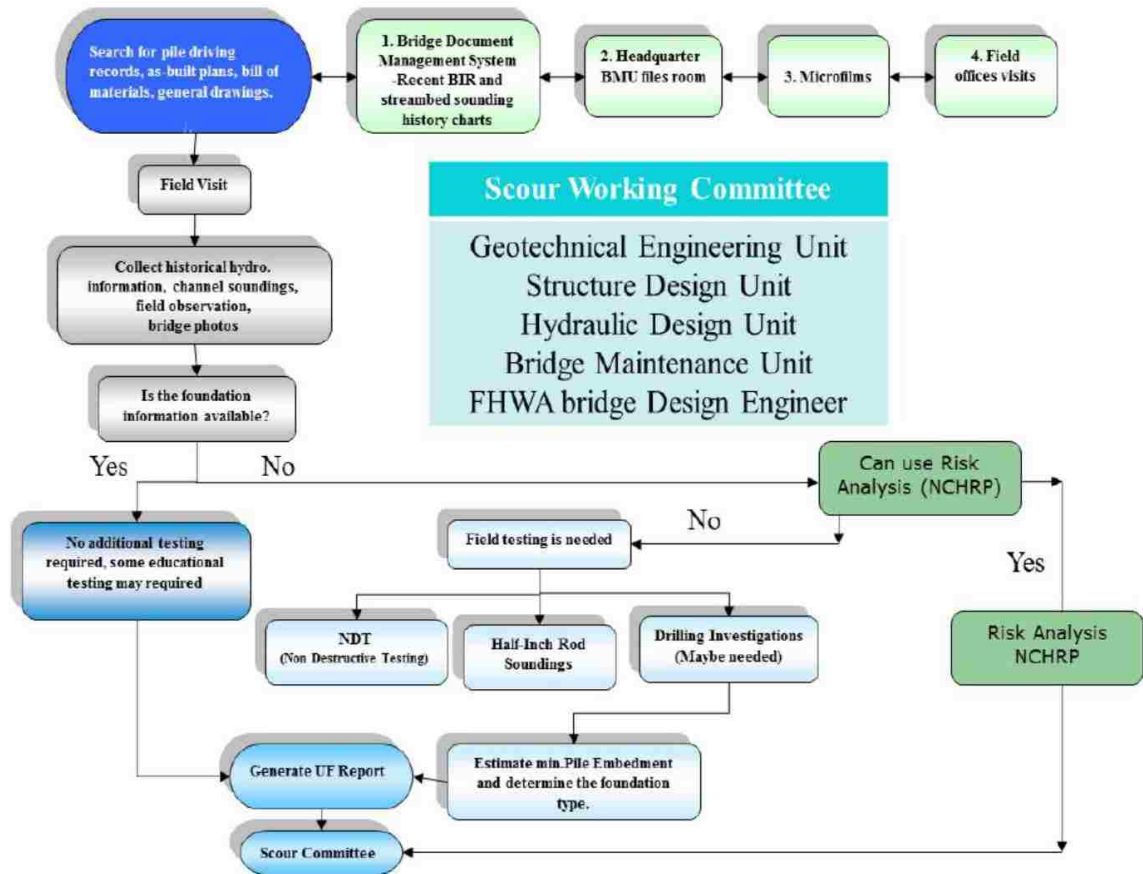


**Figure 3. Flowchart for North Carolina Unknown Bridge Foundation Process (17)**

Figure 4 illustrates the appropriate application of the NDT method as suggested by Florida DOT. Here, SE/IR tests are not recommended since other methods provide much better results.

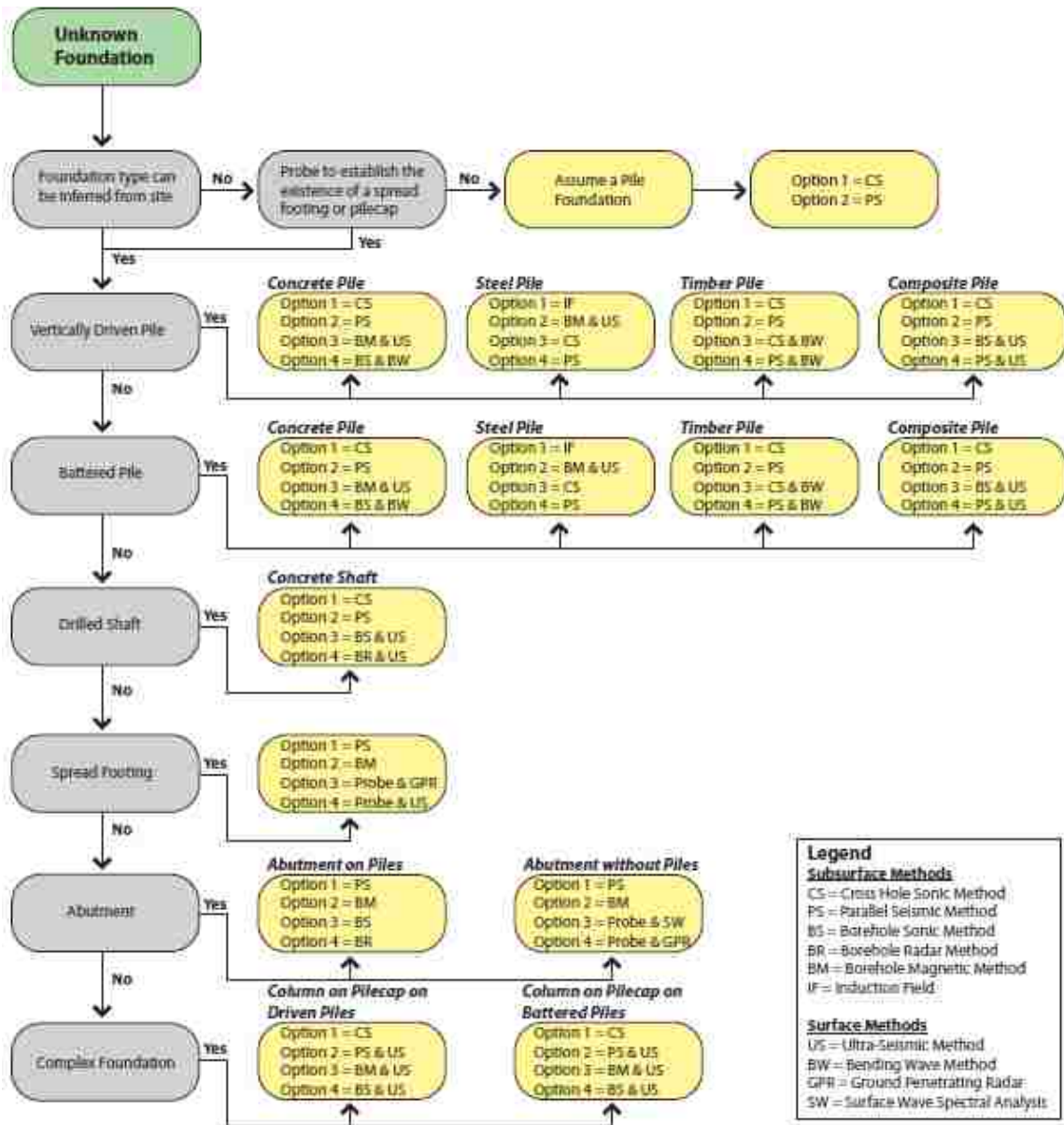


Figure 4. Various NDT Methods and Their Appropriate Use (1)

Strategic Highway Research Program (SHRP) led to the development of the NDT Toolbox for highway applications which allows DOT engineers to select appropriate NDT tools (18). According to this joint FHWA/AASHTO/TRB product, “many NDT technologies are available to owner agencies; however, each has its own set of applications, strengths and weaknesses, and practitioners need clear information to help them select the best NDT method to evaluate the condition of a specific feature. The NDTToolbox provides

an independent assessment to allow owner agencies to be confident in their choice of technology and method. The NDTtoolbox enables owners to:

- Provide information, quickly and reliably, about the under-the-surface conditions of bridge decks without causing undue additional wear to the bridges themselves.
- Yield faster measurements in the field by using hand-held stereoscopic “fingerprinting” equipment for testing the quality assurance of materials.
- Use automated thermal profiling systems and other technologies to reliably prevent deterioration and segregation of hot-mix asphalt construction.
- Detect easily and efficiently the extent, depth and severity of de-lamination in hot-mix asphalt pavements.
- Meet smoothness requirements for Portland cement concrete pavements, more easily and less expensively, by detecting surface irregularities in real-time before the cement hardens.
- Use continuous deflection measuring devices to determine the structural capacity of pavement with better spatial coverage and less impact on traffic.
- Monitor more thoroughly the condition and deterioration of tunnel linings while providing less disruption of traffic.

Hossain et al. (19) presented research on the determination of the depth of the foundation of a previously unknown bridge foundation at Fort Worth, Texas. The bridge was supported by driven steel H-piles. Three NDT techniques were utilized: (1) PS method, (2) SE/IR method, and (3) resistivity imaging (RI). The main objective of this study was to compare the suitability of these three different NDT techniques to determine the unknown bridge foundation depth. Based on the field test results, both PS and RI methods provided foundation depth close to actual foundation depth. However, the SE/IR method was determined to be unsuitable for determining the unknown steel H-pile depth.

In one such case (20), a construction project was delayed by a state inspector after it was noted that a field inspector was not present during shaft construction. In order to resume construction, the state required that SE/IR testing be performed on the 12 shafts to verify their integrity. It was determined that all 12 shafts had bulbs (or widening) between approximately 8 and 13 ft. Several of the shafts were partially uncovered by the contractor,



and the bulbs were confirmed. After testing and approval by the design engineer, the state allowed construction to continue.

In addition to the abovementioned literature search, emails have been sent to various state DOTs including Alabama, Arizona, Colorado, Florida, Illinois, Louisiana, North Carolina, Minnesota and Texas to determine the current state of practice of NDT testing for UBF. A summary of the responses is listed below:

**Arizona DOT** No information on nondestructive testing on bridge piles in Arizona

**Colorado DOT** used consultants to work on the unknown foundation bridges. NDT tests have been carried out on eleven bridges the type of NDT tests were not disclosed.

**Florida DOT** hired consultants to evaluate 2,500 unknown foundation bridges. The consultants developed the methodology and carried out the production work. Structures Maintenance Office is responsible for NDT testing of bridges with unknown foundations. For a large majority of the bridges, the consultants used a statistically based evaluation method instead of performing NDT. Only PS method has been used on 3 bridges which had a high importance.

**Illinois DOT** did not use NDT testing on unknown bridge foundations. They have bridge plans for most of the bridges in Illinois which specify which type of foundation is used. Only 7 bridges were found with unknown foundations out of 7500 state owned structures. For those structures in a water environment subject to scour an unknown foundation would be assumed to be scour critical and either monitored during significant hydraulic events or remediated with stone rip-rap. The responsible unit for unknown bridge foundations is the bridge management unit. They would use a consultant to do the NDT if necessary.

**Minnesota DOT** has just started the investigation on the unknown bridge foundations. Some preliminary PS tests were performed to determine the unknown pile lengths by using a special cone in the cone penetration testing as the receiver.

**North Carolina DOT** has completed their unknown bridge foundations program. 6,000 bridges have been identified as having unknown foundations. They have tried almost all of the NDT methods in the past to estimate the minimum depth of piles. The most often used two methods are the Bending Wave method and the Low Strain Pulse Echo method

(SE method). They tried to stay away from any borehole methods due to additional drilling cost, time consuming, and sometimes require specialty equipment to perform the drilling. The Geotechnical Engineering Unit was responsible for NDT testing of bridges with unknown foundations. The NDT was performed by both the consultants and the Geotechnical Engineering Unit staff. Low Strain Pulse Echo was performed by trained staff members. The average cost of unknown bridge foundation evaluation by consultants is \$800 to \$1600 per bridge. The half-inch sounding rod was used to provide some information concerning the subsurface conditions (rock depth) as addition method to clarify the estimation of the minimum depth prediction from the NDT.

**Texas DOT** has 111 bridges on-system and 7637 off-system bridges that have unknown foundations. However, they do not currently use nondestructive testing methods to estimate the depth and/or other characteristics of bridge foundations with unknown foundations.

#### **2.4 Selection of the Three NDT Methods**

Based on information provided by NMDOT, there are 266 bridges in New Mexico that have insufficient information regarding bridge substructure and can be considered scour critical. NMDOT and FHWA prioritized these bridges by placing them into 3 categories (high risk, moderate risk, and low risk). They are categorized based on available information and visual assessments with the criteria defined by NMDOT. The database of the bridge foundations has been updated with the results of this study and the work of a consultant. Tables 1 and 2 summarize the inventory of the bridges with unknown foundations in terms of their priority and the superstructure material in New Mexico.

**Table 1. Inventory of Bridges with Unknown Foundations in New Mexico.**

	High Risk	Moderate Risk	Low Risk	Total
State	2	14	46	62
Local	20	22	162	204
Total	22	36	208	266

**Table 2. Superstructure Materials of Bridges with Unknown Foundations in New Mexico.**

	Steel	Timber	Concrete	Aluminum	Masonry	Total
State	14	38	10	0	0	62
Local	71	24	103	5	1	204
Total	85	62	113	5	1	266

Since these bridge foundations are made of concrete, timber, or steel, the selected NDT methods should work properly on these materials. Considering the advantages and limitations of the previously mentioned NDT methods, three methods (SE/IR, PS, and IF) were selected. All selected methods are proven techniques (2). The surface SE/IR method and two borehole methods (PS and IF) are easy to operate compared to other NDT methods. The equipment of these three NDT methods are inexpensive. Although these NDT tests can be performed by one person, it is more efficient with two persons. The pros and cons of the methods can be found in previous section. In addition, NMDOT engineers already have experience on the equipment for SE/IR tests. It has been used on determining the length and integrity of the drilled shaft foundations placed at the I-40-Coors interchange in Albuquerque, NM. The existing equipment can be used to perform SE/IR tests without modification and it can be upgraded easily to perform PS tests. The detailed reasons for selecting these three methods (SE/IR, PS, and IF) are described first. Then, the principles and important facts of each method are explained in detail.

The SE/IR method was selected because it is the most economical NDT method and can be used for timber and concrete foundations. Moreover, the SE/IR method was selected because the setup is quick and straightforward. The setup time for each test takes only 15 minutes. Each test can then be conducted in minutes. Every pile at a bridge site can be tested within a reasonable time. In addition, The SE/IR method has less requirement for the exposed length of the pile. Bending Wave and Ultra-seismic methods need a 4-5 ft of accessible exposed part of the pile. The SASW method requires a flat access to generate the surface wave.

The two borehole methods (PS and IF) were selected because of the limitations of SE/IR method. The SE/IR method does not work on steel piles (H-piles or steel pipe piles without concrete filling). It cannot detect the pile toe reflection for complex foundations

(the pile is fully embedded underneath a massive pier wall). The result of SE/IR method is doubtful for long piles (embedded length to diameter ratios greater than 30:1).

Among the borehole methods, the PS method not only is a proven technique but also has the widest range of application for determining the depth of unknown foundation regardless of depth, substructure type, geology, and materials. The test is also quick. The number of data points needed to be obtained in each PS test depends on the depth of the borehole. Each data point can be obtained in less than 2 minutes. Although the method imposes an additional cost of drilling a borehole, soil exploration can be conducted during the excavation to obtain valuable geotechnical information. It should be noted that the purchased equipment from Olson for this project was able to conduct both PS and SE/IR tests.

Although PS method can work on steel piles, IF method is the best proven technology for determining the depth of steel piles. IF tests are quicker than PS tests. Unlike PS method, IF method is not affected by traffic vibration. The data interpretation is very straightforward. In addition, the equipment is inexpensive. A device has been purchased for this project. Reliability of the result can be improved by performing an additional PS test in conjunction with the IF test. The major challenge of this method is that the borehole must be within 1.5 ft from the pile edge. This may be accomplished by the purchased Geoprobe Model 7822DT drilling rig for low clearance bridges.

## **2.5 Sonic Echo/Impulse Response Method**

Figure 5 shows the SE/IR test setup underneath a bridge. A small hammer equipped with an electronic trigger is utilized to generate the impact (source). The impact can be applied at the top of the pile (pile top striking), on the striking block that attached on the pile surface, or at the pile cap (Point A, Point B, or Point C). The generated stress wave travels down the pile and reflects (or echoes) back at the interface of the pile toe and foundation soil. The wave is recorded through a sensor (a geophone or an accelerometer) mounted on the side of the pile (13). More than one sensor can be attached to improve the reliability of the test if the length of the exposed pile is long enough to accommodate the sensors. Figure 6 shows a typical velocity amplitude-time graph obtained from a sensor. This type of presentation will be called as velocity graph from here on. In this figure, the

indicated impulse and echo points show the moments of the waves passing through the sensor location while traveling down and returning respectively. Once the propagated wave velocity is known, the total pile length ( $L_t$ ) and buried length ( $L_b$ ) shown in Figure 5 can be calculated using following equations.

$$L_{tr}: \text{Distance between the sensor location and pile toe } (= \frac{v \times \Delta t}{2}) \quad (1)$$

Where  $\Delta t$ : Time difference between the impulse and first echo

$v$ : Propagated wave velocity

$$L_t: \text{Total pile length} = L_{tr} + L_a \quad (2)$$

$$L_b: \text{Buried pile length} = L_t - L_e \quad (3)$$

$L_e$ : Exposed pile length between the pile cap and ground surface

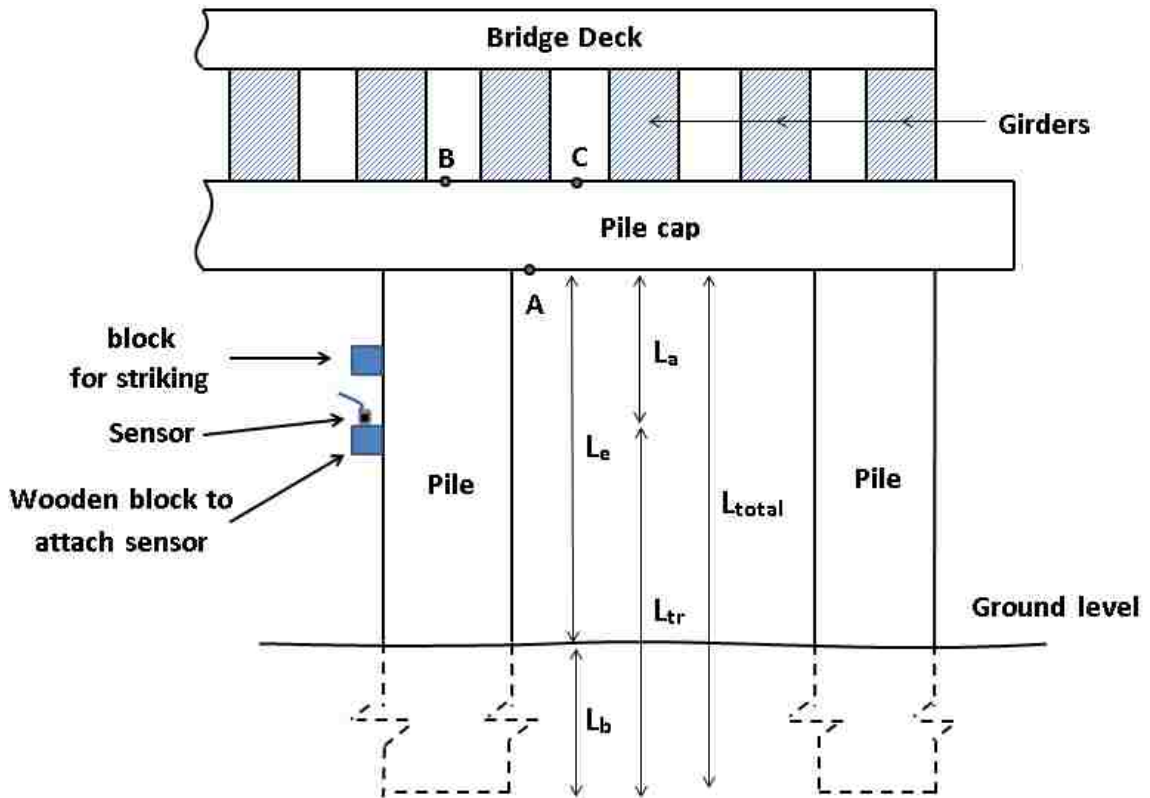
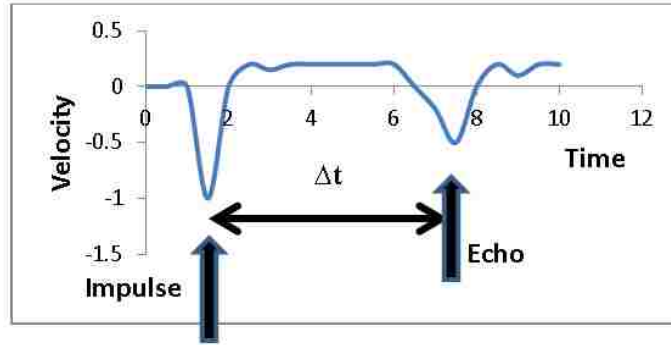


Figure 5. SE/IR Test Setup for Piles Underneath a Bridge



**Figure 6. A Typical Velocity Amplitude-time Graph**

The signals obtained from sensors can also be investigated by Impulse Response (IR) analysis. The force and velocity time history signals are converted into frequency domain using the Fast Fourier Transform. Mobility is then defined as the ratio between the converted frequency-base velocity and the frequency-base force. The result is commonly presented as a plot of mobility versus frequency as shown in Figure 7. For the generated wave lengths greater than the diameter of a prismatic pile, there are resonant frequencies that depend on the pile length and the propagated wave velocity as shown in Figure 7 (21). The length of the pile can be estimated from the difference of successive resonant frequencies ( $\Delta f$ ) as:

$$L_{\text{total}} = \frac{v}{2 \times \Delta f} \quad (4)$$

The  $\Delta f$  is the difference between consecutive *resonant* frequencies.

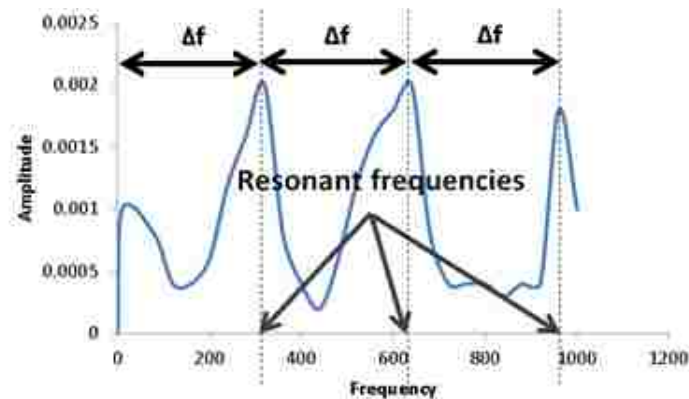


**Figure 7. Resonant Frequencies on a Typical Mobility Graph**

Factors affecting SE/IR testing are listed in Table 3 (22). Although the SE/IR method is easy to conduct in the field, some precautions regarding its applicability are listed in the table (22). The pile-to-soil stiffness ratio and length-to-diameter ratio of the pile are two major factors affecting the success of the SE/IR test (23). Since the impact force energy is radiated from the pile shaft into the surrounding soil. It is difficult to determine the length of a long pile with a high slenderness ratio (24). The surrounding soil absorbs energy and dampens the measured response (echo). The maximum detectable pile length-to-diameter ratio reported in literature varies from 10 to 30, depending on the stiffness ratio of the pile and the surrounding soil (25). It was found that the SE/IR method can be applied on drilled shafts if the shaft to soil stiffness ratio is more than 77 (23).

**Table 3. Factors Affecting SE/IR Testing (22).**

Factors	Consequences	Proposed Corrective measures
Incorrect hammering	Generation of poor longitudinal waves.	Striking perpendicular to the top surface of pile head.
Incorrect hammers	Too small a hammer with a stiff head generates high frequency waves which attenuates too fast and cannot reach the deeper part of the pile. Too large a hammer with a soft head generates a wave with a large contents of low frequencies and a large pulse period which may mix up with reflections from small defects in shallow depth of the pile.	Using an adequate hammer. If defects are in the shallow part of the pile, a small and very hard tipped hammer should be tried. The correct selection and use of hammers depend on the experience and judgment of the operator.
Soil resistance and damping	(a) Abrupt change in soil stiffness may induce a reflected wave. (b) Soil layers may induce secondary waves. (c) Soil's damping (radial and viscous) may reduce the strength of the wave propagation in the pile by attenuation.	Differentiating between the secondary waves from the soil layers and the reflections from pile toe and anomalies.
Wave velocity of piles assumed in analysis	Wrongly assumed wave velocity leads a wrong estimation of pile length (or defect location).	Calibrating the wave velocity on a pile (known length) of the same material as the pile under testing.
Large diameter pile	On a large diameter pile, there is a problem in generating plane waves propagating longitudinally along the pile's axis.	The wave length should be larger than the pile's diameter. If the pile diameter is too large, use other alternative methods.
Long pile	The wave reflection may be too weak or there is no reflection at all due to attenuation of the wave for a long pile.	(a) Increase the hammer impact energy. (b) Increase the resolution of sampling and signal-to-noise ratio of the measurement. (c) Use other alternative methods.
Defects near the pile head and multiple defects	(a) Defects near the pile head may lead to dispersion of the initial impact wave and a distortion of echo wave. (b) Multi-reflections reduce the wave energy transmitted to the deep part of the pile and lead to wave superposition.	(a) To overcome the effects of defects near the pile head and to detect defects in the deep part of the pile, try to use heavy and less stiff tipped hammer. (b) Experienced interpretation is needed. (c) Development of more sophisticated programs for modeling and interpretation.
Instrument	Poor resolution cannot differentiate the reflections from two close reflectors. Low signal-to-noise ratio may not pick up weak signals from the toe of a long pile.	The instrument shall have adequate resolution (minimum 50(s) and signal-to-noise ratio and other advanced features such as signal filtering, auto-ranging, auto-averaging, and auto-correlation.

The quality of the source and the location of the sensor are important for a successful SE/IR test. The source should have enough energy to produce a detectable echo from the pile's bottom in the velocity graph. A standard hammer with a hard tip usually produces desirable impulses. However, it sometimes generates unfavorable high frequency waves that make it difficult to interpret the test results. This problem is associated with the

sensor location, placing the sensor at different locations may produce successful interpretation (26).

The propagated wave velocity depends on the quality of the material. Knowing the wave velocity accurately yields accurate results in SE/IR tests. The application of a multi-sensors array on wood timber utility poles was proposed for more reliable and accurate results (27).

The presence of a pile cap and superstructure can undermine the success of determination of foundation depth using SE/IR tests. Two main geometric factors were reported that limit the applicability of the SE/IR method (21). They are the ratio of the intervening structure tributary area above the shaft to the drilled shaft area and the pile cap thickness to shaft diameter ratio. The result of two scenarios is shown in Figure 8. The darkened curves are the results obtained while the head is inaccessible. The light-colored curves represent the result where the pile head is accessible. With inaccessible the pile head, the length of the pile is difficult to determine. Echoes from multiple cap reflection can be seen in the velocity graph (see Figure 8a) and identifying the resonance frequencies corresponding to the reflection of the toes are difficult (see Figure 8b). However, the result is very clear with an accessible head (see light colored curves).

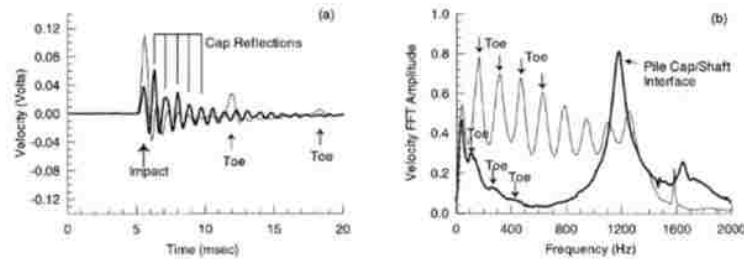


**Figure 8. Effect of Accessible and Inaccessible Heads on Velocity Graph (21)**

The determination of the length of a pile is affected by any echo reflections from the impedance changes such as changes in pile dimensions, cracks, voids, variations in material quality and variations in the surrounding soil layers affect (28).

Anomalies such as consecutive bulges and necks also result in reflections between the impulse and the echo from the pile bottom on the velocity graph. Such reflections should be considered when the echo from pile bottom is sought. A study showed that the



defects with sizes greater than 10–30% and 45% can be identifiable by SE and IR analyses, respectively (29). An example of a defective pile with a bulge and a neck and the corresponding velocity signal is indicated in Figure 9 (30).

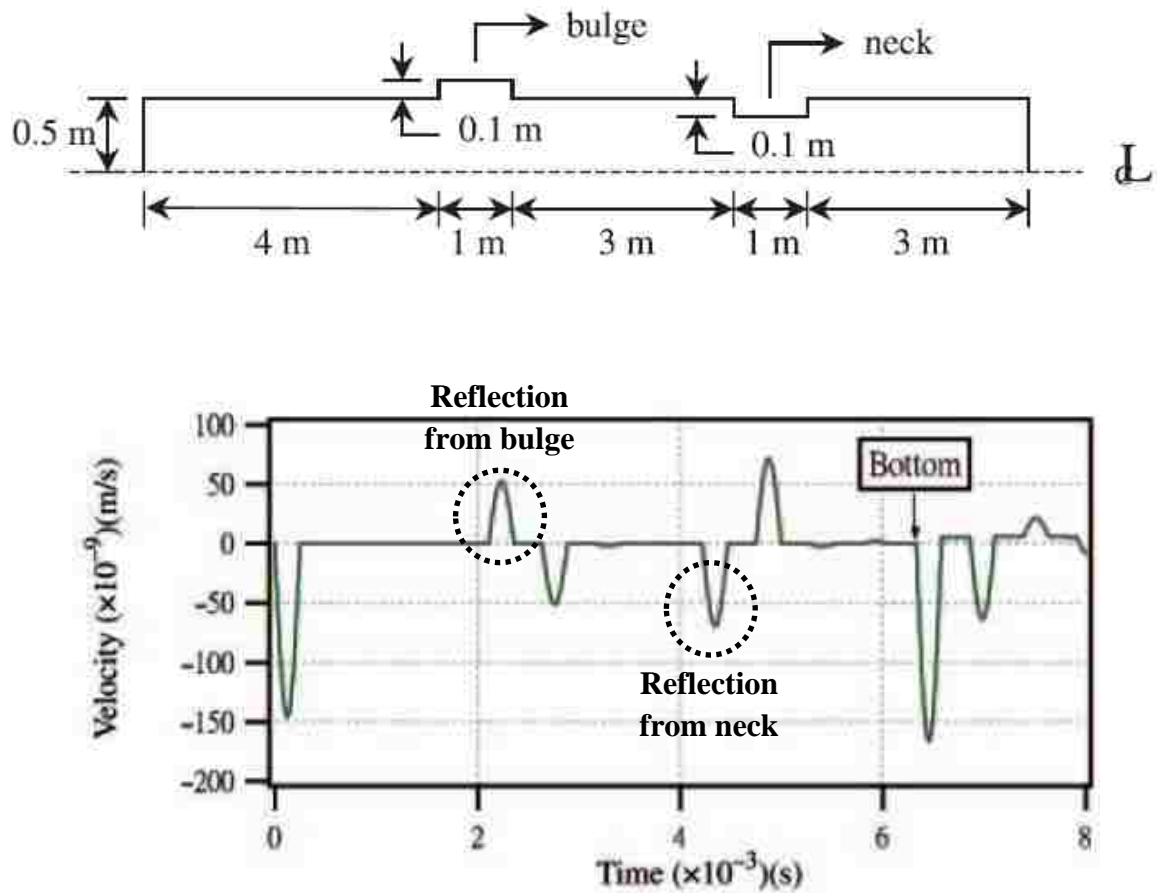


**Figure 9. Velocity Graph of a Defective Pile with a Bulge and a Neck (30)**

The impedance change along a pile also produces oscillation on the mobility graph. An example of a mobility graph affected by impedance change along a pile is shown in Figure 10 (31). The  $\Delta f = 200$  Hz corresponds to the reflection from the pile bottom, whereas the  $\Delta f = 980$  Hz corresponds to the cross-section change at 2 m below the pile top.

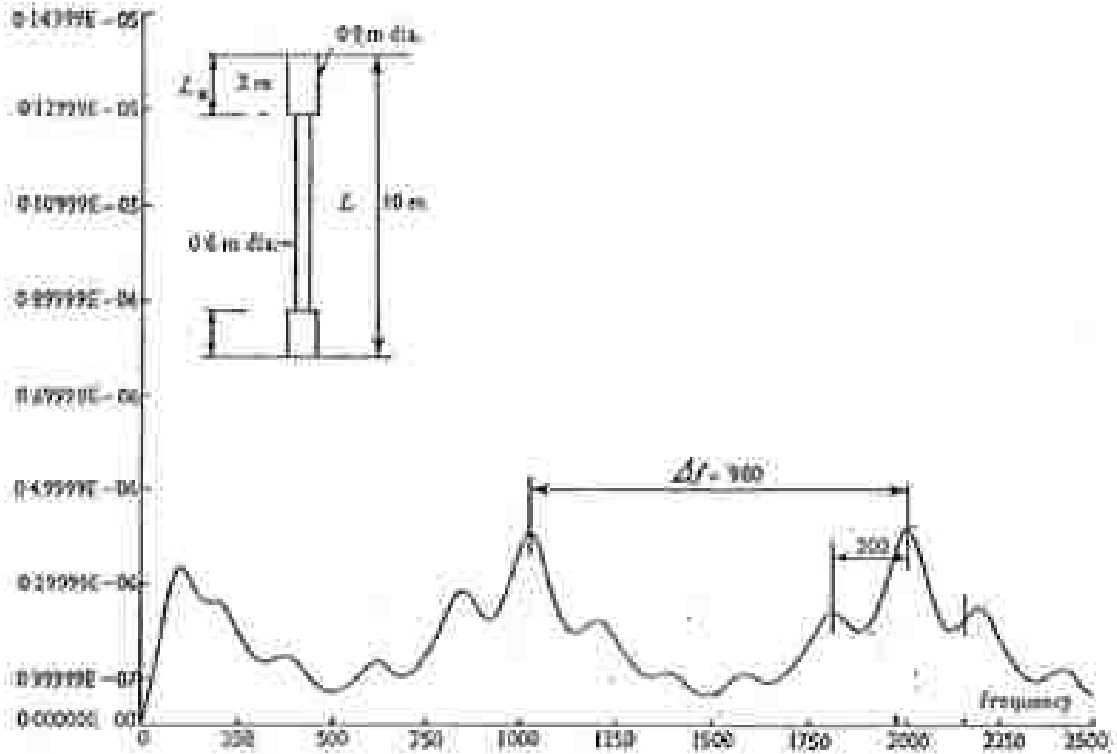


**Figure 10. An Example of a Mobility Graph with Impedance Change in the Pile (31)**

## 2.6 Parallel Seismic Method

The PS method is one of the common low strain methods that can be used to detect the length of piles. However, this method is more expensive than the SE/IR method because it requires drilling a hole parallel to the test pile. The borehole is cased with a 2-in capped-end PVC tube and filled with clean water for better coupling with the sensor (hydrophone).

In the PS test, an instrumented hammer produces an impulse that travels downward through the pile. As the stress wave travels down the pile, a portion of the wave is transmitted into the surrounding soil. The transmitted wave is recorded by a hydrophone that is inside a nearby borehole. The hydrophone is raised or lowered in uniform increments and the test is repeated at each increment. The velocity graph is recorded at each depth. The first arrival time of the wave is defined at each velocity graph. These velocity graphs are stacked together as shown in Figure 11. A typical setup is also shown in this figure.

Since the wave velocity of the pile material is significantly higher than the wave velocities of soils, the arrival times differ between two consecutive depth increments, one tested when the hydrophone is parallel to the pile and the second when the hydrophone is

below the pile. Two straight lines can be determined from these arrival times and the intersection of the two lines is then identified as the foundation depth (32, 33). An additional benefit of the PS test is that the wave propagation through the soil provides information about the soil condition (such as stiffness) adjacent to the foundation (34).

A newly developed combined Parallel Seismic and Cone Penetration Test (PS/CPT) system allows collecting soil data and conducting a PS test simultaneously during a CPT test. The new combined technique has a great advantage over conventional PS tests since no borehole is required (35). Olson et al. (36) presented details of the principles and operations of the combined (CPT+PS) system.

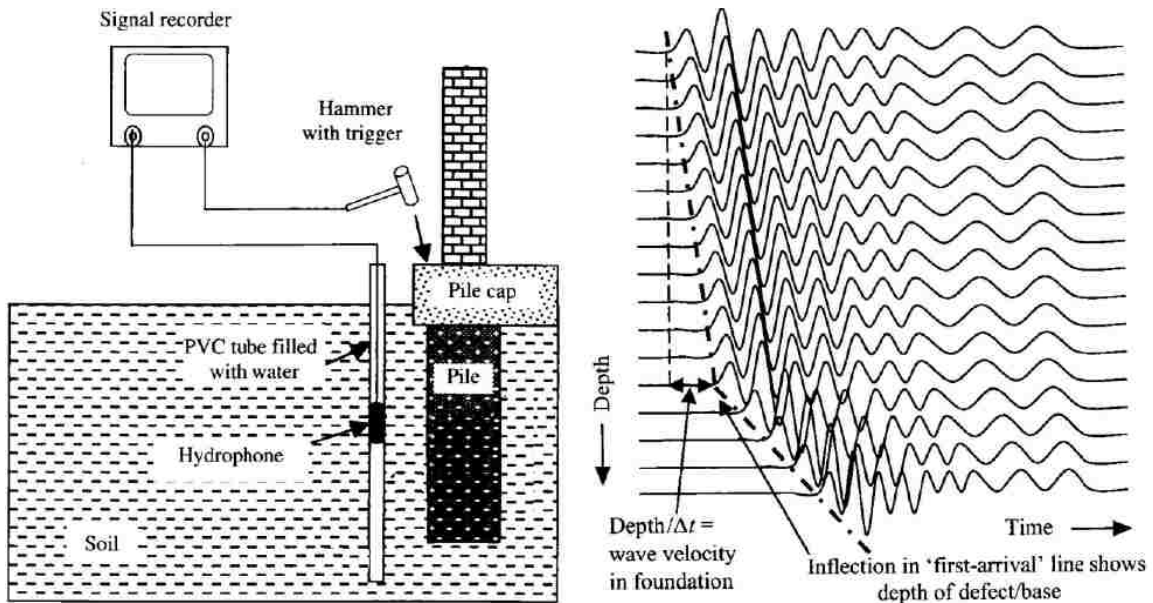


**Figure 11. Typical Setup and Test Data of PS Test (12)**

## 2.7 Induction Field Method

The IF method is used to measure the depth of steel foundations (H-piles or pipe piles) or concrete piles with continuous reinforcing steel. This method can be performed in conjunction with the PS method, since the installed borehole for IF tests can also be used for PS tests.

The IF method involves determining the length of the metal within the foundation by inducing an electro-magnetic field through a soil-foundation system and detecting the change of the magnetic field due to the nearby metal objects. The testing is implemented

by passing a DC current through a polarized magnetic field sensor which is lowered into a PVC cased borehole adjacent to the test pile. A magnetic field is consequently induced in the pile's metal which can be detected by the probe. The depth of the foundation is determined by measuring the magnetic field strength at various depths, and identifying the changes in magnetic field strength. A typical IF setup and associated data are indicated in Figure 12.

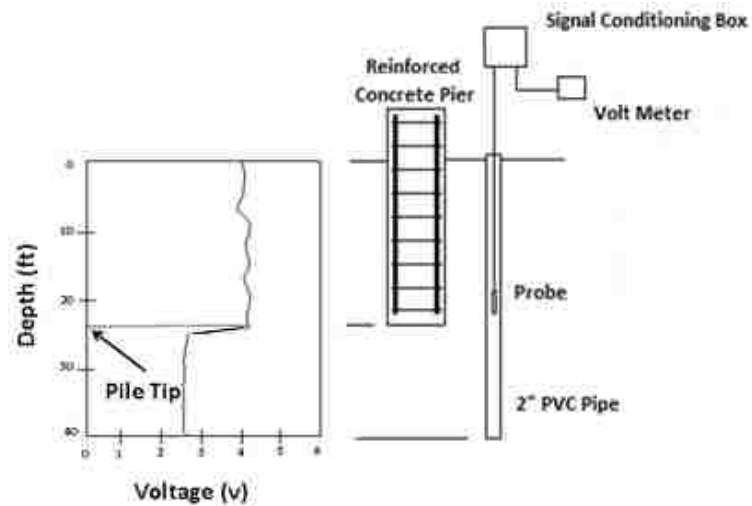


**Figure 12. The IF Result and a Typical IF Setup**

## 2.8 Research Methodology

SE/IR, PS, and IF were used to determine the conditions of unknown bridge foundations. As mentioned before, the three NDT methods have different requirements regarding degrees of site access. SE/IR generally requires access to the substructure of a bridge. Borehole methods (PS and IF) require a soil boring that must be installed as close as possible to the test pile before conducting testing. The borehole methods require a borehole to extend at least 10 feet deeper than the expected embedment pile depth. The PS method requires a borehole to be located within 6 feet from the test pile while the IF method requires a borehole to be located within 18 inches (preferably within 12 inches). Two-inch inner diameter PVC tube with an end cap should be placed in the hole and the spacing between the PVC tube and the hole should be backfilled with compacted native soil. The tube must be filled with water before conducting PS tests.

Two devices and ancillary equipment were purchased for the project from Olson Instruments, Inc. for SE/IR and PS tests and from Pile Dynamics Inc. for IF tests. The equipment pursuant to ASTM D5882-07-2013 (37), ACI 228.2R-13 (38) were acquired. Equipment purchased from Olson consists of the Freedom Data PC platform, two 100mv/g 1D accelerometers, a hydrophone, and a hammer with force transducer and 4 hammer tips. The hammer tips are hard, medium hard, medium soft, and soft. The contact time for hard tip is mainly between 1200 to 2000 milliseconds. The contact time increases with the degree of softness of the hammer tip. For IF tests, the Length Inductive Test Equipment (LITE) comprises a signal conditioner, multimeter, Probe (sensor) and battery.

Before conducting the field tests, preliminary tests were performed under controlled environmental conditions to study the applicability and limitations of the selected NDT methods. The tests were conducted in the Civil Engineering Structural Lab, on the University of New Mexico (UNM) campus, and at a test site off campus. It was expected that the knowledge obtained from these controlled tests should improve the success rate of conducting NDT tests in the field. After performing initial tests, numerous NDT field tests have been performed at each bridge location in coordination with the NMDOT. For each bridge, the foundation was investigated in detail to determine the foundation depth as well as to reveal any possible difficulties that might be encountered. Since it was crucial to provide test procedures to conduct the SE/IR, PS and IF tests, initial test procedures were developed based on numerous sources in the literature review. However, they were regularly modified during the preliminary and field tests based on the success and failure of various tests conducted in the project. It should be noted that such procedures allow efficient collection of high quality data in the limited timeframe assigned for field testing. The tests procedures for each selected NDT method will be presented later. The specifications of all NDT tests performed in this project are summarized in Table 4. Details of the setup of NDT tests and the results will be elaborated later. The foundations were known for Bridge Nos. 1676 and 7480 since the as-built drawings are available. Validation of SE/IR and PS tests was confirmed by conducting these two tests on Bridge No. 1676 while validation of PS tests was examined on Bridge No. 7480. All the bridge numbers are based on NMDOT database. The purpose of selecting the bridges is explained in the sequel:

**Table 4. Specifications of Preliminary and Field NDT Tests.**

Test Type	Test Object	Foundation Material	NDT Test
Preliminary	Centennial Building Column (UNM)	Reinforced Concrete	SE
	Structural Lab Concrete Wall (UNM)	Reinforced Concrete	SE
	Centennial Library Column (UNM)	Reinforced Concrete	SE
	Biology Annex Building Column (UNM)	Wood	SE
	Buried Cylinder in Ground (Private Test Site)	Reinforced Concrete	IF, PS
	Constructed Wooden Box Test-bed (UNM)	Steel	IF
Field	Highway Bridge No. 7480 - H-pile foundation	Steel	SE, PS
	Highway Bridge No. 5899 - Pier wall foundation	Reinforced Concrete	SE
	Highway Bridge No. 6922 - Pile foundation	Wood	SE
	Highway Bridge No. 1190 - Pile foundation	Wood	SE
	Highway Bridge No. 1676 - Pile foundation	Wood	SE, PS
	Railroad Santo Domingo Bridge- Pile foundation	Wood	SE
	Partially Dismantled Bridge near Route 419 (Bridge No. 6253)	Wood	SE

**Santo Domingo Bridge** This railroad bridge was the first bridge recommended by Mr. Bob Meyers and Ms. Michelle Mann of NMDOT on which preliminary SE/IR tests were performed because of the bridge location and the foundation material. In addition, the bridge is far away from any automotive traffic. NMDOT has the equipment that has been used regularly for Pile Integrity Tests. It was decided to use NMDOT's equipment to start

the project before the completion of the purchase of the required equipment for the research project. The new equipment has the capability for conducting PS tests and for an additional sensor. The SE/IR tests were implemented while NMDOT's engineers were the observers.

**Bridges Nos. 1190 and 6922** It was expected that a great amount of unknown bridge foundations in New Mexico were supported by timber piles, therefore it was crucial to investigate the performance of SE/IR tests on such foundations. The communication with NMDOT revealed that performing NDT on the unknown foundations of state-owned bridge of high risk was their highest priority. Therefore, SE/IR tests were suggested for 7 high risk state-owned timber bridges from the NMDOT database including bridges Nos. 312, 1190, 1873, 1876, 4069, 5893, and 6922. Since the bridge inspection reports and pictures of Bridges No. 1190 and 6922 were available to the UNM research group, it was decided to perform the NDT tests on those two bridges.

**Bridge No. 1676** Validation of the research results was essential, therefore the UNM research group requested NMDOT to provide a bridge with *known* foundation. Bridge No. 1676 was introduced to the research group for conducting the NDT tests (SE/IR and PS tests). The selection of the bridge was based on the following reasons:

- The as-built drawings of the bridge foundation were available.
- The bridge site was conveniently located (just 66 miles from UNM).
- There was no accessibility problem and the bridge had sufficient clearance to install boreholes for PS tests.
- The capability of Geoprobe Model 7822DT could be examined.

**Bridge No. 6253** In 2015, the research group obtained the information that some bridges in District 4 near NM Route 419 were being replaced. Since the timber piles of these bridges was supposed to be pulled out, validation of NDT tests can be performed on these timber piles. With the help of the technical panel, SE/IR tests were able to be conducted on one bridge prior to exhumation of the timber piles.

**Bridge No. 5899** The foundation of Bridge No. 5899 was selected due to following reasons:

- The bridge was categorized as state own and high risk.
- The material of the foundation was concrete that provides a means to examine the performance of SE/IR equipment on concrete foundations.

- The bridge foundations were massive pier walls. The literature review indicated that most of SE/IR studies were on foundations of slender elements. The research group did not have adequate information on the performance of the SE/IR tests on massive pier walls. Therefore, this bridge foundation could provide valuable information of SE/IR tests on pier wall foundations.

**Bridge No. 7480** This bridge was supported by steel H-piles and the as-built drawing was available. It was a great site to examine the performance of IF tests. However, due to the difficulty of drilling boreholes close enough to the piles, only PS method could be conducted. Although SE/IR tests were not recommended for steel piles, SE/IR tests with different setups were also conducted.

In addition to the physical NDT tests, Finite Element Method (FEM) simulations were conducted in this study. The full-waveform inversion method was carried out and the results were compared against the field observation. The comparison provides a means of better understanding and conducting the SE/IR tests and better interpreting the results. In the current study, major factors, such as a foundation's bottom condition, a foundation's material damping, hammer tip type, superstructure reflections, pier geometry and characteristics of striking, were studied using FEM models of piles, pier walls and complicated foundations composed of piles and pier walls.



## CHAPTER 3 PHYSICAL TESTS

### 3.1 Sonic Echo/Impulse Response Tests

#### 3.1.1 Introduction to SE/IR Test Setup

In the presence of superstructure, it is crucial to identify the best locations of source and receiver to capture the intended echo from foundation bottom. For wing piles, the top surface of the pile is accessible. SE/IR tests can be conducted by placing the sensor on the pile top or attaching the sensor to the side of the pile and striking the pile top. When the top of the foundation is inaccessible due to the presence of superstructure, the sensor must be mounted on the side of a pile to record vertical vibrations. Since geophones are heavier and larger than accelerometers, it is easier to attach an accelerometer than a geophone. Therefore, accelerometers were used as the sensor. The source must be created by striking the hammer on other areas rather than the pile top.

In this section, various options for striking and sensors attachments are presented. They have been utilized in both preliminary and field tests. They are presented in detail and prioritized throughout this report.

##### 3.1.1.1 Striking Setup

In SE/IR tests, sonic waves are generated by striking a hammer on a surface of the foundation. P waves or S waves will be generated depending on the direction of the hammer strike. If a portion of the top of a pile is accessible, the best longitudinal P-waves can be generated by striking on its top. For piles with inaccessible top, the research group examined other options such as striking on a block attached on the side of the pile. When attached blocks to the side surface of the piles are used, they must be properly secured by nails and screws to prevent any detachments during striking.

When a horizontal strike is applied on the side of a pile, S-waves are primarily generated. P-waves will be generated at any interface when the incident waves are not propagated perpendicular to the interface. The energy of the indirect P-wave is significantly smaller than that of the P-wave produced by vertical striking. However, the side strikes are very attractive since it is much easier to apply when the top of a pile is inaccessible. It is

worthy to examine the velocity graphs from the horizontal and vertical strikes. This issue will be discussed later in the preliminary and field tests.

**Striking Setup for Piles with Accessible Top** When either the entire or a portion of the pile top is accessible, a vertical strike can be applied on the top surface of the pile as shown in Figure 13. In this case, the longitudinal P-waves travelling down the pile is generated directly.

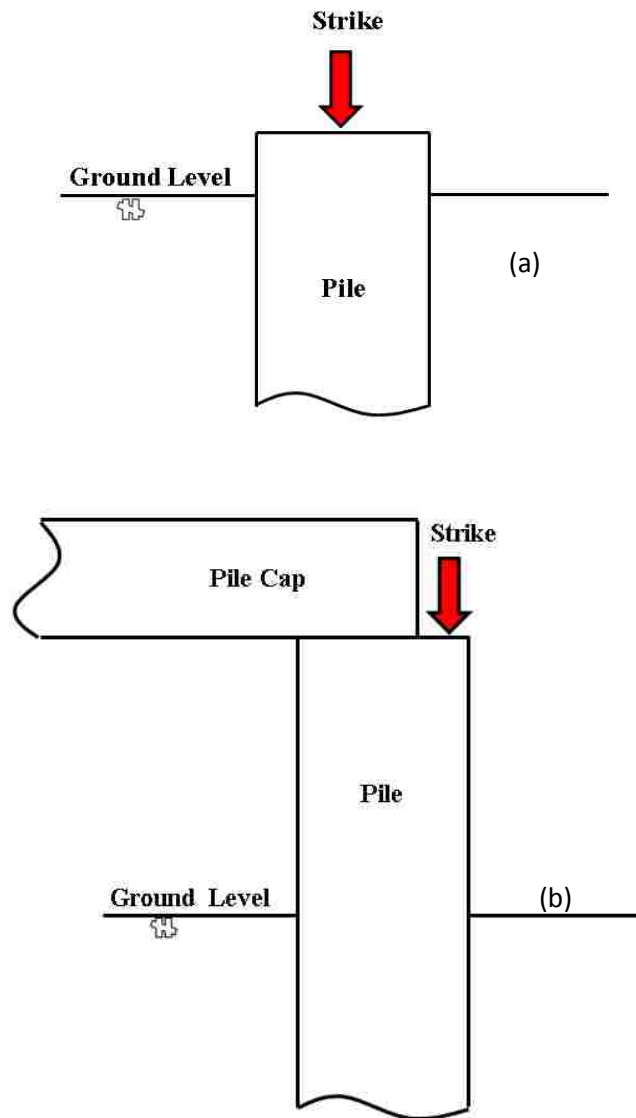


**Figure 13. Vertical Striking on Piles with Accessible Top**

**Setup for Striking on Piles with Inaccessible Top** For piles with inaccessible top, the longitudinal wave can be generated by striking other parts of the foundation as shown in Figures 14 to 19. When the superstructure is not placed exactly atop the pile, longitudinal waves can be produced by striking the top surface of the pile cap as indicated in Figure 14. If the presence of the girders on the top of the pile cap does not allow striking on the pile cap top surface, other options indicated in Figures 15 to 19 can be applied.

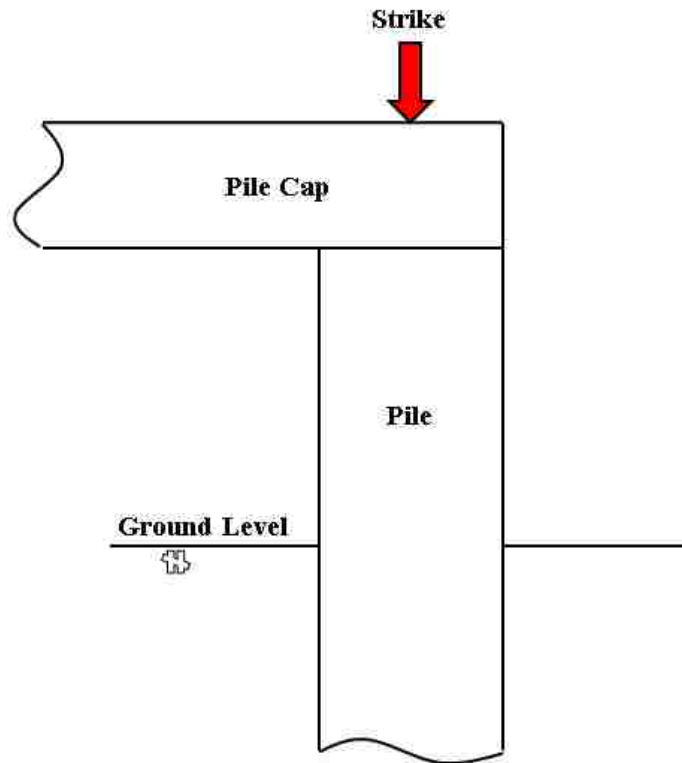


**Figure 14. Vertical Striking on the Top Surface of Pile Cap**

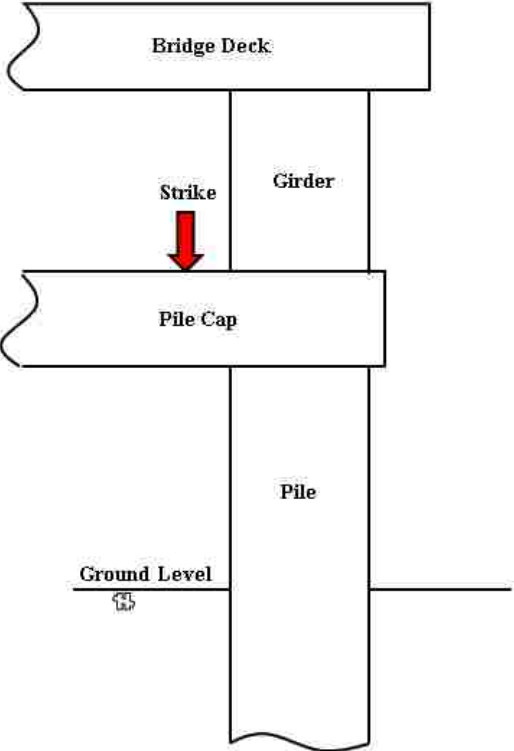


Figure 15. Eccentric Vertical Striking on the Top Surface of Pile Cap

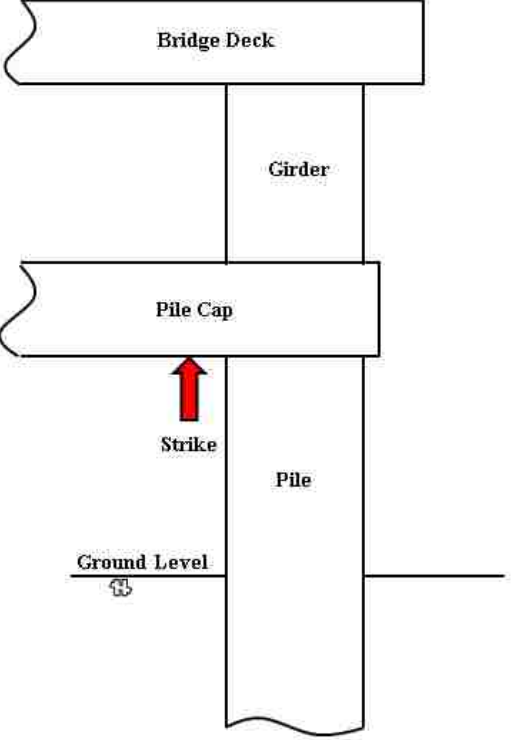
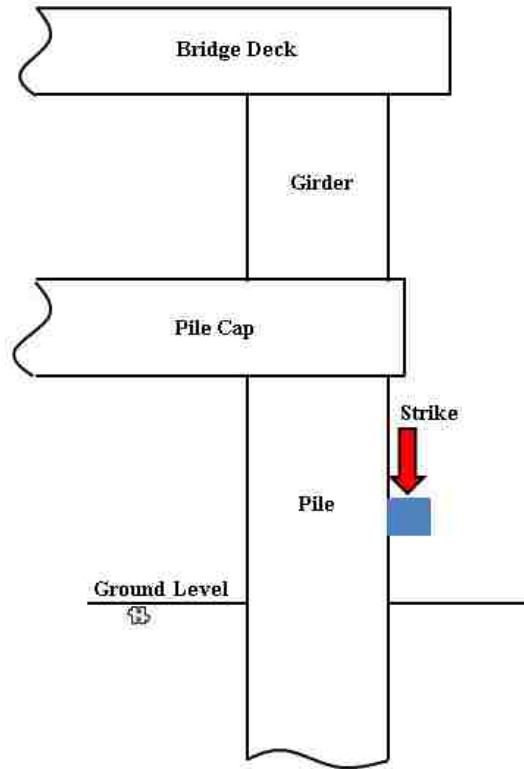
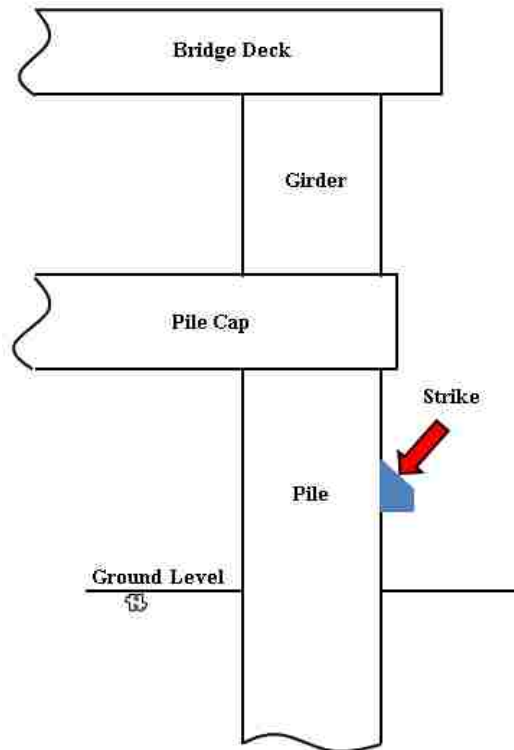


Figure 16. Upward Vertical Striking on the Bottom Surface of Pile Cap



**Figure 17. Vertical Striking on a Block Attached to the Side of a Pile**



**Figure 18. Inclined Striking on a Wedge Block Attached to the Side of a Pile**

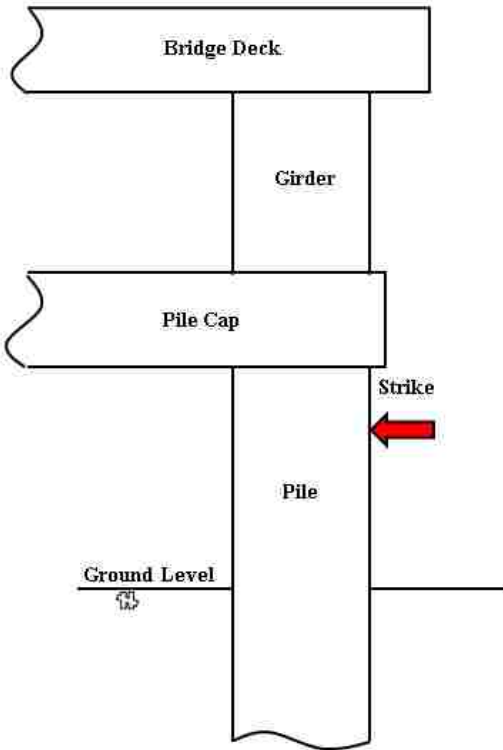


**Figure 19. Horizontal Striking on the Side of a Pile**

### 3.1.1.2 Sensor Setup

**Accelerometer Setup on Piles with Accessible Top** When the top of a pile is accessible, the accelerometer can be placed vertically to capture the longitudinal vibrations as indicated in Figure 20. Vaseline is commonly applied at the interface between the accelerometer and the pile surface for better wave transmission.

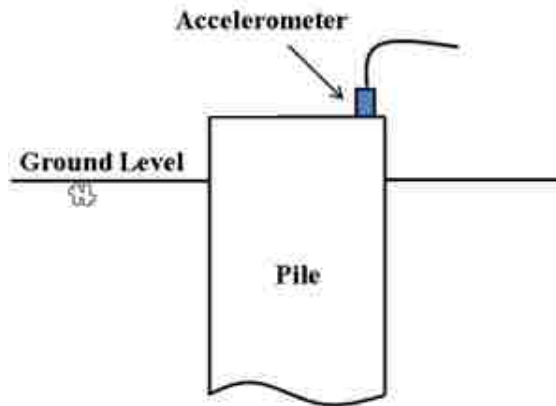


**Figure 20. Accelerometer Setup for Piles with Accessible Top**

**Accelerometer Setup on Piles with Inaccessible Top** When the top of a pile is inaccessible, a block is attached onto the pile's side as indicated in Figure 21. Then, the sensor is placed vertically on the mounted block to capture the vertical vibration of the pile.

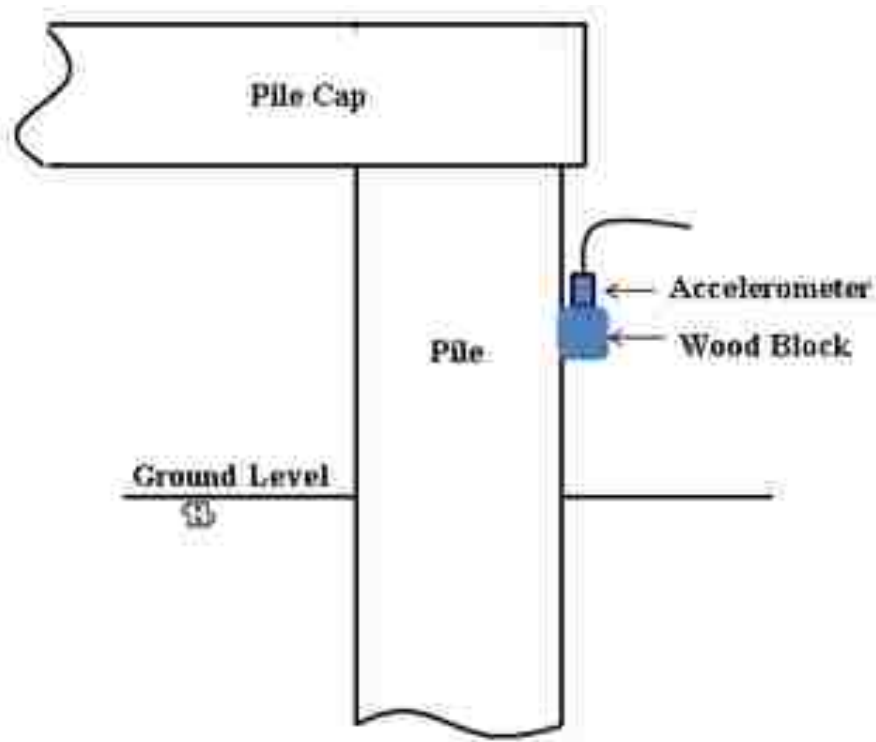


**Figure 21. Accelerometer Setup for Piles with Inaccessible Top**

Small wooden blocks (1.5" × 1.5" × 1.5") shown in Figure 22 can be used to mount the accelerometers. The dimensions of the block are noncritical as long as they are greater than the size of the accelerometer. The blocks are attached to the side surface of the piles using nails (screws) or superglue. The accelerometer is placed vertically on the top surface of the blocks to receive longitudinal vibrations. Appropriate nuts are attached to the top surface of the blocks to ease the attachment of the accelerometer. Since the accelerometer is securely mounted on the wooden block, no Vaseline is needed between the accelerometer and the wooden block.

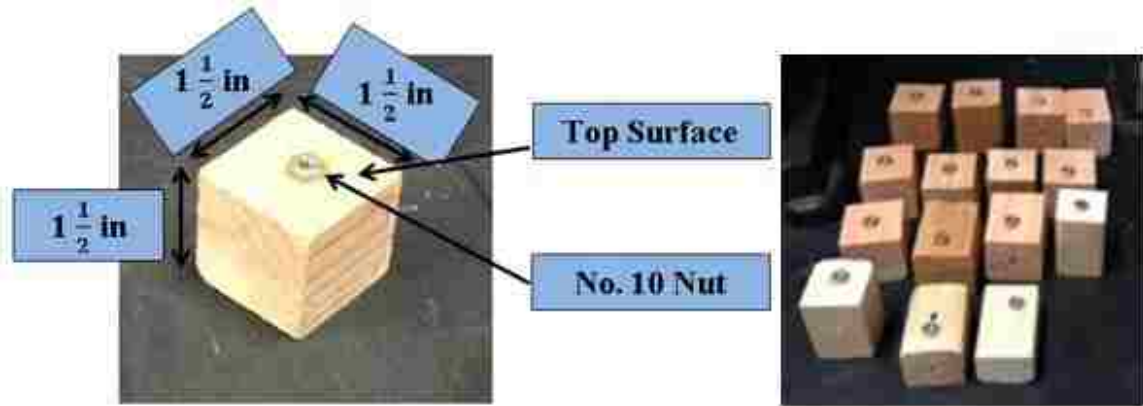


**Figure 22. Wooden Blocks Used for Accelerometers Attachments**

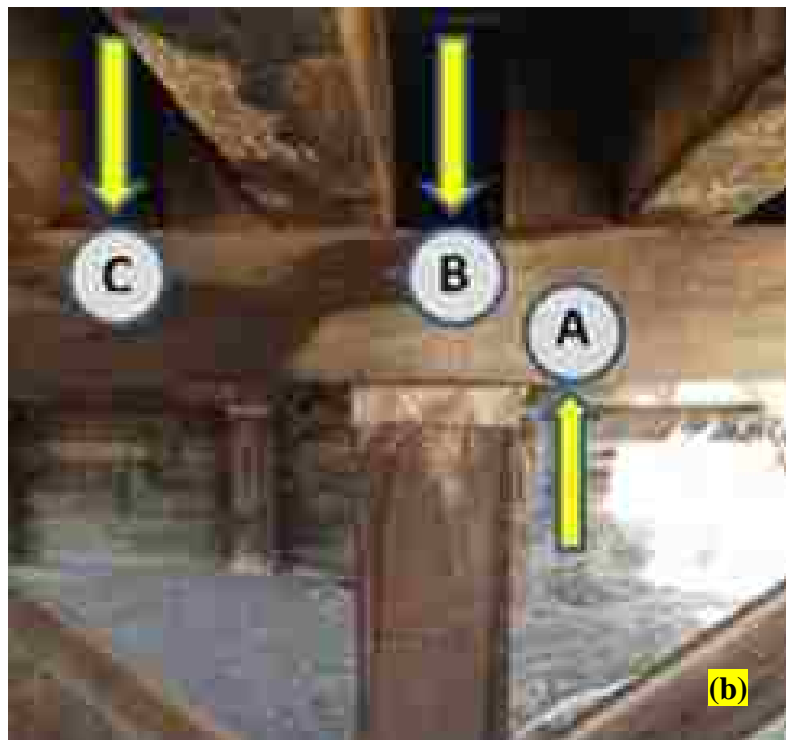
### **3.1.2 SE/IR Test Procedure**

Initial SE tests procedure was developed prior to conducting the preliminary and field tests. An SE/IR test includes the selection of the method of striking, accelerometers locations, equipment assemblage, and data acquisition.

#### **3.1.2.1 Method of Striking**

A successful SE/IR test is strongly affected by the source location. Therefore, proper striking methods should be selected to obtain interpretable results. Based on the SE/IR tests setup introduction presented in the previous section, proper practical source locations are indicated in Figure 23. Such striking methods can be used depending on the accessibility of the pile top. These source locations were extensively utilized in the field. They are prioritized based on the quality of the produced data and the preferred options are discussed later.





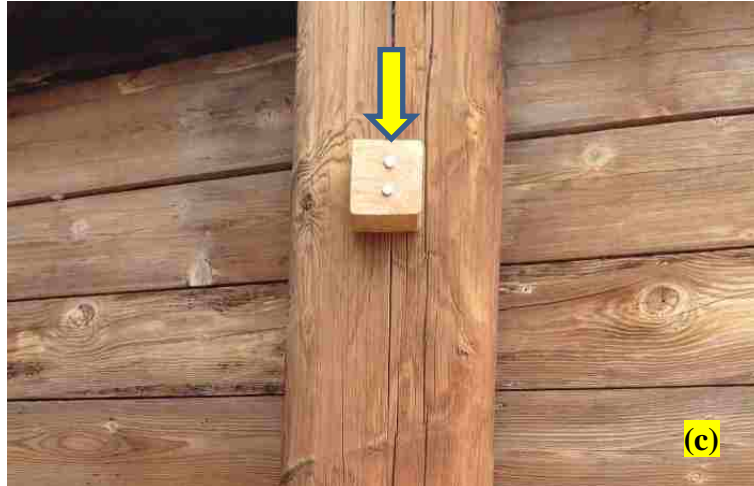


**Figure 23. Proper Practical Source Locations, (a) Striking on top of the test pile (b), Downward striking on Point B (top of the pile cap directly above the test pile), C (top of the pile cap next to the test pile) and upward striking on Point A (bottom of the pile cap next to the test pile), (c) Striking on top surface of a block tightly attached onto the test pile**

The dimensions of the wood and aluminum blocks used for striking in this project are indicated in Figure 24. The actual dimensions of the striking blocks are noncritical as long as they are larger than the size of the hammer head. The cubic aluminum block was machined with an internal curvature to provide better contact with the curved surface of the piles. The internal curve increases the contact surface between the block and the pile's side surface. The blocks must be tightly attached onto the test pile by nails or screws as indicated in Figure 25. This method will be more difficult for concrete surface since concrete screws only have a maximum embedment of 1 ¾ inch. If more embedment depth is required, threaded holes have to be installed into the concrete which will significantly increase the cost and time.

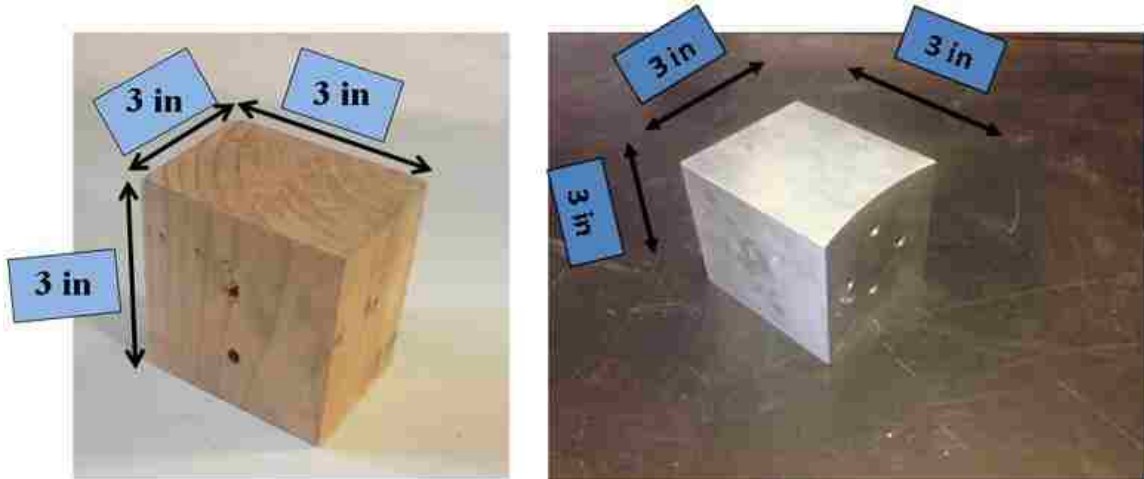


**Figure 24. Dimentions of Wood and Aluminum Striking Blocks**



**Figure 25. Attachment of a Wooden Striking Block onto the Test Pile**

### 3.1.2.2 Location of Receivers

The sensor (accelerometer) can be placed atop the wing piles. If the pile top is inaccessible, the accelerometers will be mounted on wooden blocks attached onto the side of the test pile with nails, screws, or glue. The dimensions of the wooden blocks used in this project can be found in Figure 22. Examples of accelerometer attachment to the pile surface is indicated in Figure 26. If two accelerometers are used, the second accelerometer should be placed far away from the first accelerometer as possible.



**Figure 26. Accelerometers Mounted on a Pile by Wooden Blocks.**

### 3.1.2.3 Hardware Assembly

The equipment utilized for conducting SE/IR tests should be assembled as indicated in Figure 27. Four different hammer tips are available as shown in Figure 28.



1. Olson Freedom Data PC
2. Input Module
3. Impulse Hammer
4. Accelerometer
5. BNC Cable
6. BNC to 4 Pin Adapter Cable
7. Female-Female BNC Adapter
8. Microdot to BNC Cable

**Figure 27. SE/IR Test Equipment**



**Figure 28. A Hammer and Four Different Tips**

### 3.1.2.4 SE/IR Data Acquisition

The WinTFS software was used to acquire the data in this project. Figure 29 shows an example of the acquired data including raw data (top graph) and velocity graph (middle graph).

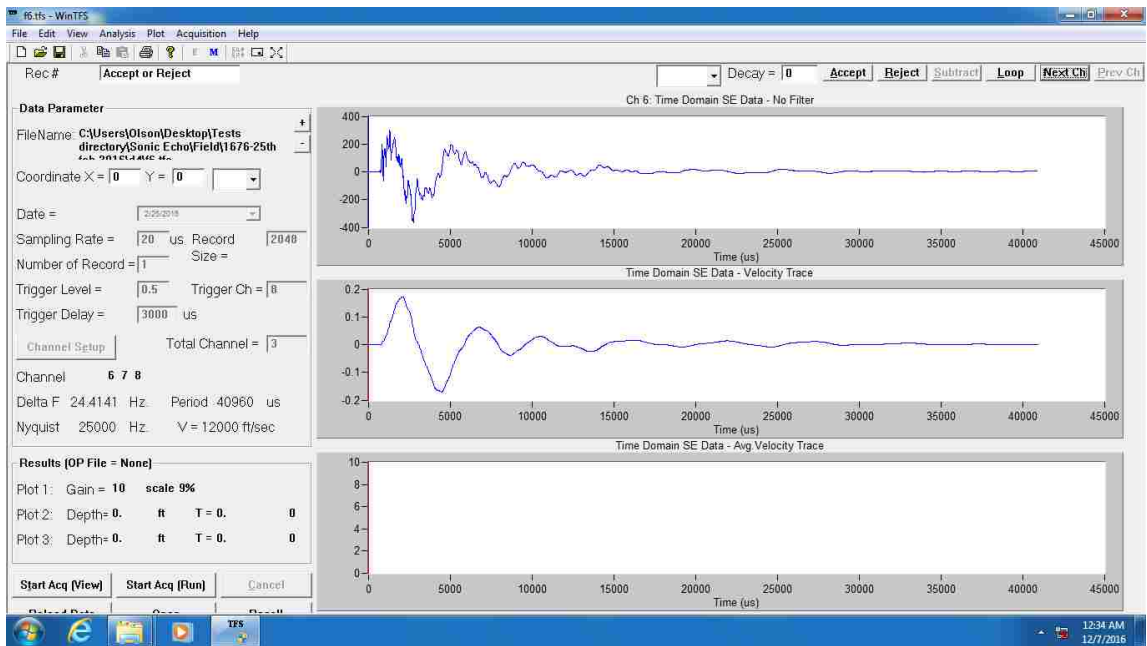


**Figure 29. An Example of Acquired SE Data Including Raw Data (Top Graph) and Velocity Trace (Middle Graph)**

The flowchart shown in Figure 30 was designed to acquire consistent SE/IR data. Based on the flowchart, each SE/IR test should be repeated adequately to achieve the desired level of reliability.

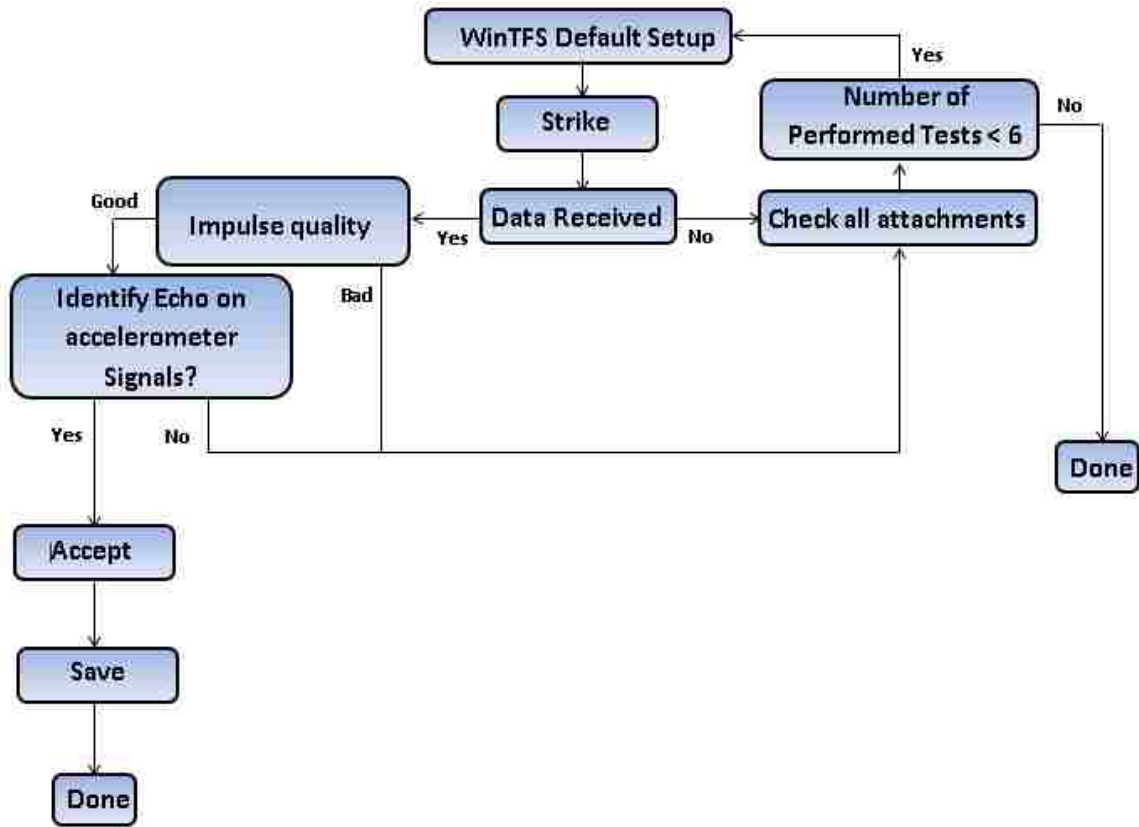


**Figure 30. Flowchart for Conducting SE/IR Tests**

### 3.1.2.5 SE/IR Data Processing and Length Determination

For each SE/IR test, the obtained velocity graph indicated in Figure 29 was used to determine the time difference between the impulse (source) and the echo from pile toe ( $\Delta t$ ).  $\Delta t$  is used therein to represent the time difference and used to determine the pile length associated with SE analysis through Eq. 1. The software was also able to process the data and perform an IR analysis. An example of the result of an IR analysis is indicated in Figure 31. If the resonant frequencies were distinguishable in the mobility plot (bottom graph), the difference in frequency between the resonant frequencies ( $\Delta f$ ) could be used to determine the embedment depth of a pile. Similar to  $\Delta t$ ,  $\Delta f$  was used to denote the difference

in frequency between the resonant frequencies in this report.  $\Delta f$  was used to determine the pile length associated with IR analysis through Eq. 4.

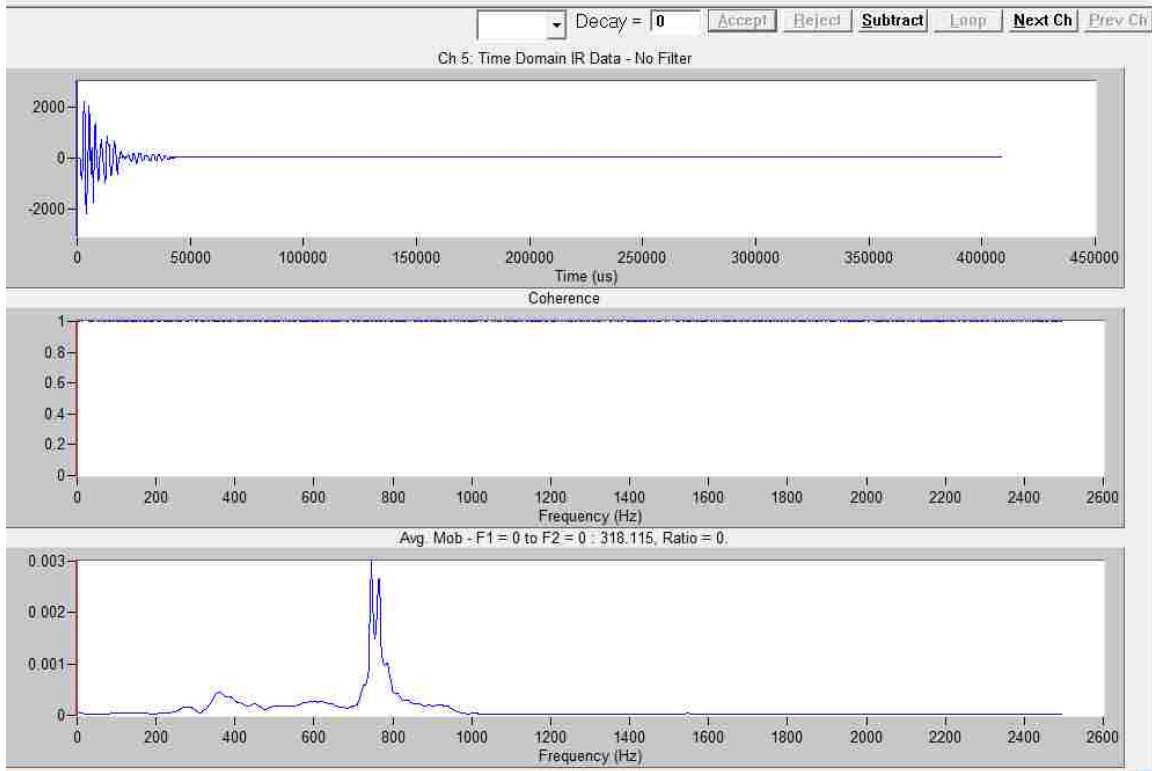


**Figure 31. Produced Graphs from IR Analysis, Tme domain IR data (top), Coherence (middle) and Average Mobility (bottom)**

In both analyses of time and frequency domains, the length measurements were based on the propagated wave velocity in the foundation material. In the current research, the utilized wave velocities were chosen based on the material quality observed in the field as well as in the literature. For example, the literature indicates the wave velocity in wood ranging from 9,900 to 15,000 ft/s that depends on the type of wood, the number of knots, and rottenness (39, 40). There is no means to determine the wave velocity in the pile below ground although the wave velocity may be determined for the exposed pile. Therefore, a variation of 20% in calculated lengths is usually expected. The wave velocity in the foundation should be obtained as accurately as possible to produce more accurate results. The compressional wave velocity could be measured between two mounted receivers to

improve the accuracy of the estimated length. Using two receivers can also distinguish the up-going and down-going waves.

The most important outcome of an SE test is the velocity graph. A *good* SE test should show a clear impulse and echo in the velocity graph. A *consistent* SE test should have three similar good SE tests. The measured length is considered as "*in accordance*" with the actual length when the measured length is within 90% to 110% of the actual length.

### **3.1.3 Preliminary SE Tests**

The preliminary tests were conducted on wood and concrete elements to examine the applicability of the equipment on such materials. The elements were similar to individual piles and pier walls in real bridges. Therefore, conducting SE tests on such elements not only revealed the equipment performance but also provided guidelines to conduct tests on bridge foundation more efficiently.

#### **3.1.3.1 SE Tests on A Wood Column**

SE tests were conducted on a decorative wooden column on UNM campus. The SE test setup is shown in Figure 32. The tests were carried out only with a hard-tip hammer. The source was applied in three different ways. The impulse was produced by striking horizontally at point C, vertically on the concrete pavement next to the column, and upward on the capital. Although the hammer was not struck on the column directly, vertical striking on pavement produced a reflected longitudinal wave that traveled upward along the column and reflected from the top of column. Two accelerometers were mounted at points A and B. The accelerometers were attached on the top surface of wooden blocks glued onto the side surface of the column as shown in Figure 32.



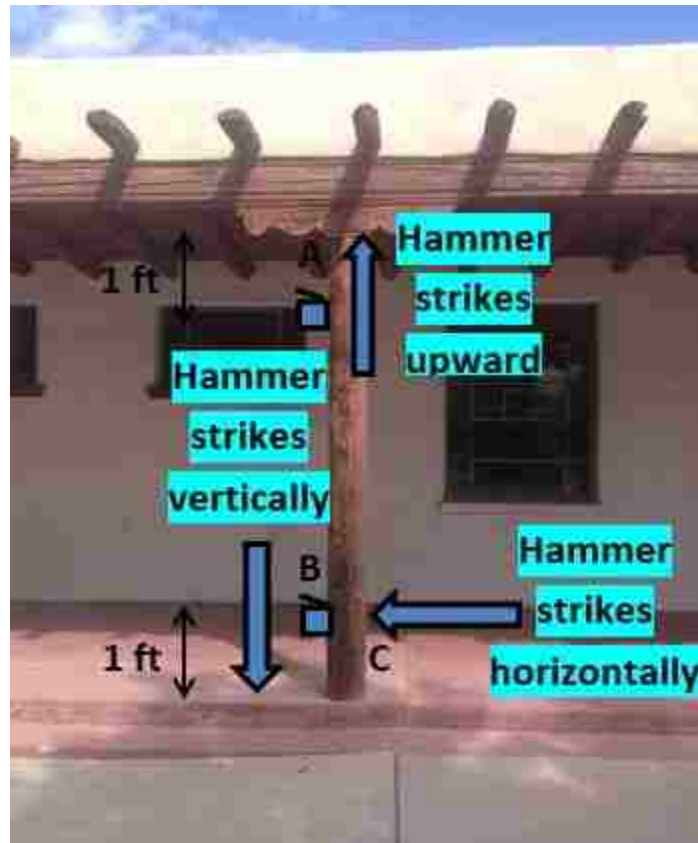


**Figure 32. Source and Receiver Locations on Investigated Wooden Column**

As mentioned before, upon striking, three graphs including raw acceleration data, velocity graph (integrated from acceleration), and impulse signal will appear on the computer screen. The velocity graph is used to determine the length of the column.

The results showed that horizontal striking did not produce good velocity graphs that could be used to determine the length of the column. An example of velocity graphs obtained from horizontal striking is indicated in Figure 33. Identifying the echo corresponding to the reflection from column top is difficult. Also, the signals should decay with time which is not the case here. On the other hand, the velocity graph obtained from vertical striking on pavement and upward striking on the capital were similar. The echo from the reflection of the end of the column can be identified. An example of good velocity graph is shown in Figure 34; the graph is produced by upward striking on the capital with the accelerometer at point A. The echo corresponding to the reflection from the bottom of the column (a part of the column is embedded in ground) is indicated on the graph. The

amplitude of the signal decayed as expected.  $\Delta t$  can be estimated clearly as shown in the figure.

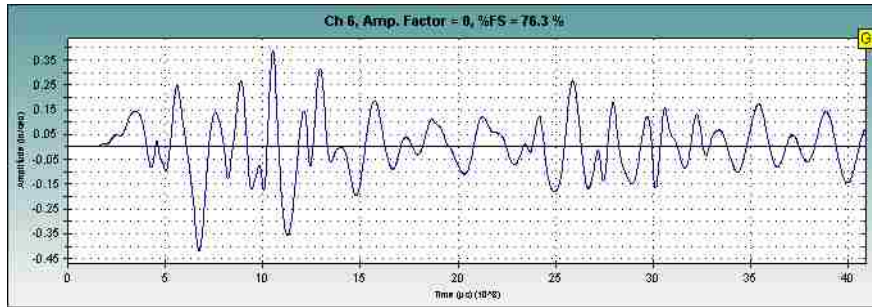


**Figure 33. A Velocity Graph Obtained from Horizontal Striking on Investigated Wood Column**

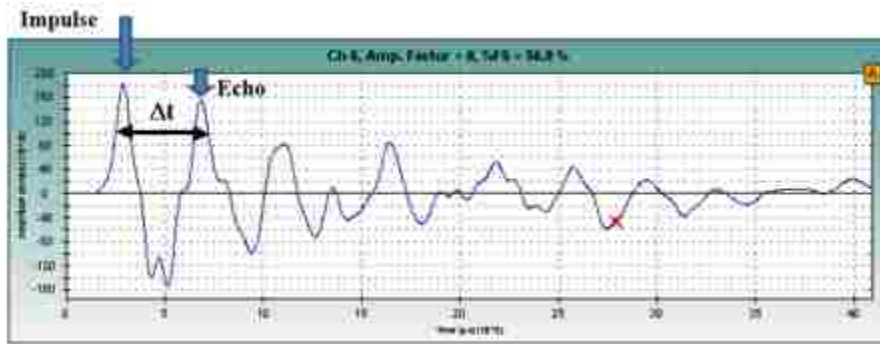


**Figure 34. A Velocity Graph Obtained from Vertical Upward Striking on Investigated Wood Column**

As an example, using  $\Delta t = 3920 \mu\text{s}$  in Figure 34 and the sensor location is 1 ft from the top, the column length is:

$$L_t = \frac{v \times \Delta t}{2} + 1 = \frac{10000 \times 3920 \times 10^{-6}}{2} + 1 = 20.6 \text{ ft}$$

Wave velocity in wood  $v = 10,000 \text{ ft/s}$  (based on column's material quality)

### 3.1.3.2 SE tests on A Concrete Column

Twelve SE tests were conducted on one of the concrete columns of the Centennial Engineering Building on UNM campus to study the behavior of SE tests on concrete material while an accelerometer was attached onto the side surface of the column. A

wooden block was attached on the column surface with superglue. The accelerometer was placed vertically on the top surface of the block. In this column, it was decided to explore if horizontal striking on the capital and column itself can produce useful velocity graphs that yields the determination of the length of concrete column. The concrete column and the test setup are shown in Figure 35. The direction and the location of the strikes are indicated in Table 5.

It was found that horizontal striking cannot produce good results. An example of poor velocity graphs is indicated in Figure 36. Again, the signals did not decay with time. On the other hand, the echoes were clear for the SE tests by vertical striking on the top above the column.  $\Delta t$  from the velocity graphs were measured and the length of the column was determined.

$$L_t = \frac{v \times \Delta t}{2} + \text{distance between accelerometer and the bottom of the capital.}$$

The wave velocity is assumed to be 10,000 ft/s. The wave velocity of concrete is very similar to the wave velocity of wood.

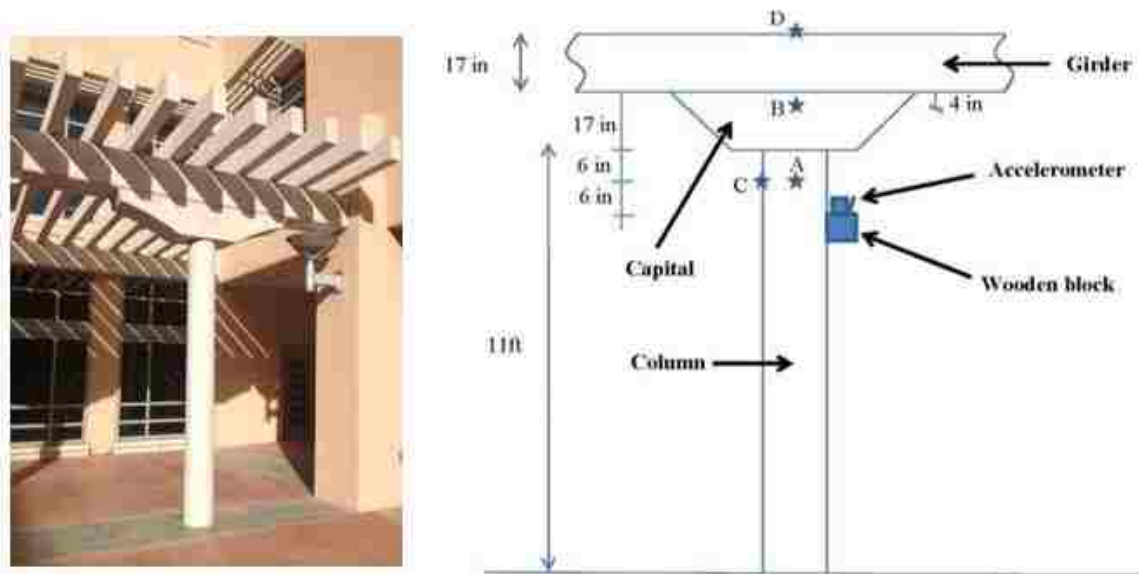


**Figure 35. Picture and Details of Centennial Engineering Concrete Column**

**Table 5. Direction and Location of Strikes on a Concrete Column at the Centennial Engineering Center.**

Test No.	Hammer Tip	Direction and Location of Strike
1	Hard	A (horizontally)
2	Hard	A (horizontally)
3	Hard	B (horizontally)
4	Hard	B (horizontally)
5	Hard	C (horizontally)
6	Hard	C (horizontally)
7	Hard	D (vertically)
8	Hard	D (vertically)
9	Medium-hard	D (vertically)
10	Medium-hard	D (vertically)
11	Medium-soft	D (vertically)
12	Medium-soft	D (vertically)

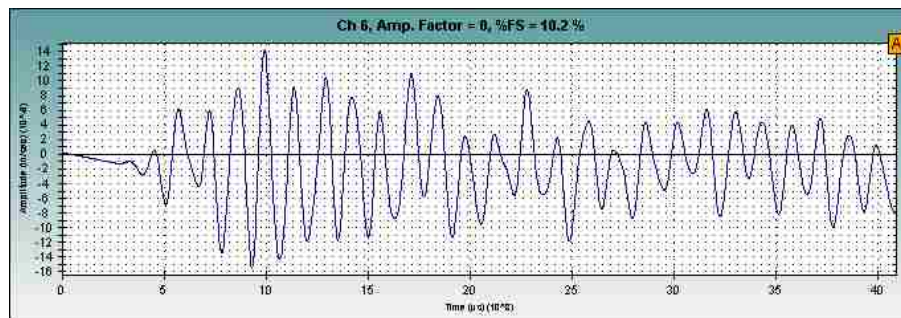


**Figure 36. An Example of Poor Velocity Signal Produced by Horizontal Striking**

The calculated lengths are summarized in Table 6.  $L_t$  is the total height of the column which is the sum of the exposed and buried part. The average calculated length (15.8 ft) is in accordance with the approximated total height of the column.

**Table 6. Calculated Lengths of Centennial Engineering Concrete Column.**

Test No.	$\Delta t$ ( $\mu s$ )	$L_t$ (ft)
1 ~ 6	--	--
7	2900	15.5
8	2900	15.5
9	3012	16.1
10	3020	16.1
11	3120	16.6
12	2820	15.1

### **3.1.3.3 SE Tests on A 3-story Concrete Column**

Twelve SE tests were conducted on a reinforced concrete column on UNM campus shown in Figure 37. The column is one of the 3-story columns of the Centennial Engineering Library on UNM campus. The total length of the column is 43 ft. Only the top 7.5 ft of the column is visible as shown in the photo.



**Figure 37. The Reinforced Concrete Column of Centennial Library on UNM Campus**

SE tests were carried out with different hammer tips. Since the top of the column was accessible, the accelerometer was placed on the top surface of the column and vertical strike at top and horizontal strikes were applied as shown in Figure 38. The characteristics of all SE tests are listed in Table 7.

**Table 7. Characteristics of SE Tests on the Concrete Column of Centennial Library on UNM Campus.**

Test No	Hammer tip	Strike Direction
1	Hard	Vertically at A
2	Hard	Vertically at A
3	Medium-hard	Vertically at A
4	Medium-hard	Vertically at A
5	Medium-soft	Vertically at A
6	Medium-soft	Vertically at A
7	Hard	Horizontally at B
8	Hard	Horizontally at B
9	Medium-hard	Horizontally at B
10	Medium-hard	Horizontally at B
11	Medium-soft	Horizontally at B
12	Med-soft	Horizontally at B

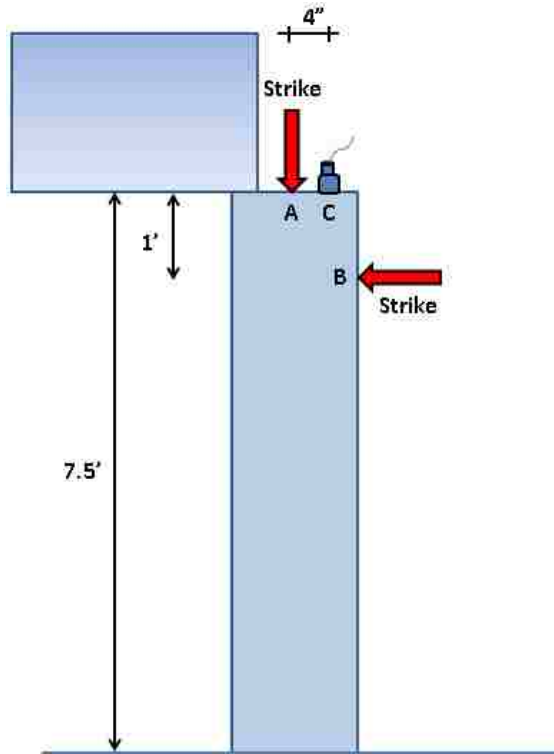


**Figure 38. Source and Receiver Locations on the Concrete Column of Centennial Library on UNM Campus**

**Results of Vertical Striking with Hard Tip** The velocity graphs obtained from the accelerometer in Tests 1 and 2 are depicted in Figure 39. Although high frequency noise at the beginning was clearly observed in Figure 39b, the impulse and echoes were identifiable as shown as arrows in the figure. When the accelerometer was placed at least 1 ft away from the source, the high frequencies at the beginning disappeared. Therefore, accelerometers are recommended to be placed at least 1 ft from the source.

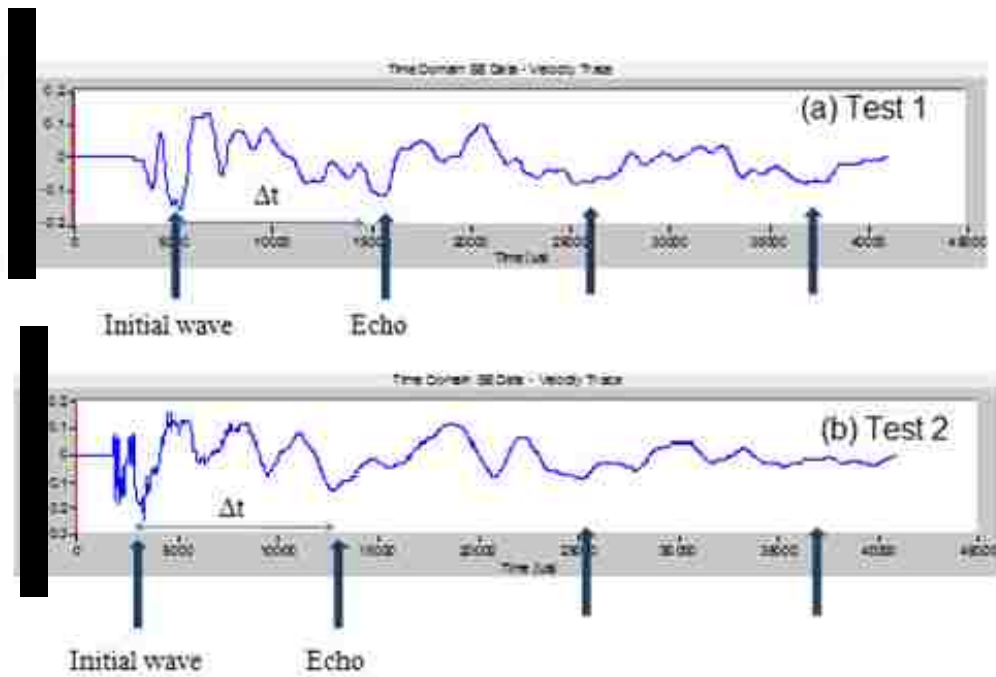


**Figure 39. Velocity Graphs for Tests 1 and 2 on the Concrete Column of Centennial Library on UNM Campus**

The time differences between the initial wave and the first echo were similar for these two tests. The first and second arrows from the left are the impulse and the echo from the bottom respectively. It should be noted that the wave reflection from any change of impedance in the direction of the traveling wave along the column may be shown in the velocity graph. Valleys between marked arrows may also be due to the wave reflections at the junctions of each floor.  $\Delta t = 10$  ms and the wave velocity is 10,000 ft/s, the length of the column is determined as:

$$L = \frac{v \times \Delta t}{2} = \frac{10000 \times 10 \times 10^{-3}}{2} = 50 \text{ ft}$$

The calculated length is close to the expected length of the column.

**Results of Vertical Striking with Medium-hard Tip** SE tests were repeated using a medium-hard tip. The velocity graphs for Tests 3 and 4 are shown in Figure 40. There are no high frequencies at the beginning of the velocity graphs. The time differences between the impulse and echo are similar to tests conducted by the hard tip (see Figure 39).  $\Delta t$  is still 10 ms and the calculated length is 50 ft.



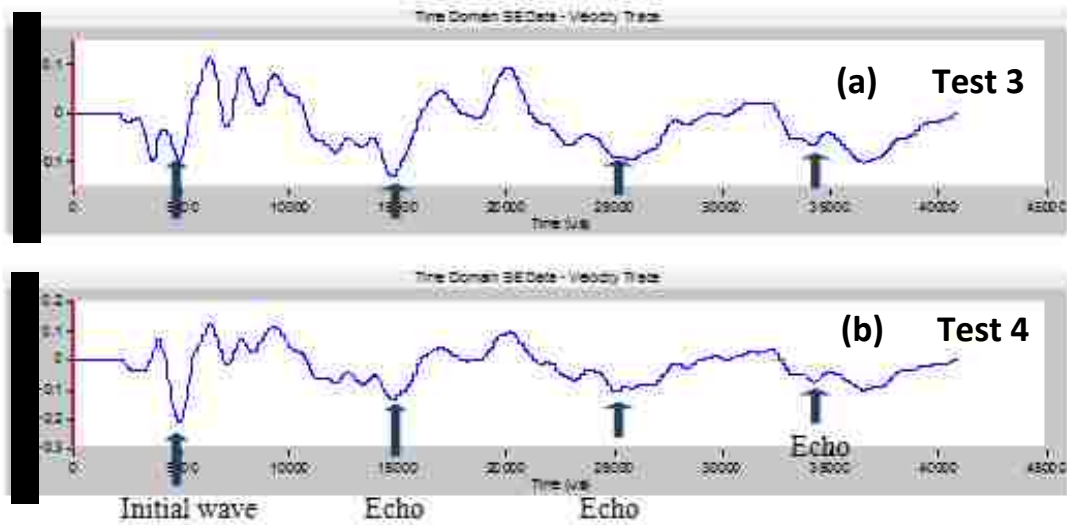


**Figure 40. Velocity Graphs for Tests 3 and 4 on the Concrete Column of Centennial Library on UNM Campus**

**Results of Vertical Striking with Medium-soft Tip** Medium-soft tip was used and the obtained velocity graphs are shown in Figure 41. Again, the results are similar to the velocity graphs using medium-hard tip (see Figure 40). In addition, no high frequency content can be found as seen in the velocity graph of hard tip (Figure 39b).  $\Delta t$  is still 10 ms and the calculated length is 50 ft.

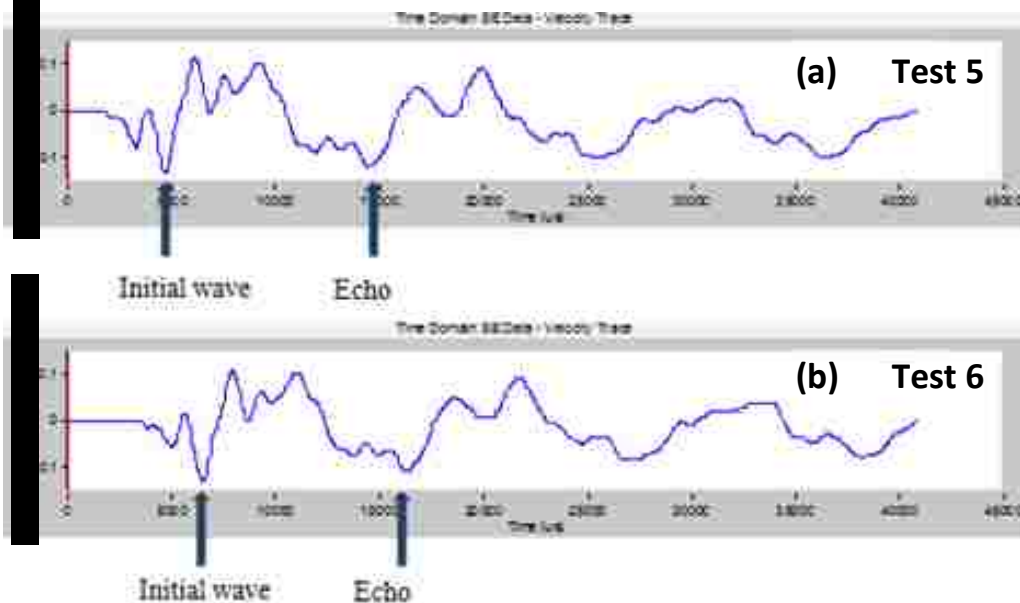


**Figure 41. Velocity Graphs for Tests 5 and 6 on the Concrete Column of Centennial Library on UNM Campus**

**Results of Horizontal striking** The hammer striking was applied horizontally with various hammer tips as listed in Table 6 (Tests 7 to 12). None of the results were good. A typical result is shown in Figure 42 for hard tip. There are many echoes in the graph but it is difficult to identify the echo from the column end.  $\Delta t$  between echoes are too short to represent the length of the column. The reflections are due to other sources.

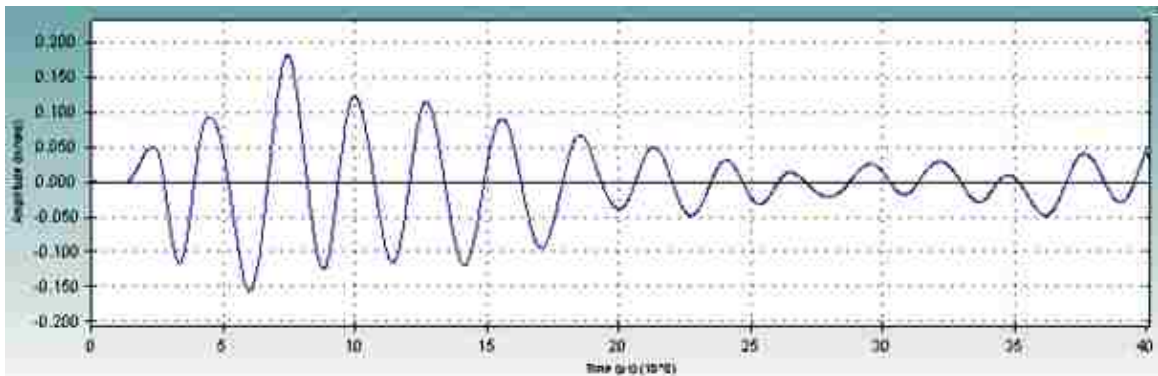


**Figure 42. Velocity Graph for Horizontal Hammer Striking with Hard Hammer Tip on the Concrete Column of Centennial Library on UNM Campus**

#### 3.1.3.4 SE Tests on a Reinforced Concrete Wall

Since there are similarities in relative dimensions between a pier wall foundation and the reinforced concrete strong-wall at the Structural Lab of the Department of Civil Engineering at UNM (Figure 43), SE tests were conducted in the lab to study the applicability of the method on non-slender foundations. SE tests were carried out using vertical and horizontal striking with hard, medium-hard, medium-soft and soft hammer tips. Figure 44 shows the source (A~D) and the accelerometer locations (E, F and G). The accelerometer was mounted vertically on Points E, F or G. Wooden blocks were utilized to mount the accelerometers at Points F and G. Figure 49 shows the setup of one SE test.



Figure 43. The Reinforced Concrete Wall in the Structural Lab

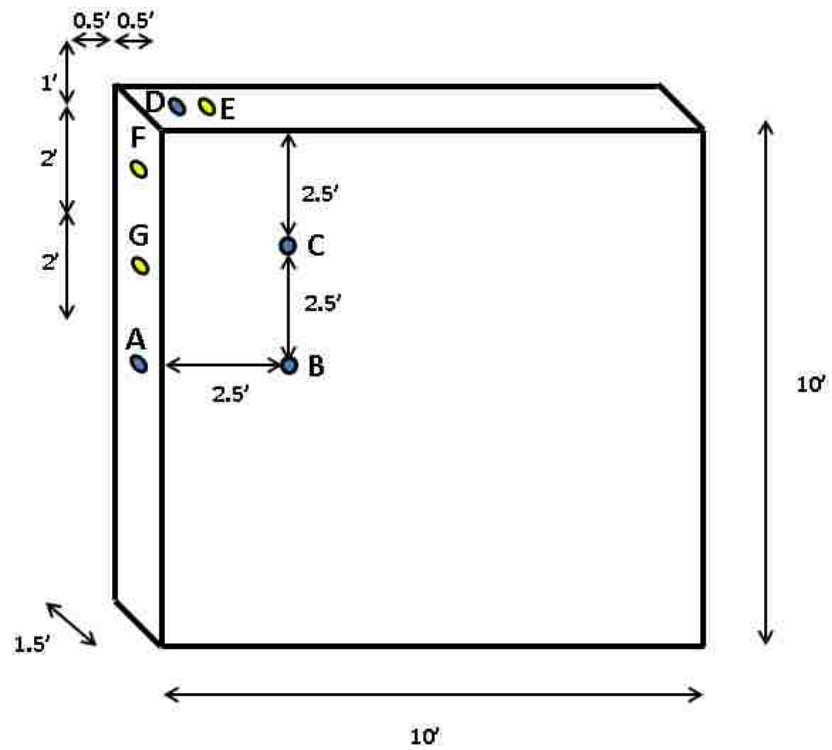


Figure 44. Locations of Striking Points (A to D) and Accelerometers (E, F and G) on the Reinforced Concrete Wall



**Figure 45. An SE Setup on the Reinforced Concrete Wall**

When the sources were applied by striking vertically on Point D and mounting the accelerometer at either points E, F and G, good signals were obtained with all hammer tips. We are able to determine the height of the wall. Figure 46 shows a velocity graph obtained at Point E when Point D was stroke at with a hard-tip hammer. The  $\Delta t$  was determined from the time difference between impulse and echo.  $\Delta t = 2400 \mu\text{s}$ . The wave velocity of the concrete was assumed to be 10,500 ft/s. Since the sensor was mounted at the top, the wall's height with the concrete floor ( $L_t$ ) was determined as follows:

$$L_t = \frac{v \times t}{2} = \frac{10500 \times 2400 \times 10^{-6}}{2} = 12.6 \text{ ft}$$

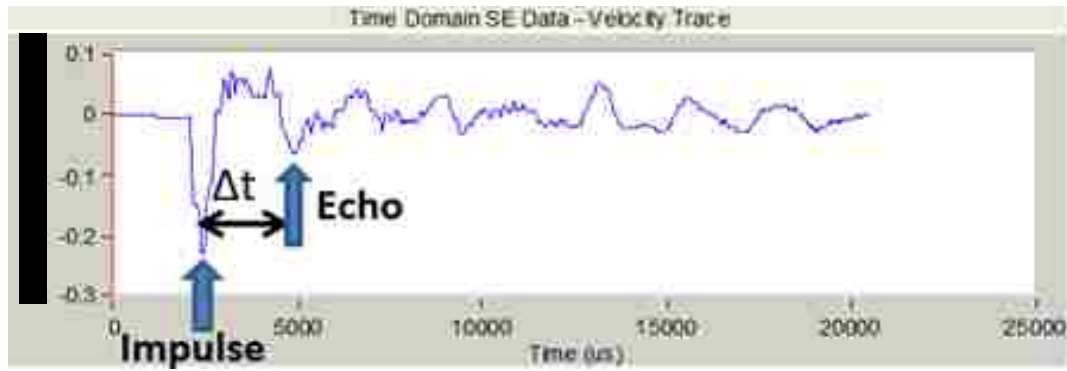


**Figure 46. Velocity Trace of the Accelerometer at Point D with Hard Tip**

On the other hand, when the source was applied by striking horizontally at Points A, B and C, the echoes from the bottom could not be determined since multiple echoes were shown near the expected echo from the bottom. This may be due to the lateral vibration of the wall. An example of poor velocity graphs is shown in Figure 47 obtained from horizontal striking at Point B.

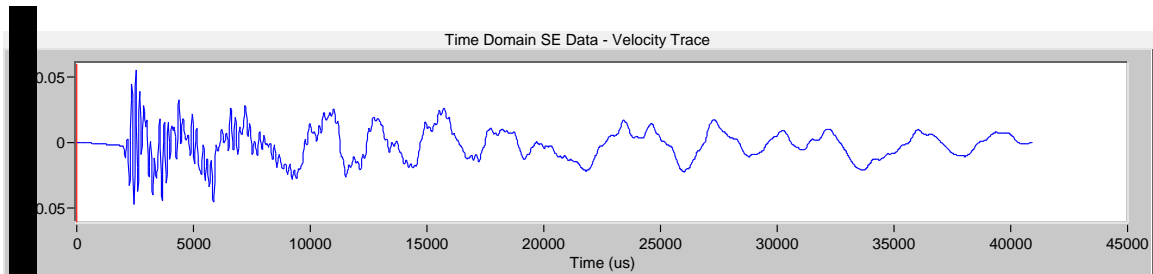


**Figure 47. A Poor Velocity Graph Produced by Horizontal Striking**

### 3.1.3.5 Conclusions of Preliminary SE Tests

SE tests were performed on a concrete wall and three columns composed of wood and concrete. The effect of striking direction, accelerometer location, and hammer tip type were investigated. When the top of the wall (or columns) was accessible, striking on the top surface produced the most interpretable results (highest success rate in the determination of the length). While the top of the column was inaccessible, striking on the pavement next to the column could introduce proper longitudinal waves through the column (medium success rate due to the reduction of energy). Horizontal striking produced lateral vibrations in lieu of longitudinal waves which complicated the velocity graphs. No

success in SE tests performed by horizontal striking has been obtained in the preliminary SE tests.

In addition to selecting the best striking method, the sensors should be properly placed to capture the longitudinal vibration. The preliminary SE tests result indicates that vertical placement of a sensor on the side of the wall or columns produces good results. However, when the sensor was placed too close to the striking point (less than 1 ft), the noise of initial high frequency vibrations may contaminate the velocity graph. Thus, it is recommended that the sensors be placed 1-2 ft away from the striking point to prevent the disturbing effect of the high frequency vibrations. It should be noted that using softer hammer tips decreases the high frequency content of the velocity signal which may ease the interpretation in some cases.

Based on the preliminary tests' observations, the following instructions are suggested for implementation in the field:

- 1) A combination of a vertical strike and vertically placed sensors is a proper way to conduct SE/IR tests.
- 2) Since the outcome of SE/IR tests depends on the energy (strength) of the longitudinal wave, vertical striking on the top of the foundation is the best method to use.
- 3) When the top of the foundation is inaccessible, the accelerometers should be placed vertically on the side of the foundation no closer than 1-2 feet from the striking point.
- 4) If high frequencies conceal either impulse or echo in the velocity graphs, using softer hammer tips may remove the disturbing high frequencies and consequently eases the interpretation.
- 5) Although the wave propagation inside a reinforced concrete wall was different from slender elements (columns or piles), applying a vertical strike at the top of the wall yielded successful tests. Placing the accelerometers vertically on the top or on wooden blocks attached to the side of the wall produced good results.

### 3.1.4 Field SE/IR Tests

#### 3.1.4.1 Santo-Domingo Bridge

The Santo Domingo Railroad Bridge was selected by NMDOT for initial SE field tests. The tests were carried out with the existing SE equipment owned by NMDOT. The bridge is located 42 miles northeast of Albuquerque. The latitude and longitude coordinates of the location for this railroad bridge are: 35.488752, -106.385058. The bridge is supported by round timber piles. Figures 48 and 49 show the location and street view of the bridge, respectively.



**Figure 48. Location of the Santo Domingo Bridge**



**Figure 49. Street View of the Santo Domingo Bridge**

Sixteen SE tests were conducted on two timber piles at Bents 7 and 8. Figure 50 depicts the foundation plan and test piles.

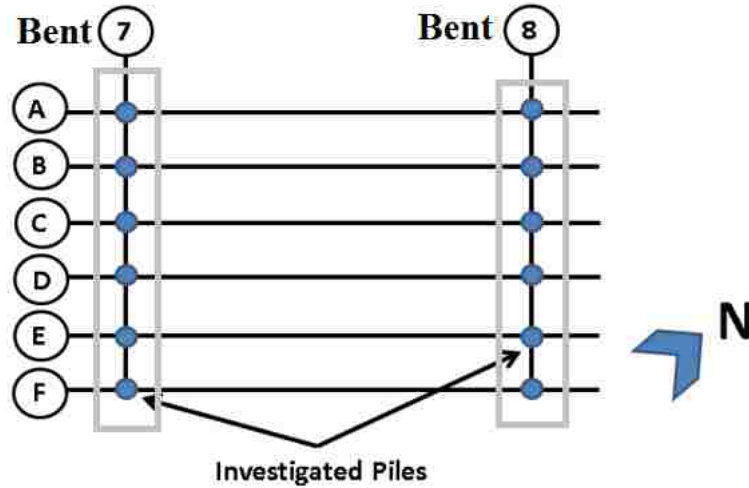


**Figure 50. Foundation Plan and Investigated Piles of Santo Domingo Bridge**

Six SE tests were performed on Pile 7-F and seven on Pile 8-E. The test setup is shown in Figure 51. Although horizontal striking did not result in interpretable velocity signals in preliminary tests, it was decided to examine if horizontal striking on the side of a pile could produce useful result in the field. Vertical striking on a metal block was used on Pile 8-E as the source. The metal block used for vertical striking was attached to the pile surface tightly. The accelerometer was attached vertically on a metal block attached to the pile. The specifications of SE tests are indicated in Table 8.



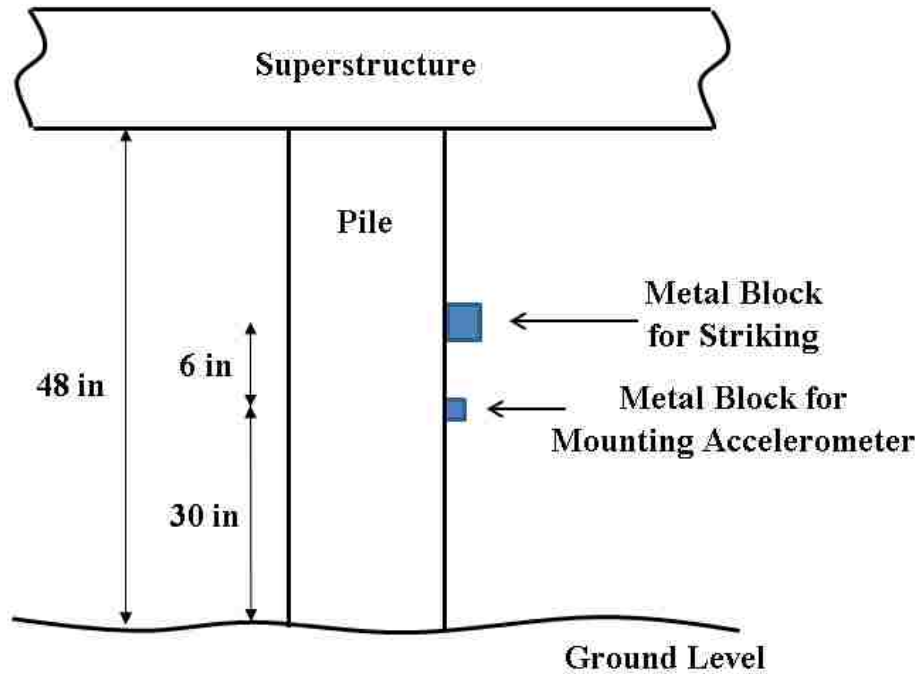


**Figure 51. SE Tests Setup for the Santo Domingo Bridge Piles (Not to Scale)**

**Table 8. Specifications of SE Tests Performed on the Santo Domingo Bridge Piles.**

Pile	Test No.	Hammer Tip	Direction of Strike
7-F	1 - 4	Hard	Horizontal
7-F	5 - 6	Medium-hard	Horizontal
8-E	7 - 8	Medium-hard	Vertical
8-E	9 - 10	Medium-Soft	Vertical
8-E	11 - 13	Hard	Vertical

Tests 1 to 6 were performed on Pile 7-F with horizontal striking. The results were not useful and the length of the pile could not be determined. A typical velocity graph (Test 1) is shown in Figure 52. The arrows in the figure indicate the high frequency vibrations. These high frequencies may be due to the reflections of impedance change in the pile or may relate to the lateral vibration of the pile. Reflections from the pile toe were not found.

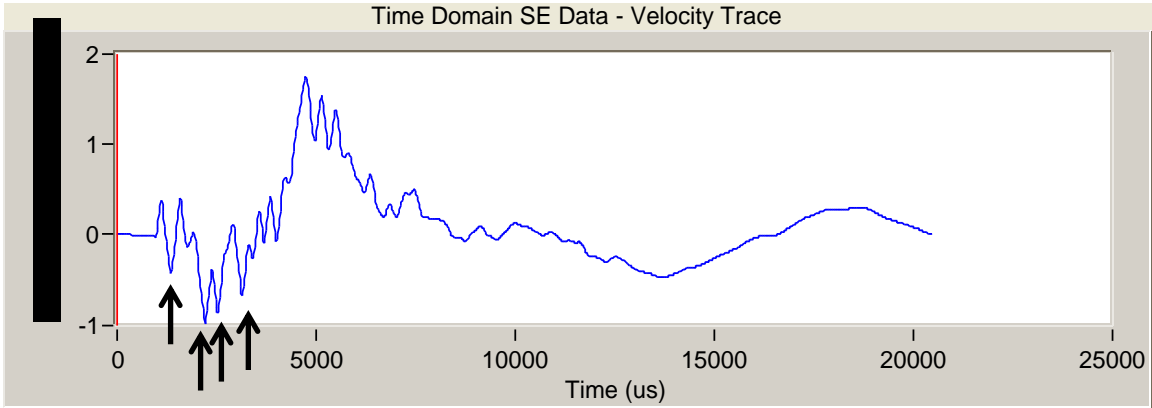


**Figure 52. Velocity Graph from the Accelerometer (Pile 7-F)**

For Pile 8-E, the accelerometer was mounted vertically on a block attached to the pile and the source was applied by vertical striking with medium-hard and medium-soft tips (Tests 7 to 10) and hard tip (Tests 11-13). The velocity graphs of medium-hard and medium-soft tips are shown in Figures 53 to 56. Poor results were obtained since the impulse was difficult to identify in the velocity graph (too many valleys at the beginning of the velocity graph). Also, we cannot pick one of valleys because the velocity magnitude of the impulse should be greater than the magnitude of the echoes. It was identified in the field that the attachment of the accelerometer was loose. The attachment was then corrected and the tests were repeated with hard tip (Tests 11 to 13). The velocity graphs of these three tests are shown in Figures 57 to 59. The impulses and echoes (shown as arrows) are clearly visible in the velocity graphs.

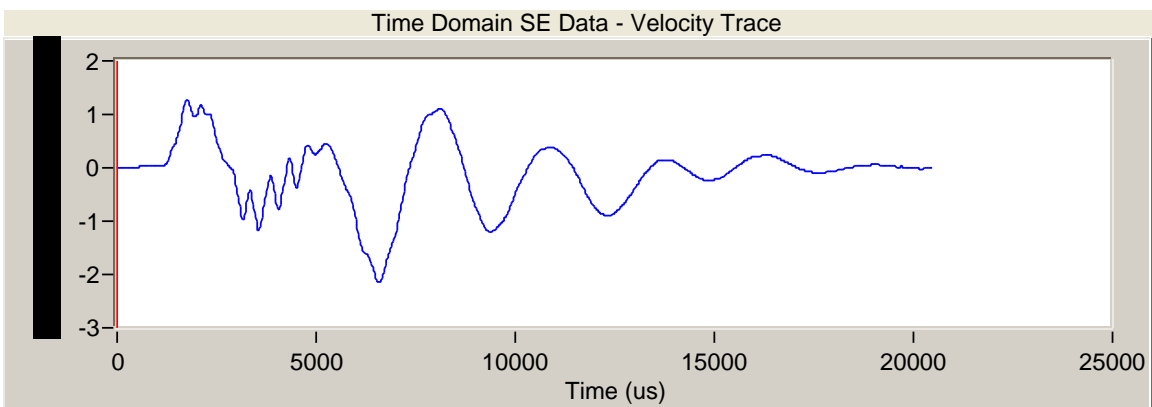


**Figure 53. Velocity Graph of Test 7**

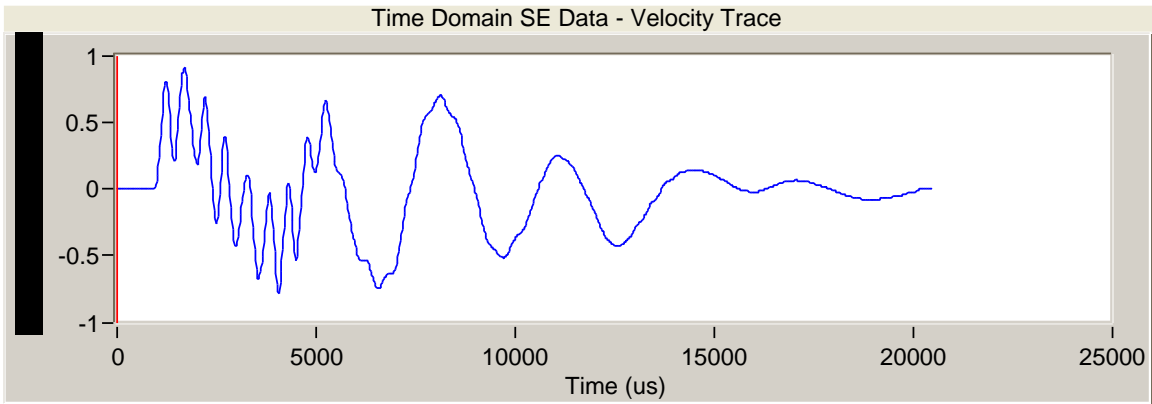


**Figure 54. Velocity Graph of Test 8**

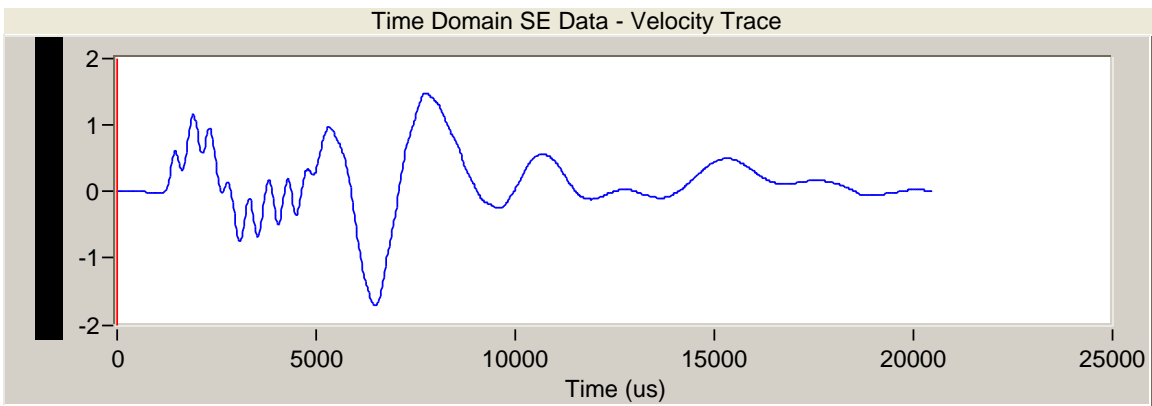


**Figure 55. Velocity Graph of Test 9**

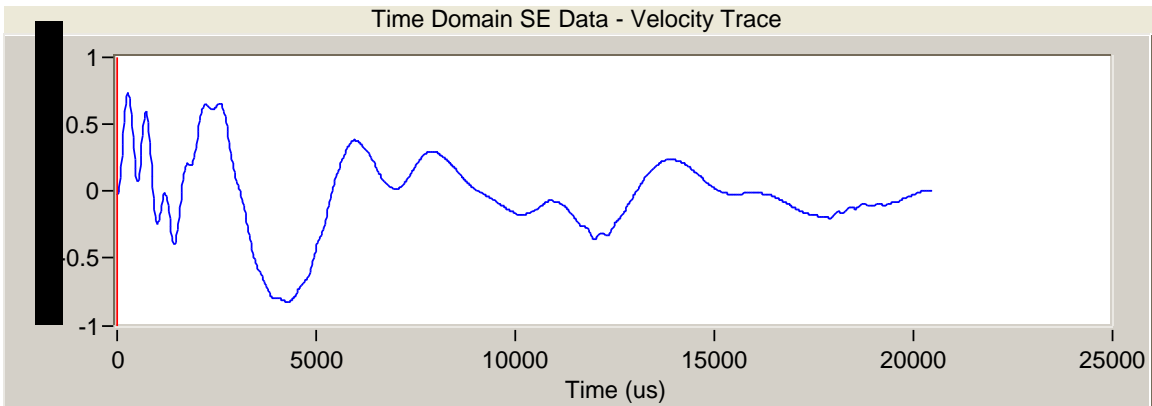


**Figure 56. Velocity Graph of Test 10**

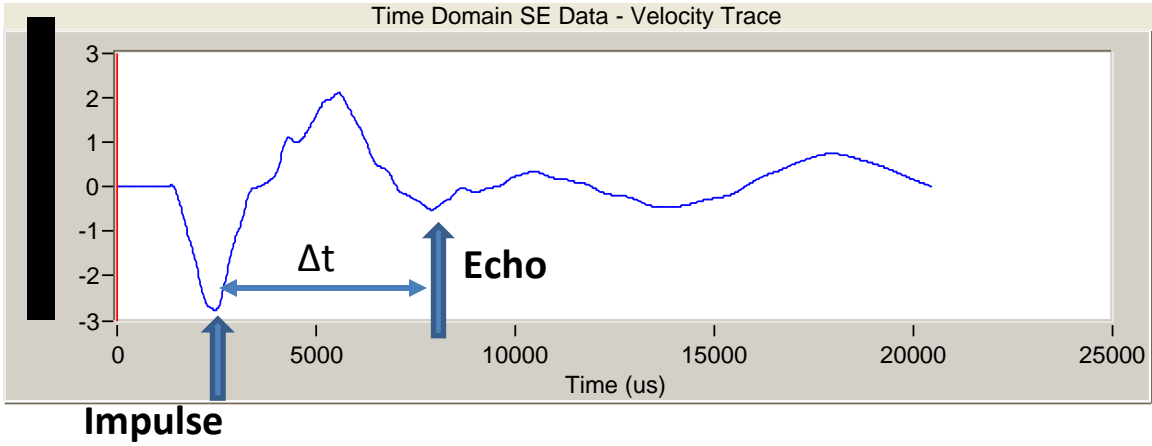


Figure 57. Velocity Graph of Test 11

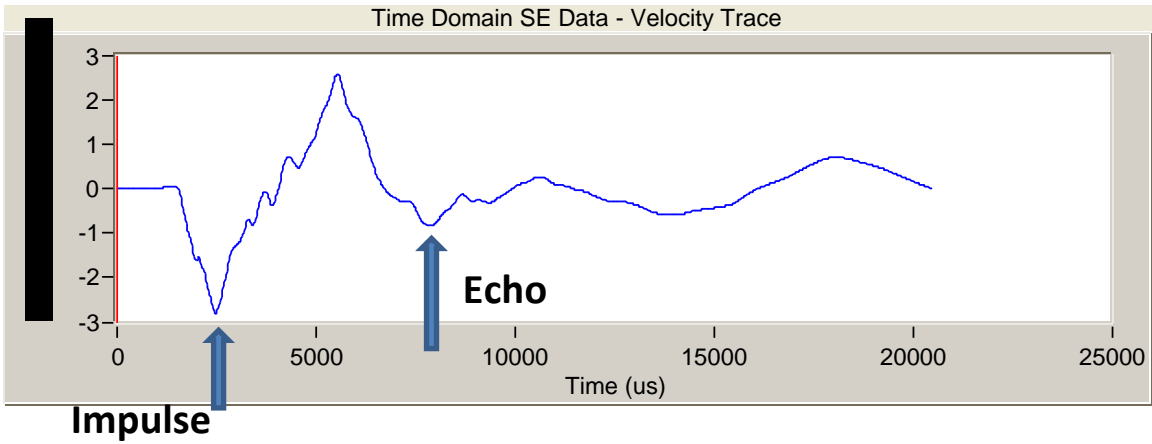


Figure 58. Velocity Graph of Test 12

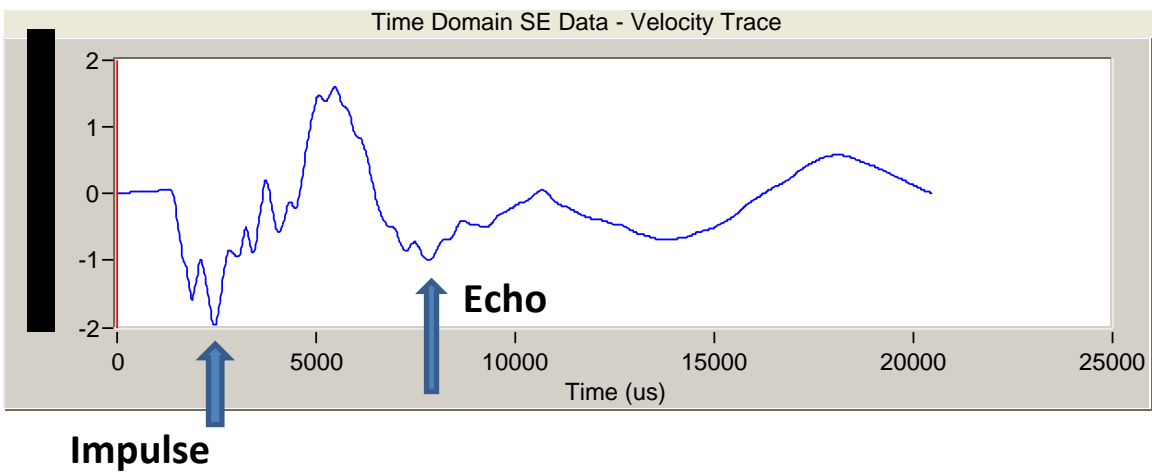


Figure 59. Velocity Graph of Test 13

The velocity graph of Test 11 (see Figure 57) was used to demonstrate the calculation of the total ( $L_t$ ) and embedment depth ( $L_b$ ) of Pile 8-E. As shown in Figure 57,  $\Delta t = 5,500 \mu s$ . The wave velocity of the pile is 11,500 ft/s and the sensor was located 1.5 ft from the top of the pile. The length of the pile was determined as:

$$L_t = \frac{v \times \Delta t}{2} + 1.5 = \frac{11500 \times 5500 \times 10^{-6}}{2} + 1.5 = 33.1 \text{ ft}$$

The embedment length is 29.1 ft since the exposed length is about 4 ft. Table 9 shows the calculated embedment depths and the lengths of Pile 8-E.

**Table 9. Calculated Pile Lengths of Pile 8-E.**

Test No.	$\Delta t$ ( $\mu s$ )	Embedment Depth (ft)	Total Length (ft)
11	5500	29.1	33.1
12	5420	28.7	32.7
13	5400	28.5	32.5

**Summary of Results** The test results for the two investigated piles are summarized in Table 10. Based on the numbers of tested piles, the success rate is 50% (1 out of 2).

**Table 10. Estimated Lengths of Piles of Santo Domingo Bridge.**

Pile	Embedment Pile Length (ft)	Exposed Pile Length (ft)	Total Pile Length (ft)
7-F	--*	4.1	--
8-E	28.8	4	32.8

Note \* -- denotes unsuccessful tests

### 3.1.4.2 Bridge No. 6922

Bridge No. 6922 is located 40 miles east of Las Vegas on NM 104. The latitude and longitude coordinates of the bridge are 35.477197, -104.613580. The bridge location and street view of the bridge are shown in Figures 60 and 61 respectively. Numerous SE

tests were conducted on 5 round timber piles. The foundation plan and investigated piles are indicated in Figure 62.



**Figure 60. Location of Bridge No. 6922**



**Figure 61. Street View of Bridge No. 6922**

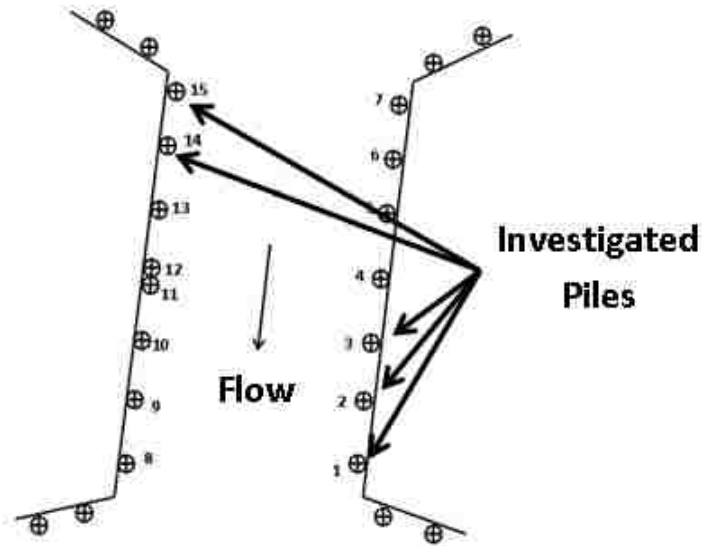


**Figure 62. Foundation Plan and the Investigated Piles of Bridge No. 6922**

The source was applied by three different hammer strikes:

- Vertical strike at the top of the pile (when the girder does not cover the entire pile's top surface such that part of the top surface of a pile is exposed)
- Vertical strike on a wooden block attached to the side of the piles
- Vertical strike on an aluminum block attached to the side of the piles

Two accelerometers were placed vertically on wooden blocks attached to the pile's side surface. The typical SE test setup is shown in Figure 63. The locations of the blocks in each tested pile are depicted in Figures 64 to 68 for Piles 1, 2, 3, 14, and 15 (see Figure 62).

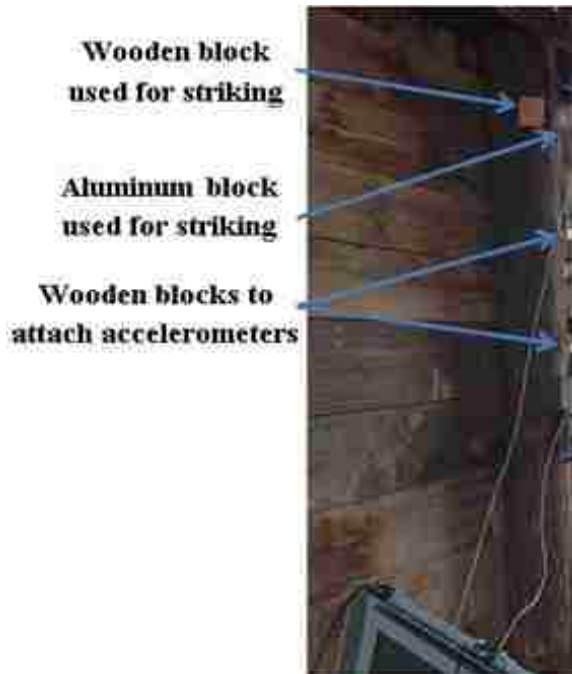


Figure 63. Typical SE Test Setup for Piles of Bridge No. 6922

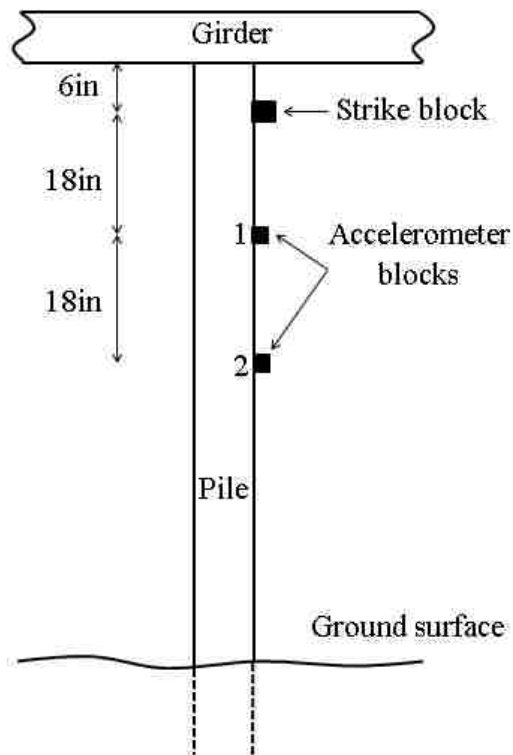
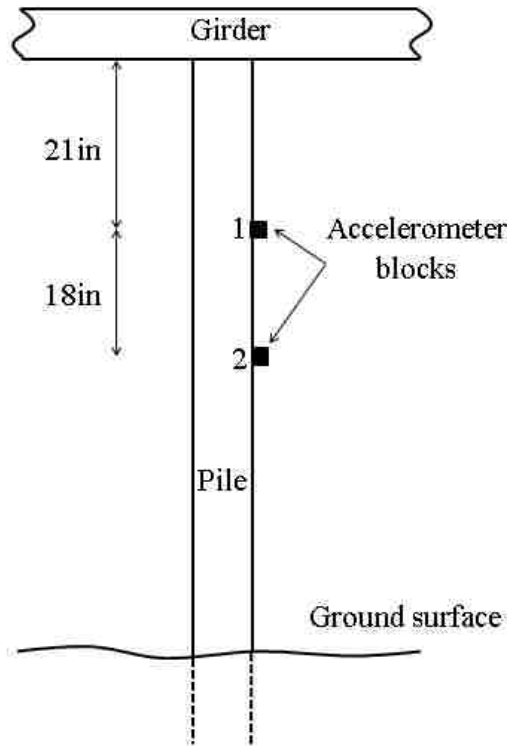
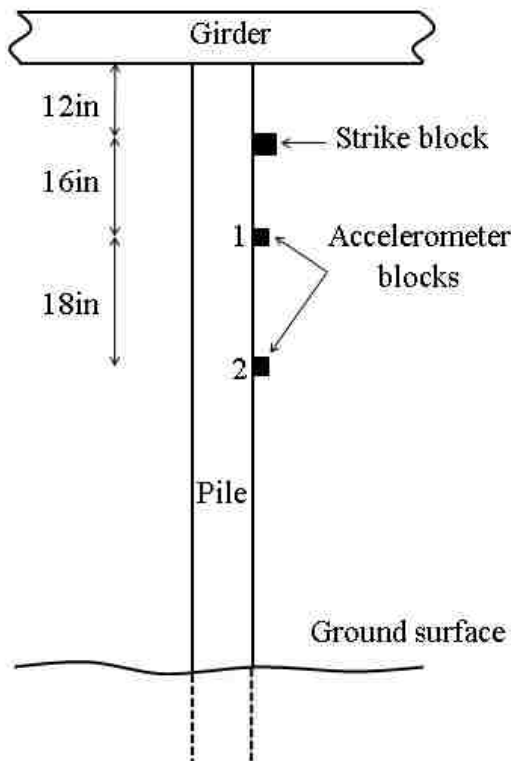


Figure 64. Location of Source and Accelerometers on Pile 1





**Figure 65. Location of Source and Accelerometers on Pile 2**



**Figure 66. Location of Source and Accelerometers on Pile 3**

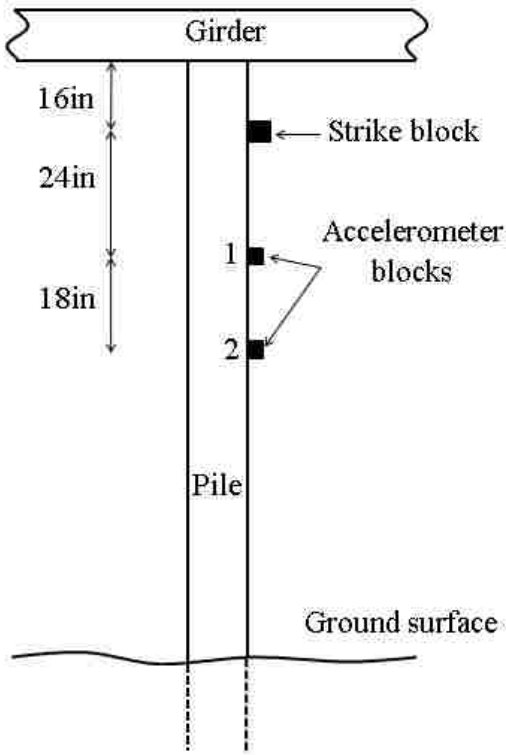


**Figure 67. Location of Source and Accelerometers on Pile 14**

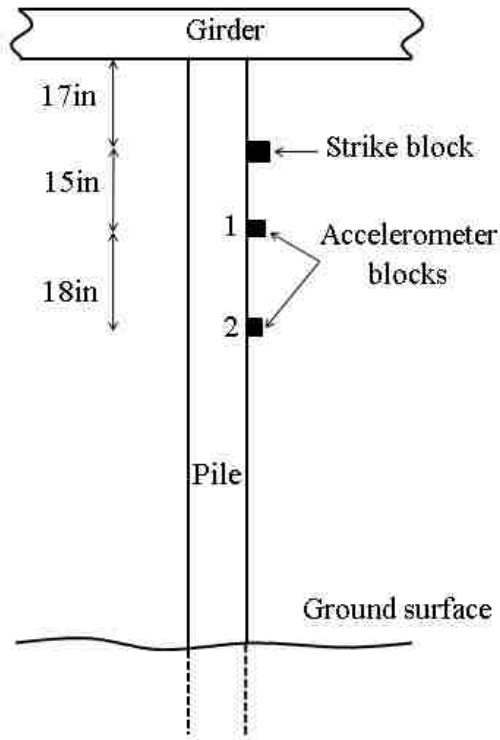


**Figure 68. Location of Source and Accelerometers on Pile 15**

**Determining Propagated Wave Velocity in a Pile** The propagated wave velocity was measured at Pile 2. Two accelerometers were placed far apart (79 in) so that the arrival times at these two sensors are distinguishable. Accelerometer 1 was closer to the top of the pile while accelerometer 2 was closer to the ground. This test is different from other SE tests that the distance between two accelerometers are 18 in. The time difference between the two arrival times was used to determine the wave velocity. The velocity graphs of accelerometers 1 and 2 are shown in Figure 69.

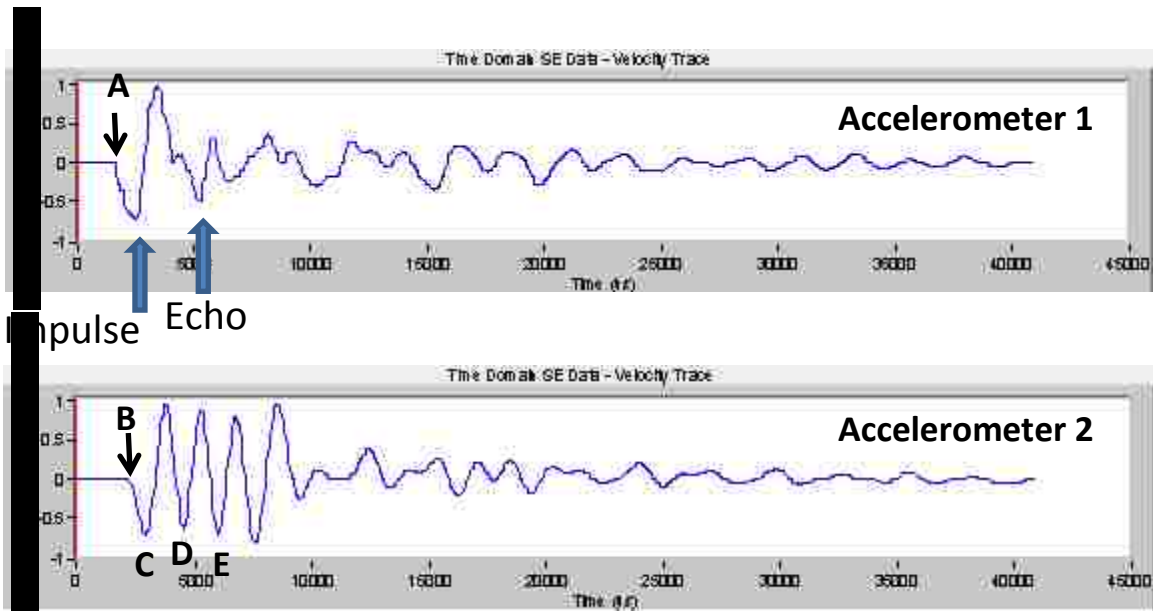


**Figure 69 Velocity Graphs of Accelerometers 1 and 2**

Points A and B show the first arrival times at accelerometers 1 and 2. The time difference ( $\Delta t$ ) between points A and B was used to estimate the wave velocity. Since the distance between accelerometers ( $\Delta L$ ) is 79 in (6.58 ft) and  $\Delta t = 1.96 - 1.46 = 0.5$  ms, the wave velocity is estimated as:

$$v = \frac{\Delta L}{\Delta t} = \frac{6.58}{0.0005} = 13,160 \text{ ft/s}$$

The appearance of these two velocity graphs is very different due to the locations of the two sensors. For accelerometer 1,  $\Delta t$  was found to be 2.76 ms and the calculated length of the pile is 19.9 ft using 13,160 ft/s as the propagated wave velocity.

Many echoes are shown in the velocity graph for accelerometer 2. The time difference between Points C (first valley) and D (second valley) is 1.62 ms. The estimated distance between the sensor and the bottom is:

$$L_{tr} = \frac{v \times \Delta t}{2} = \frac{13160 \times 1.62 \times 10^{-3}}{2} = 10.7 \text{ ft}$$

Since the distance between the accelerometer and pile top is 8.35 ft, the total pile length is estimated as  $L = 10.7 + 8.35 = 19.05$  ft. This value is very close to the estimated pile length from accelerometer 1 (19.9 ft). The reflected up-going wave continued to go upward. Then the wave was reflected at the pile top and became a down-going wave arriving at the sensor at Point E. Since the distance between the accelerometer and pile top is 8.35 ft, the wave traveled 16.7 ft ( $\Delta L$ ) before returning to the accelerometer. The required time for this path is:

$$\Delta t = \frac{\Delta L}{v} = \frac{16.7}{13160} = 0.00127 \text{ sec} = 1.27 \text{ ms}$$

This calculated time is close to the time difference between Points D and E in Figure 69b.

The above-mentioned calculations show that the multiple peaks observed at the accelerometer located far from the pile top was related to the multiple reflections from both the top and the bottom of the pile. The accelerometer closer to the top of the pile provided result that was easy to interpret. Reflections from both ends can complicate the velocity graphs. Additional discussion is presented later in the finite element analysis.

**SE/IR Tests on Pile 1** Six SE/IR tests were conducted on Pile 1. A portion of the pile top surface was accessible; therefore, half of the tests were carried out by striking at the top of the pile. Table 11 indicates the specification of the six SE/IR tests conducted on Pile 1.

*SE/IR Tests with Striking on Top of the Pile* Results obtained from top striking showed that, hard and medium-hard hammer tips produced good data. However, poor results were found for medium-soft tip as shown in Figure 70. The impulse, the first largest magnitude, was expected to be a valley (compression down-going wave) and not a peak

(tensile wave) as shown in this figure. The first valley was not related to the direct down-going compression wave. Since the impulse was difficult to identify,  $\Delta t$  cannot be determined.

**Table 11. SE Tests Conducted on Pile 1.**

Test No.	Hammer Tip	Strike at
1	Hard	Top (edge)
2	Medium-hard	Top (edge)
3	Medium-soft	Top (edge)
4	Hard	Aluminum block
5	Medium-hard	Aluminum block
6	Medium-soft	Aluminum block

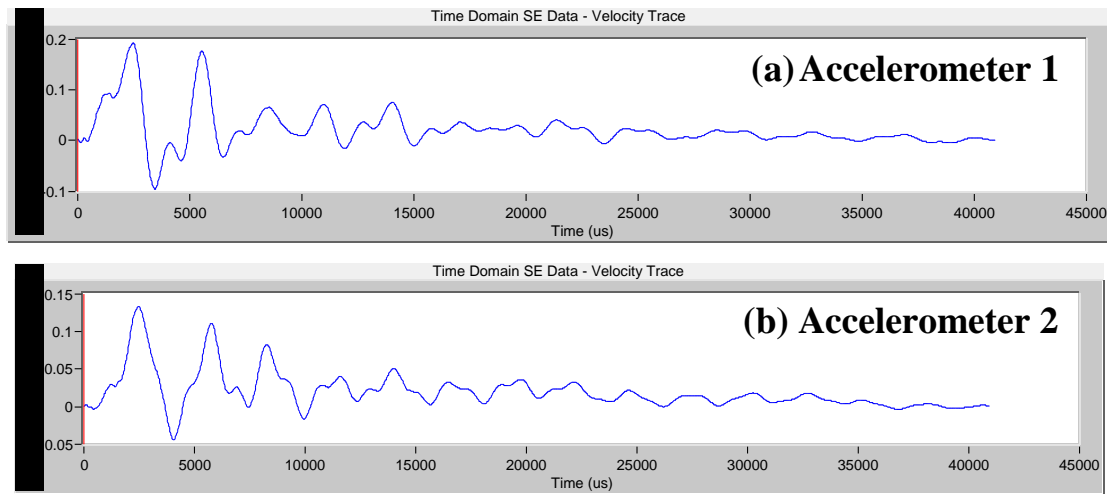


**Figure 70. Velocity Graphs of Test 3**

Table 12 shows the calculated length of Pile 1 using the  $\Delta t$  determined in the velocity graphs of Tests 1 and 2.

**Table 12. Estimated Length of Pile 1 from SE Analysis.**

Test No.	Accelerometer 1				Accelerometer 2			
	$\Delta t$ (ms)	$L_{tr}$ (ft)	$L_a$ (ft)	$L_t$ (ft)	$\Delta t$ (ms)	$L_{tr}$ (ft)	$L_a$ (ft)	$L_t$ (ft)
1	2.84	18.7	2	20.4	2.28	15	3.5	18.5
2	3.52	23.2	2	25.2	3.64	24	3.5	27.5

As stated before, the Impulse Response (IR) analysis based on the frequency content of the entire waveform can provide additional information to validate the results of time domain analyses in some cases. The obtained mobility graphs obtained from Tests 1 to 3 indicated clear resonant frequencies. The mobility graph obtained from accelerometer 1 in Test 1 is shown in Figure 71 as an example. The arrows indicate the resonant frequencies of the pile. The total length of the pile was calculated as:

$$L_t = \frac{v}{2 \times \Delta f} = \frac{13160}{2 \times 363} = 18.1 \text{ ft}$$

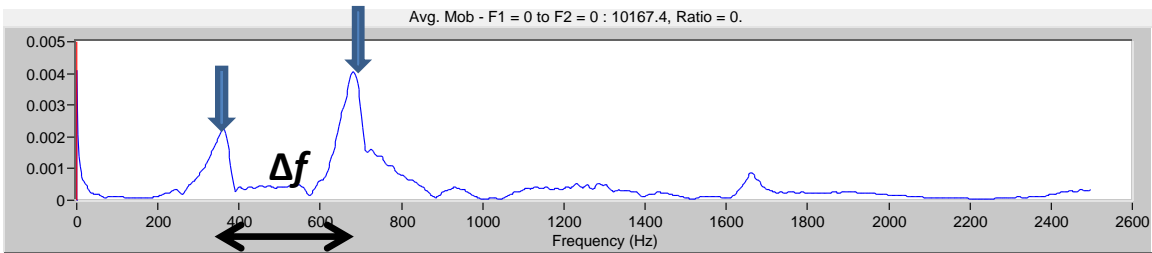


**Figure 71. Mobility Graph Obtained from Accelerometer 1 (Test 1)**

The calculated lengths of Pile 1 based on IR analysis are summarized in Table 13. Note that the variation of the calculated length is smaller than the variation calculated by SE analysis (see Table 12). Also, the IR analysis of Test 3 could estimate the length of the pile but the SE analysis was not. Therefore, IR analysis should be carried out when poor results are observed from SE analysis.

**Table 13. Estimated Length of Pile 1 from IR Analysis.**

Test No.	Accelerometer 1		Accelerometer 2	
	$\Delta f$ (Hz)	$L_t$ (ft)	$\Delta f$ (Hz)	$L_t$ (ft)
1	363	18.1	357	18.4
2	364	18.1	364	18.1
3	358	18.4	363	18.1

**SE/IR Tests with Aluminum Striking Block** Three SE/IR tests were conducted by striking an aluminum block with hard, medium-hard and medium-soft hammer tips (Tests 4 to 6 respectively). The force graphs of the hammer for Tests 4 and 5 are shown in Figure 72. The shapes of the impulses are different from the typical hammer impulse shown in Figure 73. Multiple peaks were shown in the graphs produced by striking on the aluminum block. The peaks may be due to the small sliding of the block on the surface of pile and occurrence of a momentary contact loss or multiple contacts between the block and pile surface.

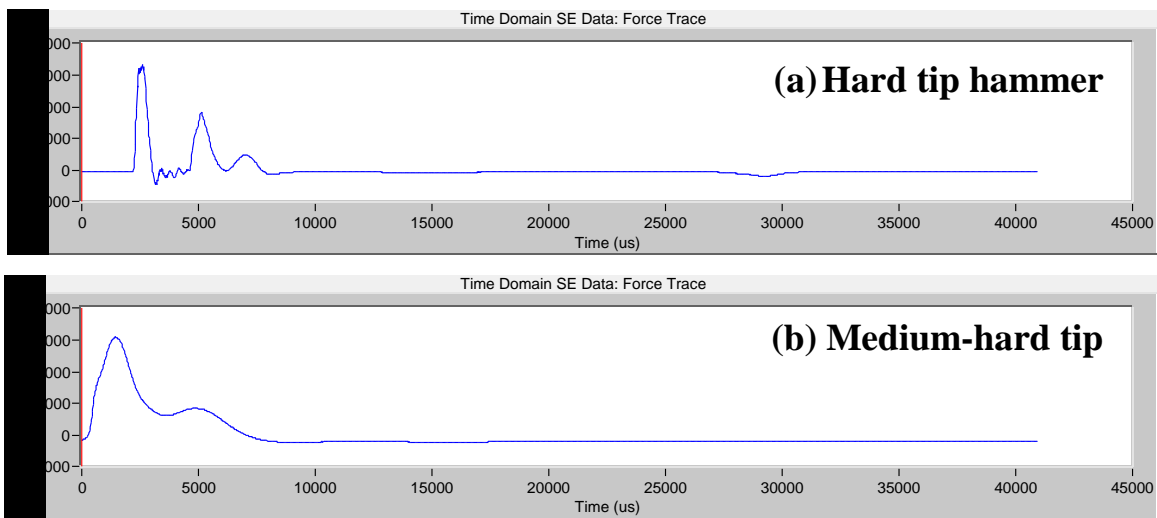


**Figure 72. Impulse Signals of Striking on an Aluminum Block**

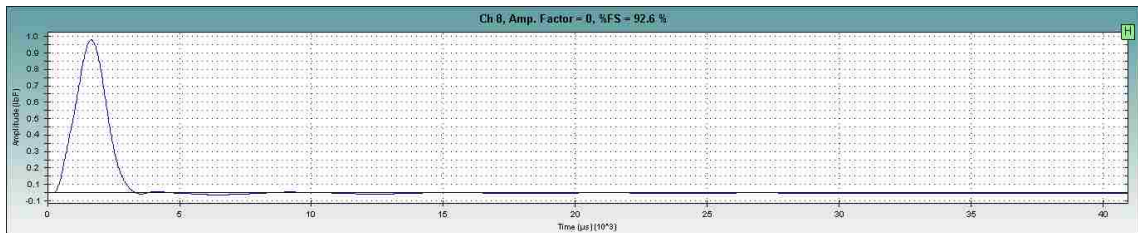


**Figure 73. Impulse Signal of Striking on a Solid Surface**

In some cases, the velocity graphs from the accelerometers showed complicated vibrations in the initial part of the graphs as shown in Figure 74. The impulse and echo could not be identified. Table 14 summaries the SE results on this pile.

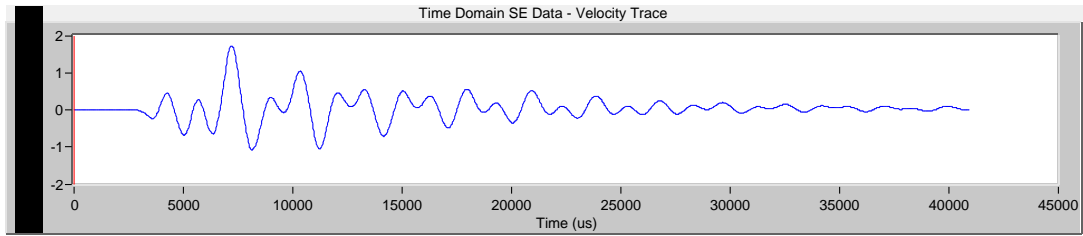


**Figure 74. Velocity Graph Obtained from Accelerometer 1 (Test 4)**

**Table 14. Estimated Length of Pile 1 from SE Analysis (Tests 4 to 6).**

Test No.	Accelerometer 1				Accelerometer 2			
	$\Delta t$ (ms)	$L_{tr}$ (ft)	$L_a$ (ft)	$L_t$ (ft)	$\Delta t$ (ms)	$L_{tr}$ (ft)	$L_a$ (ft)	$L_t$ (ft)
4	-	-	2	-	2.36	15.5	3.5	19
5	3.24	21.3	2	23.3	-	-	3.5	-
6	2.96	19.5	2	21.5	-	-	3.5	-

IR analyses were performed for Tests 4-6. A mobility graph obtained from Accelerometer 1 in Test 5 indicating clear resonant frequencies shown in Figure 75. Table 15 indicates the calculated length of the pile based on  $\Delta f$ . Unlike the previous case (striking on the top of the pile), IR analysis did not always work. Therefore, IR analysis could determine the pile length in some cases.

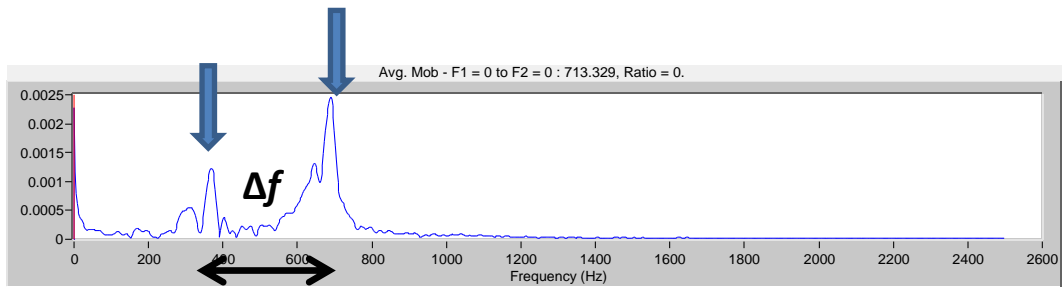


**Figure 75. Mobility Graph of Test 6**

**Table 15. Estimated Length of Pile 1 from IR Analysis (Tests 4 to 6).**

Test No.	Accelerometer 1		Accelerometer 2	
	$\Delta f$ (Hz)	$L_t$ (ft)	$\Delta f$ (Hz)	$L_t$ (ft)
4	-	-	-	-
5	354	18.6	357	18.4
6	372	17.7	-	-



**SE/IR Tests Pile 2** Four SE tests were performed on Pile 2. Hard hammer tip was used for Tests 7 and 10. Medium-hard and medium-soft tips were utilized in Tests 8 and 9 respectively. The source was applied by striking the top of the pile for all tests. All results were poor except for one velocity graph shown in Figure 76. This was for Accelerometer 1 in Test 7 and the impulse and echo were clearly identifiable in the figure.  $\Delta t$  is 2.76 ms and the corresponding pile length is 19.9 ft. Figure 77 shows an example of poor results. The use of softer tips did not help here.

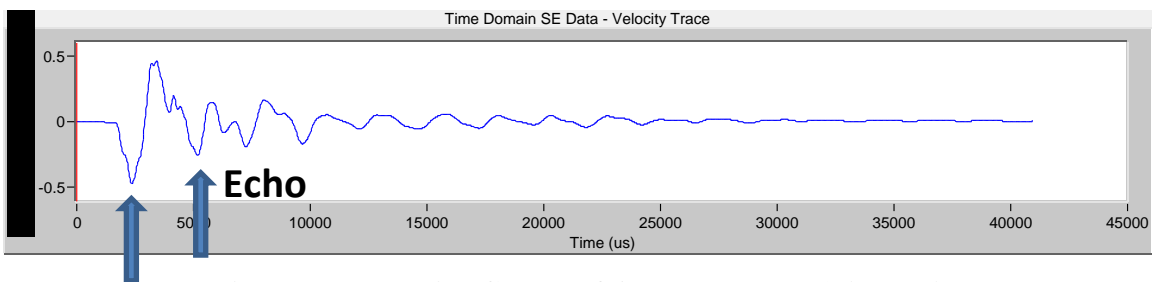


**Figure 76. Velocity Graph of Accelerometer 1 (Test 7)**

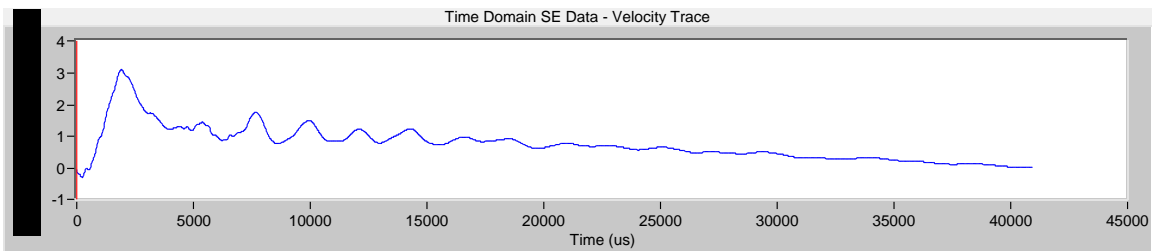


**Figure 77. Velocity Graph of Accelerometer 1 (Test 9)**

IR analysis of the data did not reveal any resonant frequencies. IR analysis could not aid the determination of pile length in this case.

**SE Tests on Pile 3** Since the top of the pile was inaccessible, a wooden block and an aluminum block were attached onto the side of the pile and hard and medium-hard hammer tips were used.

*SE Tests Performed with Wooden Striking Block and Hard tip Hammer* SE tests were conducted by hard hammer tips in Tests 11 to 13. Since the source was applied manually, the only difference between Tests 11 to 13 was the difference between their input energies and impulse shapes (Figure 78). These source signal graphs show more regular

shapes compared to sources produced by aluminum blocks (Figure 72). The corresponding velocity graphs for Tests 11 to 13 are indicated in Figures 79 to 81 respectively.



**Figure 78. Initial Impulse from the Hammer's Force Sensor (Wooden block, Hard-tip)**

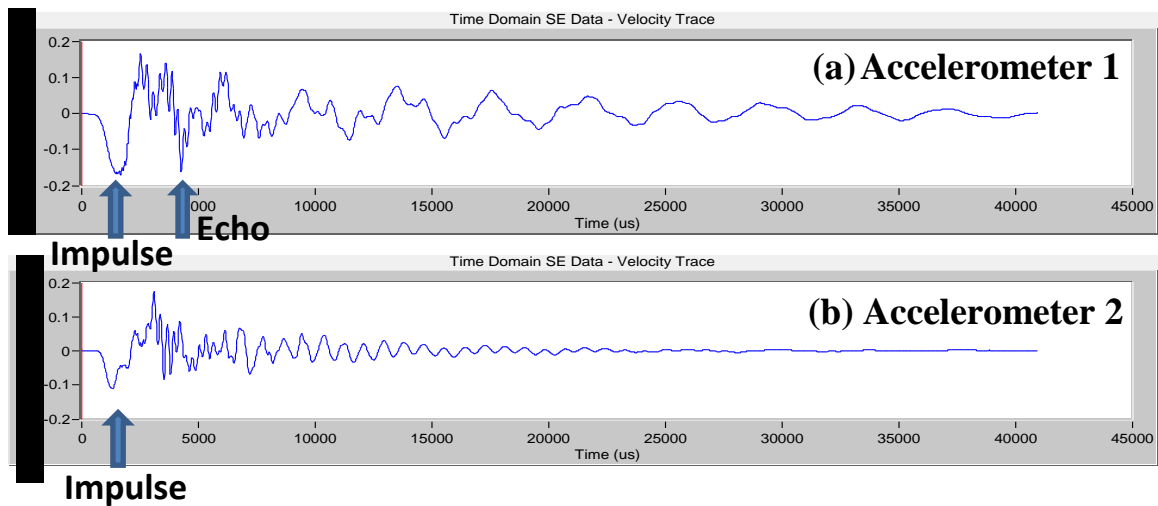


**Figure 79. Velocity Graphs of Test 11**

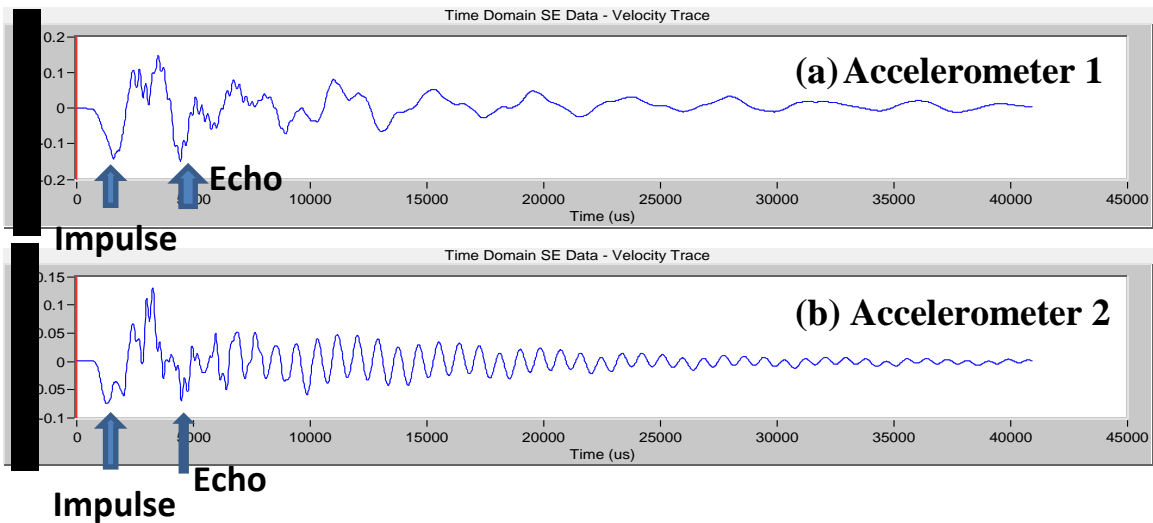


**Figure 80. Velocity Graphs of Test 12**

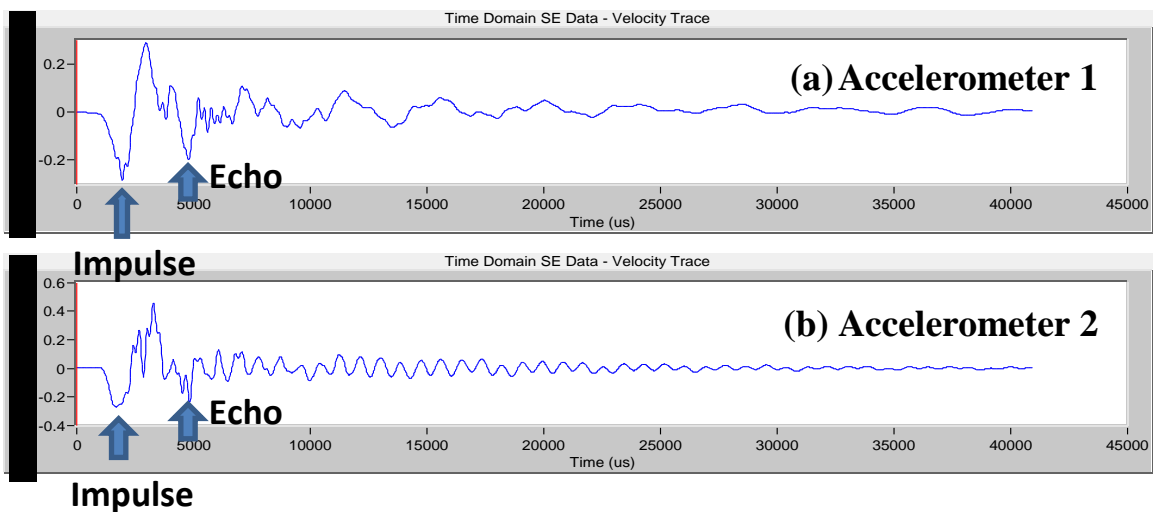


**Figure 81. Velocity Graphs of Test 13**

The result shows recognizable impulses and echoes except for Accelerometer 2 in Test 11. The clarity of these impulses and echoes implies that marginally irregular impulse shapes of the source may produce useful velocity graphs. Table 16 shows the calculated length of Pile 3 from Tests 11 to 13.

*SE/IR Tests Performed with Wooden Striking Block and Medium-hard Tip Hammer*

Three SE tests were conducted with medium-hard tip hammer in Tests 14 to 16. The source signals in Tests 14 to 16 are shown in Figure 82; the shape of the source signal is better

that of hard tip (see Figure 78). The corresponding velocity graphs obtained from Accelerometer 1 and 2 are shown in Figures 83 to 85 for Tests 14 to 16 respectively.

**Table 16. Estimated Length of Pile 3 (Tests 11 to 13)**

Test No.	Accelerometer 1				Accelerometer 2			
	$\Delta t$ (ms)	$L_{tr}$ (ft)	$L_a$ (ft)	$L_t$ (ft)	$\Delta t$ (ms)	$L_{tr}$ (ft)	$L_a$ (ft)	$L_t$ (ft)
11	2.8	18.4	2	20.4	-	-	3.5	-
12	2.84	18.7	2	20.7	3.22	21.2	3.5	24.7
13	2.84	18.7	2	20.7	3.16	20.8	3.5	24.3



**Figure 82. Initial Hammer Impulses (Wooden blocks, Medium-hard-tip)**

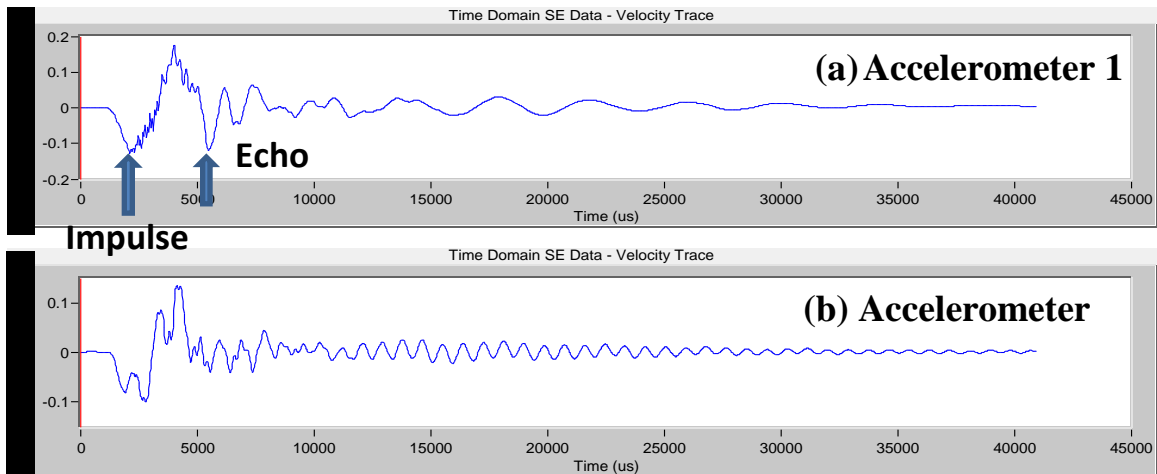


Figure 83. Velocity Graphs of Test 14

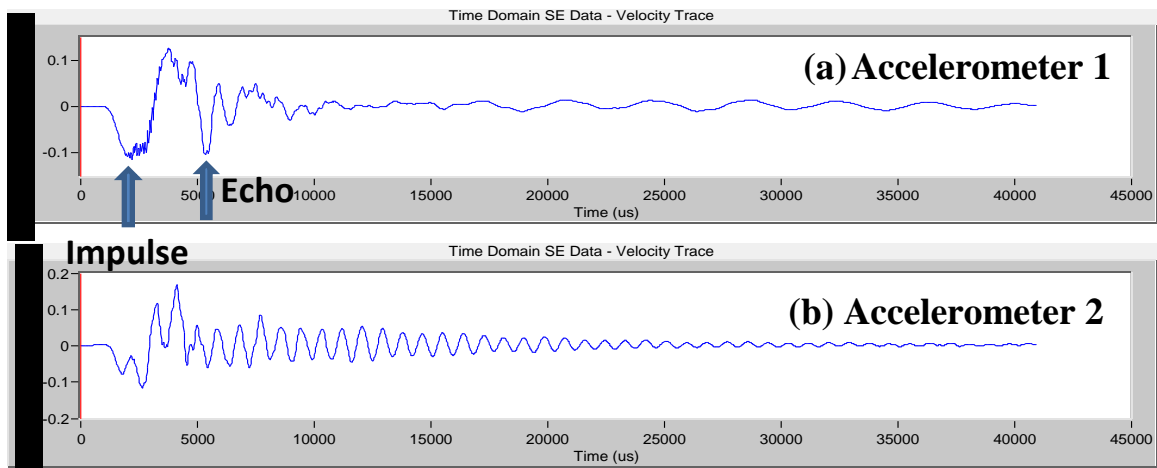


Figure 84. Velocity Graphs of Test 15

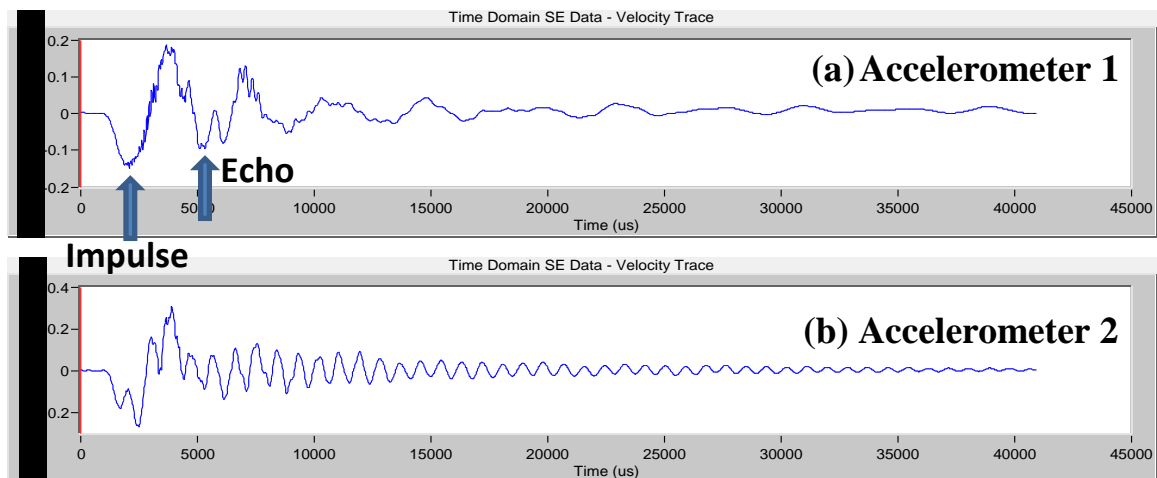


Figure 85. Velocity Graphs of Test 16

Results of Accelerometer 1 are much better than those obtained from Accelerometer 2. The accelerometer attachment was checked and functioned correctly. Better results of Accelerometer 1 may be due to the location of the accelerometer for this particular pile. The calculated pile lengths are summarized in Table 17.

**Table 17. Estimated Length of Pile 3 (Tests 14 to 16).**

Test No.	Accelerometer 1				Accelerometer 2			
	$\Delta t$ (ms)	$L_{tr}$ (ft)	$L_a$ (ft)	$L_t$ (ft)	$\Delta t$ (ms)	$L_{tr}$ (ft)	$L_a$ (ft)	$L_t$ (ft)
14	3.34	22.0	1.75	23.8	-	-	3.25	-
15	3.18	20.9	1.75	22.7	-	-	3.25	-
16	3.24	21.3	1.75	23.1	-	-	3.25	-

Table 18 shows the pile length determined by IR analyses (in frequency domain) for the data of Accelerometer 2. IR analyses yielded an estimated pile length around 14.5 ft although the pile length could not be determined by the SE analysis (in time domain). This estimated pile length from IR analyses is different from the 22.7 to 23.8 ft determined from SE tests (see Table 17). Although IR analysis provides a pile length, the result may be unreliable comparing the pile length determined by SE analysis since SE analysis is more reliable in general. In addition, IR analysis on the data of Accelerometer 1 did not produce reasonable pile lengths.

**Table 18. IR Results for Accelerometer 2 (Tests 14 to 16).**

Test No.	$\Delta f$ (Hz)	$L_t$ (ft)
14	446	14.8
15	460	14.3
16	456	14.4

*SE/IR Tests Performed with Aluminum Striking Block* In Tests 17 to 19, different energies were imparted into the piles by striking an aluminum block attached to the side of the pile with hard hammer tip. As shown in Figure 86 the impulse graphs show multiple peaks similar to the previous observations of Pile 1 (see Figure 72).



**Figure 86. Impulse Signals Generated by Striking the Aluminum Block with Hard Hammer Tips (Tests 17 to 19)**

Poor velocity graphs were obtained for both accelerometers. Examples of poor velocity graphs are indicated in Figure 87. Only one velocity graph shown in Figure 88 (Accelerometer 2 in Test 18) could determine the length of the pile ( $L_t = 20.5$  ft,  $\Delta t = 2.76$  ms). The resonant frequencies from IR analyses did not reveal the correct pile length.

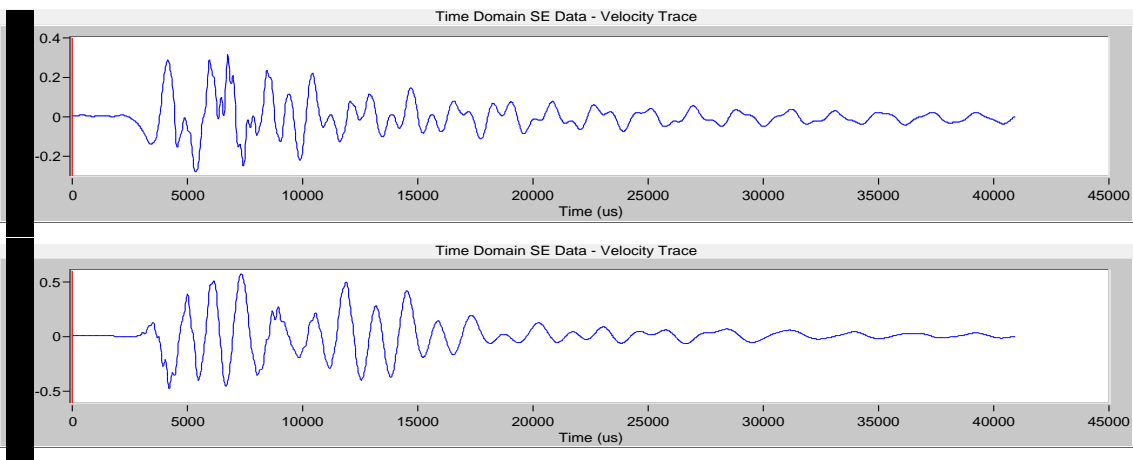


**Figure 87. Examples of Poor Velocity Graphs Obtained by Striking the Aluminum Block**

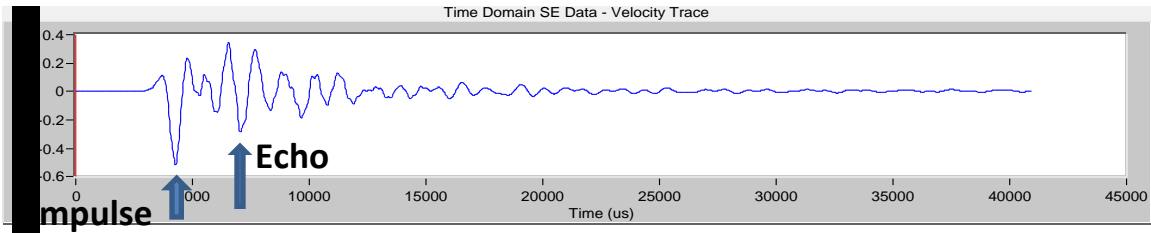


**Figure 88. Velocity Graph Obtained from Striking the Aluminum Block (Test 18, Accelerometer 2)**

Using the medium-hard tip hammer did not improve the results too. This leads to the conclusion that the aluminum block was unsuitable as the striking block for SE/IR tests. Thus, the use of aluminum block for striking is not recommended.

**SE Tests on Pile 14** Three SE tests were conducted on Pile 14. The impulse and hammer tip characteristics for each test are shown in Table 19. The velocity graphs from Accelerometer 1 for Tests 20 to 22 are shown in Figure 89.

The velocity graphs are very complicated. Closely located valleys indicated as arrows are shown in Figure 89. This is due to the presence of a huge longitudinal crack shown in Figure 90 which caused multiple internal reflections. The arrow in the figure indicates the big crack along the pile.

**Table 19. Specification of Tests Conducted on Pile 14.**

Test No.	Hammer tip	Strike
20	Medium-hard	Top
21	Hard	Wooden block
22	Medium-hard	Wooden block



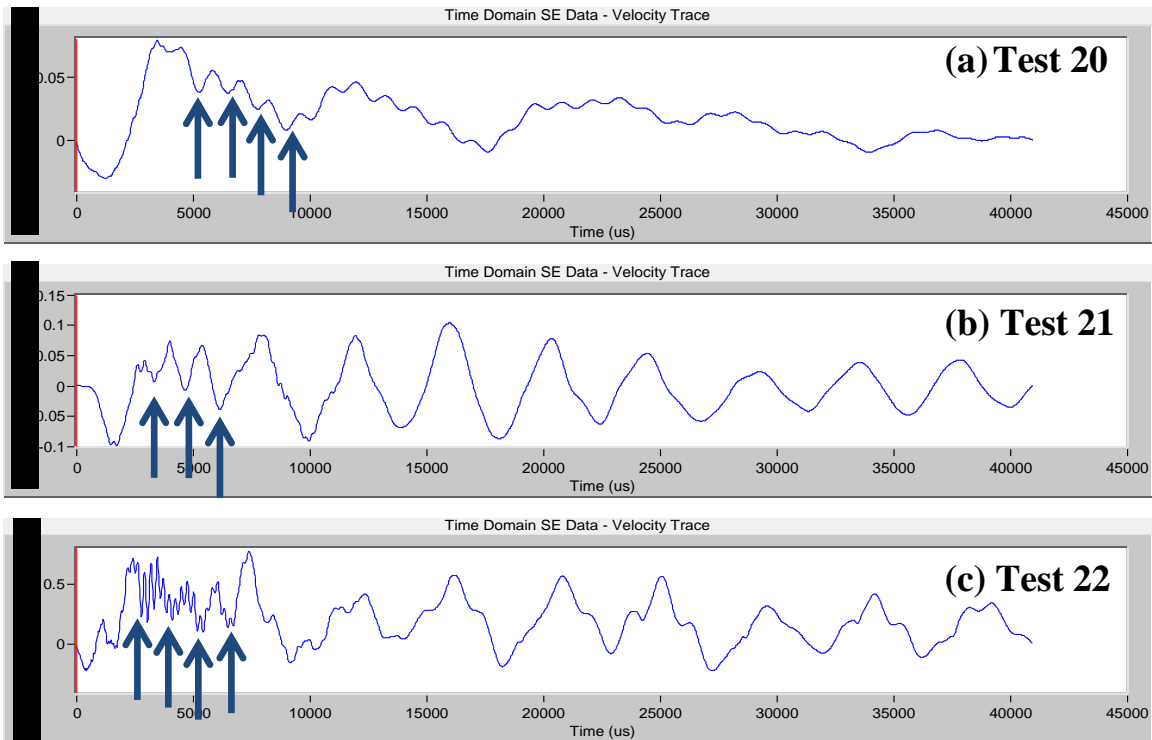


**Figure 89. Velocity Graph Obtained from Accelerometer 1 (Tests 20 to 22)**

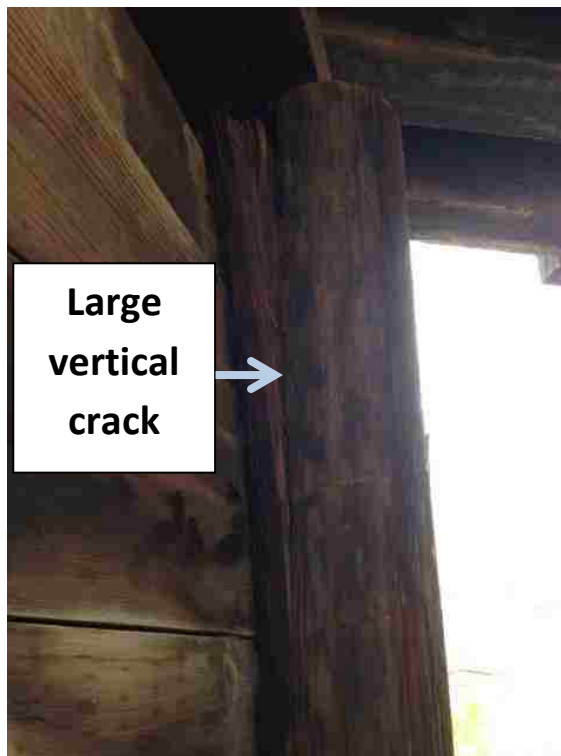


**Figure 90. Picture of a Crack along Pile 14**

**SE/IR Tests on Pile 15** Six SE/IR tests were conducted on Pile 15. The characteristics of source and hammer tip for each test are shown in Table 20.  $\Delta t$  cannot be determined in all the velocity graphs, however, IR analysis on the data from Accelerometer 1 reveal reasonable pile length. The mobility graph of Accelerometer 1 in Test 27 is shown in Figure 91. The length of the pile was calculated from IR analysis and the results are summarized in Table 21.

**Table 20. Specification of Tests Conducted on Pile 15.**

Test No.	Hammer tip	Strike
23	Hard	Top (edge)
24	Med-hard	Top (edge)
25	Med-soft	Top (edge)
26	Hard	Wooden block
27	Med-hard	Wooden block
28	Med-soft	Wooden block

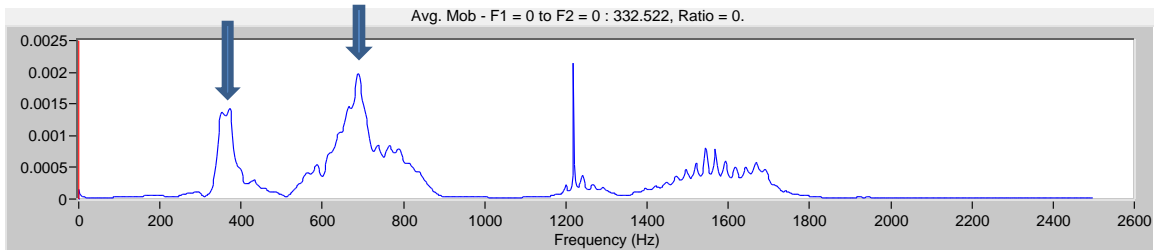


**Figure 91. Mobility Graph of Accelerometer 1 (Test 23)**

**Table 21. Estimated Length of Pile 15 from Mobility Graphs (Tests 23 to 28).**

Test No.	$\Delta f$ (Hz)	$L_t$ (ft)
23	363	18.1
24	363	18.1
25	363	18.1
26	377	17.4
27	372	17.7
28	367	17.9

**Summary** The inferred lengths of the five piles of Bridge No. 6922 are summarized in Table 22. Only the embedment depth of Pile 14 cannot be determined. The success rate at this site is 80% (4 out of 5 piles).

**Table 22. Estimated Average Length of Piles of Bridge No. 6922.**

Pile	Embedment Pile Length (ft)	Exposed Pile Length (ft)	Total Pile Length (ft)
1	12.7	9	21.7
2	10.2	9.4	19.6
3	12.1	8.8	20.9
14	-	8.8	-
15	12.4	8.2	20.6

### 3.1.4.3 Bridge No. 1190

Bridge No. 1190 is located 23 miles west of Springer, NM on NM 21 crossing over Rayado Creek. The coordinates of the bridge are 36.368383, -104.929533. It is a 2-span bridge supported by round timber piles. The location of the bridge is shown in Figure 92. Figure 93 and 94 show the condition of the running water during the first and second visits respectively.



**Figure 92. Location of Bridge No. 1190**



**Figure 93. Street View of Bridge No. 1190 Showing Running Water Surrounding Intermediate Bent during the First Visit**



**Figure 94. Photo of Bridge No. 1190 during the Second Visit**

During the first visit, the accessibility of the intermediate bent was hindered by the running river water as indicated in Figure 93. Only the piles beneath the end bents were accessible. Due to seasonal reduction in the water level, all piles beneath the intermediate bent became accessible during the second visit as indicated in Figure 94. SE tests were conducted on the intermediate piles and the piles beneath the end bents. The investigated piles are indicated in Figure 95.

A trailer-mounted inspection platform (mobile scaffold) from NMDOT District 4 was arranged at the second visit to explore the feasibility of conducting SE tests on piles with the help of the inspection platform. Figure 96 shows the mobile scaffold that was used for attaching the blocks for accelerometer and for striking. Figure 97 shows NMDOT staff preparing the scaffold to conduct SE tests.

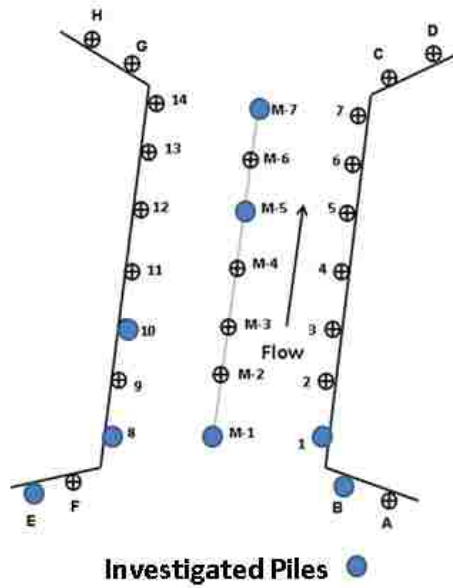


**Figure 95. Foundation Plan and Investigated Piles of Bridge No. 1190**



**Figure 96. Mobile Scaffold from NMDOT District 4**



**Figure 97. Preparing the Mobile Scaffold**

**SE Tests on Pile B** The accelerometer was placed at the top of the pile since the top of this wing pile was accessible, Three different hammer tips were used. The results are shown in Figure 98. As shown in this figure,  $\Delta t$  can be identified for medium-hard and medium-soft hammer tips but not the hard tip. This is interesting as our experience indicates that hard tip performs better than softer tips in general. The wave velocity was assumed to be 13,160 ft/s. Table 23 lists the calculated lengths of Pile B.

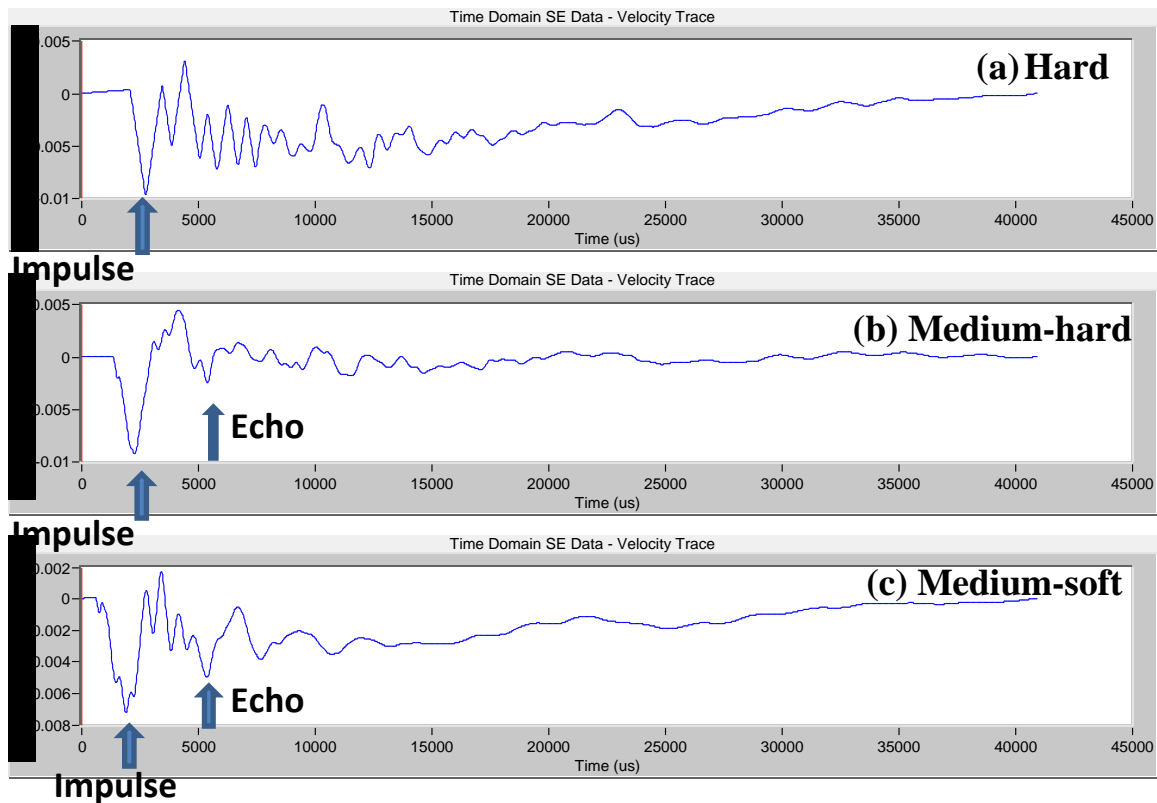


**Figure 98. Velocity Graphs Obtained by Striking with Different Hammer Tips (Pile B)**

**Table 23. Calculated Length of Pile B.**

Test No.	Hammer Tip	$L_t$ (ft)
1	Hard	-
2	Medium-hard	20.5
3	Medium-soft	22.6

**SE Tests on Pile E** Three SE tests were performed on Pile E (Tests 4 to 6). Similar to Pile B, the source and receiver were placed at the top of the pile. Figure 99 shows the velocity graphs of all three tests. Distinguishable impulses and echoes can be identified in the velocity graphs for hard and medium-hard tips but not the medium soft tip. There are two echoes of similar magnitudes (shown as two arrows in Figure 99c), however, it is difficult to choose the correct one. The first one is wrong compared with the results of other SE tests. The second echo yields the pile length that is similar to those of SE tests with hard and medium-hard tips. It is suggested not to use medium-soft tip as the primary tip. Table 24 indicates the calculated pile lengths.

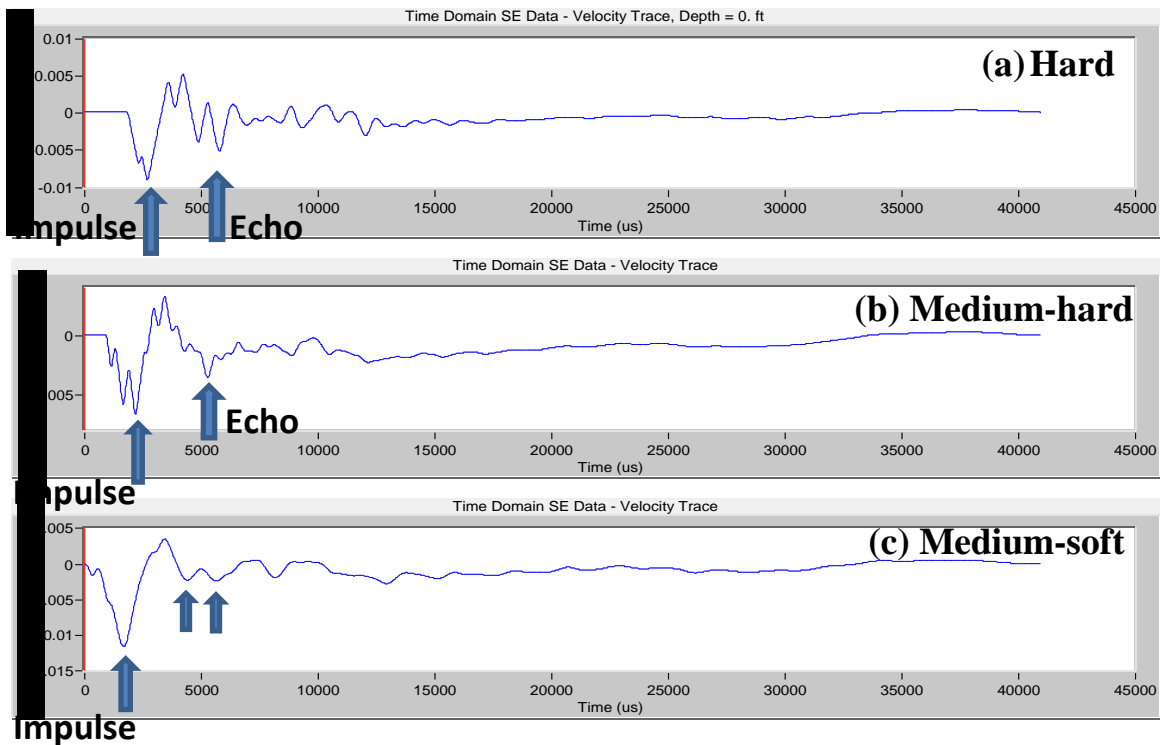


**Figure 99. Velocity Graphs of Pile E with Different Hammer Tips (Tests 4 to 6)**

**Table 24. Calculated Length of Pile E.**

Test No.	Hammer Tip	$\Delta t$ (ms)	$L_t$ (ft)
4	Hard	3.08	20.3
5	Medium-hard	3.06	20.1
6	Medium-soft	-	-

**SE Tests on Pile 1** Three SE tests (7 to 9) were conducted on Pile 1 with hard, medium-hard and medium-soft hammer tips respectively. Since the top of the pile was inaccessible, a wooden block was attached with screws for striking. The accelerometer was mounted on a wooden block. Figure 100 shows the locations of the blocks for the source and receiver. The obtained velocity graphs are shown in Figure 101 for these three hammer tips. The echo is undistinguishable again when using medium-soft tip. However, the bad response was due to accelerometer's insecure attachment in this particular case. The average pile lengths are listed in Table 25.

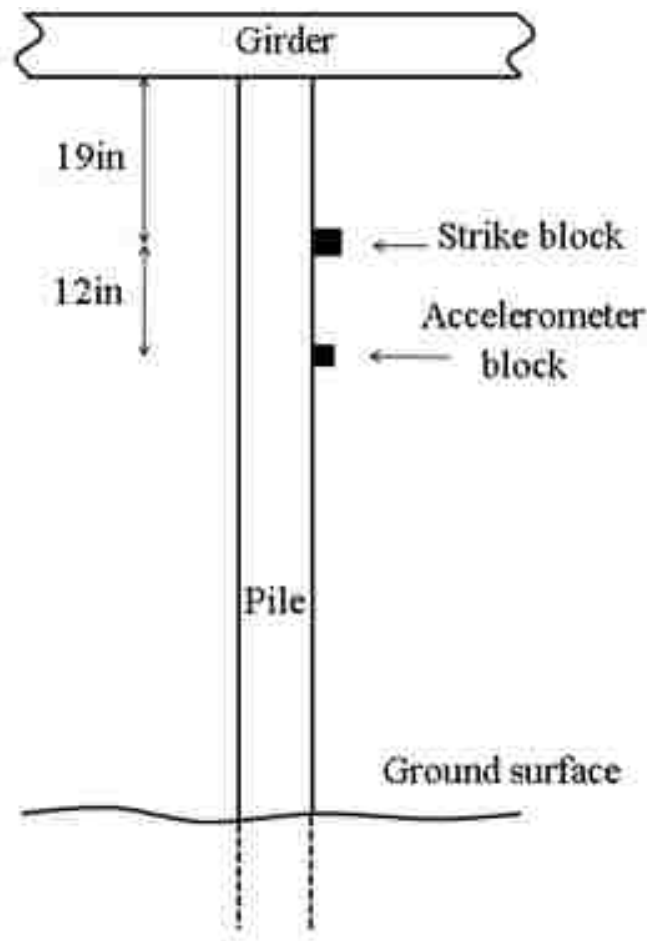


**Figure 100. Locations of Source and Receiver for Pile 1**



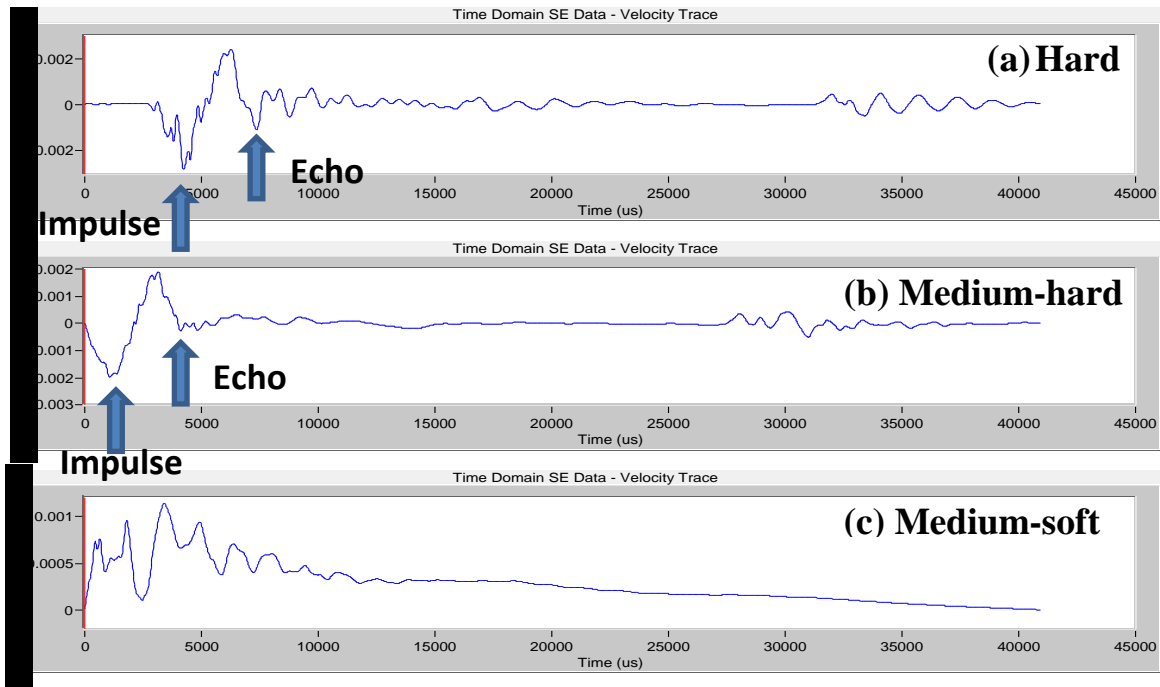


**Figure 101. Velocity Graphs of Different Hammer Tips (Tests 7 to 9)**

**Table 25. Calculated Length of Pile 1.**

Test No.	Hammer Tip	$\Delta t$ (ms)	$L_{tr}$ (ft)	$L_a$ (ft)	$L_t$ (ft)
7	Hard	3.08	20.3	2.6	22.9
8	Medium-hard	3.04	20	2.6	22.6
9	Medium-soft	-	-	-	-

**SE Tests on Pile 8** Three SE tests (10 to 12) were conducted on Pile 8 with hard, medium-hard and medium-soft hammer tips again. The top edge of the pile was accessible; therefore, the source was applied by striking the top surface. Due to the size of the pile, the accelerometer was mounted 1 ft below the top of the pile. The velocity graphs are shown in Figure 102. Recognizable impulse and echo were found in all three velocity graphs. Unlike the SE test on Pile 1, the result of medium-soft tip was acceptable when striking at the top of the pile. The estimated pile lengths are listed in Table 26.

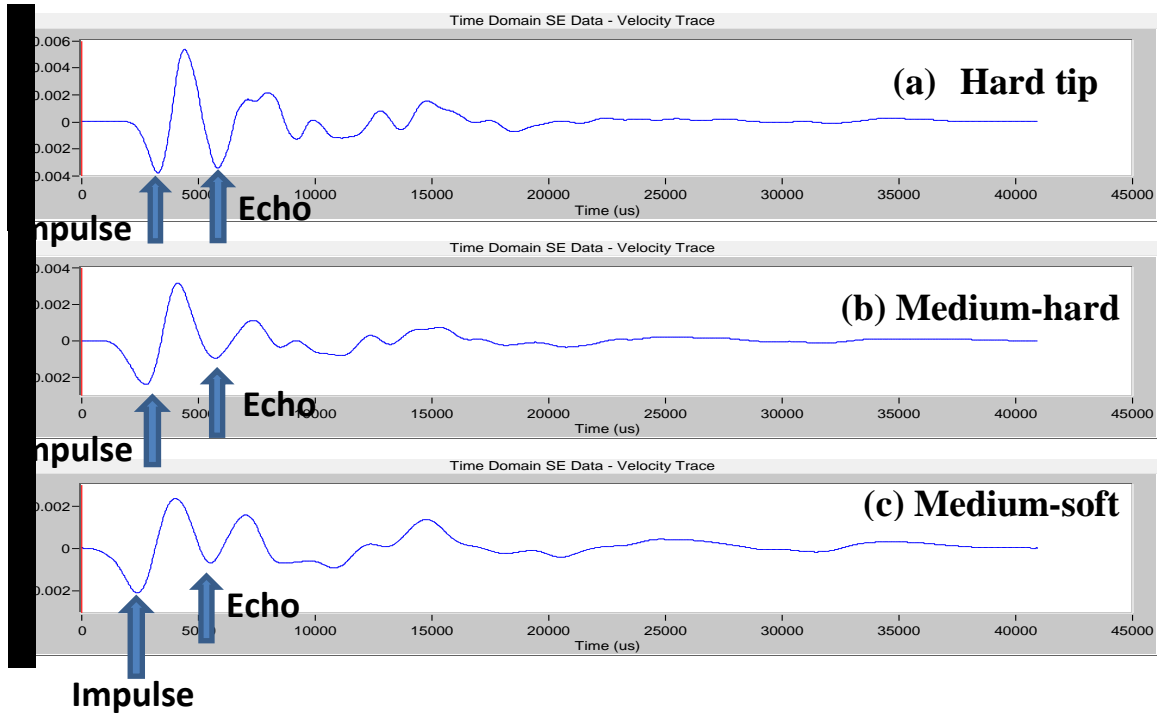


**Figure 102. Velocity Graphs of Pile E with Different Hammer Tips (Tests 10 to 12)**

**Table 26. Calculated Length of Pile 8.**

Test No.	Hammer Tip	$\Delta t$ (ms)	$L_{tr}$ (ft)	$L_a$ (ft)	$L_t$ (ft)
10	Hard	2.66	17.5	1	18.5
11	Medium-hard	3.02	19.9	1	20.9
12	Medium-soft	3.00	19.8	1	20.8

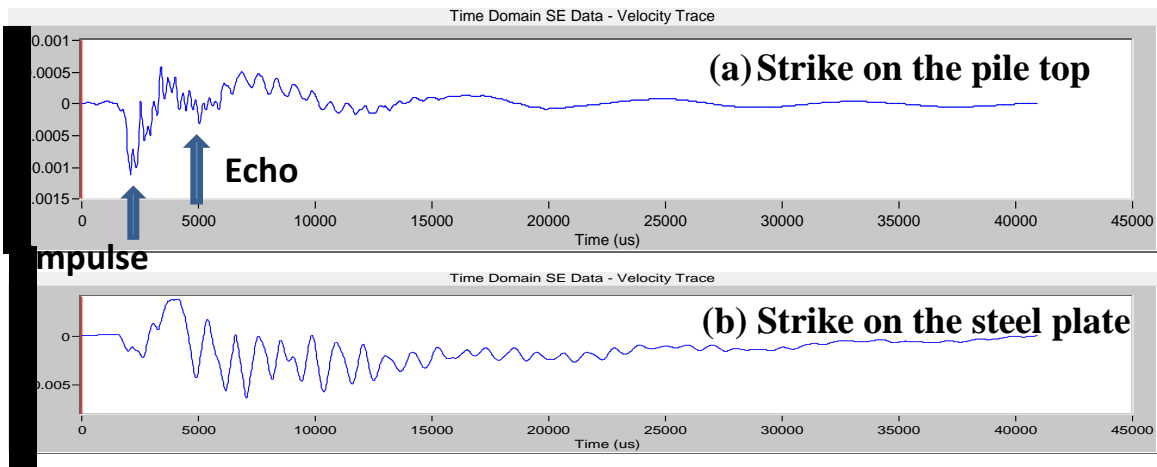
**SE Tests on Pile 10** Two SE tests (13 and 14) were conducted on Pile 10 with hard tip. Since the top was accessible, Test 13 was performed by striking the top surface of the pile. A ½ in thick steel plate was attached on this pile as shown in Figure 103 that could be used as the striking block. The steel plate was connected to the pile with thick metal bolts but the contact was loose. There was also a gap between the steel plate and the pile. In Test 14, the source was applied by vertical striking at the edge of the steel plate. The accelerometer was mounted 40 inches below the top of the pile.

Figure 104 shows the velocity graphs of these two tests. Good result was found for vertical striking at the top (Test 13).  $\Delta t = 2.92$  ms and the estimated pile length is 22.5 ft. Poor results of striking the steel plate were found which might be due to the poor coupling between the steel plate and pile. Energy transmitted only through the steel bolts and a

complex source signal was created due to the vibration of the plate. Thus, mounting the striking block on a pile tightly and securely is very essential to yield good results.



**Figure 103. A Steel Plate Attached to Pile 10**



**Figure 104. Velocity Graphs of Vertical Striking on the Pile Top and on the Steel Plate**

**SE Tests on Piles M-5** Twenty-one SE tests were performed on this pile. Two accelerometers were mounted on the wooden blocks attached to the side of the test pile. As mentioned before, when the top of either pile or pile cap are inaccessible, upward striking on the pile cap next to the test pile can be used as the alternative mean to produce longitudinal waves along the test pile. Figure 105 shows the locations of striking on the pile cap. Upward striking on pile cap will produce a strong tensile wave accompanied by a weak reflected compression wave. The source of some SE tests was also applied through

striking block. The locations of the sensor and striking block can be found in Figure 106. Cubic and wedge wooden blocks were attached onto the pile surface with screws for striking. The striking was accomplished with four different hammer tips including hard, medium-hard, medium-soft, and soft. Table 27 lists the characteristics of all SE tests conducted on Pile M-5.



**Figure 105. Photo of Pile M-5 and the Pile Cap**

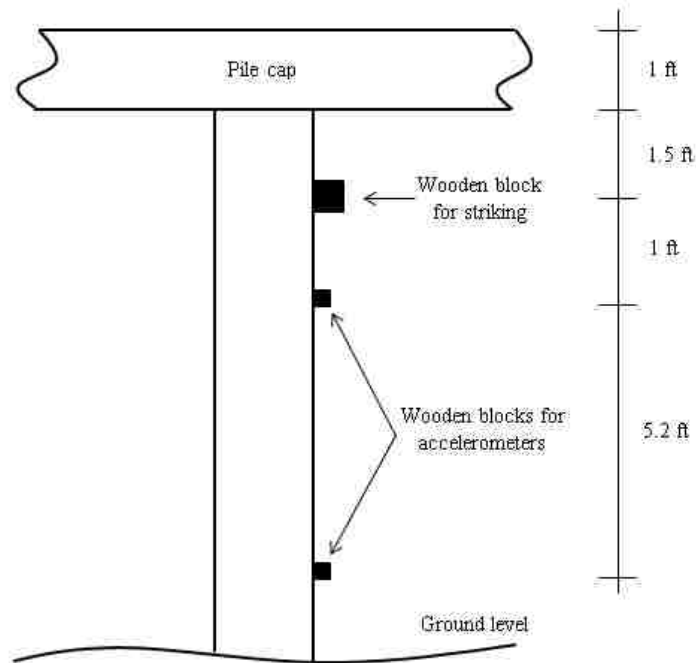


**Figure 106. Locations of Source and Receivers Blocks for Pile M-5**

**Table 27. Specifications of SE Tests Conducted on Pile M-5.**

Test No.	Hammer tip	Striking Condition
1	Hard	On block
2	Medium-soft	On block
3	Medium-soft	On block
4	Medium-soft	On block
5	Hard	Upward on pile cap
6	Hard	Upward on pile cap
7	Hard	Upward on pile cap
8	Medium-hard	Upward on pile cap
9	Medium-hard	Upward on pile cap
10	Medium-hard	Upward on pile cap
11	Medium-soft	Upward on pile cap
12	Medium-soft	Upward on pile cap
13	Medium-soft	Upward on pile cap
14	Hard	On wedge (1 screw)
15	Medium-hard	On wedge (1 screw)
16	Medium-soft	On wedge (1 screw)
17	Medium-soft	On wedge (1 screw)
18	Hard	On wedge (2 screws)
19	Medium-hard	On wedge (2 screws)
20	Medium-soft	On wedge (2 screws)
21	Soft	On wedge (2 screws)

The length of the pile was estimated from the  $\Delta t$  determined in the velocity graphs of both accelerometers. The specification and result of the SE tests are listed in Table 28.

**Table 28. Results of SE Tests Conducted on Pile M-5.**

Test No.	Hammer Tip	Striking Condition	Accelerometer 1		Accelerometer 2	
			$\Delta t$ (ms)	$L_t$ (ft)	$\Delta t$ (ms)	$L_t$ (ft)
1	Hard	On block	4.74	33.7	2.64	25.1
2	Medium-soft	On block	4.64	33.0	-*	-
3	Medium-soft	On block	4.54	32.4	2.78	26.0
4	Medium-soft	On block	4.72	33.6	2.84	26.4
5	Hard	Upward on pile cap	-	-	-	-
6	Hard	Upward on pile cap	4.26	30.5	2.78	26.0
7	Hard	Upward on pile cap	4.1	29.5	3.86	33.1
8	Medium-hard	Upward on pile cap	4.26	30.5	2.98	27.3
9	Medium-hard	Upward on pile cap	4.3	30.8	-	-
10	Medium-hard	Upward on pile cap	-	-	-	-
11	Medium-soft	Upward on pile cap	4.34	31.1	3.18	28.6
12	Medium-soft	Upward on pile cap	4.32	30.9	3.18	28.6
13	Medium-soft	Upward on pile cap	4.82	34.2	3.32	29.5
14	Hard	On wedge (1 screw)	3.28	24.1	2.44	23.8
15	Medium-hard	On wedge (1 screw)	3.74	27.1	3.5	30.7
16	Medium-soft	On wedge (1 screw)	-	-	-	-
17	Medium-soft	On wedge (1 screw)	-	-	-	-
18	Hard	On wedge (2 screws)	-	-	-	-
19	Medium-hard	On wedge (2 screws)	3.3	24.2	2.86	26.5
20	Medium-soft	On wedge (2 screws)	3.42	25.0	3.24	29.0
21	Soft	On wedge (2 screws)	3.94	28.4	3.56	31.1

-\* :  $\Delta t$  cannot be determined from the velocity graph

Following observations were inferred based on the hammer and velocity graphs of the SE tests conducted on Pile M-5:

- The data from Accelerometer 1 (mounted close to the end of the pile) were slightly more consistent than the results from Accelerometer 2 mounted closer to the

ground. It may be due to the interference of the natural waves existing in the ground (strong water current). The river is running on one side (see Figure 97)

- The results of the upward striking on the pile cap were consistent. The calculated buried lengths were similar to those calculated by striking on the blocks. The finding indicates that the accompanied transmitted compression wave did not affect the SE result. Therefore, upward striking on pile cap next to the test pile is acceptable as the input source.
- Care must be taken on mounting the striking block onto the test pile. Clean and clear source signal may not be generated due to imperfect coupling between the block and pile surface. The result also depends on the hammer tip as shown in Figures 107 and 108 Multiple peaks in the impact signal were found while using a hard tip (see Figure 107a). These peaks interfered with the determination of the echo in the velocity graph (see Figures 107b and 107c). When a softer hammer tip was used, the multiple peaks disappeared for the accelerometer mounted farther from the source (see Figure 108a).

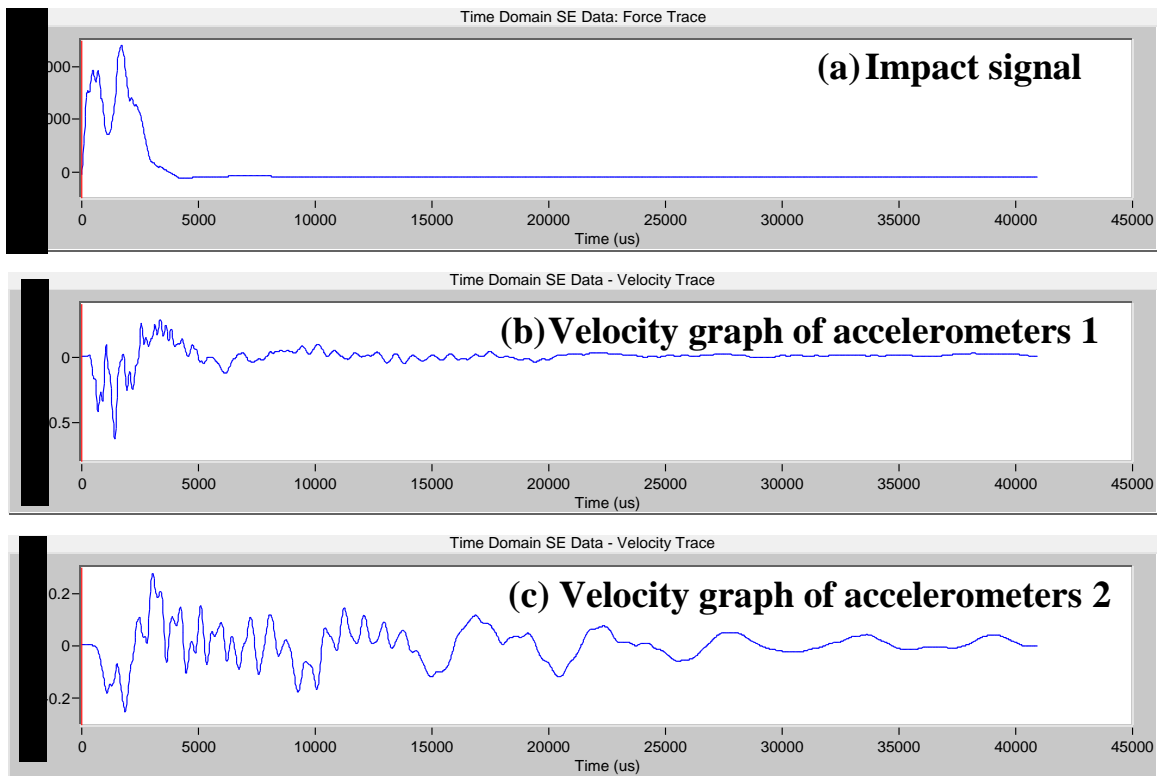


**Figure 107. Impact Signal and Velocity Graphs using a Hard Tip**

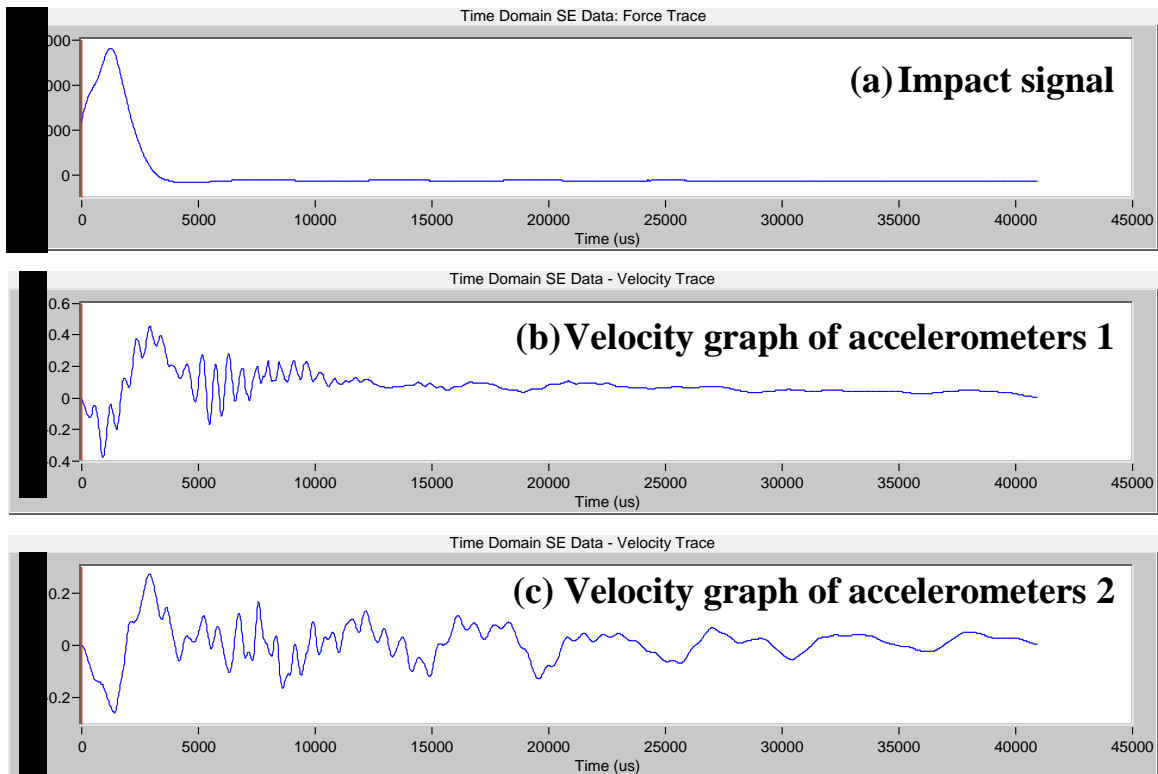


**Figure 108. Impact Signal and Velocity Graphs Using a Medium-soft Tip**

- Although striking on the wedge block produces horizontal wave as well as vertical compression wave that may complicate the velocity graphs, the increase of lateral compressive force should benefit the coupling between the block and the pile. The investigation showed that inclined hammer strikes produced similar results to those of vertical strikes on the cubic striking blocks. Multiple peaks in the hammer force history have also been found due to imperfect coupling in some cases.
- In general, all hammer tips produced good results when there was good coupling between the striking block and the pile. However, upward striking with hard hammer tip did not produce good velocity graphs (Tests 5, 9 and 11). Figure 109 shows three SE tests with three different hammer tips. As shown in Figure 109a, there are two echoes with similar magnitudes which made it difficult to select the correct echo. High frequency vibrations were seen in the velocity graph for hard tip but not for medium-hard and medium soft tips. The softer tips produced waves with lower frequencies that resulted in better data for this particular pile.



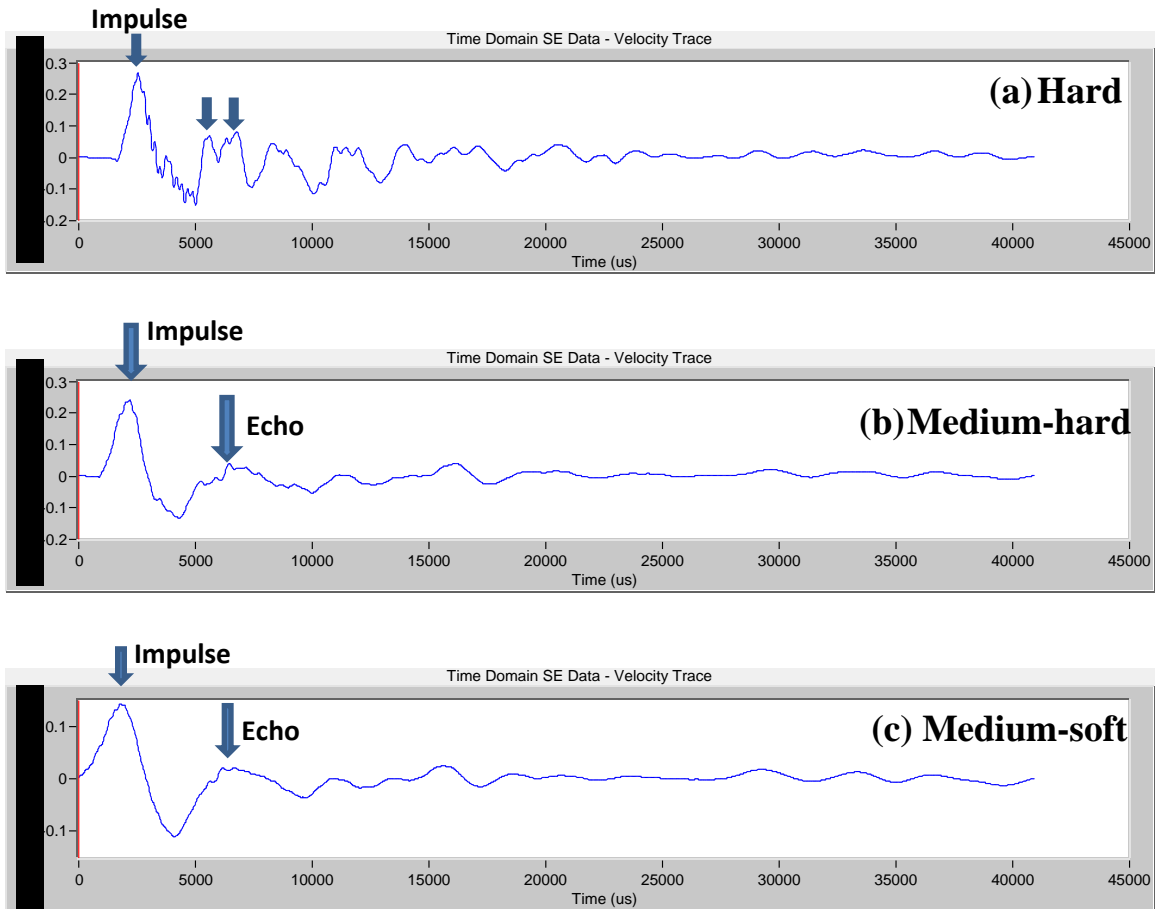


**Figure 109. Velocity Graphs for Various Hammer Tips Conducted on Pile M-5**

**SE Tests on Piles M-7** Twenty-four SE tests were performed with two accelerometers attached to the side of the pile. Figure 110 shows the locations of the receivers for Pile M-7. Eight different scenarios were considered and each scenario was repeated three times. Different hammer tips including hard, medium-hard, medium-soft, and soft were utilized to perform the tests. The striking was applied on the top of the pile cap and on the cubic and wedge wooden blocks attached to the pile surface for striking. The specifications of the SE tests conducted on Pile M-7 are indicated in Table 29.

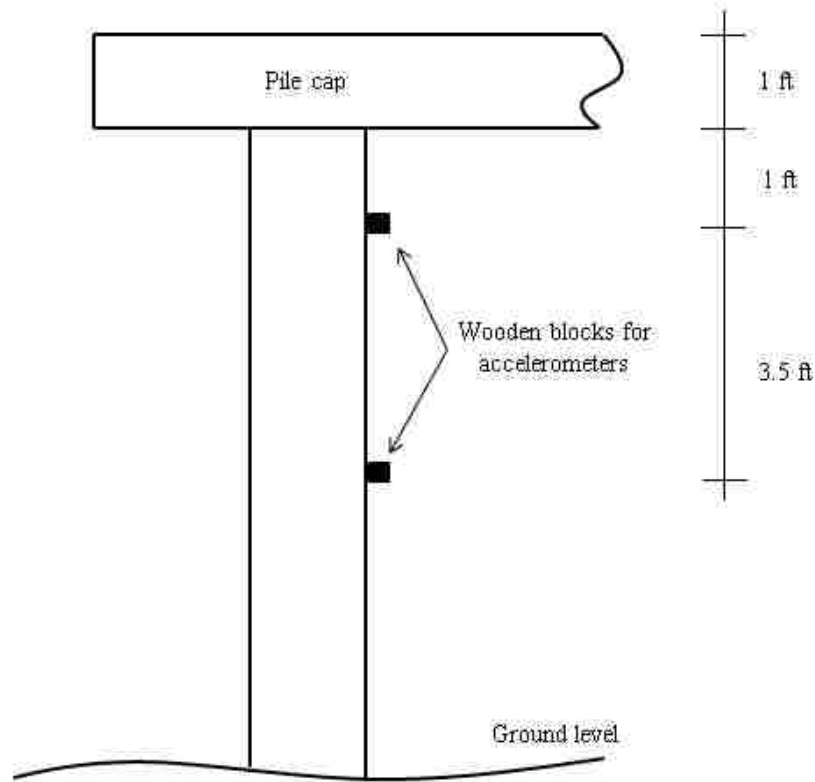


**Figure 110. Locations of the Receivers Blocks on Pile M-7**

The results of the SE tests on Pile M-7 obtained from both accelerometers are also shown in Table 29. This result is more consistent than those of Pile M-5 (see Table 28). First, striking on the pile cap directly above the pile produced excellent results. Second, there is no interference of reflections from superstructure. As shown in Figure 111, Pile M-7 is the exterior pile with only a pile cap above the pile. There is no superstructure above the pile cap. When the source is applied by upward striking at the pile cap, the generated up-going tension wave is reflected from the cap as a down-going compression wave. More complicated superstructures produce more complicated velocity graphs. This is the reason that the results of Pile M-5 is less consistent than Pile M-7. Once again, the results show that upward striking on pile cap next to the test pile is acceptable.

**Table 29. Specifications and Results of SE Tests Conducted on Pile M-7.**

Test No.	Hammer Tip	Striking Condition	L <sub>t</sub> (ft) (Accelerometer 1)	L <sub>t</sub> (ft) (Accelerometer 2)
1	Hard	Top of pile cap	22.5	24.4
2	Hard	Top of pile cap	27.2	29.9
3	Hard	Top of pile cap	24.7	27.5
4	Medium-hard	Top of pile cap	22.6	25.6
5	Medium-hard	Top of pile cap	22.7	26.2
6	Medium-hard	Top of pile cap	22.6	26.1
7	Medium-soft	Top of pile cap	23.0	26.2
8	Medium-soft	Top of pile cap	25.2	28.6
9	Medium-soft	Top of pile cap	23.2	27.4
10	Soft	Top of pile cap	23.8	27.8
11	Soft	Top of pile cap	24.8	28.3
12	Soft	Top of pile cap	24.7	28.1
13	Hard	Upward on pile cap	20.7	22.9
14	Hard	Upward on pile cap	21.1	24.6
15	Hard	Upward on pile cap	21.0	24.5
16	Medium-hard	Upward on pile cap	21.3	24.4
17	Medium-hard	Upward on pile cap	20.9	23.6
18	Medium-hard	Upward on pile cap	21.1	23.6
19	Medium-soft	Upward on pile cap	21.0	23.2
20	Medium-soft	Upward on pile cap	21.8	24.5
21	Medium-soft	Upward on pile cap	21.4	24.1
22	Soft	Upward on pile cap	21.3	22.0
23	Soft	Upward on pile cap	20.3	23.7
24	Soft	Upward on pile cap	20.6	22.8



**Figure 111. Exterior Pile M-7 and the Pile Cap**

**SE Tests on Pile M-1** Twenty-eight SE tests have been performed on Pile M-1. The specifications of the tests are listed in Table 30. The accelerometers were placed at various locations. The SE setup for Pile M-1 is shown in Figure 112. Despite numerous attempts, none of the results could be used to determine the length of the pile.

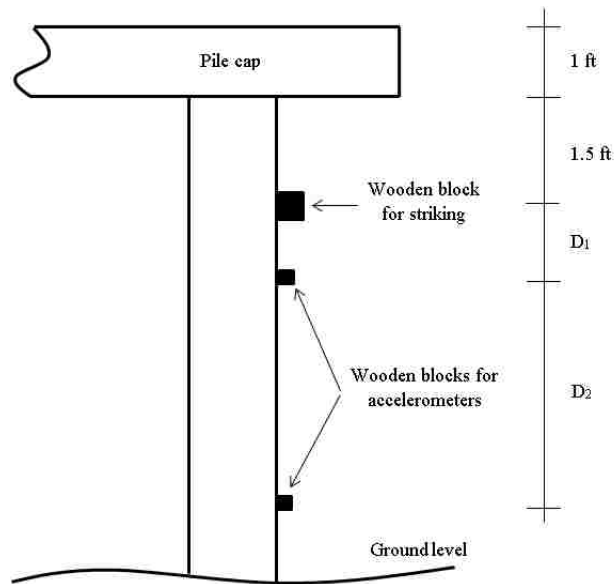


**Figure 112. Locations of Source and Receivers blocks for Pile M-1**

Although numerous SE tests with different striking conditions and hammer tips, placement of the receivers were carried out on Pile M-1, poor results were obtained. The echo from the pile toe could not be identified in the velocity graphs. We expected that either the presence of a big anomaly adjacent to ground level (such as a big internal crack)

or the noise due to the running water (river current hits the pile constantly) hinders the determination of the echo from the pile toe. The velocity graphs received from the two sensors were very different and typical velocity graphs are shown in Figures 113 and 114. The arrows on the graphs of the Accelerometer 1 (closer to pile top) show a reflection from an impedance change but the echo did not appear in Accelerometer 2 (close to the ground level). Therefore, the echoes shown in Figures 113a and 114a are not considered as the echoes from the pile toe.

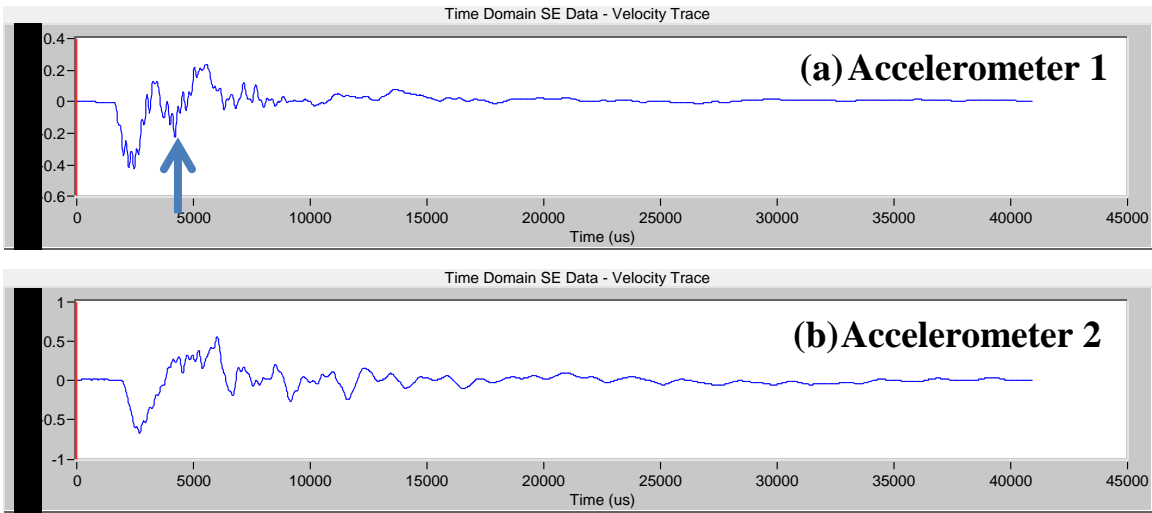


**Figure 113. Velocity Graphs Obtained from Accelerometers 1 and 2 (Test 19)**

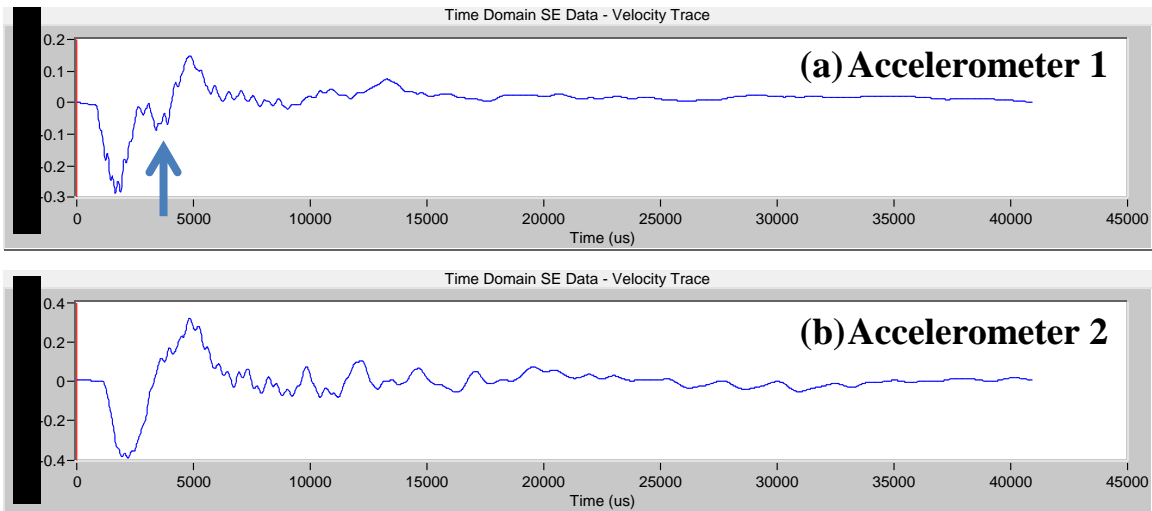


**Figure 114. Velocity Graphs Obtained from Accelerometers 1 and 2 (Test 20)**

**Table 30. Specifications of SE Tests Conducted on Pile M-1.**

Test No.	Hammer Tip	Striking Condition	D <sub>1</sub> (ft)	D <sub>2</sub> (ft)
1	Hard	On block	1	6
2	Hard	On a nail of the bracing	1	6
3	Hard	Top of pile cap	1	6
4	Hard	Top of pile cap	1	6
5	Hard	Top of pile cap	2	5
6	Medium-hard	Top of pile cap	2	5
7	Medium-hard	Top of pile cap	2	5
8	Medium-hard	Top of pile cap	2	5
9	Medium-soft	Top of pile cap	2	5
10	Medium-soft	Top of pile cap	2	5
11	Medium-soft	Top of pile cap	2	5
12	Hard	Upward on pile cap	2	5
13	Hard	Upward on pile cap	2	5
14	Medium-soft	Upward on pile cap	2	5
15	Medium-soft	Upward on pile cap	2	5
16	Soft	Upward on pile cap	2	5
17	Soft	Upward on pile cap	2	5
18	Hard	On wedge	2	5
19	Hard	On wedge	2	5
20	Medium-hard	On wedge	2	5
21	Medium-hard	On wedge	2	5
22	Medium-hard	On wedge	2	5
23	Medium-soft	On wedge	2	5
24	Medium-soft	On wedge	2	5
25	Medium-soft	On wedge	2	5
26	Soft	On wedge	2	5
27	Soft	On wedge	2	5
28	Soft	On wedge	2	5

**Summary of Results of Bridge No. 1190** The results of all the tested piles are summarized in Table 31. The success rate of SE tests at this site is 87.5%.

**Table 31. SE Tests Results for Piles of Bridge No. 1190.**

Pile	Embedment Pile Length (ft)	Exposed Pile Length (ft)	Total Pile Length (ft)
B	15.1	5.3	20.4
E	15.7	4.6	20.3
1	15.5	7.4	22.9
8	13.9	6.1	20
10	15.3	7.7	23
M-1	-	-	-
M-5	18.4	11.5	29.9
M-7	11	11.5	22.5

#### **3.1.4.4 Bridge No. 1676**

Bridge No. 1676 is located 11 miles north of Socorro on I-25 Frontage Road (coordinates 34.211303, -106.921087). It is a 4-span bridge supported by square timber piles. The location and street view of the bridge are shown in Figures 115 and 116, respectively. The as-built foundation depth of this bridge was used to verify the results of SE/IR tests.



**Figure 115. Location of Bridge No. 1676**



**Figure 116. Street View of Bridge No. 1676**



The foundation plan and the investigated piles are indicated in Figure 117. SE tests were performed on three timber piles indicated in the figure. The SE tests were done with four different hammer tips including hard, medium-hard, medium-soft, and soft. Two accelerometers were attached to the side of the piles as shown in Figure 118. The wooden blocks were glued onto the pile surface.

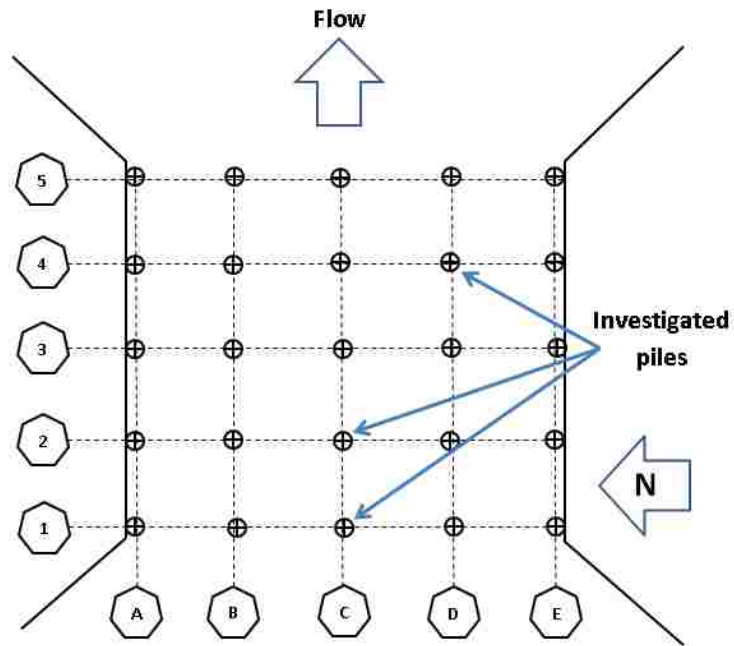


**Figure 117. Foundation Plan and Investigated Piles of Bridge No. 1676**



**Figure 118. Accelerometers Attached onto a Pile**

**SE/IR Tests on Piles C-1 (SE Analysis)** Eighteen SE/IR tests were performed on this pile. The source was applied by three different methods: downward striking at the top of the pile cap, upward striking at the pile cap near the pile, and inclined striking on a wooden wedge attached on the side of the pile. The source by inclined striking on a wedge wooden block was examined on this pile. The striking points (A and B), the locations of the wooden wedge and the accelerometers are shown in Figure 119. The location and the direction of hammer strikes of each test are indicated in Table 32.

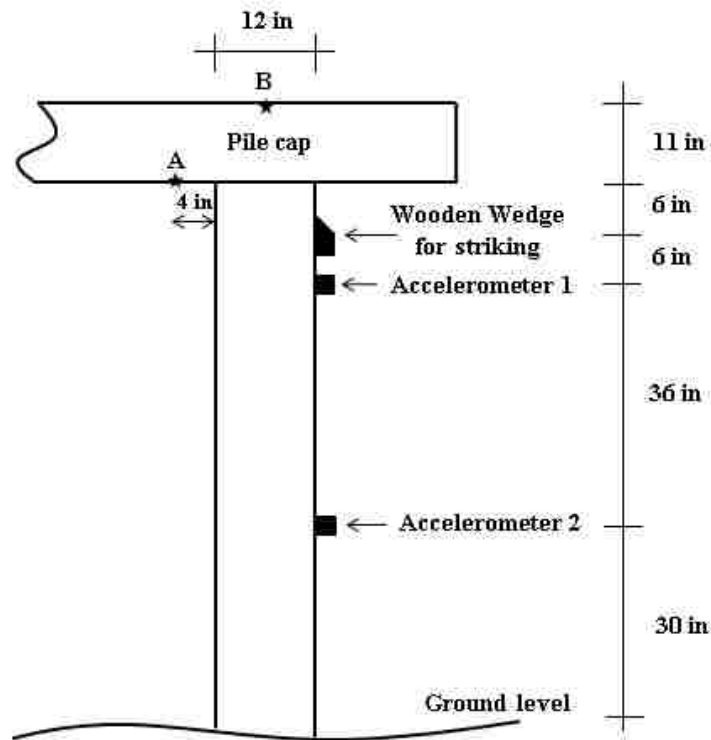


**Figure 119. SE Setup for Pile C-1**

Out of those eighteen SE tests, only the SE tests performed by striking on the pile cap above the pile produce useful velocity graphs. The other two striking methods did not produce good results. An example of useful velocity graph is shown in Figure 120. The impulse and the echo can be identified in the velocity graph (Test 4, Accelerometer 1).  $\Delta t$  is 4.56 ms. With the assumed velocity of 10,000 ft/s, the buried length is 22.8 ft and the length of the pile is 23.8 ft. Table 33 shows the pile lengths determined from the four successful SE tests. The average length of the pile is 24.4 ft.

Echoes could not be identified in the velocity graphs of the SE tests by upward striking at Point A (at the pile cap near the pile). It may be due the small energy of the down-going compressive wave along the pile such that the echo from the pile toe cannot be detected. The shape of the source signal when striking the wooden wedge showed multiple peaks. It indicated poor connection between the wedge and the pile. Very complicated vibration phenomenon was observed in the velocity graphs that made the echo determination difficult.

**Table 32. Location and Direction of Hammer Strikes for Pile C-1.**

Test No.	Hammer Tip	Striking Condition
1	Hard	Downward at B
2	Medium-hard	Downward at B
3	Med-soft	Downward at B
4	Soft	Downward at B
5	Hard	Upward at A
6	Hard	Upward at A
7	Hard	Upward at A
8	Hard	Upward at A
9	Medium-hard	Upward at A
10	Medium-soft	Upward at A
11	Soft	Upward at A
12	Soft	Upward at A
13	Hard	Inclined on wedge
14	Hard	Inclined on wedge
15	Hard	Inclined on wedge
16	Medium-hard	Inclined on wedge
17	Medium-soft	Inclined on wedge
18	Soft	Inclined on wedge

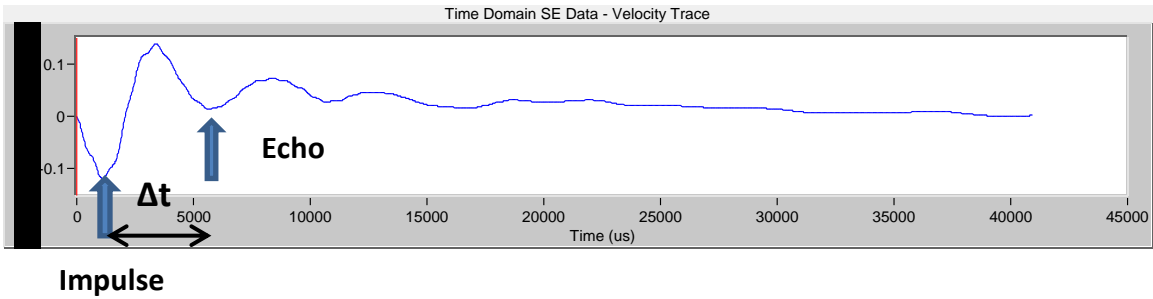


**Figure 120. Velocity Graph of Test 4 Conducted on Pile C-1**

**Table 33. Calculated Pile Lengths of Pile C-1.**

Test No.	Accelerometer 1		Accelerometer 2	
	$\Delta t$ ( $\mu s$ )	$L_t$ (ft)	$\Delta t$ ( $\mu s$ )	$L_t$ (ft)
1	4600	24	- *	-
2	4580	23.9	4380	25.9
3	4500	23.5	4020	24.1
4	4560	23.8	4320	25.6

**SE/IR Tests on Piles C-1 (IR Analysis)** IR analyses were carried out for the eighteen SE/IR tests mentioned previously. The first resonant frequencies and the estimated length of the pile for these eighteen tests are indicated in Table 34.

The pile length was estimated from the first resonant frequencies and the pile length was calculated:

$$L_t = \frac{v}{2 \times \Delta f}$$

$\Delta f$ : First resonant frequency (Hz)

$v$ : Assumed wave velocity = 10000 ft/s

**Table 34. First Resonant Frequencies of IR Analysis for Pile C-1.**

Test No.	Accelerometer 1 (Hz)	Accelerometer 2 (Hz)
1	210	210
2	210	210
3	208	208
4	208	208
5	-	210
6	208	-
7	208	-
8	208	208
9	208	-
10	208	-
11	208	-
12	210	210
13	-	-
14	-	-
15	-	-
16	-	-
17	-	-
18	-	-

The average pile lengths determined by IR analysis for the three source applications are listed in Table 35. Downward striking at Point *B* produced good estimation of pile length. The time domain analysis on the results of upward striking on Point *A* did not reveal the pile length. In contrast, IR analysis did produce a reasonable pile length (24 ft) from the data of Accelerometer 1 (closer to the pile top). The value is similar to 24.4 ft, the average pile length determined from SE analysis. We should try our best to place one accelerometer as close as to the pile top in SE/IR tests.

Poor results were obtained when the source was applied by striking the wedge. Thus, wooden wedge is not recommended as striking blocks.

**Table 35. Average First Resonant Frequencies and Calculated Lengths of Pile C-1.**

Striking Condition	Average $\Delta f$ (Hz)	$L_t$ (ft)
Downward at Point B	209	23.9
Upward at Point A	208.6	24
Inclined on wedge	-	-

**SE/IR Tests on Pile C-2 (SE Analysis)** Twelve SE/IR tests were conducted on Pile C-2 with different hammer tips. The source was created by downward striking on pile cap above the pile, downward striking on the pile cap near the pile, and upward striking on the pile cap near the pile. Figure 121 shows the source (Points A, B, and C) and receiver locations and Table 36 lists the specifications of these SE/IR tests.

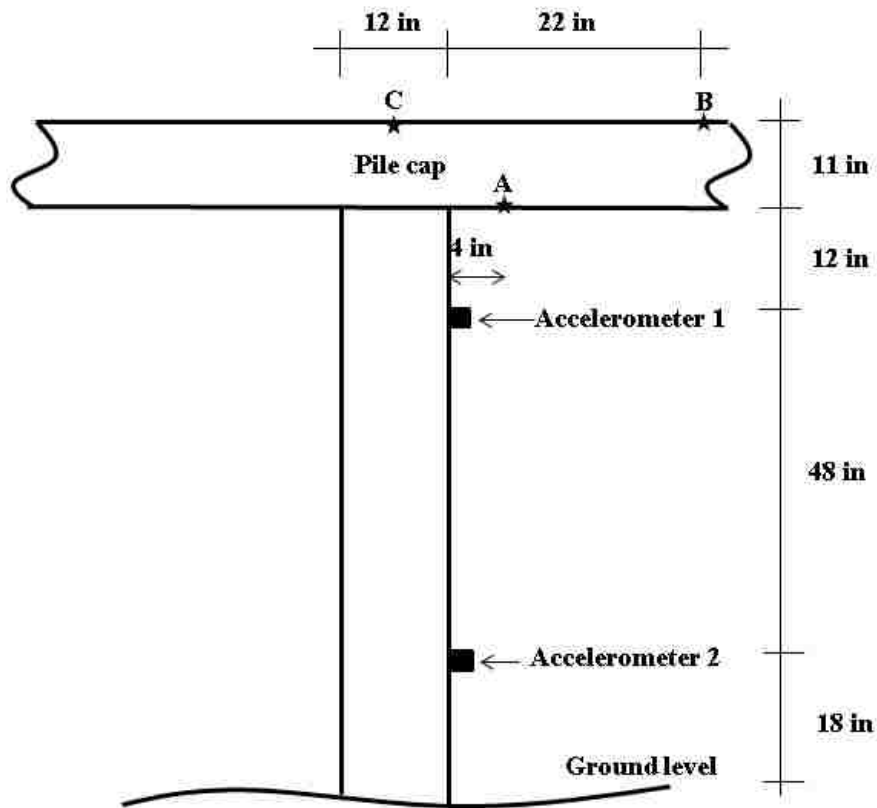


**Figure 121. SE/IR Setup for Pile C-2**

**Table 36. Location and Direction of Hammer Strikes for Pile C-2.**

Test No.	Hammer Tip	Location and Direction of Hammer Strike
1	Hard	Downward at C
2	Medium-hard	Downward at C
3	Medium-soft	Downward at C
4	Soft	Downward at C
5	Hard	Downward at B
6	Medium-hard	Downward at B
7	Medium-soft	Downward at B
8	Soft	Downward at B
9	Hard	Upward at A
10	Medium-hard	Upward at A
11	Medium-soft	Upward at A
12	Soft	Upward at A

When the impulse and echo were identified on the velocity graphs, the buried pile length and the total pile length were calculated. The calculated pile lengths from these SE/IR tests are indicated in Table 37. More successful SE tests were found when the striking point was closer to the pile. This is because more energy can be transmitted down the pile. If the impulse and echo were identified from the SE tests of different sources (Striking at Points A, B, or C), similar pile lengths were obtained.

**Table 37. Calculated Pile Lengths of Pile C-2.**

Test No.	Accelerometer 1		Accelerometer 2	
	$\Delta t$ ( $\mu s$ )	$L_t$ (ft)	$\Delta t$ ( $\mu s$ )	$L_t$ (ft)
1	-	-	-	-
2	-	-	3860	24.3
3	4520	23.6	4140	25.7
4	4980	25.9	4820	29.1
5	-	-	-	-
6	4540	23.7	3720	23.6
7	-	-	-	-
8	-	-	-	-
9	-	-	-	-
10	4320	22.6	3700	23.5
11	-	-	-	-
12	-	-	3860	24.3

The average length of each striking method was calculated and the result is presented in Table 38.

**Table 38. Average Calculated Pile Lengths of Pile C-2.**

Striking Condition	Average $L_t$ (ft)
Downward at C	24.5
Downward at B	23.6
Upward at A	23.5

**SE/IR Tests on Pile C-2 with IR analysis** The IR Analysis were carried out for these twelve SE/IR tests. The success rate was low and the first resonant frequencies were identified for some tests as indicated in Table 39. The first frequency is equal to 210 Hz for Tests 2, 5, 6, and 7. The estimated pile length is 23.8 ft with an assumed wave velocity of 10,000 ft/s. For upward striking at A, IR analysis did not lead to pile length while SE analysis did. However, the overall success rate from IR analysis was unacceptable.



Therefore, it is recommended that the IR analysis should be used as the secondary and SE analysis be considered as the primary analysis tool.

**Table 39. First Resonant Frequencies (Hz) for Pile C-2.**

Test No.	Accelerometer 1	Accelerometer 2
1	-	-
2	210	-
3	-	-
4	-	-
5	-	210
6	210	-
7	-	210
8	-	-
9	-	-
10	-	-
11	-	-
12	-	-

**SE/IR Tests on Piles D-4 (SE Analysis)** Twelve SE/IR tests were conducted on Pile D-4 with different hammer tips. Figure 122 shows the locations of the three sources (A, B, and C) and the locations of the two accelerometers. The longitudinal wave was created by striking downward at C, upward at A, and downward at B. The specifications of the SE/IR tests are indicated in Table 40.

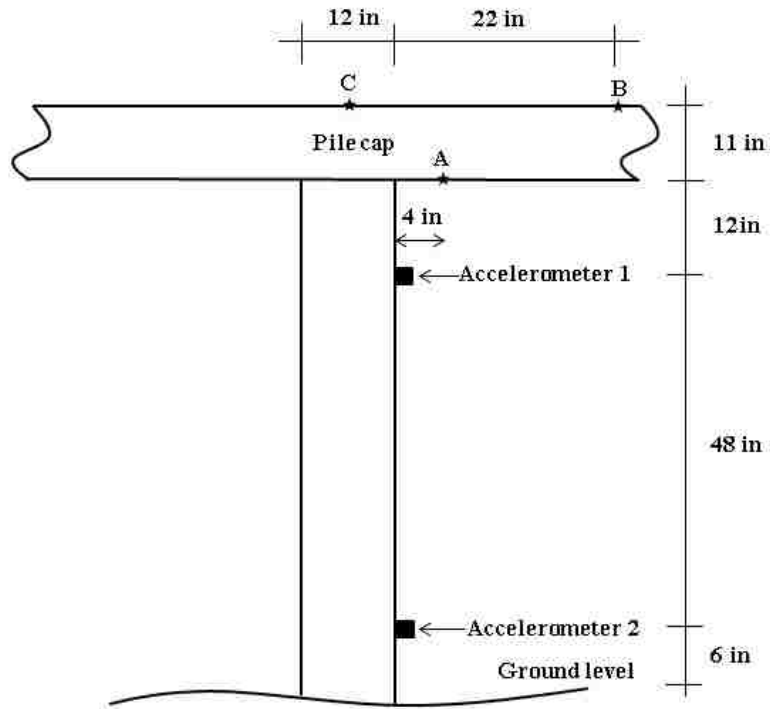


**Figure 122. SE Setup for Pile D-4**

**Table 40. Location and Direction of Hammer Strikes for Pile D-4.**

Test No.	Hammer Tip	Location and Direction of Hammer Strike
1	Hard	Downward at C
2	Medium-hard	Downward at C
3	Medium-soft	Downward at C
4	Soft	Downward at C
5	Hard	Upward at A
6	Medium-hard	Upward at A
7	Medium-soft	Upward at A
8	Soft	Upward at A
9	Hard	Downward at B
10	Medium-hard	Downward at B
11	Medium-soft	Downward at B
12	Soft	Downward at B

Table 41 shows the pile lengths calculated from these SE tests. For SE tests with clear impulse and echo in the velocity graphs, the lengths of the pile were calculated. The calculated pile lengths are indicated in Table 41.

**Table 41. Calculated Pile Lengths of Pile D-4.**

Test No.	Accelerometer 1		Accelerometer 2	
	$\Delta t$ ( $\mu s$ )	$L_t$ (ft)	$\Delta t$ ( $\mu s$ )	$L_t$ (ft)
1	-	-	4580	27.9
2	4420	23.1	-	-
3	4920	25.6	-	-
4	-	-	-	-
5	4280	22.4	-	-
6	4640	24.2	4600	28
7	4660	24.3	-	-
8	-	-	-	-
9	-	-	-	-
10	-	-	-	-
11	-	-	-	-
12	-	-	-	-

The success rate of downward striking at Point B (22 inches away from the test pile) is lower than the success rates of downward striking at Point C (above the pile) and upward striking at Point A (4 inches from the pile). Once again, the result indicated that the striking point should be as close to the pile as possible to guarantee the generation of waves with the greatest possible energy.

The average lengths for downward striking at C and upward striking at A are 25.5 and 24.7 ft, respectively.

**SE/IR Tests on Piles D-4 (IR analysis)** The IR analysis was carried out to supplement the SE analysis. The first resonant frequencies of all tests are indicated in Table 42. A single resonant frequency (208 Hz) was identified and the corresponding pile length

is 24 ft. This value supported the finding obtained from the time domain analysis (23.1 to 28 ft).

**Table 42. First Resonant Frequencies (Hz) for Pile D-4.**

Test No.	Accelerometer 1	Accelerometer 2
1	208	208
2	208	208
3	208	208
4	208	208
5	-	208
6	208	208
7	208	208
8	208	208
9	-	-
10	208	208
11	208	208
12	208	208

**Summary of SE/IR Results at Bridge No. 1676** The results of all test piles are summarized in Table 43. The error is less than 10% that is within the accuracy range of SE/IR tests. The success rate in determining the pile length is 100% at this site.

**Table 43. SE Tests Results of Piles at Bridge No. 1676.**

Pile	Embedment Pile Length (ft)	Exposed Pile Length (ft)	Total Pile Length (ft)	As-built Pile Length (ft)	Error(%)
C-1	17.6	6.5	24.1	23	4.8
C-2	17.3	6.5	23.8	23	3.5
D-4	18.9	5.5	24.4	23	6.1

### 3.1.4.5 Partially Dismantled Bridge near Route 419 (Bridge No. 6253)

The partially dismantled bridge (Bridge No. 6253) is located 64 miles east of Las Vegas. The bridge was used to be on Route 419 (coordinates 34.211303, -106.921087). Figure 123 shows the location of the bridge. Route 419 was realigned and the bridge was no longer in service. The superstructure of the bridge was removed when the research team arrived at the site. Only pile caps and round timber piles were presented as shown in Figure 124.



**Figure 123. Location of the Partially Dismantled Bridge near Route 419**



**Figure 124. Photo of the Partially Dismantled Bridge near Route 419**

This site was selected because the piles are going to be pulled out. The actual pile length finally become known which enables the research team to verify the results of nondestructive tests. SE/IR tests were conducted on five piles as shown in Figure 125. Since the findings were very similar to the conclusions of previous bridges on timber piles the results are not elaborated here. The results including the embedment pile lengths and the total pile lengths are listed in Table 44.

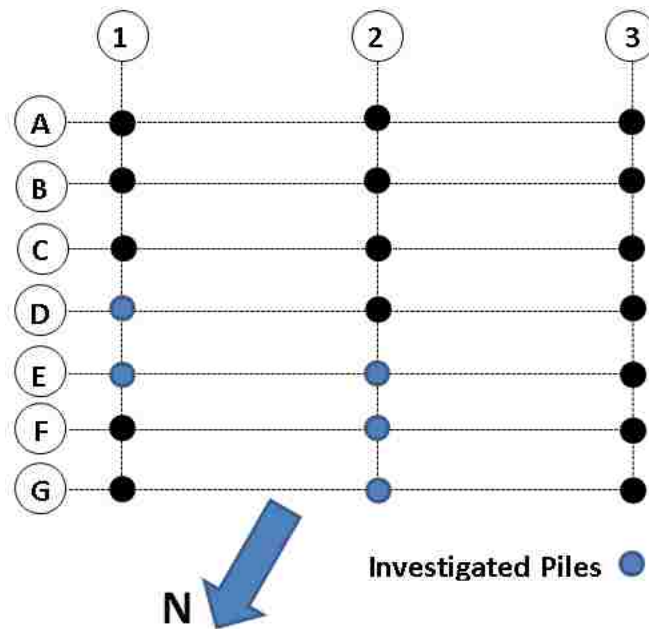


**Figure 125. Investigated Piles of the Partially Dismantled Bridge near Route 419**

**Table 44. SE Tests Results of the Partially Dismantled Bridge near Route 419.**

Pile	Embedment Pile Length (ft)	Exposed Pile Length (ft)	Total Pile Length (ft)
D-1	8.60	6.2	14.8
E-1	8.15	6.25	14.4
E-2	8.74	7.0	15.7
F-2	7.66	7.42	15.1
G-2	6.95	7.25	14.2

### 3.1.4.6 Bridge No. 7480

Bridge No. 7480 is located north of Shiprock, NM, on NM 491 crossing, over the Salt Creek. The coordinates of the bridge are 36.826389, -108.692500. Figures 126 and 127 show the location of the site and the street view of the bridge, respectively. The bridge is supported by 11 battered and 11 straight steel-H piles. The piles were extended from the bottom of the superstructure to the ground level, and continued under the ground surface to form the foundation.



**Figure 126. Location of Bridge No. 7480**



**Figure 127. Street View of Bridge No. 7480**

Although SE tests were found unsuitable for H-piles in the literature (2, 19), the research team also elected to conduct SE tests to explore the possibility of the piles depths detection by various test configurations.

Holes had been predrilled by NMDOT engineers. Metal blocks for striking and mounting accelerometer were attached onto the web of the H-pile with bolts. Two accelerometers were used. A nonconventional SE test setup is shown in Figure 128. The source (hammer striking) was between two accelerometers. Although numerous SE tests of different setups were performed on different piles, none of the results were successful.

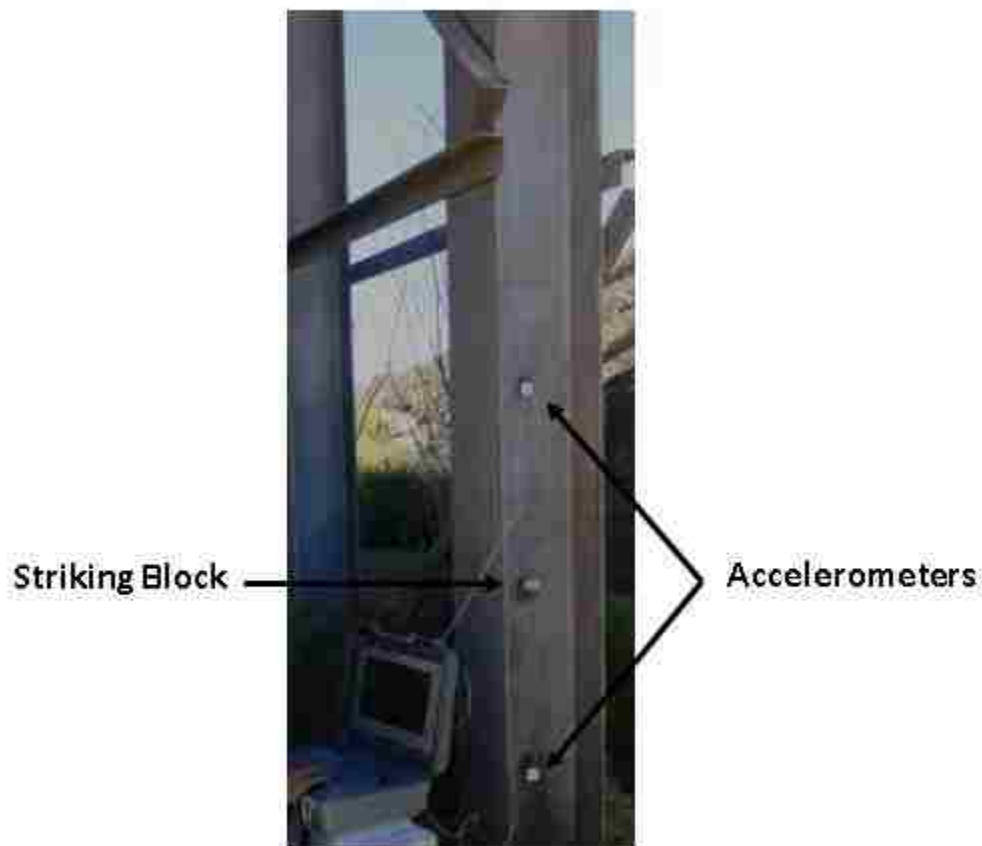


**Figure 128. SE Test Setup for a H-pile of Bridge No. 7480**

Figure 129 shows a typical velocity graph obtained from a vertical striking on the metal block attached to the H-pile web. High frequency vibrations are evident in this figure. The high frequency response corresponds to the reflections from the boundaries of the steel cross section. When a strike is applied at the middle of the web, the wave travels



horizontally as well as vertically through the thin-walled members, unlike circular (or square) solid piles in which most energy travels downward. The sensor picks up the reflected waves from the free boundaries, which in turn interfere with the expected reflected longitudinal wave from the pile bottom.

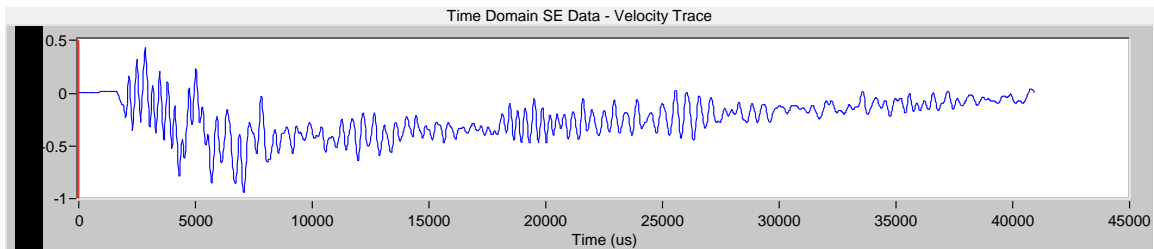


**Figure 129. Velocity Time History Signal Obtained from Vertical Striking on a Metal Block Attached to a H-pile**

Apart from the difficulties mentioned above, steel H-piles transmit a large portion of the wave energy into the surrounding soil due to their specific cross section configuration. Less energy is transmitted to the pile bottom, which significantly decreases the amplitude of the echo from the pile toe.

#### **3.1.4.7 Bridge No. 5899**

In addition to the NDT tests performed on timber piles, the research team decided to conduct SE tests on concrete piers. Bridge No. 5899 in District 5 was selected for testing since there are three intermediate concrete piers. The bridge is located 66 miles north of Santa Fe on NM 111 crossing over the Rio Vallecitos as shown in Figure 130. The coordinates of the bridge are 36.49485, -106.1124972. The street and aerial views of the bridge are shown in Figure 131. The bridge is a 4-span concrete bridge supported by three intermediate concrete piers. The side view of one of the piers is indicated in Figure 132.



**Figure 130. Location of Bridge No. 5899**

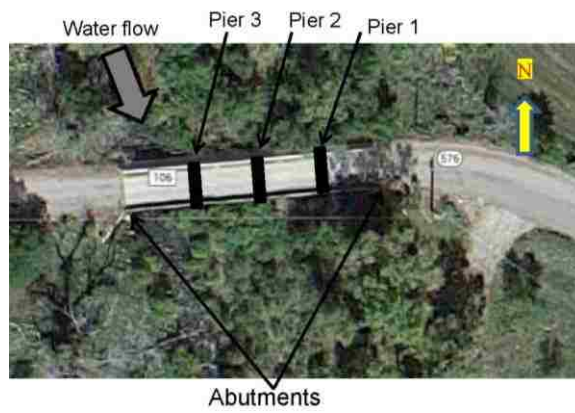


**Figure 131. Street and Aerial Views of Bridge No. 5899**



**Figure 132. Side View of One of the Piers**





**Figure 134. Attached Accelerometers on the Pier Side**

**Wave Velocity Measurement** Before conducting SE tests to determine the buried lengths of the piers, the propagated wave velocity in the concrete pier was measured. Three horizontal strikes with hard hammer tip were applied at Point F (see Figure 133) and the time difference between the impulse and echo obtained from a horizontally placed accelerometer at Point 3 were measured. The generated wave from the horizontal strike reaches the accelerometer, reflects from the opposite side of the pier and arrives at the accelerometer again. Since the horizontal pier width is known, the wave velocity can be determined. The results are indicated in Table 46.

**Table 46. Estimated Wave Velocities of the Concrete Pier.**

Test No.	$\Delta t$ ( $\mu s$ )	$v$ (ft/s)
1	3,060	10,784
2	3,100	10,645
3	3,100	10,645

The average velocity (10,700 ft/s) was used to calculate the buried lengths of the piers for all SE tests conducted on the piers. For each SE test, the impulse and echo were sought in the velocity graphs and the  $\Delta t$  was used to determine the buried length.

**SE tests on Pier 1** Fifteen SE tests were conducted on the north side of Pier 1. Three different hammer tips (hard, medium-hard, and medium-soft) and two striking directions (horizontal and vertical) were used. Table 47 shows the hammer tips and the striking locations and directions for each test. The locations can be found in Figure 133.

**Table 47. Hammer Tips and Striking Locations and Directions for Testing at the North Side of Pier 1.**

Test No.	Hammer Tip	Location (Direction) of Hammer Strike
1	Hard	A(horizontal)
2	Hard	A(horizontal)
3	Hard	A(horizontal)
4	Hard	B(horizontal)
5	Hard	B(horizontal)
6	Hard	B(horizontal)
7	Hard	E(vertical)
8	Hard	E(vertical)
9	Hard	E(vertical)
10	Medium-hard	E(vertical)
11	Medium-hard	E(vertical)
12	Medium-hard	E(vertical)
13	Medium-soft	E(vertical)
14	Medium-soft	E(vertical)
15	Medium-soft	E(vertical)

Table 48 shows the estimated lengths of the pier wall based on the SE results. The measured concrete wave velocity of 10700 ft/s was used to calculate the length of the pier wall. Horizontal striking did not produce useful results (echo from the bottom cannot be identified in the velocity graphs). Vertical striking generated good velocity graphs such that the echo from the bottom was identified easily. The average embedment depth of the pier wall is 22 ft and the height of the pier wall is 23.8 ft.

**Table 48. Results of SE Tests Conducted at the North Side of Pier 1.**

Test No.	Striking Direction	Accelerometer 1		Accelerometer 2	
		$\Delta t$ ( $\mu s$ )	$L_t$ (ft)	$\Delta t$ ( $\mu s$ )	$L_t$ (ft)
1	Horizontal	--	--	--	--
2	Horizontal	--	--	--	--
3	Horizontal	--	--	--	--
4	Horizontal	--	--	--	--
5	Horizontal	--	--	--	--
6	Horizontal	--	--	--	--
7	Vertical	4000	21.9	3220	21.7
8	Vertical	3900	21.4	3080	21.0
9	Vertical	--	--	3420	22.8
10	Vertical	4280	23.4	3340	22.4
11	Vertical	4200	23.0	3320	22.3
12	Vertical	4300	23.5	3360	22.5
13	Vertical	4420	24.1	3280	22.0
14	Vertical	4440	24.3	3140	21.3
15	Vertical	4000	21.9	3220	21.7

**SE/IR Tests at South Side of Pier 2 by SE Analysis** Twenty SE/IR tests were conducted at the south side of Pier 2. The source was applied on five different points with three different hammer tips. The strikes were the horizontal striking on the south (or west) side of the pier wall, upward striking on the pile cap (or on the bottom of the bridge deck), and vertical downward striking on the bridge deck above the pier wall. Figure 135 shows the application of upward striking on the pile cap and on the bottom surface of the bridge deck. Table 49 shows the used hammer tips and the location and direction of the hammer strike for each test at the south side of Pier 2. Table 50 shows the results of SE tests conducted at the south side of Pier 2. Similar to Pier 1, horizontal striking (Tests 1-3 and 9-11) did not produce useful data and consequently the pier length was not determined. The length of the pier was determined from SE tests of all vertical striking. The average length of Pier 2 at the south side is 26.8 ft.

**Table 49. Hammer Tips, Location, and Direction of Hammer Strikes at the South Side of Pier 2.**

Test No.	Hammer Tip	Location (Direction) of the Hammer Strike
1	Hard	A (Horizontal)
2	Hard	A (Horizontal)
3	Hard	A (Horizontal)
4	Hard	C (Vertical-upward)
5	Hard	C (Vertical-upward)
6	Hard	C (Vertical-upward)
7	Hard	D (Vertical-upward)
8	Hard	D (Vertical-upward)
9	Hard	B (Horizontal)
10	Hard	B (horizontal)
11	Hard	B (horizontal)
12	Hard	E (vertical)
13	Hard	E (vertical)
14	Hard	E (vertical)
15	Medium-hard	E (vertical)
16	Medium-hard	E (vertical)
17	Medium-hard	E (vertical)
18	Medium-soft	E (vertical)
19	Medium-soft	E (vertical)
20	Medium-soft	E (vertical)



**Figure 135. Upward Striking on the Pile Cap and on the Bridge Deck**

**Table 50. Results of SE Tests Conducted at the South Side of Pier 2.**

Test No.	Accelerometer 1		Accelerometer 2	
	$\Delta t$ ( $\mu s$ )	$L_t$ (ft)	$\Delta t$ ( $\mu s$ )	$L_t$ (ft)
1 ~ 3	--	--	--	--
4	--	--	4020	26.5
5	4,740	26.4	3880	25.8
6	-	-	4040	26.6
7	4,880	27.1	--	--
8	4,800	26.7	--	--
9 ~ 11	--	--	--	--
12	5,240	29.0	3660	24.6
13	5,220	28.9	3800	25.3
14	5,200	28.8	3800	25.3
15	5,020	27.9	3880	25.8
16	5,100	28.3	3720	24.9
17	5,100	28.3	3880	25.8
18	4,960	27.5	3960	26.2
19	5,020	27.9	4040	26.6
20	5,020	27.9	3880	25.8



**SE/IR tests at South Side of Pier 2 by IR Analysis** The IR analysis has been previously applied to SE/IR tests on timber piles. It was demonstrated that IR analysis may provide additional information on determining the length of the pile. When the impulse and echo are undistinguishable in the velocity graph of SE analysis, IR analysis may be able to provide a reasonable estimation regarding the buried depth by using the resonant frequencies. The resonant frequencies and corresponding calculated buried pier lengths at the south side of Pier 2 are indicated in Table 51. Similar to the SE analysis, horizontal striking (Tests 1-3 and 9-11) did not work either. Data of both accelerometers of all vertical striking produced useful and consistent results. The average height of Pier 2 at the south side is 24.5 ft. This value is less than the average height obtained from SE analysis (26.8 ft).

**Table 51. Resonant Frequencies and Calculated Pier Lengths at the South Side of Pier 2.**

Test No.	Accelerometer 1		Accelerometer 2	
	$\Delta f$ (Hz)	$L_t$ (ft)	$\Delta f$ (Hz)	$L_t$ (ft)
1 ~3	--	--	--	--
4	218	24.5	224	23.9
5	218	24.5	224	23.9
6	218	24.5	224	23.9
7	218	24.5	220	24.3
8	218	24.5	220	24.3
9 ~ 11	--	--	--	--
12	218	24.5	218	24.5
13	216	24.8	218	24.5
14	216	24.8	218	24.5
15	220	24.3	222	24.1
16	218	24.5	220	24.3
17	218	24.5	220	24.3
18	215	24.9	217	24.7
19	215	24.9	217	24.7
20	216	24.8	217	24.7

**SE Tests at the North Side of Pier 2** Twelve SE tests were performed at the north side of Pier 2. Only hard hammer tip was used. The source was applied in four different ways as shown in Table 52. The results of the SE analysis are shown in Table 53.

Again, the results of horizontal striking did not work. Vertical striking produced good velocity graphs that can be used to determine the height of the pier. Examples of good SE velocity graphs (impulse and echo can be identified easily) for the downward and upward vertical strikes are shown in Figures 136 and 137 respectively. Comparing these two figures indicates the change of polarity for upward striking on the pile cap (or the deck) that generated tension wave.

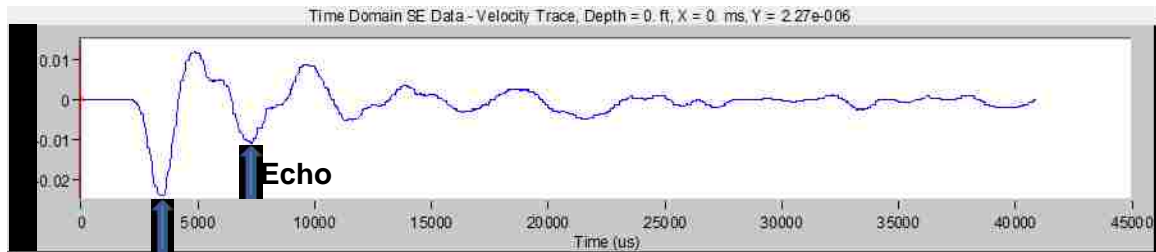
Table 54 shows the average buried depths of Pier 2 at south and north sides for different source applications. The NDT tests show that the embedment depth of pier at north side is 4.6 ft deeper than that of the south side. This may due to the existence of an abnormality at the south side that causes the impedance change.

**Table 52. Hammer Tips, Location, and Direction of Hammer Strikes at the North Side of Pier 2.**

Test No.	Location (Direction) of the Hammer Strike
1	A (Horizontal)
2	A (Horizontal)
3	A (Horizontal)
4	C (Vertical-upward)
5	C (Vertical-upward)
6	C (Vertical-upward)
7	D (Vertical-upward)
8	D (Vertical-upward)
9	D (Vertical-upward)
10	E (Vertical)
11	E (Vertical)
12	E (Vertical)

**Table 53. Results of SE Tests Conducted at the North Side of Pier 2.**

Test No.	Accelerometer 1		Accelerometer 2	
	$\Delta t$ ( $\mu s$ )	$L_t$ (ft)	$\Delta t$ ( $\mu s$ )	$L_t$ (ft)
1 ~ 3	--	--	--	--
4	--	--	5120	32.4
5	--	--	5120	32.4
6	--	--	5060	32.1
7	5940	32.8	5200	32.8
8	5540	30.6	5120	32.4
9	5800	32.0	5200	32.8
10	--	--	5160	32.6
11	--	--	5100	32.3
12	--	--	4860	31.0



**Impulse**

**Figure 136. Typical Velocity Graph of Downward Striking at Point E**

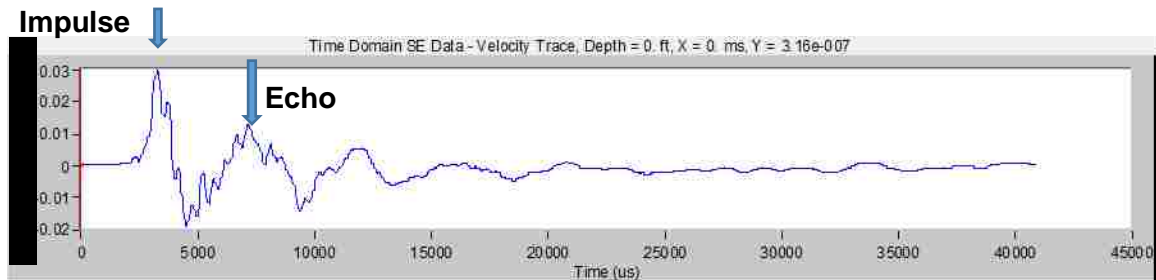


**Figure 137. Typical Velocity Graph of Upward Vertically Striking at Point C**

**Table 54. Average Buried Depths at the South and North Sides of Pier 2.**

Input Method	South Side (ft)	North Side (ft)
Downward striking at E	20.9	25
Upward striking at C	20.3	25.7
Upward striking at D	20.9	25.1

**SE/IR Tests on Pier 3** Fourteen SE tests were conducted at the north end of Pier 3 with the hard hammer tip. The source was applied in four different ways as indicated in Table 55.

**Table 55. Direction and Location of Hammer Strike at the North Side of Pier 3.**

Test No.	Location (Direction) of the Hammer Strike
1	A (Horizontal)
2	A (Horizontal)
3	A (Horizontal)
4	C (Vertical-upward)
5	C (Vertical-upward)
6	C (Vertical-upward)
7	D (Vertical-upward)
8	D (Vertical-upward)
9	D (Vertical-upward)
10	E (Vertical)
11	E (Vertical)
12	E (Vertical)
13	E (Vertical)
14	E (Vertical)

Table 56 shows the results of SE tests conducted at the north end of Pier 3. Some of the velocity graphs of Accelerometer 1 showed multiple echoes of similar magnitudes which made it difficult to determine the right echo from the toe. This was not expected since the accelerometer was close to the bridge deck. It was not due to the mounting or the

malfunctioning of the accelerometer. Therefore, it is a good practice to use more than one accelerometer for SE/IR tests.

Table 57 lists the buried lengths and the total lengths of the pier at the north side using different striking methods. Consistent results were found and the average buried and total length are 16.3 ft and 23.5 ft respectively.

**Table 56. Results of SE Tests Conducted at the North Side of Pier 3.**

Test No.	Accelerometer 1			Accelerometer 2		
	$\Delta t$ ( $\mu s$ )	$L_t$ (ft)	$L_b$ (ft)	$\Delta t$ ( $\mu s$ )	$L_t$ (ft)	$L_b$ (ft)
1 ~ 3	--	--	--	--	--	--
4	4000	21.4	14.2	3540	24.3	17.1
5	4480	24.0	16.8	--	--	--
6	4220	23.9	16.7	3540	24.3	17.1
7	--	--	--	3300	23.0	15.8
8	--	--	--	--	--	--
9	3940	21.1	13.9	3600	24.6	17.4
10	--	--	--	3460	23.8	16.7
11	--	--	--	3480	24.0	16.8
12	--	--	--	3480	24.0	16.8
13	--	--	--	3500	24.1	16.9
14	--	--	--	3420	23.6	16.5

**Table 57. Average Buried Lengths at the North Side of Pier 3.**

Striking Method	Buried Length (ft)	Total Length (ft)
Downward striking at E	16.7	23.9
Upward striking at C	16.4	23.6
Upward striking at D	15.7	22.9

The SE tests data obtained at this bridge are consistent. The results showed that the source applied by horizontal striking was not working at all. Upward striking on the pile cap and the bridge deck generated acceptable results. Downward striking at the bridge deck

above the pier was the best way to apply the source. Although the better location of the sensor is the one close to the top of the pier in general, bad results were obtained occasionally. The additional accelerometer provides the necessary redundancy. Otherwise, the SE test needs to be repeated by placing the accelerometer at a different location.

**Summary of SE/IR Results on Bridge No. 5899** The test results are summarized in Table 58 and the success rate is 100% for this bridge.

**Table 58. SE Tests Results for Piles of Bridge No. 5899.**

Pier	Embedment Length of the Pier (ft)	Total Length of the Pier (ft)
1-(North Side)	16.0	22.6
2-(South Side)	20.9	27.2
2-(North Side)	25.0	32.8
3-(North Side)	16.7	23.7

### 3.2 Parallel Seismic Tests

PS tests can be used to determine the pile length for piles of all materials (timber, concrete, and steel). Also, the method can detect the pile length that is too long for being detected by SE/IR tests. Moreover, the PS method can be applied to detect the lengths of buried piles underneath a pile cap or a pier wall. The major disadvantage of the method is the requirement of drilling a borehole next to the pile with a depth deeper than the pile.

To study the applicability of the method on bridge foundations with different materials, both conventional and reverse test methods were used. Preliminary conventional PS tests were carried out to investigate the performance of the equipment on concrete short piers and to study the factors that affect PS tests results. Then, PS tests were performed on two bridge foundations made of steel H-piles and square timber piles. The as-built foundation depths are available at both sites. In addition to the conventional PS tests, the reverse PS test was performed on square timber piles of a bridge foundation. The reverse PS tests was accomplished with the purchased Geoprobe 7822DT drill rig and the results were compared to that obtained from the conventional PS tests.

### 3.2.1 PS Test Procedure

Before conducting a PS test, a borehole must be drilled next to the foundation. There are requirements for the preparation of the borehole:

- The borehole must align with the test pile.
- The depth of the borehole must be at least 15 ft deeper than the expected pile toe level.
- The hole should be bored as close as possible to the test pile (no more than 6 ft away from the pile).
- A 2-in PVC tube is prepared based on the depth of borehole and the bottom of the tube is capped.
- The PVC tube is inserted into the hole and the annular space between borehole and tube is grouted or filled with compacted soil.
- The PVC tube is filled with water.

The PS test is carried out in three steps: setup the hardware, data acquisition, and data processing.

#### 3.2.1.1 Hardware Assemblage

Figure 138 shows the required equipment for conducting a PS test. The assembled equipment is shown in the figure. Engineers should follow the user manual of the equipment to assemble the device.



Figure 138. PS Equipment

### 3.2.1.2 PS Data Acquisition

The hydrophone is lowered towards the bottom of the PVC tube in an increment of either 1 ft or 2 ft. At each depth, the foundation is struck with a hammer and the software records and plots the signals of the hammer and hydrophone. The software WinGEO-T installed in the Olson Freedom Data PC has been used for data acquisition. A screen shot of the program including the obtained signals is shown in Figure 139.

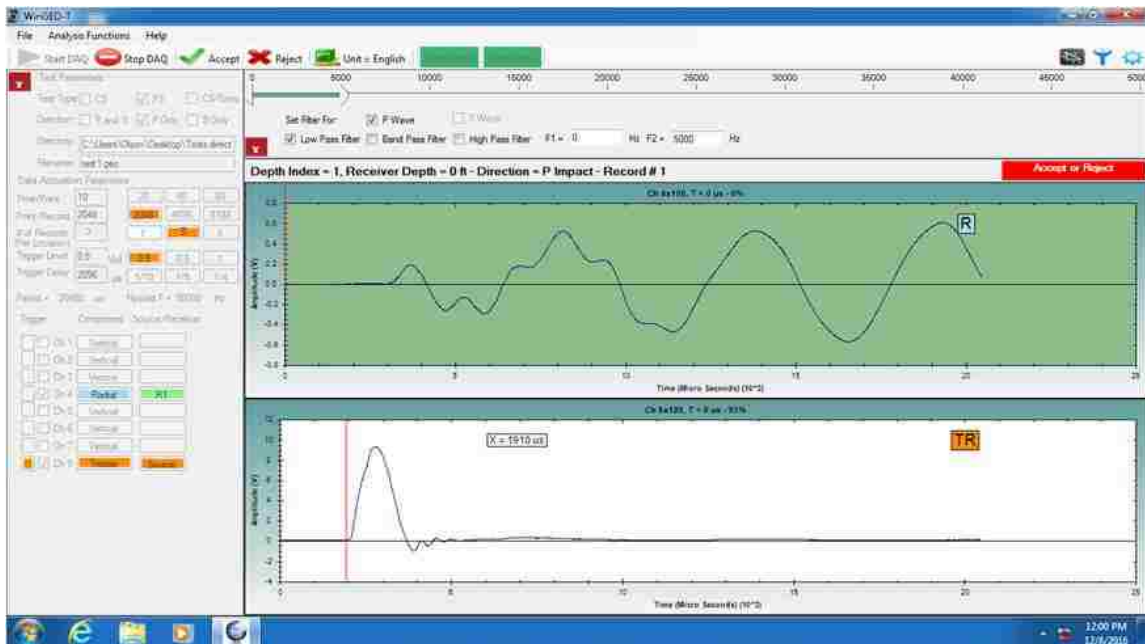
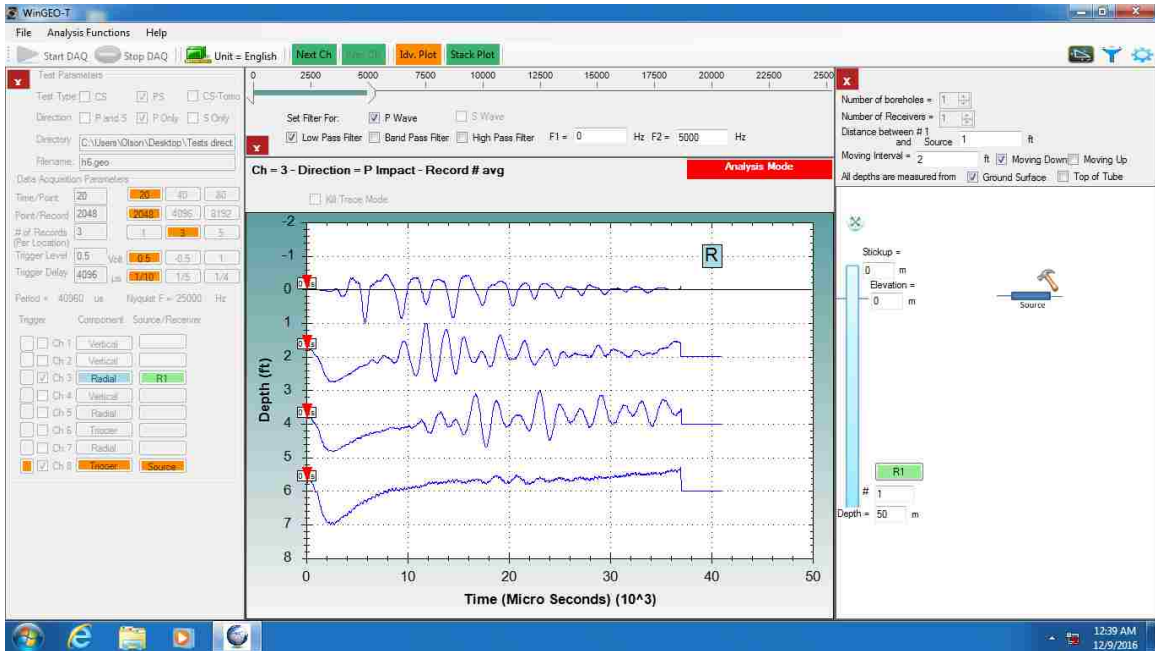


Figure 139. Screen Shot of Software WinGEO-T

### 3.2.1.3 Data Processing

After the data at each depth are gathered, the first arrival time corresponding to each depth can be determined from the velocity graph. Depending on the signal-to-noise ratio in the velocity graphs, the picking of the first arrival time may not be trivial. The correct pile length is determined if the first arrival times are picked correctly. A screen plot of a PS 'Stack Plot' of velocity graphs obtained from four consecutive depths is shown in Figure 140. The details of picking the arrival time and determining the pile toe will be discussed later.





**Figure 140. A Screen Shot of the Stack Plot with Four Consecutive Depths**

### 3.2.2 Preliminary PS Tests

Initial PS tests were conducted at a test site off UNM campus to examine the capability of the equipment. The soil of the test site is silty clay with gravel. A 10-in diameter and 3-ft long reinforced concrete cylinder (pier) was installed at the test site. The PS test setup is shown in Figure 141. The depth of the concrete cylinder is 2 feet below ground. Four 2-in PVC pipes, each 5-ft in length, were installed at various distances from the center of the pile. The PVC pipes were then filled with water. PS tests were conducted by lowering a hydrophone into each of the pipes and impacting the center of the concrete pier with a hammer. The data were collected from each of the pipes at intervals of 1 foot starting at the ground level.



**Figure 141. Configuration of the PS Testbed**

Figure 142 shows the signal generated by the hammer. Figure 143 shows the received signals when the hydrophone is at the ground level and four feet below grade. The distance between the borehole and the concrete cylinder is 2 ft. Comparing Figures 143a and 143b, a delay in arrival time was observed as expected. Figure 143a shows a peak at 8  $\mu\text{s}$  while Figure 143b shows a peak at 9  $\mu\text{s}$ . The 1<sup>st</sup> valleys in Figures 143a and 143b were found at 11  $\mu\text{s}$  and 13  $\mu\text{s}$ , respectively.

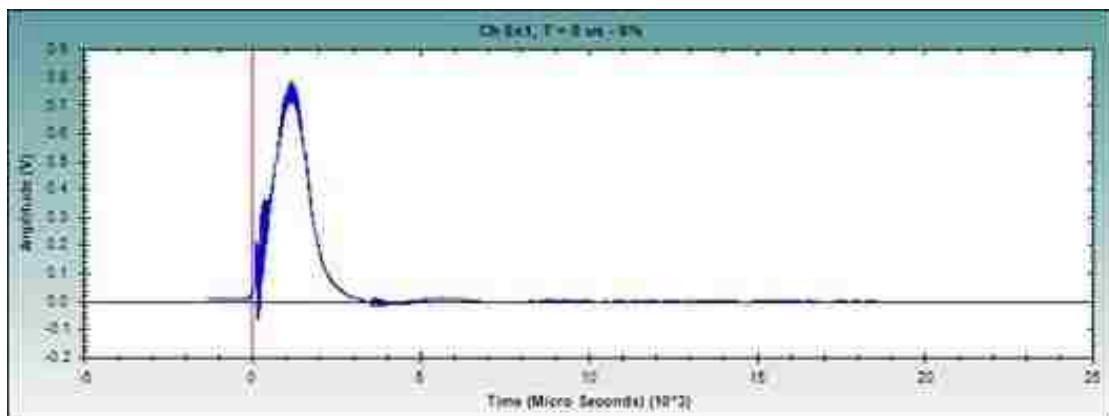


**Figure 142. Duration and Amplitude of the Source Generated by a Hammer**

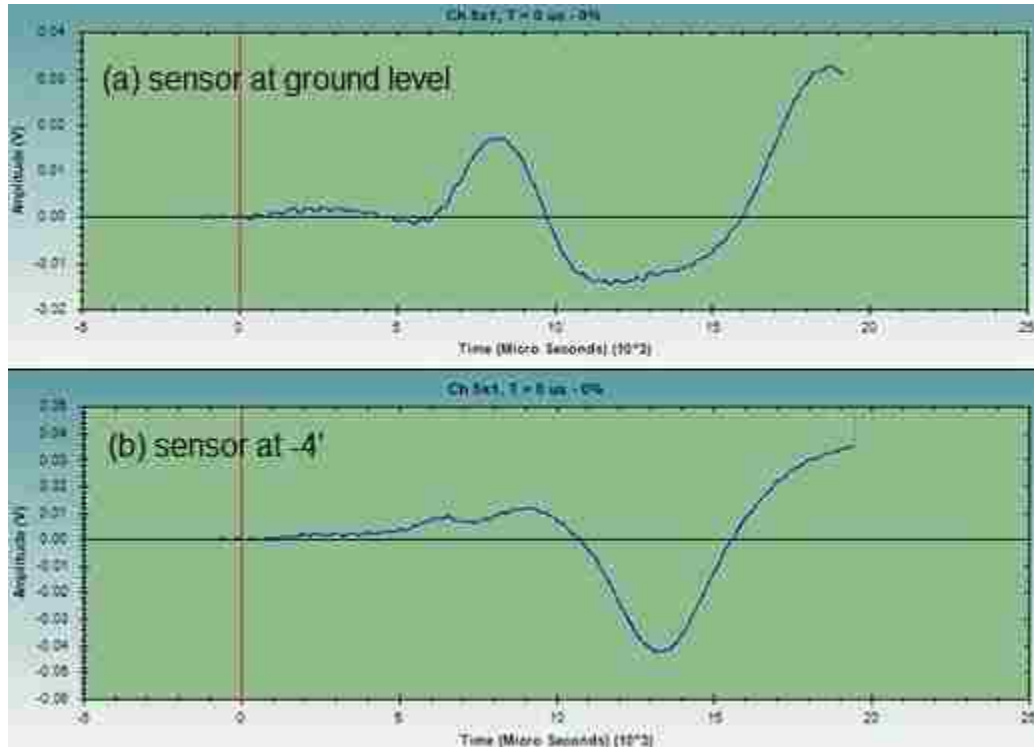


**Figure 143. PS Data at Ground Level and at a Depth of 4 Feet**

Assuming the typical wave velocities in concrete and in soil to be 12,000 ft./sec and 300 ft/sec respectively. The first arrival time should be 6.8  $\mu$ s for the sound travels through 1 ft of concrete and 2 ft of soil for the sensor at the ground level. As shown in Figure 142, the peak of the input signal occurs at approximately 1  $\mu$ s after impact. The 1<sup>st</sup> peak in Figure 143a is at 8  $\mu$ s which is very close to the analytical value ( $7.8 = 6.8 + 1$ ). The time taken for the wave to go through the concrete is insignificant compared to what it takes to go through the soil due to the much lower propagation speed in soil. When the sensor is 4 ft below ground, the analytical arrival time is 9.4  $\mu$ s. There should be a delay of 1.6  $\mu$ s. Figure 143 shows a delay of 1 and 2  $\mu$ s based on the peaks and the valleys respectively. The result is in agreement with the theory.

PS tests were performed using other pipes (3, 4, and 5 ft from the source). For the PS test performed at the pipe placed at 3 ft from the source, the 1<sup>st</sup> peak and the 1<sup>st</sup> valley were at 10 and 13  $\mu$ s respectively when the hydrophone was at the ground level. There was an additional 2  $\mu$ s delay due to the additional one foot of soil in the wave path. Similar observations were found for the PS tests at the pipes 4 ft and 5 ft from the source.

The obtained waveform is always distorted when wave travels through various media. Therefore, interpreting the delay of less than 1  $\mu$ s is unlikely to be accurate. This is likely to control the accuracy of PS tests.

The preliminary PS test results also indicated that the background noise affected the identification of the first arrival time of the wave. The good news is that the effect of the existing noise seems to decrease with depth. However, this finding may be inconclusive due to the limited depth of the PVC pipes.

### **3.2.3 Field PS Tests**

PS tests were conducted on the foundations of Bridges Nos. 7480 and 1676. SE/IR tests have been conducted on these two bridges which were discussed previously. Bridge No. 7480 is supported by steel H-piles while Bridge No. 1676 is on timber piles. The results are presented according to the testing order at these two locations.

#### **3.2.3.1 PS tests on Bridge No. 7480**

Bridge No.7480 was selected by NMDOT as the first test site for conducting both PS and IF tests. The location of the site and the street view of the bridge can be found in Figures 126 and 127 respectively. The research team was only able to perform PS tests since the holes were bored at a distance greater than 18 in from the piles.

Eight test borings were drilled by Terracon. The borings are adjacent to the existing H-piles drilled to a depth ranging from about 25 to 40 ft below the ground surface. Figure 144 shows the plan view of the locations of boreholes related to the piles. Holes B-01 to B-04 are inclined. They are approximately parallel to the closest pile. Holes B-05 to B-08 are vertical.

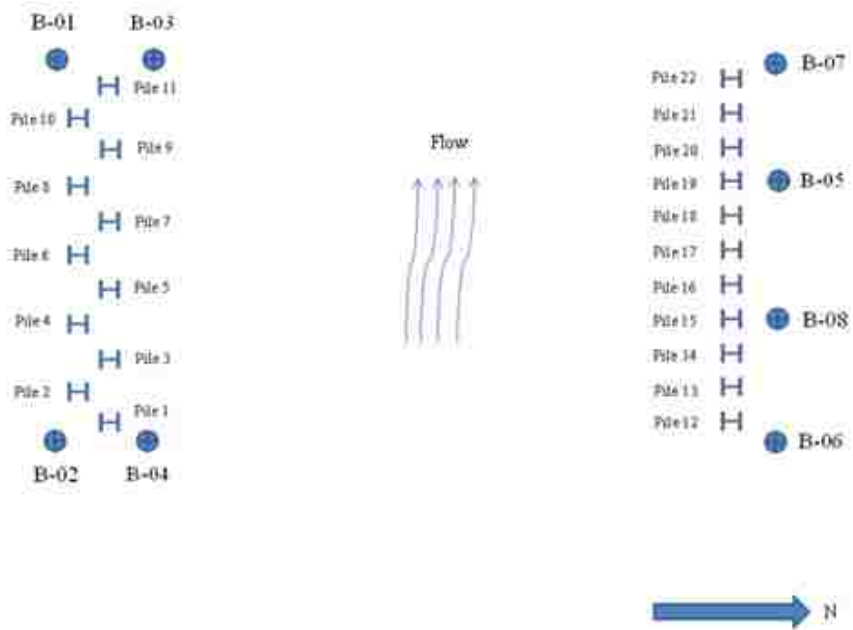


**Figure 144. Foundation Configuration and Locations of Boreholes of Bridge No. 7480**

Two-inch inner diameter PVC casings were placed in each boring with a water tight cap at the base and a removable cap at the top of the tube. The spacing between the PVC tube and the hole was backfilled with existing soil. Figure 145 shows a PVC pipe with its adjacent pile. Table 59 provides a summary of the depths for each borehole.



**Figure 145. An Aligned PVC Pipe and the Adjacent Pile**

**Table 59. Boring Depths of the Holes.**

Boring No.	Boring Depth (ft)
B-01	25
B-02	25
B-03	40
B-04	40
B-05	25
B-06	25
B-07	40
B-08	40

The contractor's report indicated three distinct soil layers at the site. The subsurface condition of the site is summarized in Table 60. The shale layer starts from a depth of 13~16 ft below grade. This layer is of interest since the as-built drawing indicates that the piles' tips were in the shale.

**Table 60. Subsurface Condition at the Site.**

Description	Approximate Depth to Bottom of Stratum (ft)	Material Encountered
Stratum 1	8 to 13	Sandy silt
Stratum 2	13 to 16	Clay, silt, sand and gravel content varied
Stratum 3	25 to 40 (termination of the borehole)	Shale bedrock

**Difficulties at Site** The original plan of the research team was to conduct PS tests at all borehole locations during the first visit. However, two problems were encountered at the site such that conducting PS tests at some holes were impossible. First, some PVC pipes (B-01, B-02, B-05 and B-08) were dry. A tentative PS test was conducted at one of the dry

holes and the obtained poor result is shown in Figure 146. The hydrophone could not record good signals without the water coupling.

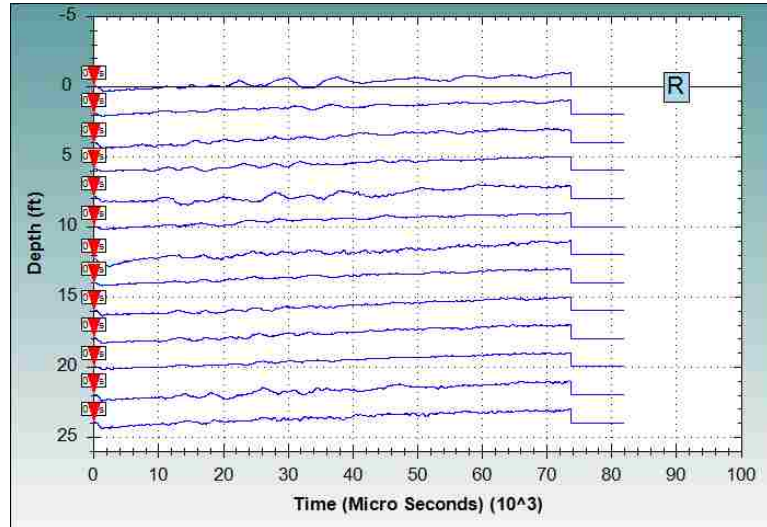


**Figure 146. PS Test Result in a Dry Hole**

The second problem was the damage of one installed PVC tube. As shown in Figure 147, the PVC pipe at B-06 was destroyed due to the movement of debris from flooding. Therefore, conducting PS test was also impossible at this borehole.



**Figure 147. Destroyed Pipe (B-06)**

Twenty PS tests were conducted during the second visit. The impulse was applied by striking the hammer vertically on the metal block that was attached on the web by bolts. Horizontal striking was applied on either the web or the flange. A hard hammer tip was used for Tests PS1 to PS19 while a medium-soft hammer tip was used in Test PS20. The strike direction, the borehole, and the borehole distance from the test pile are summarized in Table 61.

**Table 61. Specifications of PS Tests.**

Test	Pile	Strike Direction	Borehole	Borehole Distance (in)
PS1	1	Vertical	B-04	46
PS2	1	Vertical	B-04	46
PS3	1	Vertical	B-04	46
PS4	1	Vertical	B-04	46
PS5	2	Vertical	B-02	36
PS6	3	Vertical	B-04	136
PS7	10	Vertical	B-01	36
PS8	10	Horizontal (flange)	B-01	36
PS9	10	Horizontal (web)	B-01	36
PS10	11	Horizontal	B-03	72
PS11	11	Vertical	B-03	72
PS12	16	Vertical	B-07	153
PS13	16	Horizontal (flange)	B-07	153
PS14	19	Vertical	B-05	153
PS15	19	Horizontal (flange)	B-05	153
PS16	21	Horizontal (flange)	B-07	68
PS17	22	Vertical	B-07	36
PS18	22	Horizontal (flange)	B-07	36
PS19	22	Horizontal (web)	B-07	36
PS20	22	Vertical	B-07	36



**Test Results for Pile 1** Four PS tests were carried out on Pile 1. The source was introduced by a vertical striking on an aluminum block which had been attached on the pile's web by bolts. The hydrophone was inserted in B-04 that was located at 4 ft from the test pile. A velocity time history obtained from the hydrophone is shown in Figure 148. The velocity time histories were recorded at intervals of 1 and 2 ft.

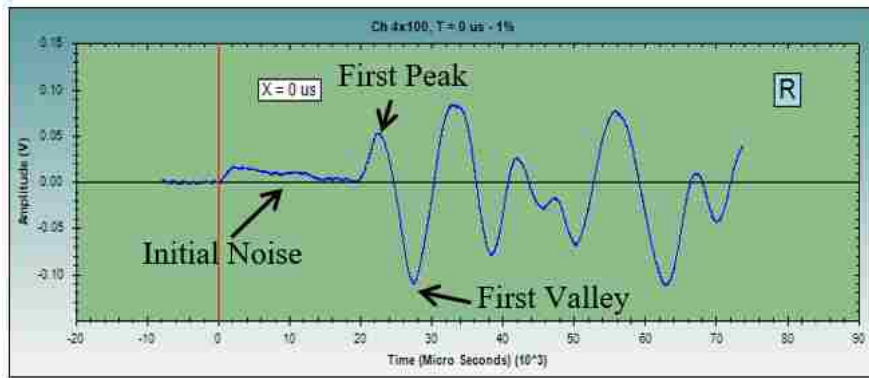


**Figure 148. An Acceleration Time History Obtained from the Hydrophone**

Because of the initial noise level shown in Figure 148, it is difficult to distinguish the arrival time of the first P-wave at some depths. For Test PS1, the first arrival times were plotted against depth in Figure 149. The figure shows three possible inflection points at three different depths below ground (8, 18, and 23 ft).

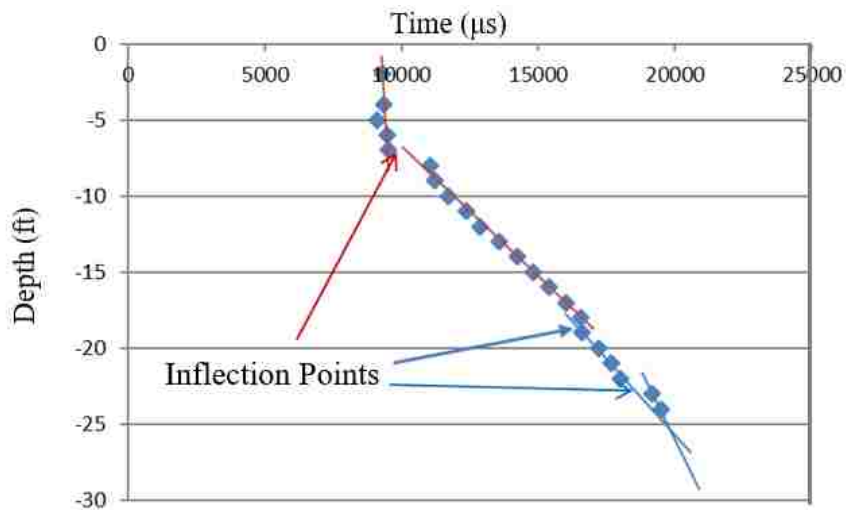


**Figure 149. First Peak Versus Depth for Test PS1**

The PS tests were repeated three more times. The results of Tests PS2, PS3, and PS4 are shown in Figures 150, 151, and 152, respectively. A first inflection point is recognizable at approximately 9 ft below the ground level for Tests PS2 and PS4 (see Figures 150 and 152). The second inflection points are at the depths of 20 and 18 ft for the Tests PS2 and PS4, respectively. In Test PS3 the first inflection point is at 8.5 ft and the second inflection point is at the depth of 22 ft (see Figure 151).

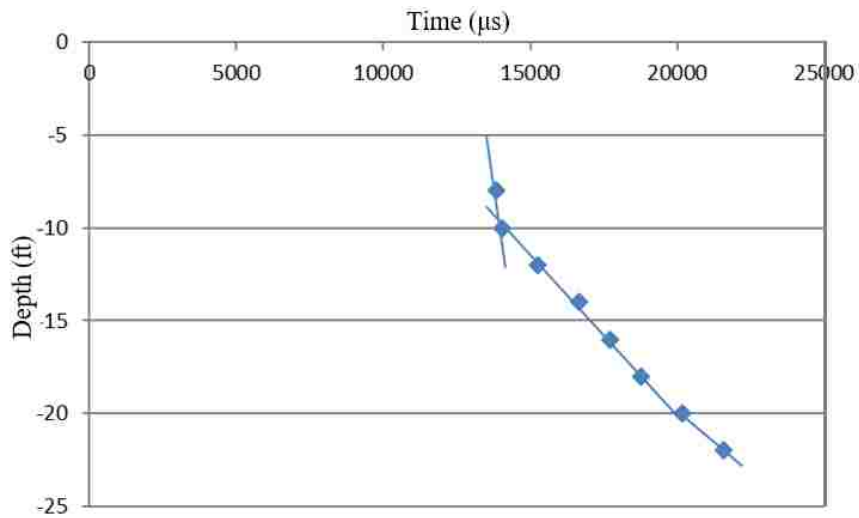


**Figure 150. First Arrival Time Versus Depth (PS2)**

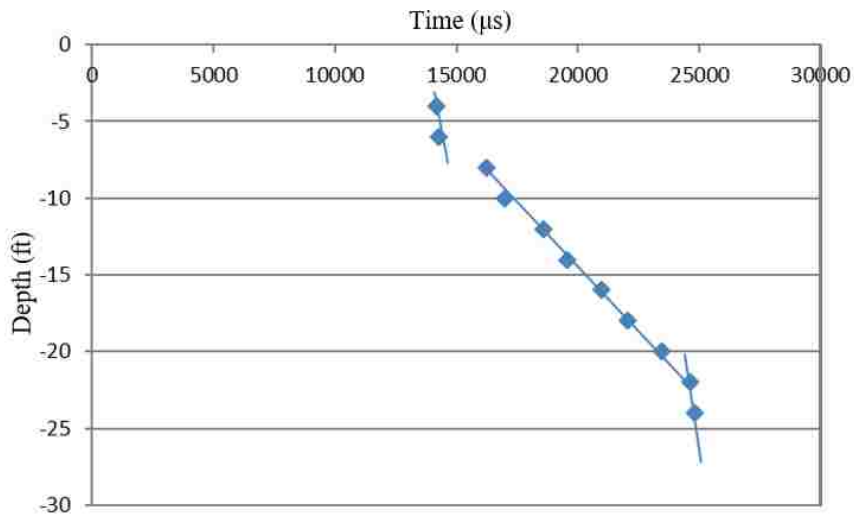


**Figure 151. First Arrival Time Versus Depth (PS3)**

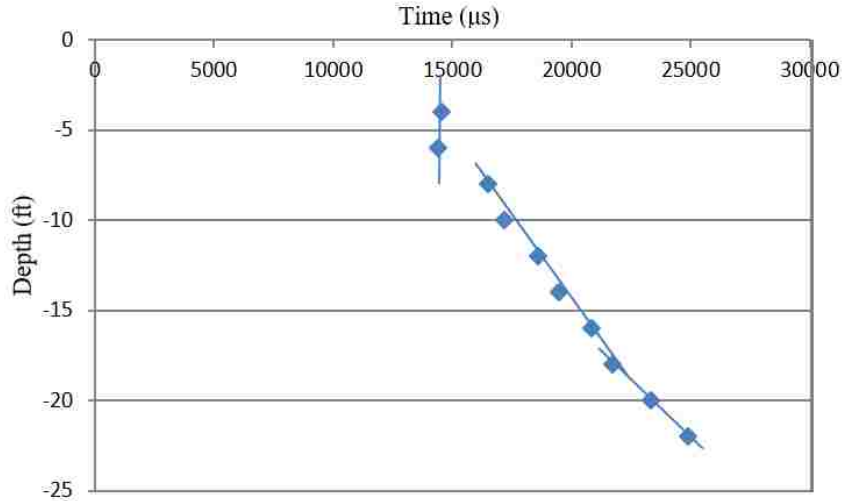


**Figure 152. First Arrival Time Versus Depth (PS4)**

It should be noted the first inflection point does not indicate the bottom of the pile. Unlike other states, unsaturated soils are common in New Mexico. The P-wave velocities usually increase with depth in non-saturated soils while the P-wave velocity in saturated soils is constant (5,000 ft/s). The increasing P-wave velocity with depth may affect the determination of the location of the pile tip. The inflection points within 18 ft below the ground level may indicate the soil layer interfaces. The second inflection points (between 18 and 22 ft) indicate the possible location of the pile's toe.

**Test Result for Pile 2** A PS test was carried out on Pile 2. The hydrophone was at B-02. The source was applied by vertical striking with a hard tip hammer. The distance between the borehole and pile is 3 ft. Figure 153 shows the result of the PS5. Here the first inflection point seen at Pile 1 disappeared. This is a textbook PS test result. The inflection point is at the depth 22 ft which is the embedded pile depth.

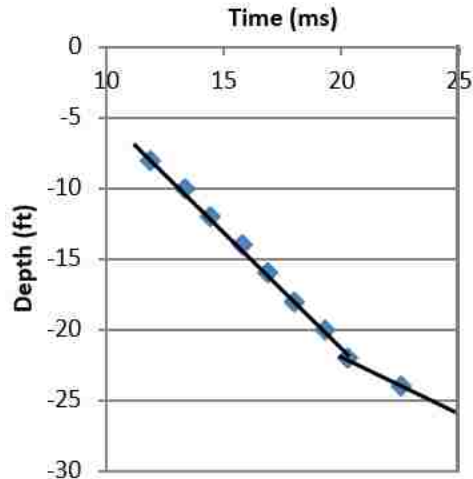


**Figure 153. Result of Test PS5 on Pile 2**

**Test Results for Pile 3** A PS test was conducted on Pile 3 while B-04 was used as the location of the receiver. This borehole was installed for testing Pile 1. The distance between the pile and the borehole is 136 in which is significantly greater than the distances of previous tests. It was a wild attempt to see if meaningful results could be obtained with a great distance.

The signals were recorded at intervals of 2 ft while the hydrophone was lowering down during testing. The stacked graph is indicated in Figure 154. As expected, the distance between the source and the receiver was too great to provide useful information. Signals were very weak at shallow depths. The obvious valleys in the stacked graphs were not related to the P-wave.

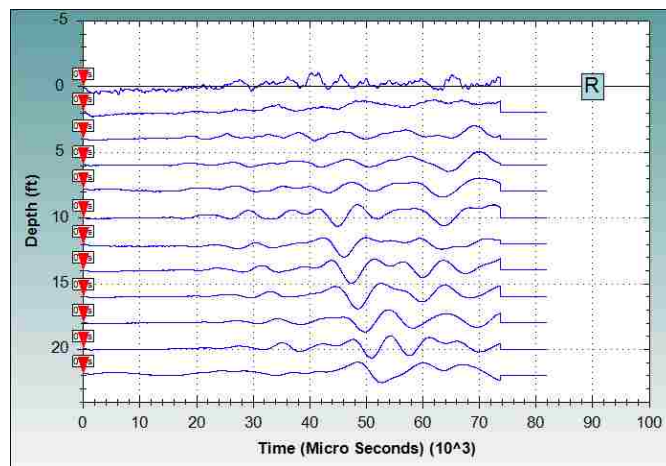


**Figure 154. Stacked Graph of Test PS6**

**Test Results for Battered Pile 10** Three PS tests were conducted on Pile 10 to investigate the effect of striking direction on the obtained signal. The receiver was located at B-01. The distance between the source and receiver is 3 ft. The source was applied along three different directions (vertical, horizontal strike at the flange, and horizontal strike at the web). When vertical striking was applied, a compression wave was generated at the striking point. In contrast, when the striking was horizontal, a shear wave was generated at the striking point. The generated wave travelled along the pile. When the traveling wave encountered an interface (a change of impedance), new compression waves and shear waves were generated and transmitted. For Test PS8, when the generated shear wave reached the ground level, a new compression wave will be developed at the soil-pile interface due to the direction of the particle movement. For Test PS9, compression wave will not be generated until the wave encounters a change in impedance.

The plots of arrival time versus depth are shown in Figure 155. Arrival times at shallow depths could not be determined due to strong initial noise. The arrival times at greater depths were identified with ease. The interface between the clay and the shale layers can be detected with the vertical striking (see Figure 155a) but not with the horizontal striking (see Figures 155b and 155c). The embedment depth of the pile was detected in all three tests. The estimated depths were determined as 24, 20, and 22 ft, respectively.

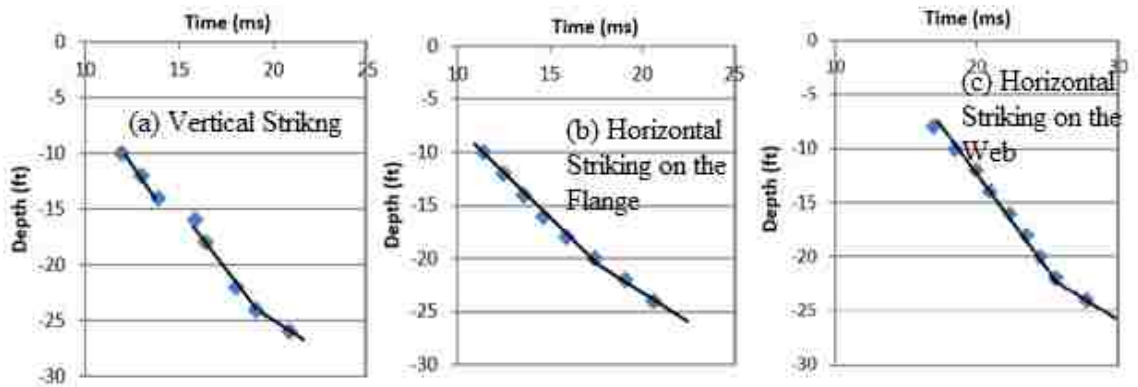


**Figure 155. Result of Three PS Tests on Pile 10**

**Test Results for Pile 11** The effect of input source (horizontal and vertical strikes) was also examined on Pile 11. The source was applied by horizontal striking at the flange (Test PS10) and vertical striking (Test PS11). The distance between the pile and the

borehole is 6 ft. The signals were recorded at intervals of 2 ft while the hydrophone lowered down the hole during testing. The results of Tests PS10 and PS11 are shown in Figures 156 and 157 respectively.

A first inflection point was determined at approximately 11 and 9 ft for horizontal and vertical striking respectively. The second inflection point at the depth of 21 ft was identified for Test PS10 but no inflection point was identified for Test PS11. This may be due to the traffic noise while conducting Test PS11. The first arrival times at depths between 19 and 23 ft were undistinguishable.

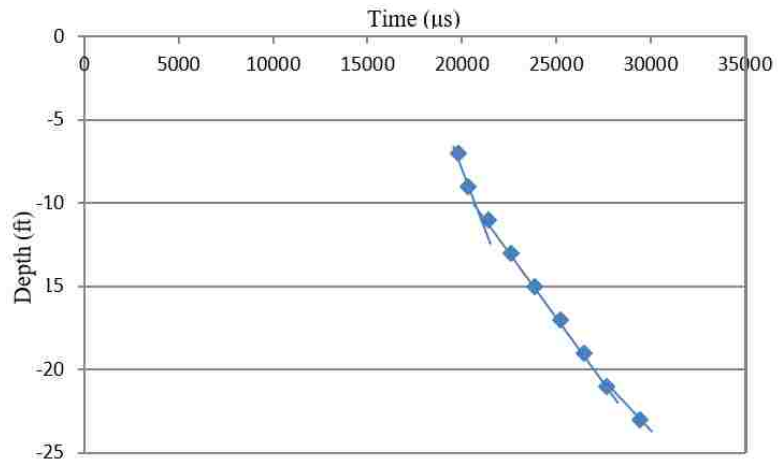


**Figure 156. First Arrival Time Versus Depth (PS10)**

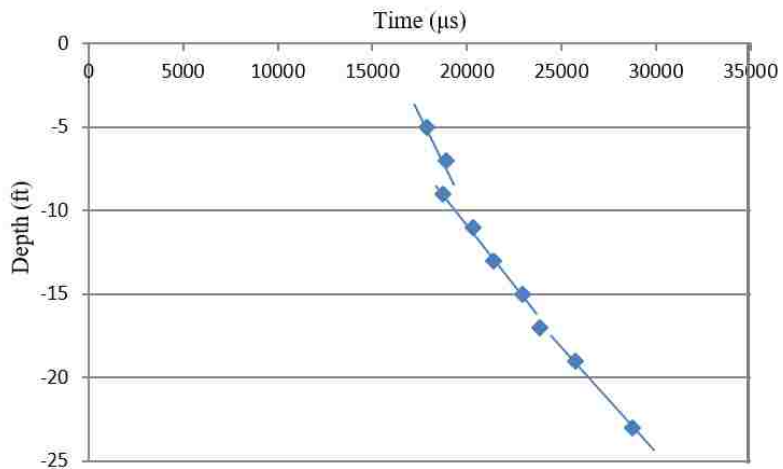


**Figure 157. First Arrival Time Versus Depth (PS11)**

**Test Results for Piles 16 and 19** This was another wide attempt to see if PS tests work in greater distance between the source and receiver (12.7 ft). The source was applied on Piles 16 and 19 while the receiver was located at B-07 and B-05, respectively. The source was applied by vertical striking and horizontal striking on the flange for each pile. A total of four PS tests were conducted with a hard tip hammer.

The results of these four PS tests are shown in Figure 158. Due to the great distance between the source and receiver, neither vertical striking nor horizontal striking can produce useful results to determine the inflection point. The hammer could not produce strong enough wave to reach the receiver. There is a certain horizontal distance between the source and the receiver. Beyond which, meaningful PS tests cannot be obtained. The certain horizontal distance depends on the strength of the input signal and soil condition. Our investigation showed that 12.7 ft was too far for our equipment to achieve interpretable results.

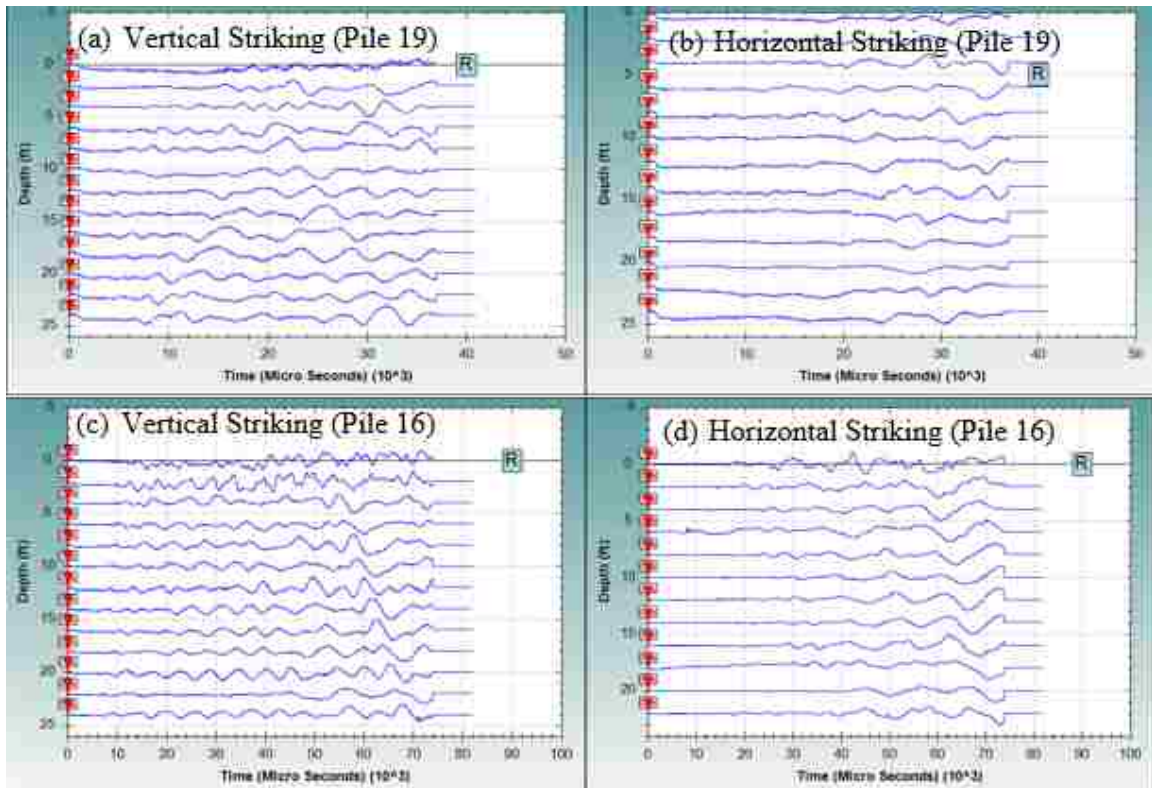


**Figure 158. Stacked Graphs of PS Tests for Piles 16 and 19**

**Test Result for Pile 21** A PS test was conducted on Pile 21. The receiver was located at B-07. The distance between the source and receiver is 5.7 ft. The source was applied by horizontal striking on the flange with a hard tip. The result is shown in Figure 159. The inflection point was identified barely at a depth of 22 ft. More data points below 24 ft will be better to support the existence of an inflection point at 22 ft. The source to receiver distance of 5.7 ft produced good result.

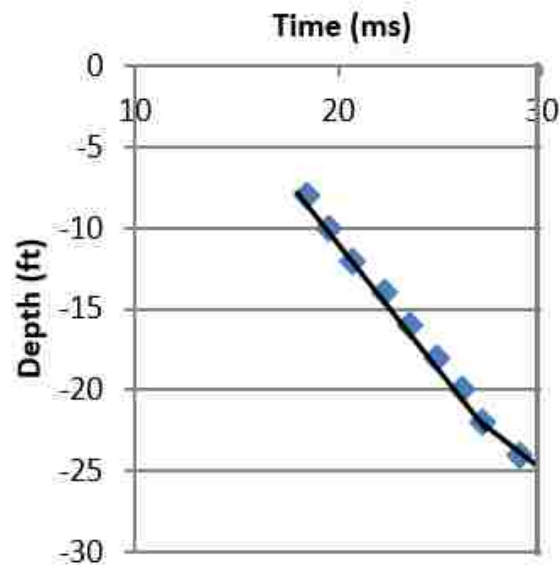


**Figure 159. Result for Test PS16**

**Test Results for Pile 22** Four PS tests were conducted on Pile 22. The receiver was located at B-07. The distance between the pile (source) and the borehole (receiver) is 3 ft. The source was applied by vertical and horizontal striking (see Table 61). A hard tip hammer was used for Tests PS17 to PS19 while a medium-soft tip hammer was used in the last test (PS20) The stacked graphs of all four tests showed initial noise at depths less than 6 ft. With the presence of noise distinguishing the arrival time was difficult. Noise was reduced when the receiver (hydrophone) was at greater depths.

The effect of striking direction was examined by comparing the results of Tests PS17, PS18, and PS19 as shown in Figure 160.



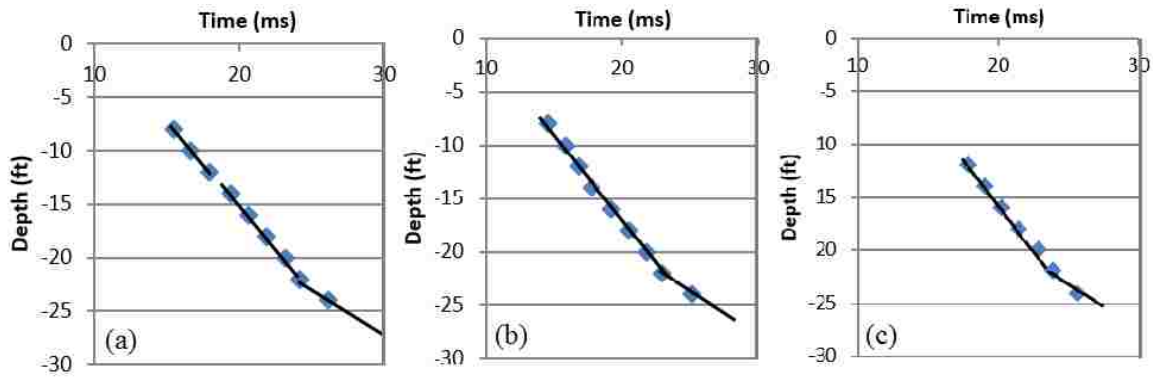


**Figure 160. Results of Tests PS17, PS18, and PS19 (a) Vertical Striking, (b) Horizontal Striking on the Flange, (c) Horizontal Striking on the Web**

The first possible inflection point was found at a depth of 13 ft. According to the soil profile of this site, the interface between the clay and shale layers is located about 13 ft below ground. This inflection point may be related to the interface. This first inflection point may not indicate the embedment depth of the foundation.

The second possible inflection point was at the depth of about 22 ft. This inflection point may indicate the location of the pile tip. The as-built drawing shows that the piles should be extended at least 5 ft into the shale layer. Therefore, this inflection point is related to the embedment depth. Due to the limited depth of the installed PVC tubes, PS tests must stop at 25 ft. The clarity of this particular inflection point could be improved if the length of the PVC pipe were more than 25 ft.

Both vertical and horizontal striking produced signals strong enough to determine the embedment depth of the pile. Good signals were received by vertical striking and horizontal striking on the flange. Only fair result was obtained by horizontal striking on the web. Although horizontal striking can be used as a source, it is more desirable to generate a shear wave such that particle movement is parallel to the direction towards the receiver.

The result of Test PS20 with a softer hammer tip (medium-soft) is shown in Figure 161. Interpretation of the PS test was still possible although the received signals were not as well-defined as that produced by hard tip (see Figure 160a). Thus, it is better to use a hammer with hard tip to generate the wave (source).

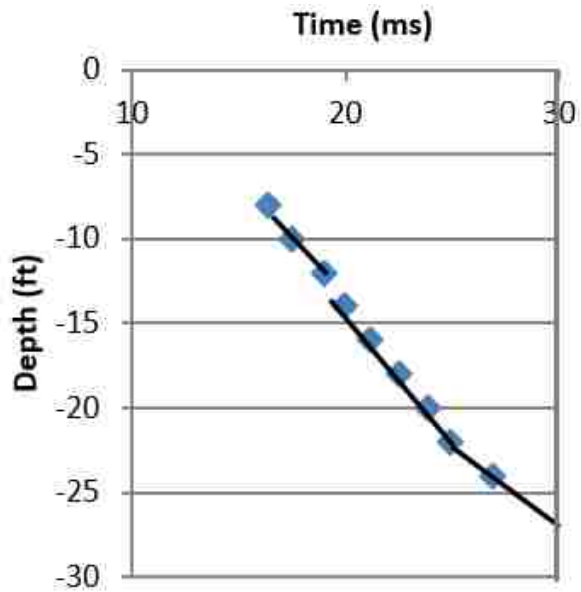


**Figure 161. Result of Test PS20**

**Summary of Results of Bridge No. 7480** The results of PS tests conducted on H-piles are summarized in Table 62. The success rate is 77.8%. The success rate is close to 100% by ignoring the results of PS tests with the source to receiver distance greater than 6 ft.

**Table 62. PS Tests Results of Bridge No. 7480.**

Pile	Embedment Pile Length (ft)
1	21
2	22
3	20
10	22
11	19
16	-
19	-
21	22
22	22

**Conclusions of PS tests on Steel H-Piles** Based on the results of the PS tests conducted in the field following observations and conclusions were inferred:

- In the presence of ambient noise, determining the arrival time of the first P-wave from the velocity graphs was very difficult.
- The stacked graphs showed initial noise in the upper soil strata. The data at a depth less than 8 ft was questionable. However, the velocity graphs showed that the initial ambient noise reduces with depth.
- Both vertical and horizontal striking can be used as the source for PS tests. However, signal provided by horizontal striking seems to be less effective than that of vertical striking. It is preferable to select the direction of the horizontal striking such that the particle movement is in the direction towards the receiver.
- Layered soils introduced difficulties in the determination of pile tip. In some PS tests, an inflection point could be interpreted as the depth of the interface between the clay and shale layers.
- The strength of the signal reduced with the increase of the distance between the source and receiver. Good results were obtained when the distance was less than 6 ft for both straight and battered piles. When the distance was 12.7 ft poor results were obtained. Thus, a borehole should be drilled less than 6 ft from the test foundation (pile or pier) for future PS tests.

### **3.2.3.2 PS tests on Bridge No. 1676**

Conventional PS tests were conducted on two timber piles at Bridge No. 1676. The location and foundation plan of the bridge are shown in Figures 115 and 117 respectively. The test piles were Pile B-1 and C-1. Two test borings were drilled adjacent to the timber piles by NMDOT using the Geoprobe 7822DT (purchased during this project). The plan view of the location of the boreholes is indicated in Figure 162. The low headroom drill rig and the drilling operation are shown in Figure 163.

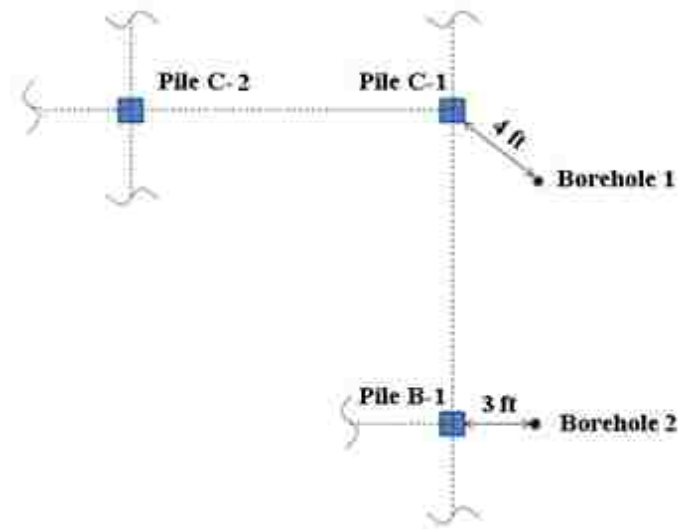


**Figure 162. Plan View of Boreholes Locations**



**Figure 163. Geoprobe Model 7822DT- Low Headroom Drill Rig**

The depths of boreholes 1 and 2 are 26 ft and 35 ft respectively. Two-inch inner diameter PVC casings were placed in each boring with a water tight cap at the base and a removable cap at the top. Native sandy soil was poured down into the hole to create a sand pack around the PVC tube.

Conventional PS tests were performed on Piles B-1 and C-1 while reverse PS tests were performed on Piles C-1 and C-2. In conventional PS tests, the source was at the pile and the receiver was at the borehole. In reverse PS tests, the source was at the borehole and the receiver was at the pile.

**Conventional PS Test Results** Nine PS tests were carried out on Piles B-1 and C-1 as shown in Table 63. In two tests, an 8-lb sledge hammer was used to impart greater impact energy into the pile. Hard tips were used for the regular hammer. The signals were recorded at an interval of 2 ft starting from the ground surface for Pile B-1. For Pile C-1, the signals were recorded starting 8 ft below the ground surface towards the PVC tube bottom with an interval of 1 ft.

**Table 63. Specifications of PS Tests.**

Test	Borehole	Pile	Striking Condition	Hammer
1	1	B-1	Vertical - Upward on pile cap	Regular
2	1	B-1	Vertical - Upward on pile cap	Regular
3	1	B-1	Vertical - Upward on pile cap	Regular
4	1	B-1	Vertical – Downward (inclined) on the connected bracing to the pile	Regular
5	1	B-1	Vertical - Upward on pile cap	8-lb Sledge hammer
6	1	B-1	Vertical - Upward on pile cap	8-lb Sledge hammer
7	2	C-1	Horizontal Striking on the side of the pile	Regular
8	2	C-1	Vertical - Downward on pile cap	Regular
9	2	C-1	Horizontal Striking on the side of the pile	Regular

Similar to the previous observation at Bridge No. 7480, noise affected the determination of the first arrival time at some depths. However, the noise was less intense at this site than that at Bridge No. 7480 due to zero traffic on the bridge during testing. Figure 164 shows the noise comparison between the data obtained at Bridges No. 7480 and 1676. The figure shows the significant effect of traffic noise on the PS tests results.

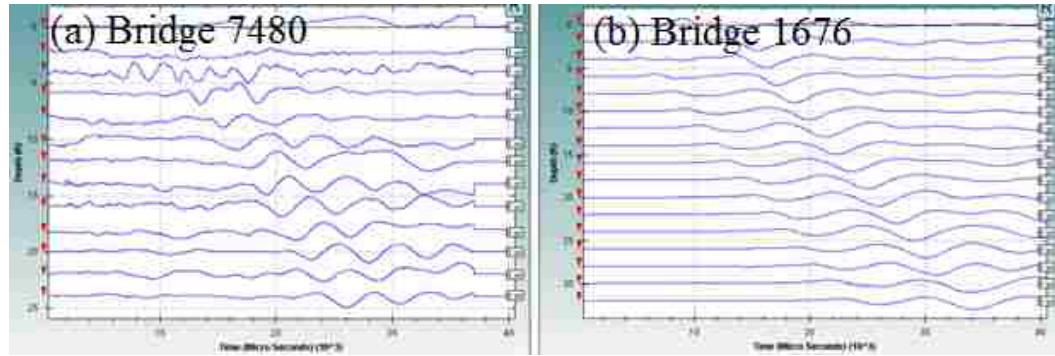


**Figure 164. Stacked Graphs for Steel H-piles and for Wood Piles**

Since the signals were generally greater than the noise at this bridge, the determination of first arrival times was not too difficult. First arrival times were determined by inspecting the background noise level in the received signals. The ‘First arrival’ was determined as the time when the signal begins to increase and consistently distinguish itself from the background noise level. Figure 165 shows the original and enlarged views of an obtained signal. The initial noise and the first arrival time are clearly identifiable in the enlarged view. The arrival times of the first P-wave were determined easily at greater depths since the ambient noise reduced with depth.

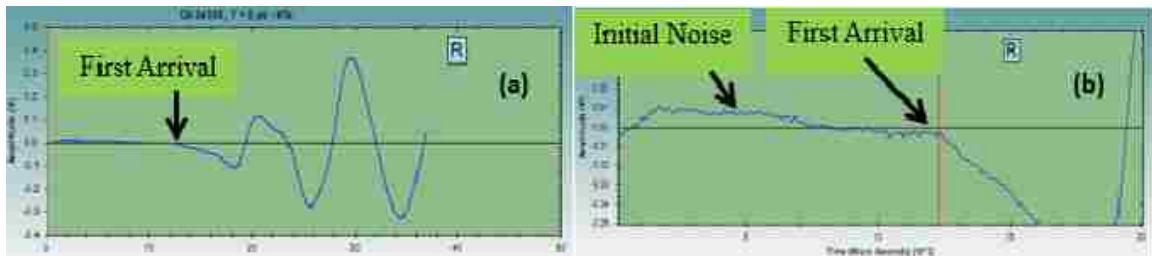


**Figure 165. Examples of (a) Original View and (b) Enlarged View Showing the Initial Noise and First Arrival**

After determining the arrival time at each depth, the arrival time versus depth was plotted for each PS test. The results of the PS tests are shown in Figures 166 to 174. Two appropriate straight lines were passed through the points and the intersection of the two lines indicated the location of the inflection point. Sometimes, identifying data points that belong to each line was based on engineering judgement. The straight lines in Figures 166 to 174 were introduced by linear curve fitting method with the selected data points.

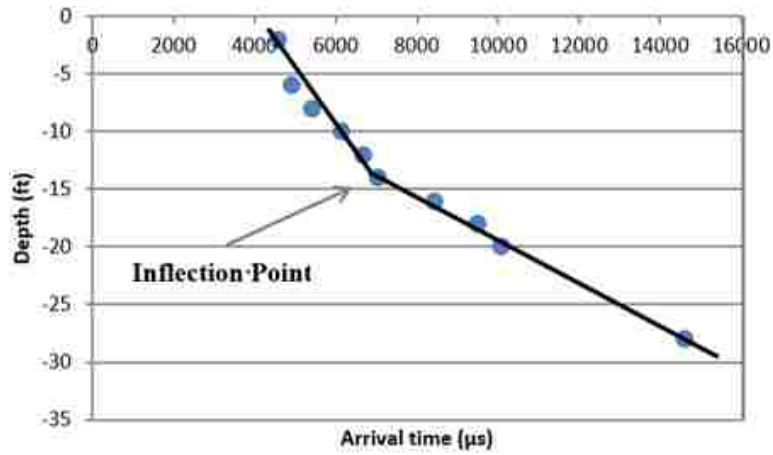


**Figure 166. First Arrival Time Versus Depth (Test 1)**

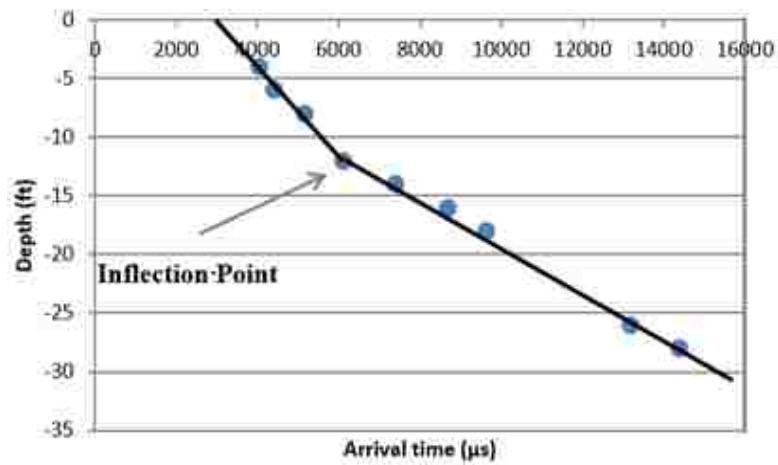


**Figure 167. First Arrival Time Versus Depth (Test 2)**

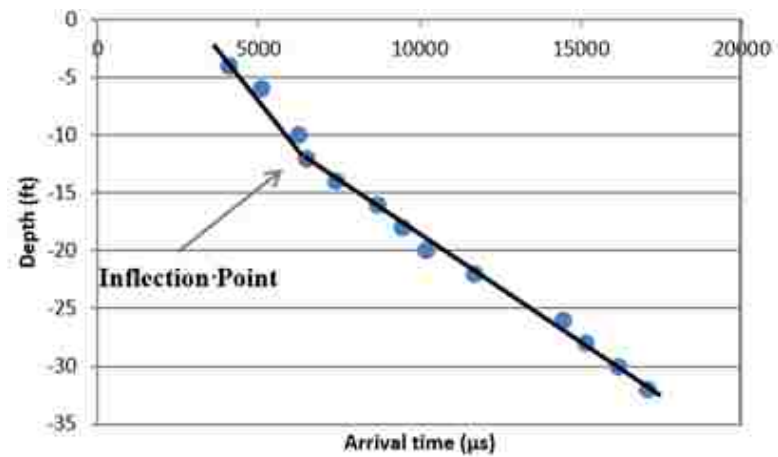


**Figure 168. First Arrival Time Versus Depth (Test 3)**

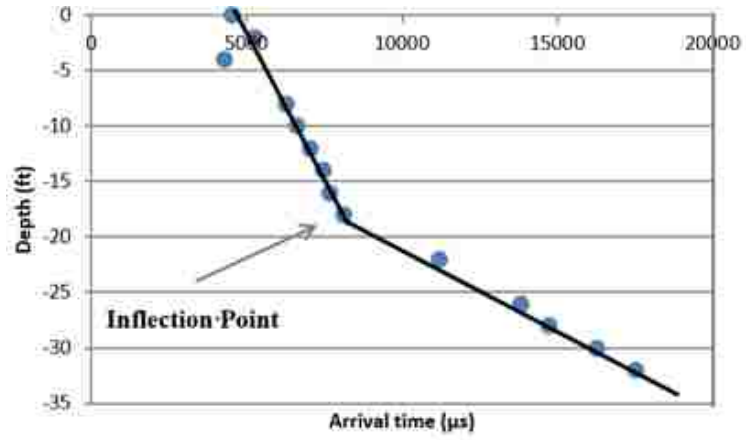


Figure 169. First Arrival Time Versus Depth (Test 4)

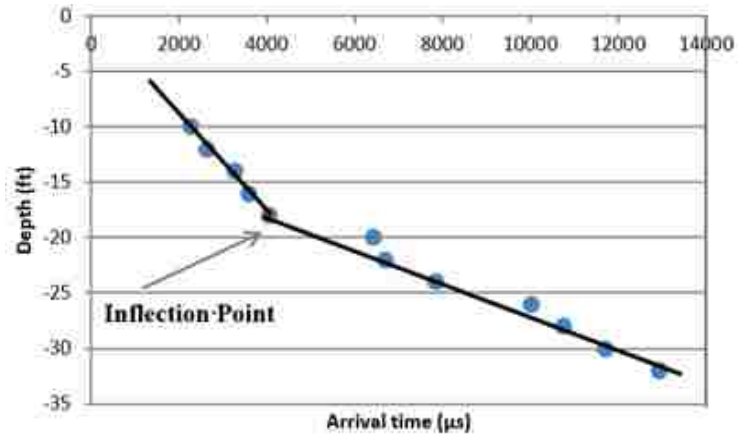


Figure 170. First Arrival Time Versus Depth (Test 5)

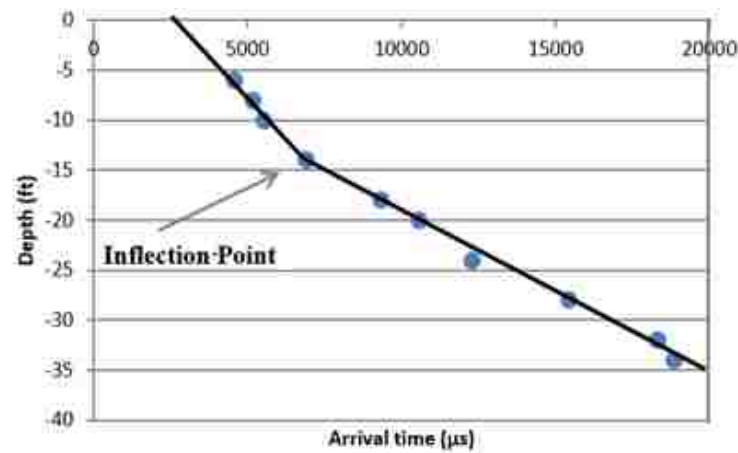
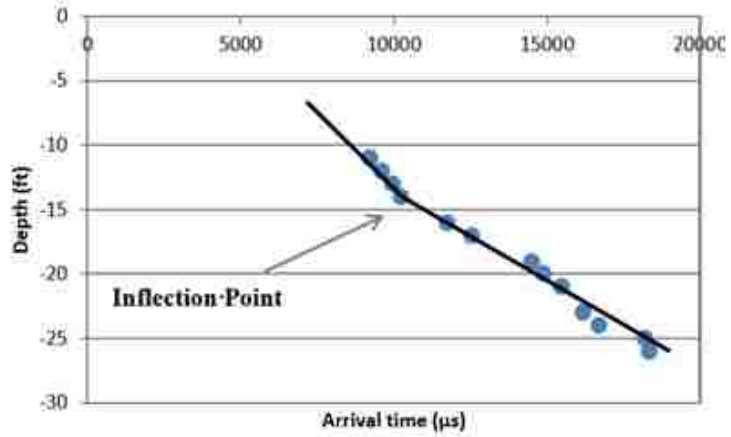
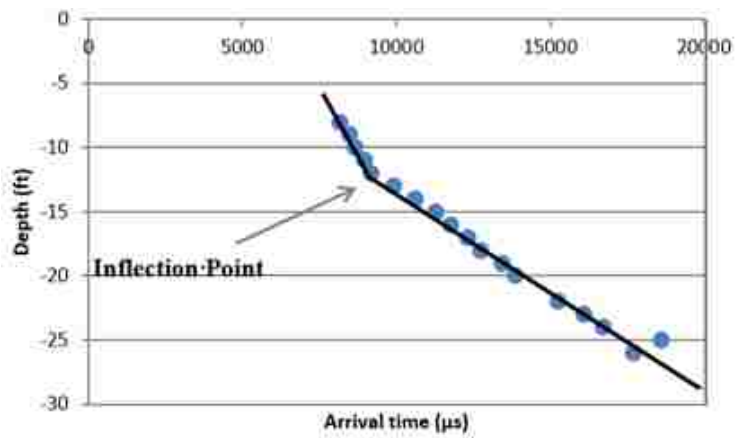


Figure 171. First Arrival Time Versus Depth (Test 6)





**Figure 172. First Arrival Time Versus Depth (Test 7)**



**Figure 173. First Arrival Time Versus Depth (Test 8)**

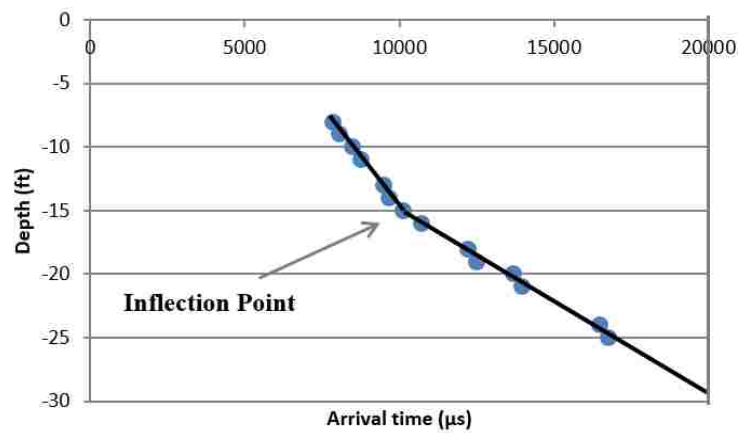


**Figure 174. First Arrival Time Versus Depth (Test 9)**

Comparing Figures 167 and 170, using an 8-lb sledge hammer did not show any improvement at this site. Applying upward striking with a regular hammer was much easier than the sledge hammer.

The depths of the inflection points for PS tests conducted on Piles B-1 and C-1 are shown in Tables 64 and 65 respectively.

**Table 64. Depths of the Inflection Points for Pile B-1.**

Test	Striking Method	Inflection Point Depth (ft)
1	Vertical - Upward on pile cap	14
2	Vertical - Upward on pile cap	12
3	Vertical - Upward on pile cap	12
4	Vertical – Downward (inclined) on the connected bracing to the pile	18
5	Vertical - Upward on pile cap	18
6	Vertical - Upward on pile cap	14

**Table 65. Depths of the Inflection Points for Pile C-1.**

Test	Striking method	Inflection point depth (ft)
7	Horizontal striking on the side of the pile	14
8	Vertical - Downward on pile cap	12
9	Horizontal striking on the side of the pile	15

**Summary of Results** Table 66 lists the range of estimated length of piles, the average value, and the value from the as-built drawings. The average pile lengths are comparable to the as-built pile length. It is difficult to determine the true errors since the actual pile length may be different from the as-built value.

**Table 66. The Range of Estimated Pile Length, Average and Known Pile Lengths.**

Pile	Range of Pile Length (ft)	Average Pile Length (ft)	As-built Pile Length (ft)
B-1	18 - 24	20.7	23
C-1	18 - 21	19.7	23

**Conclusions of Conventional PS Tests at Bridge No. 1676** Based on the PS test results the following conclusions were inferred:

- Determination of first arrival time was much easier without the traffic noise.
- Accurate arrival time determination required more detailed consideration of the background noise.
- The calculated pile lengths were similar but shorter than the as-built pile length.
- Both regular and sledge hammers produced acceptable results.
- Both vertical and horizontal striking generated acceptable results, however, vertical striking produced clearer inflection points.

**Reverse PS Tests** Two reverse PS test were conducted on two timber piles of Bridge No. 1676 during drilling the boreholes. The advantage of the reverse PS test is that no pre-knowledge of the pile depth is needed since drilling can be continued until the inflection point is identified. Moreover, multiple piles can be tested simultaneously using one borehole.

In this method, the hollow stem auger was advanced to a desired depth. A standard split-spoon sampler was inserted through the hollow stem of the auger column towards the bottom of the hole. The source for PS testing was created by striking the top of the drill rod. The receiver (accelerometer) was mounted on the test pile using wooden blocks. Figure 175 shows the reverse PS setup for Piles C-1 and C-2 at Bridge No. 1676. The propagated wave traveled through the rod, soil, and pile, and finally was received by the sensors. The procedure was repeated at various depths.

The obtained signals were stacked together for Piles C-1 and C-2 as shown in Figure 176. Very noisy signals were observed compared with the results of conventional PS tests (see Figure 164b). Since the Pile C-1 is closer to the source than Pile C-2, the signals arrived earlier at Pile C-1 than Pile C-2. Due to the noise level, it was very difficult

to pinpoint the arrival times at most depths. Thus, we do not have enough conclusive data for the determination of the inflection point. The ambient noise was more intense on the ground than at greater depths.

Another way to conduct PS tests without drilling a borehole is the use of a seismic cone as the receiver. This method can be explored in the future. The disadvantage of this method is that the PS test cannot be repeated at previous depths after the advancement of the cone due to the disturbance of the surrounding soil.

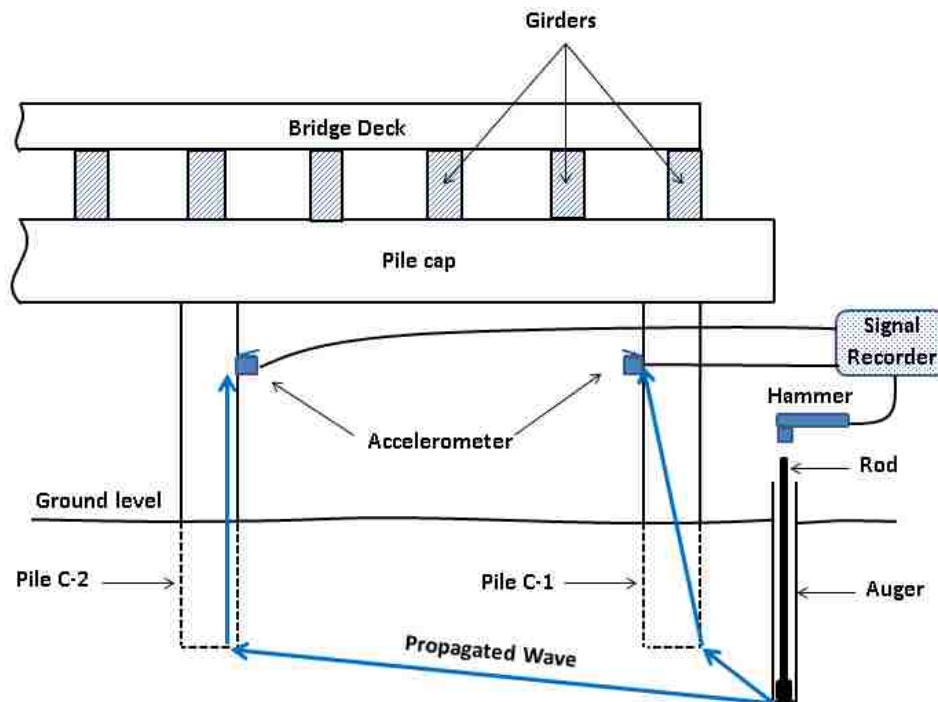


**Figure 175. Reverse PS Setup for Piles C-1 and C-2 of Bridge No. 1676**

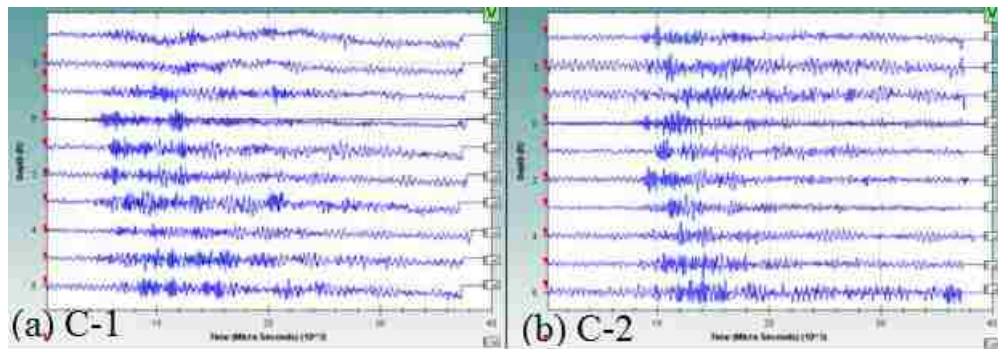


**Figure 176. Stacked Graphs for Piles C-1 and C-2**

### **3.3 Induction Field Method**

IF tests are the best NDT method for detecting the depth of steel piles. In addition, IF tests are not affected by bridge vibration.

Two testbeds were constructed to examine the capability of the equipment and to investigate various aspects of IF tests. The findings were useful for conducting IF tests in the field on foundations containing metal (steel and reinforced concrete foundations). The first testbed contained a metal I-beam placed horizontally in a wooden box full of soil. The box was filled with sand (or clay) and IF tests were conducted with the Probe placed inside the pipes at various locations. The second testbed was created off UNM campus. To conduct the desired PS tests, a reinforced concrete pier and four PVC tubes at various distances from the pier were installed. IF tests were also performed to examine the effect of the distance between the pier and the tube.

The original plan of IF field tests included performing IF tests at Bridge No. 7480. IF tests were not conducted on the bridge since the distance between the boreholes and the test piles were greater than 1.5 ft which is beyond the capability of the equipment.

#### **3.3.1 IF Test Procedure**

Before conducting IF tests, a borehole must be drilled next to the test pile. There are requirements for the preparation of the borehole:

- The borehole must align with the test pile.
- The depth of the borehole must be at least 10 ft deeper than the expected pile toe level.
- The hole should be bored as close as possible to the test pile (no more than 1.5 ft away from the pile).
- 2-in PVC tube is installed to keep the borehole from caving.
- The space between the borehole and the tube is filled with soil.

Similar to the PS tests, an IF test is carried out in three steps including hardware setup, data acquisition, and data processing.

### 3.3.1.1 IF Hardware Setup

Figure 177 shows the correct assembly of the Length Inductive Test Equipment (LITE) for IF tests. The equipment includes battery, signal conditioning box, multimeter, and the Probe (induction sensor). The details of the signal conditioning box are shown in Figure 178.

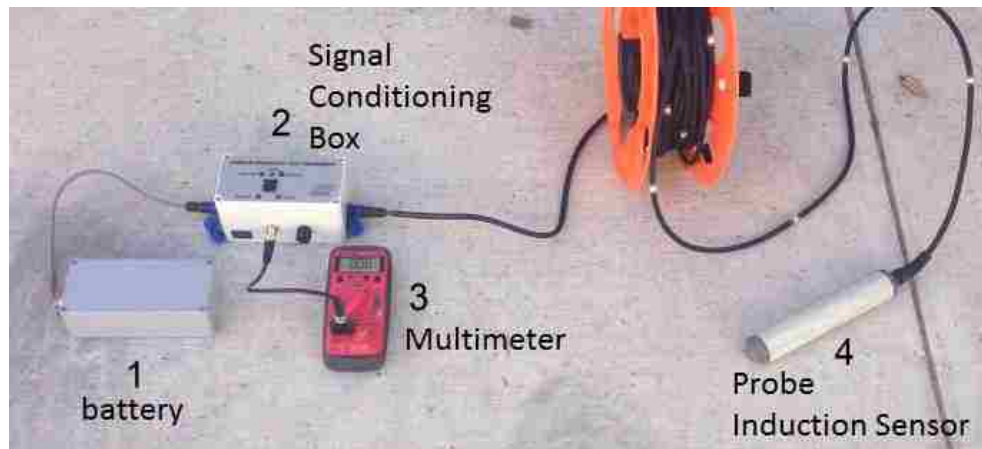


**Figure 177. Length Inductive Test Equipment (LITE) for IF tests**



**Figure 178. Details of Signal Conditioning Box**

### 3.3.1.2 IF Data Acquisition

Calibrate the system before conducting IF tests. The calibration should follow these steps.

- 1) Assemble the components as shown in Figure 177.

- 2) Set the Multimeter to “20V” in the DC.
- 3) Set the reference point
  - Place the Probe in a location such that there is no metal object within 3 ft.
  - Push down the rocker switch until one of the three lights (negative/zero/positive) illuminates.
  - Turn the knob until the green light (middle one) is on and the voltage is approximately 2.5 V.
- 4) Push down the rocker until either NO METAL or METAL illuminates.
- 5) Bring the Probe in contact with a metal object, the Multimeter should show a reading close to 5.04 V. If the readout is still less than 3V, the battery is low, either the Multimeter or the Signal Conditioning Box is defective.

The Multimeter should display a voltage between 2.5 V and 5.04 V. The voltage will be 2.5 V when there is no metal object within a distance of 2 ft from the Probe. The voltage should increase when moving the Probe closer to a metal object.

After calibration, following steps should be carried out to perform an IF test:

- 1) Insert the Probe into the previously installed PVC tube.
- 2) If the first reading remains 2.5 V, the distance between the hole and the metal in the pile is greater than 18 inches, or there is no metal in the foundation.
- 3) Lower the Probe in 1-ft increment and record the voltage at every foot till the bottom of the hole.

A successful IF test (the pile length is determined) should show a drop of voltage before the Probe touches the bottom of the hole. An example of a successful IF test is shown in Figure 179.

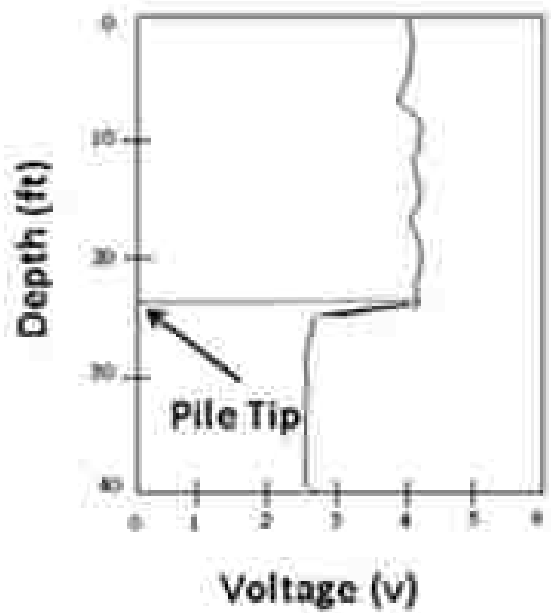


**Figure 179. A Successful IF Test Result**

### 3.3.2 IF Testing: Testbed at UNM

The first testbed contained a metal I-beam placed horizontally in a wooden box full of soil as shown in Figure 180. A metal beam buried in a wood box filled with soil was a suitable prototype of a real steel foundation of a bridge. The dimensions of the wooden box were 12 ft × 4 ft × 18 in. The I-beam was 5 ft long, 12 in depth and an 8 in flange width. The preliminary tests were supposed to be conducted in the structural lab at UNM. However, during conducting the IF tests in the structural lab, it was revealed that the test could not be conducted on the concrete floor due to the presence of steel reinforcement. The testbed was therefore moved outdoor on an asphalt paved driveway as shown in Figure 180. Before recording the data, three PVC tubes were placed horizontally at a distance of 1, 1.5 and 2 ft respectively from the steel beam.





**Figure 180. Test Configuration with Steel Beam and Wooden Box**

### **3.3.2.1 IF Results in Air**

The steel beam was placed in the box vertically and horizontally and the IF tests were conducted. The Length Induction Test Equipment (LITE) was assembled as shown in Figure 177. The system was calibrated and the Probe was then inserted into each of the PVC tubes. Data were recorded at 80 points as shown in Figures 181 and 182. The corresponding results are indicated in Tables 67 and 68. The initial voltage was 2.55 v. This implies that the voltage will be greater than 2.55 when there is metal object nearby. The italicized values in the tables designate the locations where metal was detected. The results show that the distance between the Probe and the metal beam should be limited to 18 in for the possibility of metal detection.

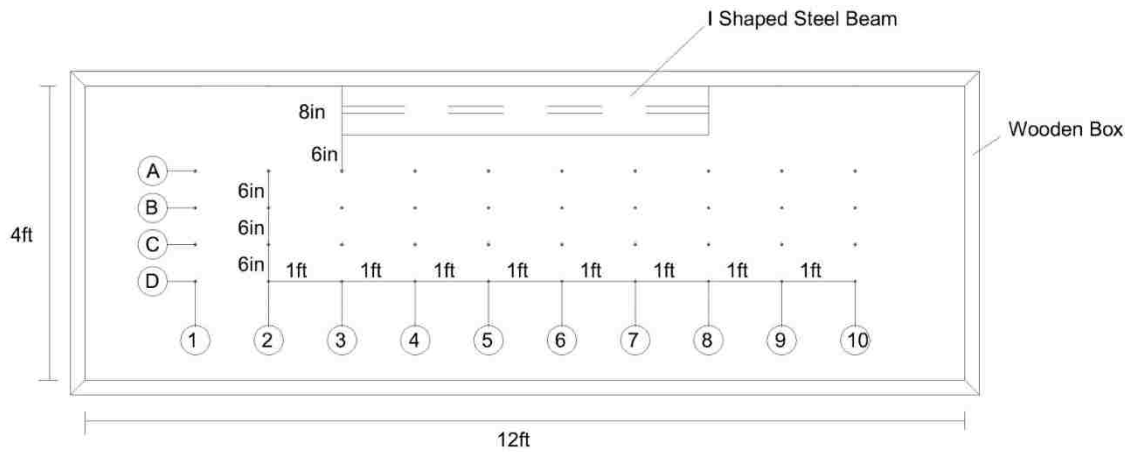


**Figure 181. Test Locations with Beam in the 1<sup>st</sup> Configuration**

**Table 67. Test Results (Locations Correspond to Figure 182).**

	1	2	3	4	5	6	7	8	9	10
A	2.45	2.97	5.04	5.04	5.04	5.04	5.04	5.04	2.74	2.45
B	2.55	2.69	3.59	4.37	4.21	4.12	4.12	3.3	2.67	2.53
C	2.4	2.4	2.62	2.72	2.77	2.64	2.64	2.55	2.47	2.42
D	2.6	2.6	2.62	2.62	2.61	2.6	2.6	2.57	2.56	2.55

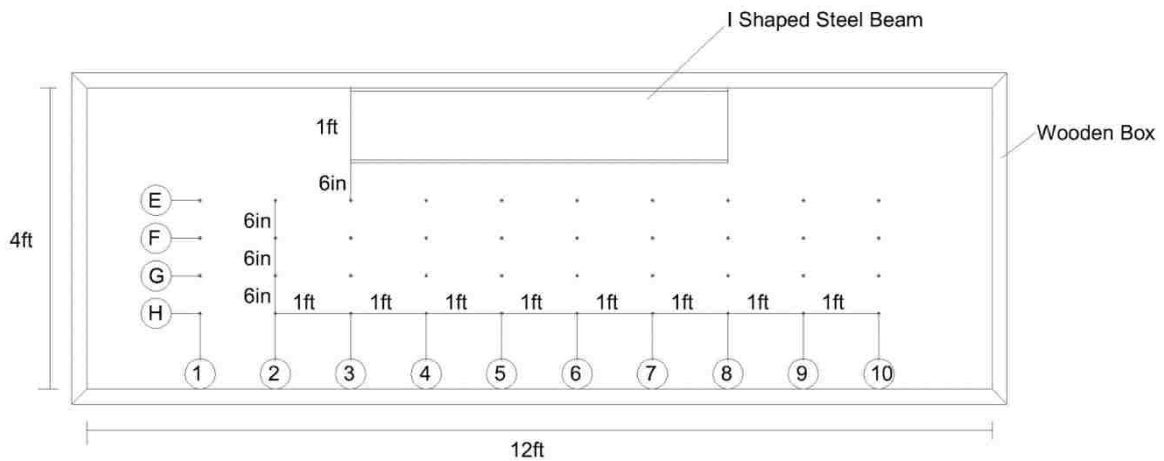


**Figure 182. Test Locations with Beam in the 2<sup>nd</sup> Configuration**

**Table 68. Test Results (Locations Correspond to Figure 183).**

	1	2	3	4	5	6	7	8	9	10
E	2.43	2.96	5.04	5.04	5.04	5.04	5.04	5.04	2.89	2.45
F	2.4	2.55	3.48	4.46	4.84	4.74	4.88	3.79	2.54	2.4
G	2.36	2.39	2.56	2.7	2.78	2.84	2.76	2.55	2.43	2.35
H	2.37	2.39	2.5	2.46	2.48	2.53	2.46	2.42	2.42	2.37

### 3.3.2.2 IF Results in Sand

In the next step, we investigated the effect of sand on IF test results. Two PVC tubes were placed horizontally at distances of 12 in and 18 in from the edge of the steel beam. The box was filled with sand at two different moisture contents. The tests were conducted with the Probe running inside the pipes at various locations. The results are shown in Tables 69 and 70 for sand at 4% moisture content and saturated sand, respectively.

**Table 69. IF Test Results for Sand with 4% Moisture Content.**

	1	2	3	4	5	6	7	8	9	10
B	3.08	3.39	5.04	5.04	5.04	5.04	5.04	5.04	3.86	3.10
C	3.08	3.20	3.29	3.41	3.56	3.63	3.62	3.52	3.38	3.18

**Table 70. IF Test Results for Saturated Sand.**

	1	2	3	4	5	6	7	8	9	10
B	3.17	3.75	5.04	5.04	5.04	5.04	5.04	5.04	5.04	3.23
C	3.06	3.22	3.36	3.43	3.53	3.56	3.51	3.37	3.20	3.00

The readings in Tables 69 and 70 are significantly higher than those in Tables 67 and 68. The presence of soil mineralization enhances the recognition of metal objects. The results of Tables 67 and 68 indicated that the steel beam cannot be clearly detected at a distance of 18 in while there is no soil in the box. However, with the presence of sand, the beam was clearly detectable at 18 in. Therefore, the borehole should be constructed within

18 in from the pile in the field. Comparing Tables 69 and 70, soil moisture content has no effect on IF tests.

### 3.3.2.3 IF Results in Clay

In the final step, the box was filled with clay and the IF tests were repeated. The measurement of voltages at the 20 recording points is shown in Table 71.

**Table 71. Measurements at Points on Axes B and C with the Presence of Clay.**

	1	2	3	4	5	6	7	8	9	10
B	2.98	3.05	3.99	5.04	5.04	5.04	5.04	4.41	3.13	2.68
C	2.91	2.95	3.04	3.18	3.22	3.28	3.22	3.12	2.91	2.69

By comparing the data from Tables 69 and 71, it was realized that there was a slight difference between the results of clayey and sandy soils; the clay was a slightly worse media for detecting the steel beam than the sand (voltages in row C are slightly lower than those in Table 69). However, the beam was clearly detectable at a distance of 18 in with the presence of clay.

### 3.3.3 IF testing: Testbed off Campus

In order to determine if an induction-based nondestructive method would be successful in locating the bottom of a reinforced concrete pier, a particular test site was established. The test site was the same as the one used for PS test presented previously.

A three-foot deep by one-foot diameter hole was excavated. A four-foot long, one-foot diameter reinforced concrete pier was cast in place at the test site. The pier was reinforced with 5-#5 vertical rebar and #3 ties at 6 in, as shown in Figure 183. There was 3 in clear cover to the outside of the #3 ties. Three two-inch diameter holes were then bored 6-ft into the ground. The boreholes run parallel to the concrete pier located distances of 6, 12, and 18 in from the outside edge of the pier as can be seen in Figure 184. A 2-in diameter PVC pipe was inserted in the holes to a depth of 3 ft below the bottom of the pier as shown in Figure 185. The LITE was assembled and calibrated. The Probe was inserted into the

tube and the voltage readings were recorded at 1 ft intervals. The results are shown in Table 72.

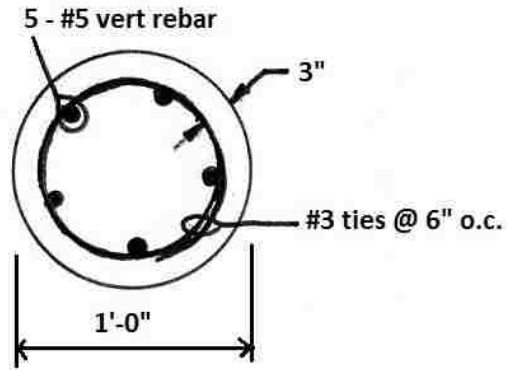


Figure 183. The 1-ft Reinforced Concrete Pier

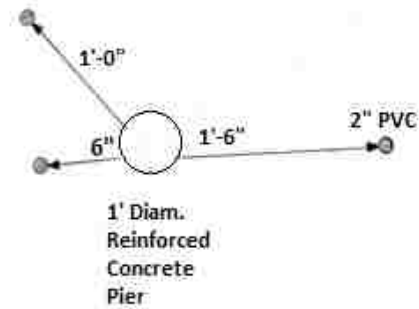
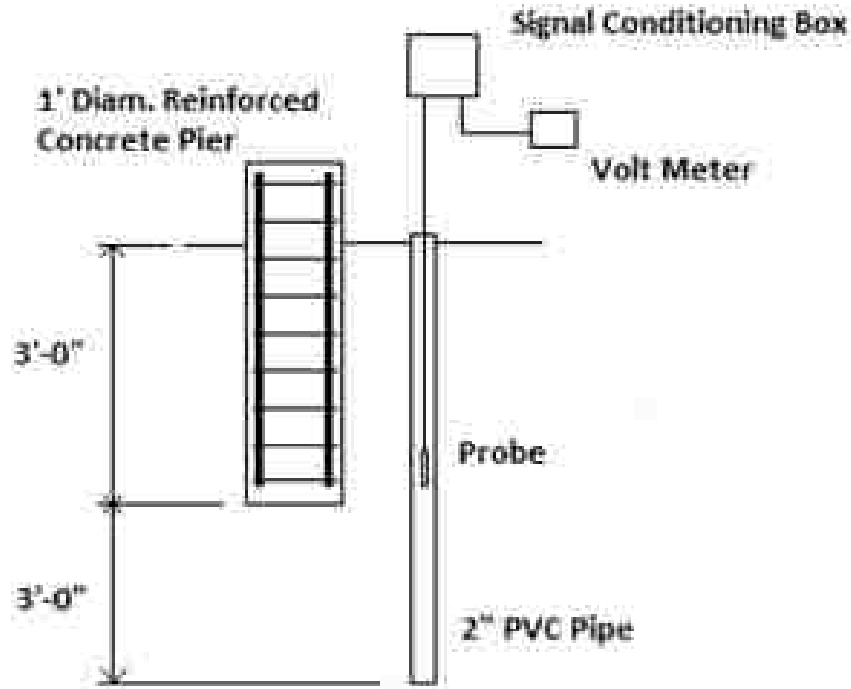


Figure 184. Layout of the Concrete Pier and Boreholes



**Figure 185. Schematics of the Reinforced Concrete Pier and the IF Test**

**Table 72. Voltage Readings Recorded at Each Borehole Location.**

Depth (ft)	Borehole @ 6"	Borehole @ 12"	Borehole @ 18"
0	5.01 V	5.04 V	3.95 V
1	5.01 V	5.04 V	3.92 V
2	5.04 V	5.04 V	3.45 V
3	5.04 V	5.01 V	3.42 V
4	3.59 V	3.62 V	2.65 V
5	2.56 V	2.75 V	2.50 V
6	2.50 V	2.50 V	2.50 V

The results show that the IF method could determine the depth of a reinforced concrete pier. It can determine the pier depth to an accuracy of approximately 6 in. It is also noted that while the bottom of the pier can be easily determined at a borehole distance of 6 and 12 in, when this distance is 18 inches the results become less conclusive.

### 3.4 Conclusions

### 3.4.1 SE/IR Tests

Numerous SE/IR tests have been conducted on a railway bridge and six highway bridges with known and unknown foundations depths. The lengths of the piles (piers) were determined using the velocity graphs obtained from the accelerometers for time domain and frequency domain analyses. Propagated wave velocity was determined when enough exposed length of the foundation was available. If not, the wave velocities were selected based on the pile condition observed in the field. In some cases, IR analyses were carried out to support and confirm the SE interpretations. Depending on the conditions of the foundations and superstructures, most tests were successful. Determination of the piles lengths was not viable in some SE/IR tests due to problems related to the method of applying the source, the location of the accelerometer, and other relevant factors that will be discussed here.

Initial testing procedures were developed and affecting factors were identified after the preliminary investigation of the columns at UNM. The selected bridges for the field tests made of various foundation materials (concrete, wood, and steel) with different geometries. Various SE/IR setups (source and receivers) were examined to identify major factors affecting the results. The conclusions of each bridge provided data leading to better understanding of those affecting factors. Then, the tests procedures were improved and modified. The conclusions inferred from field tests play a significant role in both conducting the tests and interpreting the data in the future.

Factors affecting the success of the SE/IR tests were scrutinized during the field tests. A successful SE test is the one in which the impulse and the echo from the pile bottom can be identified in the velocity graph with certainty. The effects of major factors such as striking specification, sensors location, hammer tips, environmental conditions, and pile condition are discussed

**Method of Striking** Depending on the accessibility of the pile top and the condition of the superstructure, we examined various impulse locations that are able to produce a longitudinal wave of enough energy along the test object. As shown in Figure 186 (similar to Figure 23), the impulse can be applied at Points A, B, C, and the striking block attached on the pile, as well as the top of the pile. The arrows indicate the direction of the striking.

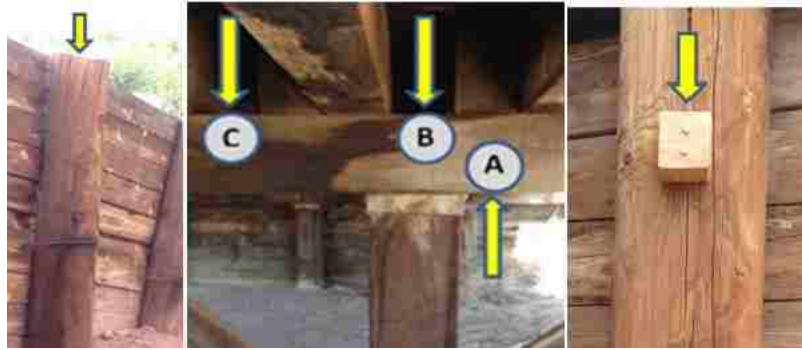


**Figure 186. Proper Source Locations**

*Pile top striking* This method can be used only when the pile top is accessible. The pile length was determined successfully in most of the cases. The impulses and echoes were clearly recognizable in the velocity graphs. Successful SE tests were obtained even for foundations for which only a small part of the pile top was exposed but large enough for a hammer strike.

*Points B and C* When the pile top is totally covered with the pile cap and superstructure, striking may be applied at Points B and C as indicated in Figure 186. However, we may only be able to apply the impact by striking at Point C due to the location of girder in some cases. The success rate of SE/IR tests is lower than the pile top striking. Higher rate of successful SE tests has been observed at Point B than at Point C due to the greater distance between the striking point and the center of the pile. In addition, the calculated length is more consistent for striking at Point B than Point C. Therefore, Point B is preferable compared with Point C.

For reinforced concrete bridges, the longitudinal waves can be generated by striking at the top surface of the concrete bridge deck above the pier. However, the result depends on the impact energy. The impact energy should be great enough to assure the determination of the foundation depth.

If downward striking at Point C is used, the striking point should be as close to the pile center as possible to maximize the input energy.

*Point A* Upward striking on the bottom surface of the pile cap adjacent to the test pile can also be considered as an alternative means to generate the impulse source. The field study indicated that fewer successful SE tests were produced than striking at Point B



since a stronger tensile wave together with a weaker reflected compression wave is transmitted down the pile rather than a stronger direct compression wave (striking at Point B).

*Striking Block* This method introduces additional uncertainty due to the problems related to the attachment of a striking block onto the pile surface. The impulse source is introduced by striking the block with a hammer. The field study indicated similar success rates for SE tests performed by striking at the wooden block and striking at Point A. The success rate was found to be much lower than striking at Point B.

Different methods of attaching the block onto the pile have been investigated. The block was mounted by nails (or screws), ties, and glue. Movement of the block was observed when the block was tied around the pile or was glued onto the pile by strong epoxy. Only secure attachment was found by mounting of the block by nails or screws. The striking block must be secured tightly onto the pile to restrict movement in order to produce good SE/IR results.

Blocks of different materials (aluminum and wood) and shapes (cube and wedge) have been tested. The aluminum block was specifically machined with a curved surface in order to provide a better contact with the side of the round piles. Table 73 shows the success rate of the SE tests in percentage performed by striking the block of different types.

**Table 73. Success Rate of SE Tests for Different Striking Blocks.**

Block Type	Aluminum Block	Wooden block	Wooden wedge
Success Rate (%)	23.3	56.8	35.7

As shown in Table 73, the success rate of using aluminum striking block is unsatisfied. The success rate is improved by using wooden blocks. The shape of the source signal for the aluminum block contained multiple peaks which was different from the typical hammer impulse on a rigid surface. The peaks may be due to either a momentary contact loss or multiple contacts between the block and the pile surface. Wedge blocks (the top surface is inclined) have been considered although striking on wedge blocks produced a horizontal compression wave as well as a vertical compression wave. The study results showed that successful SE tests were produced by using the wedge blocks, however, more

bad SE tests were found due to the imperfect coupling between the wedge block and the pile.

The problem of using striking blocks is mainly due to the appearance of multiple echoes in the velocity graphs which made the identification of the correct echo difficult.

*Comparison of striking methods* Table 74 lists the success rate of SE tests performed by different striking methods. Vertical downward striking on either the pile top or a point inside the projected pile cross section on pile cap top surface (Point B in Figure 186) transmits the most impulse energy directly to the pile, whereby the most consistent results have been obtained. Consequently, these two methods are the best to conduct SE/IR tests. If direct striking at the top of the pile is infeasible, striking on the top of the pile cap or upward striking on the bottom of the pile cap next to the pile (Points A or C in Figure 186) are alternative options. If none of these striking methods can be used, impulse source can be generated by striking on a wooden block that is tightly attached onto the pile. Striking the existing bolts or members that brace the pile sometimes produce successful SE tests.

It should be noted that each striking method will produce different levels of consistency depending on the strike quality, pile condition, and superstructure condition.

**Table 74. Success Rate of SE Tests for Different Striking Methods.**

Striking Point	Pile Top	Pile Top Edge	Pt. A	Pt. B	Pt. C	Striking Block
Success Rate (%)	83.3	52.4	54.1	81.3	37.5	56.8

**Accelerometer Location** If possible, the receiver should be placed at the top of the pile. Otherwise, the location should be selected such that the arrival time of the reflected upward wave from the pile bottom differs significantly from the reflected downward wave from the pile top. Since the pile length is not known repeating the test at a different sensor location is recommended when poor results are obtained.

As mentioned previously, when the sensor is placed too close to the striking point, the noise of high frequency was observed that significantly affected the identification of the echo in the velocity graph. The field tests indicated that successful SE tests were obtained when the accelerometer was placed 1-2 ft from the impulse source.

For the SE tests with two accelerometers, the inferred length of the pile was more consistent from the top accelerometer than the accelerometer mounted closer to the ground level, especially in the presence of running water. The accelerometer closer to the top of the pile is better because less complication from the reflections of both pile ends.

**Hammer Tips** The hard tip produced more successful SE tests than the other three softer tips. The success rate of the SE tests performed by different hammer tip types are indicated in Table 75. It should be noted, although the hard tip hammer was the best, the benefit of using softer hammer tips was found occasionally. The velocity graphs of hard tip sometimes contained multiple echoes. The input signal of the hard tip contains waves of higher frequencies. The presence of such high frequencies was verified by numerical analysis. When closely spaced multiple valleys appear in the vicinity of the expected echo, using softer tips may reveal the correct echo. When poor result of hard tip is observed, repeating the SE/IR test with a softer tip may overcome the difficulty.

**Table 75. Success Rate of SE Tests Performed by Different Hammer Tip Types**

Hammer Tip Type	Hard	Medium-hard	Medium-soft	Soft
Success Rate (%)	81.6	80	77.8	75

Besides determining the success rate of the SE tests for different hammer tips, additional investigation on the effect of the source signal amplitude was conducted for wood bridges. The success rate of SE tests performed by different hammer tips are indicated in Tables 76 to 79 based on the amplitudes of the source signals. The tables' data has following specifications:

- In each table, depending on the amount of the available data, the amplitudes of the source were broken down into multiple ranges to provide a better understanding of the SE tests success rate at specific amplitudes.
- The data of striking on the wood and aluminum blocks have not been considered since the success rate in such cases remarkably depends on the quality of the attachment of the block to the pile surface.
- All the tests conducted by hard and medium hard tips with amplitudes greater than 1 lbf produced good results. They have not been brought in the Tables.

**Table 76. Success Rate of SE tests for tests performed by hard hammer tips**

Source Amplitude Signal Range (lbf)	Success Rate (%)
0.85-1	100.0
0.65-0.85	85.7
0.4-0.65	85.7
0.2-0.4	28.6

**Table 77. Success Rate of SE tests for tests performed by Medium-hard hammer tips**

Source Amplitude Signal Range (lbf)	Success Rate (%)
0.7-1	85.7
0.6-0.7	100
0.5-0.6	71.4
0.35-0.5	71.4
0.1-0.35	42.9

**Table 78. Success Rate of SE tests for tests performed by Medium-soft hammer tips**

Source Amplitude Signal Range (lbf)	Success Rate (%)
0.8-1	85.7
0.64-0.8	85.7
0.45-0.64	100
0.35-0.45	85.7
0.1-0.35	42.9

**Table 79. Success Rate of SE tests for tests performed by Medium-soft hammer tips**

Source Amplitude Signal Range (lbf)	Success Rate (%)
0.7-1	100
0.5-0.7	100
0.4-0.5	75
0.2-0.4	25

The results indicated in Tables 76 to 79 show that the success rate of the SE tests is greater for sources with large amplitudes. It implies that stronger strikes can generate more interpretable results. As a result, for our utilized equipment, the tests performer should strike strong enough such that the amplitude of the produced signal exceeds 0.4 lbf to achieve satisfactory results for all types of the hammer tips.

**Environmental and Foundation Conditions** Environmental conditions may affect the SE/IR test results. In one of the investigated piles adjacent to water flow, the results of SE/IR tests were always bad although various setups were attempted. Successful tests were found on the next pile. It was expected that the noise due to the water flow (river current hit the pile) interfered with the SE tests. Other reasons might relate to the pile's condition such as rottenness or damage in the pile. The pile's condition has a huge effect on the clarity of signals. In one case, where there was a huge longitudinal crack in the pile, it was difficult to identify the correct echo because of the multiple wave reflections from the crack. When such abnormalities exist in piles, the actual depth of the foundation may not be determined by the SE/IR method.

**Difficulties with Steel Piles** Unsuccessful SE/IR tests were found for testing on a bridge supported by H-piles. High frequency vibrations were evident in the velocity graphs that corresponded to the reflections from the boundaries of the steel cross section. When a strike is applied at the middle of the web, the wave travels horizontally as well as vertically through the thin-walled members, unlike the results from a circular solid pile where most energy travels downward. The sensor picks up the reflected waves from the free boundaries, which in turn interfere with the expected reflected longitudinal waves from the pile bottom.

Apart from the difficulties mentioned above, steel H-piles transmit a large portion of the wave energy into the surrounding soil due to their specific cross section shape. Less energy is transmitted to the pile bottom, which significantly decreases the amplitude of the echo from the pile toe.

**IR Analysis** The IR analysis (based on the frequency content of the entire waveform) was carried out to complement the SE analysis. In some cases, IR analysis yielded the correct pile length while the echoes of SE tests could not be identified. It is recommended to perform an IR analysis when the SE data do not reveal the foundation

depth. The field results indicated that the pile length determined by IR analysis was slightly different from those of obtained from SE tests, however, the calculated pile lengths from IR analysis were more consistent than those obtained from the SE tests. This might be due to the occasional wave interference of various frequencies which might hinder pinpointing the echo from the pile toe in the velocity graphs. The IR analysis isolates the effect of each frequency.

### **3.4.2 PS Tests**

PS tests have been carried out on bridges supported by timber and steel piles. Both conventional and reverse PS tests were performed. The source was applied in testing the steel piles by either vertical striking on an aluminum block attached to the H-pile web or horizontal striking on the piles. Vertical striking on the pile cap and horizontal striking on the pile were applied by both regular and sledge hammers on the bridge supported by timber piles. Reverse PS tests were also conducted on the bridge with timber piles. The conventional PS tests were successful but the reverse PS tests did not yield good data due to the ambient noise. Therefore, the following conclusions are from the conventional PS tests only.

The first arrival times were determined by inspecting the background noise level in the signals prior to arrival of any sound wave from the source. The first arrival time was determined as the time when the signal begins to increase and consistently distinguish itself from the background noise level. The PS tests showed that determining the arrival time of the first P-wave objectively is a challenge depending on the level of ambient noise. The arrival time of the first P-wave was determined easily at greater depths since the ambient noise reduced with depth.

Both vertical and horizontal striking generated good signals although the signals provided by vertical striking were generally clearer than those of horizontal striking. The field study also showed the effect of the distance between the borehole and the test pile. Good results were obtained when the distance between the source and receiver was less than or equal to 4 ft. PS tests did not work when the distance between the source and receiver was greater than 6 ft. Other researchers recommended that the borehole should be

no more than 6 ft from the pile. Therefore, it is suggested that the borehole should be installed less than 6 ft from the test pile.

### **3.4.3 IF Tests**

Although IF field tests could not be performed in this project, two proper testbeds were constructed to investigate various aspects of IF tests. The findings were valuable and provided guidelines to perform IF tests on steel and reinforced concrete foundations.

The first testbed contained a metal I-beam placed horizontally in a wooden box full of soil. The box was filled with sand (or clay) and IF tests were conducted with the Probe placed inside the PVC tubes at various locations. IF tests were also performed on a reinforced concrete pier to study the performance of IF tests on reinforced concrete foundations.

The IF tests conducted at UNM indicated that the soil type affected the quality of detection. It was easier to detect the I-beam in sand than in clay although the beam could be detected in both types of soil at a distance less than 18 in. The results also showed that the moisture content of soils had no effect on the IF tests.

IF tests performed on the reinforced concrete cylinder located off campus showed that the IF method could be used effectively for determining the depth of a reinforced concrete pier. An accuracy level of approximately 6 in was obtained. The method worked at a borehole distance of 6 in and 12 in from the test pier. When the distance between the pier and the hole increased to 18 in or more, the results were less conclusive. It might be due to the location of the rebar that are 3 in from the pier surface. Therefore, the bore hole for IF tests must be drilled closer than 18 in in order to detect the reinforced concrete foundation.

IF tests can be used to detect steel and reinforced concrete foundations. For steel foundations, a borehole must be drilled within 18 inches from the test object. For reinforced concrete piers, a borehole must be drilled closer than 16 inches for a typical 2 in cover of concrete.

## CHAPTER 4 FINITE ELEMENT SIMULATIONS

Finite Element Modeling (FEM) is used to provide insight on the physical results of SE tests. Finite element simulations of 1D wave propagation in square-section timber piles and 3D wave propagation in concrete pier walls and complicated foundations were carried out using ABAQUS/EXPLICIT. The lengths of the timber piles and pier walls were calculated based on the velocity (or acceleration) responses at different nodes in the models. The effect of pile cap, input signal shape, the method of impulse application, and the location of sensor were investigated on timber piles. The effect of pier width, hammer tip type, the reflection from the deck, and the direction of striking were examined on models of pier walls. The effect of the material damping was also considered in the analysis. Rayleigh damping coefficients were taken into account based on the foundation resonant frequencies (41). In addition to the individual pier walls, a more complicated foundation comprising a pier wall and a pile was investigated.

### 4.1 Wave Propagation in Piles and Columns

In this section, proper FEM models were developed for better understanding of the wave propagation in the wood column at UNM and the timber piles of the Santo Domingo Bridge and Bridge No.1676 (see Table 4). The lengths of the piles were calculated based on the acceleration and velocity response at a node (the location of a sensor). The effect of the presence of pile cap and shape, location and direction of the input signal on the result of SE tests were investigated. Artificial damping was applied in some of the FEM simulations. The element type is C3D8R (8-node linear brick, reduced integration, hourglass control).

#### 4.1.1 Individual Wood Column

The simulated FEM model of an individual wood column is shown in Figure 187. The length and diameter of the wood column used in the FEM analysis are 3 m and 0.24 m respectively. The modulus of elastic (E) and the Poisson ratio ( $\nu$ ) of wood are 10 GPa and 0.3 respectively. The density ( $\rho$ ) is 500 kg/m<sup>3</sup>. The P-wave velocity is:



$$\text{P-wave velocity} = \sqrt{\frac{E}{\rho}} = \sqrt{\frac{10000000000}{500}} = 4470 \text{ m/s}$$

The impulse, a uniform pressure, was applied at the top surface of the column as shown in Figure 187. The bottom of the pile was free. The waveform of the impulse has a rectangular shape with a duration of 2 ms. This duration is similar to those observed in physical SE tests.

The impulse (wave) traveled through the column and reflected from any changes in impedance along the pile. Figure 188 shows a snap shot of the stress distribution along the column.

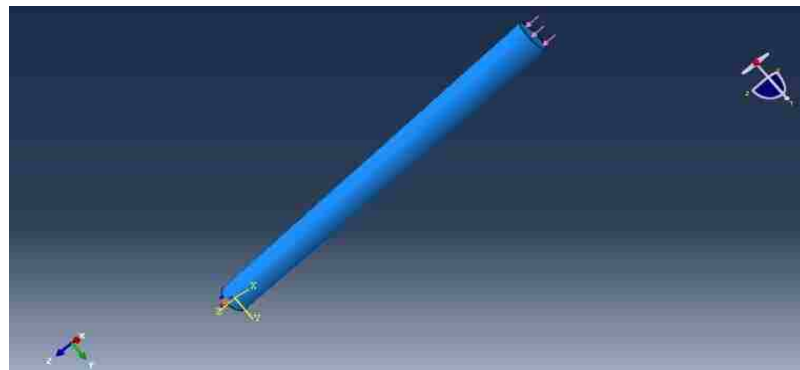


**Figure 187. An FEM Model of a Wood Column**

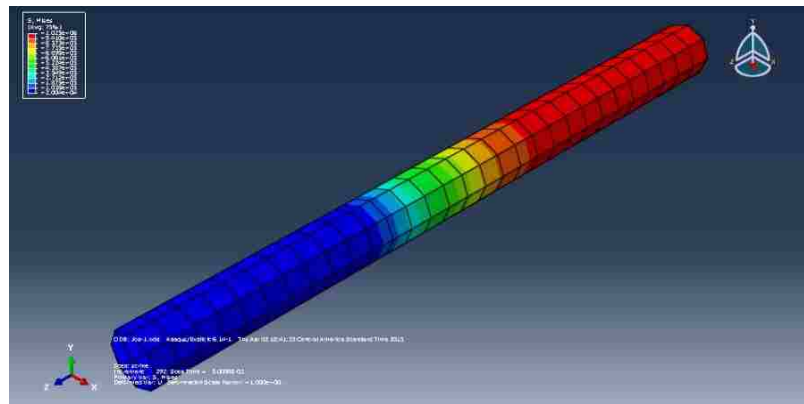


**Figure 188. A Snap Shot of the Distribution of Stresses along the Column**

The responses of acceleration and velocity at a node 0.1 m below the top of the column are shown in Figure 189.

Unlike the physical SE tests, there is no energy dissipation (zero damping) in this FEM model. More wave reflections are shown in the figure. Since the model contains a free end, the polarity of the reflected wave will change (incoming compression wave becomes outgoing tension wave). The time difference between two consecutive positive peaks (or negative valleys) corresponds to twice the length of the pile. The acceleration and velocity have 90 degrees' phase difference. Maximum acceleration occurs at zero velocity. The arrows in the figure show the moments of zero velocity at the targeted node.  $\Delta t$  (the difference between impulse and echo) was determined from two consecutive zeros (1.34 ms) to avoid the polarity change because of the free surface. The length of the column is calculated as:

$$L = v \times \Delta t = \frac{1}{2} \times 1.34 \times 10^{-3} \times 4470 = 3 \text{ m}$$

The calculated length is in accordance with the actual length (3 - 0.1 = 2.9 m) of the column.

Three other different input signals (triangular, trapezoidal, and sinusoidal impulses) were also used. Figure 190 shows the responses of the acceleration and velocity for trapezoidal, sinusoidal, and triangular impulses. The reflections can be identified clearly in these figures. The time differences between the impulses and echoes are the same as that obtained with rectangular impulse. Therefore, the shape of the impulse does not affect the determination of  $\Delta t$ .

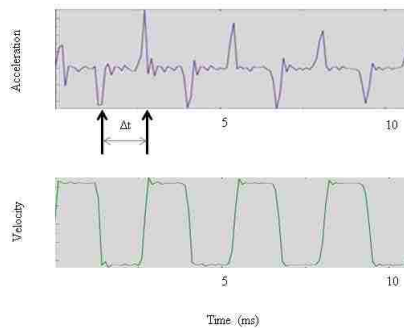


**Figure 189. Acceleration and Velocity Time Histories**

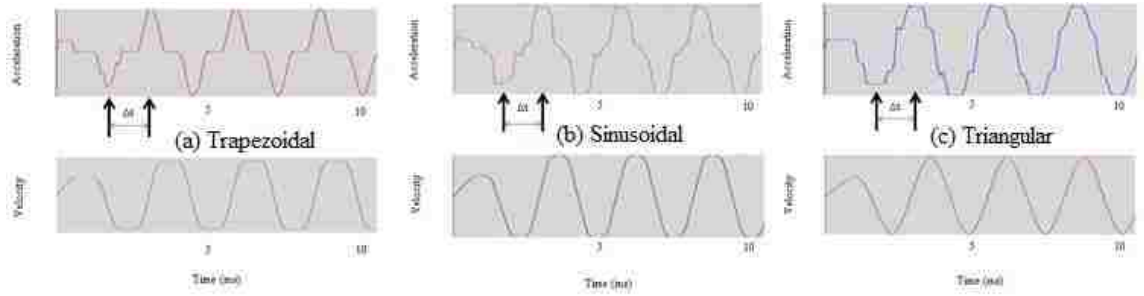


**Figure 190. Acceleration and Velocity Time Histories for Different Input Signals**

In physical SE tests a hammer applies a load on a small area rather than uniformly across the cross section of a pile. As shown in Figure 191, impulse of a rectangular waveform was applied on a 2-in diameter circle. It is to mimic the non-uniformity of stress wave across the cross-sectional area at the striking point in the physical SE tests. The result is shown in Figure 192. The general response is similar to the model in which the load was applied on the entire area of the column's top (see Figure 187).  $\Delta t$  is still 1.34 ms.

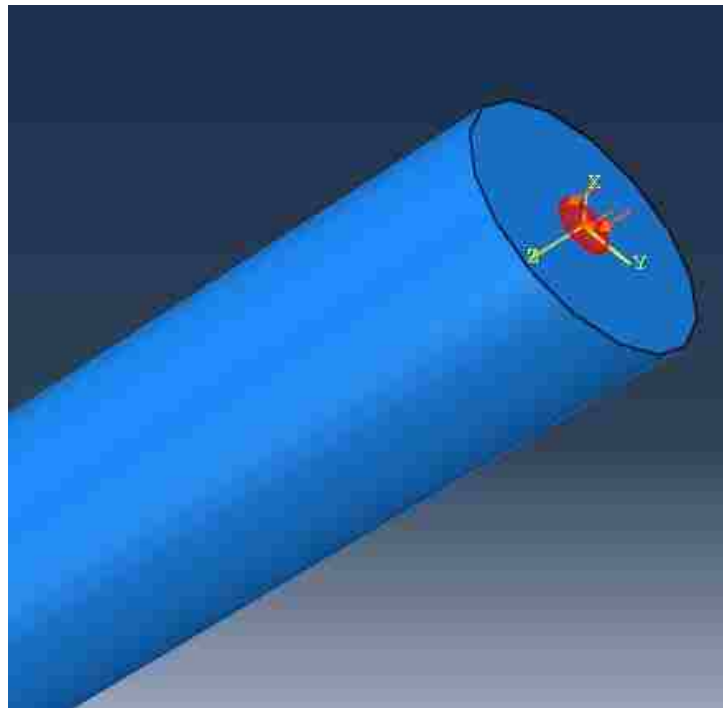


**Figure 191. Input Signal is Applied on Limited Area**

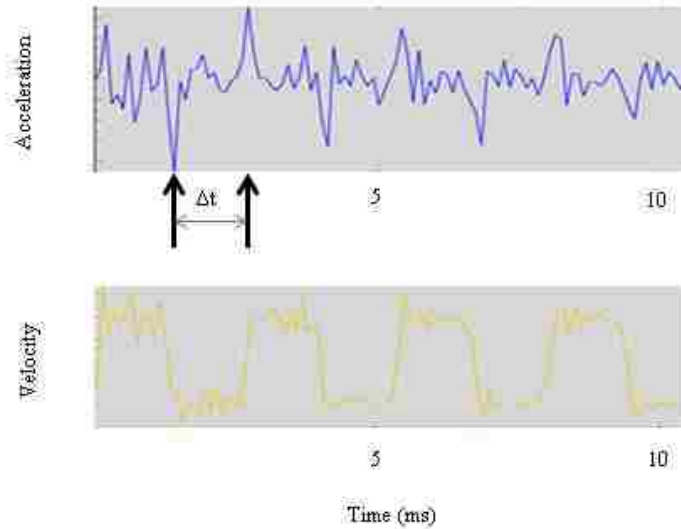


**Figure 192. Result of Input on a Limited Area**

#### 4.1.2 Wood Column with Foundation

In the next step, a structure composed of a concrete foundation ( $1.5 \times 1.5 \times 0.3$  m) and a wood column was simulated. The FEM model is indicated in Figure 193. The concrete's properties are:  $E = 20$  GPa,  $\rho = 2400$  kg/m<sup>3</sup>,  $\nu = 0.2$ . Figure 194 shows the model with the snap shot of the stress distribution.

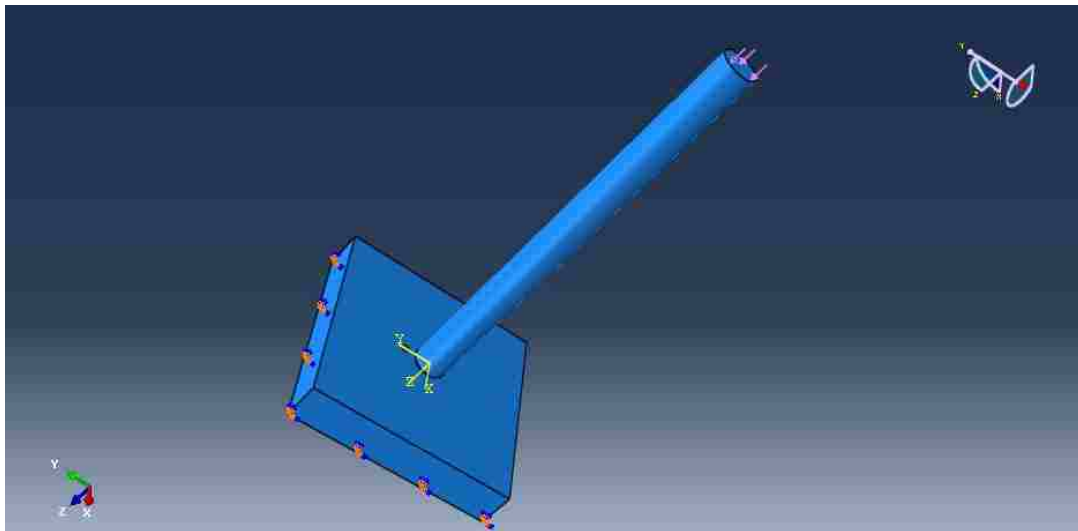


**Figure 193. A FEM Model of a Wood Column with Foundation**

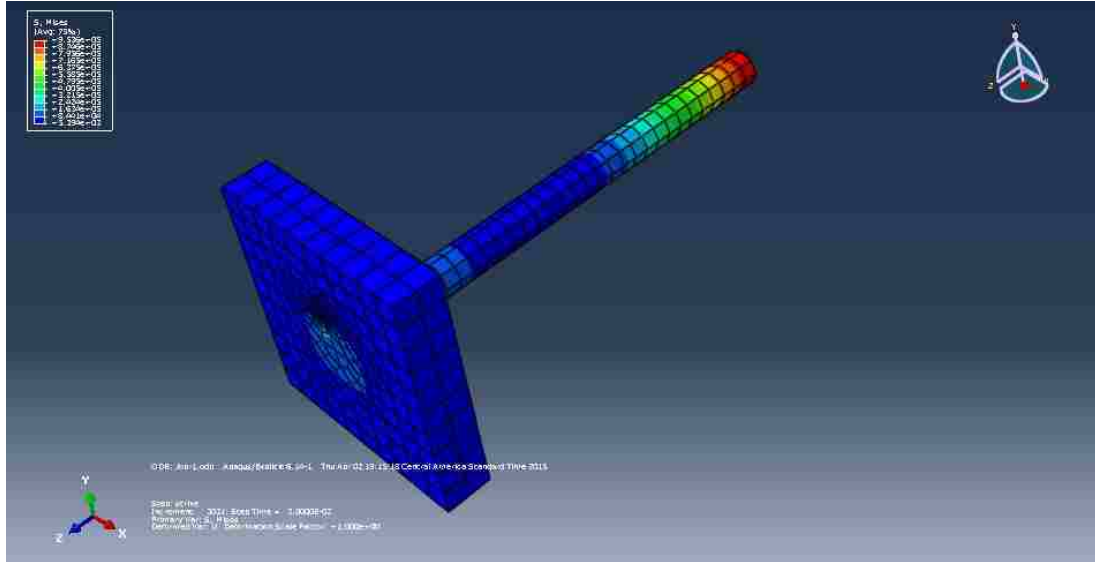


**Figure 194. Distribution of Stresses along the Column with Foundation at a Moment**

Rectangular and triangular impulses were applied. The acceleration and velocity graphs for the rectangular and triangular impulses are shown in Figure 195.

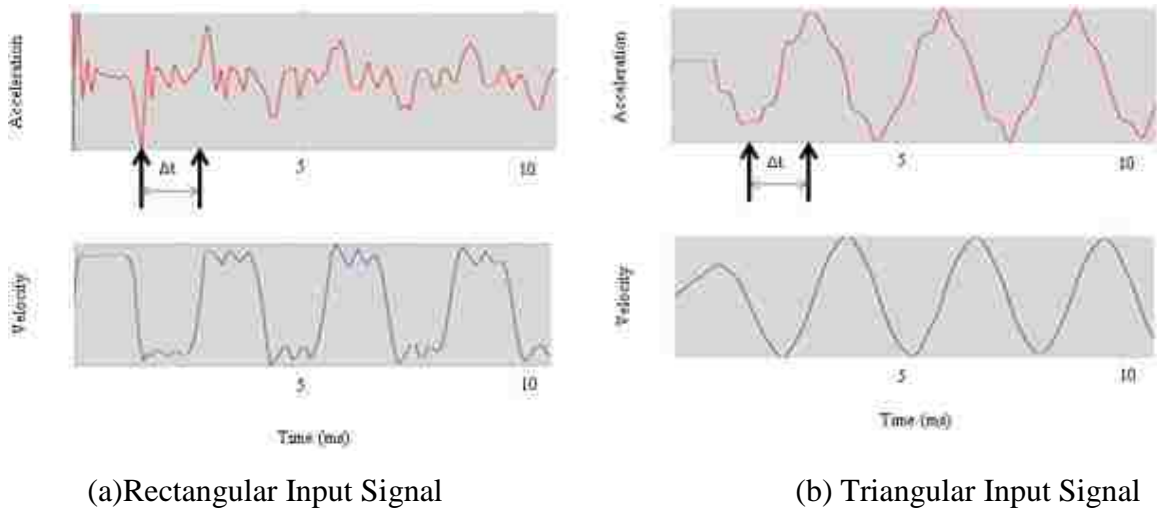


**Figure 195. Results of Rectangular and Triangular Input Signals**

Wave reflection can be seen in these figures. The interpretation of  $\Delta t$  is easier for triangular input signal than for rectangular signal. The length of the column is estimated as:

$$L = v \times \Delta t = \frac{1}{2} \times 1.44 \times 10^{-3} \times 4470 = 3.2 \text{ m}$$

This calculated length is similar to the actual length.

#### 4.1.3 Piles of Santo Domingo Bridge

SE tests have been performed on the timber piles at the Santo Domingo Bridge. Finite Element models were used to simulate these SE tests. The initial inputs for one of the bridge piles are:

Length = 9 m

Diameter = 0.33 m

E = 10 GPa

$\rho = 700 \text{ kg/m}^3$

$\nu = 0.1$

$$\text{P-wave velocity} = \sqrt{\frac{10000000000}{700}} = 3780 \text{ m/s}$$

The surrounding soil was not included in this numerical model. Only a simple FEM model of the pile was created. A snap shot of the stress distribution is shown in Figure 196.

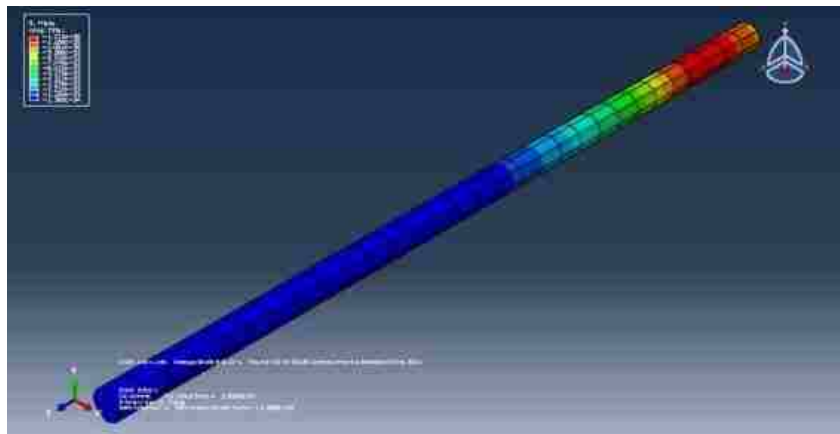


**Figure 196. Snap Shot of the Distribution of Stresses of a Model of the Santo Domingo's Pile**

Different forms of impulses were applied at the top of the pile. The graphs of the acceleration and velocity time histories for rectangular, triangular, trapezoidal, and

sinusoidal impulses are shown in Figure 197. They are the obtained response at a node located 0.3 m below the top of the pile.

Wave reflections are recognizable from these graphs. The  $\Delta t$  (time difference between the impulse and echo) is 4.7 ms and the pile length is calculated as:

$$L = \frac{1}{2} \times v \times \Delta t = \frac{1}{2} \times 4.7 \times 10^{-3} \times 3780 = 8.9 \text{ m}$$

The calculated length is in accordance with the actual length ( $9 - 0.3 = 8.7 \text{ m}$ ) of the pile.

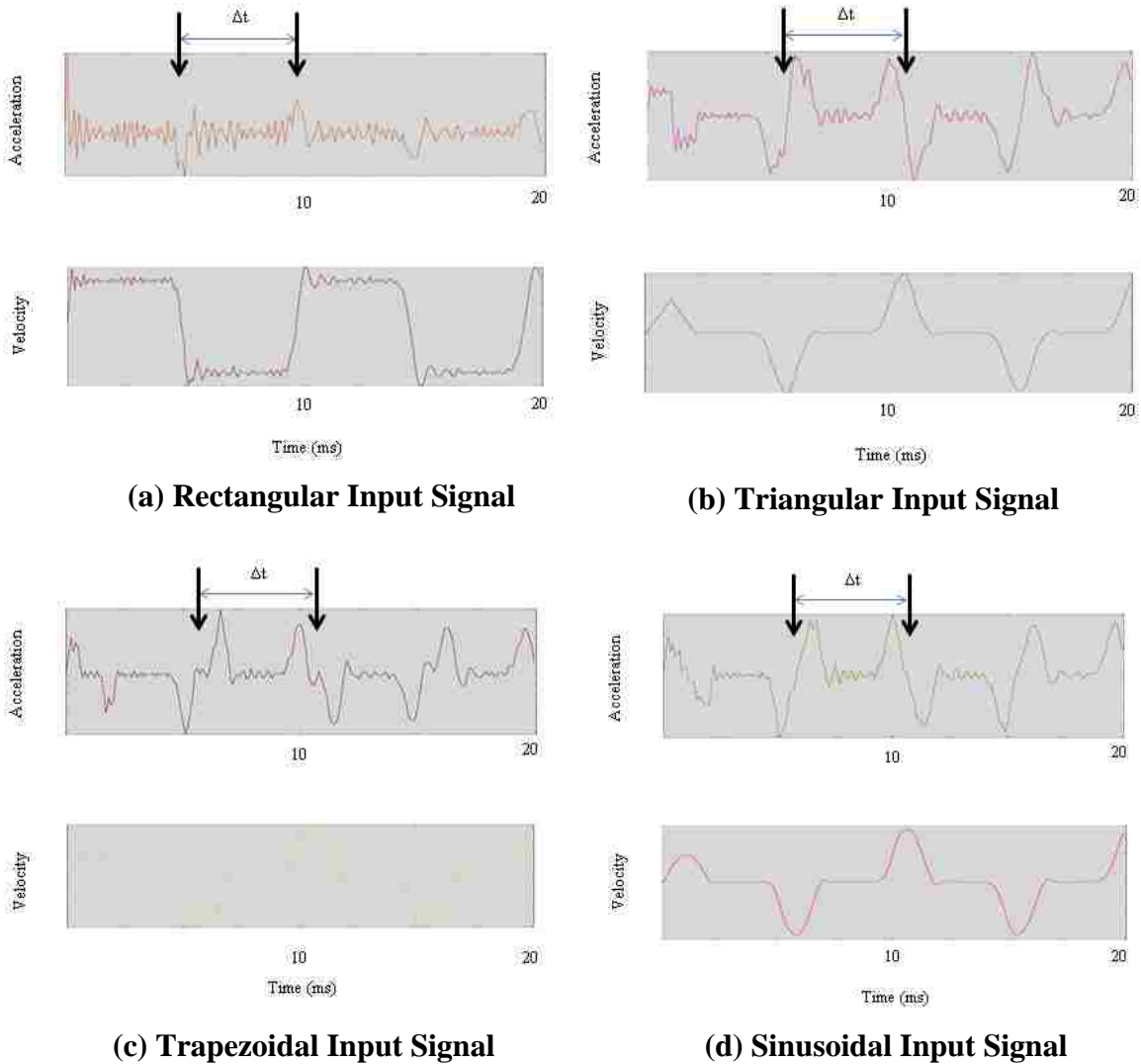


**Figure 197. Results of Input Signals of Different Shapes**

#### 4.1.4 Piles of Bridge 1676

Since the signals obtained from an accelerometer attached on the pile surface might be affected by the interference of pile cap, it was decided to investigate a foundation comprising piles and pile cap. The selected foundation FEM model has the same dimension as the foundation on bent C at Bridge No. 1676. The FEM models also provide means to compare signals obtained from different striking methods. The properties of the models are indicated in Table 80. The assumed wave velocity is 3,048 m/s which is the same as the velocity utilized to calculate the lengths of piles C-1 and C-2.

**Table 80. Specifications of Foundation Models in Bridge No.1676**

V (wave velocity)	3048 m/s
E (modulus of elasticity)	7.43 GPa
$\rho$ (density)	800 kg/m <sup>3</sup>
$\nu$ (Poisson's ratio)	0.3
Impulse amplitude	1 MPa
Impulse shape	Parabola
Impulse duration	1.2 ms
Simulation time duration	20 ms
Elements type	C3D8R (8-node linear brick)
Approximate mesh dimensions	0.2 m

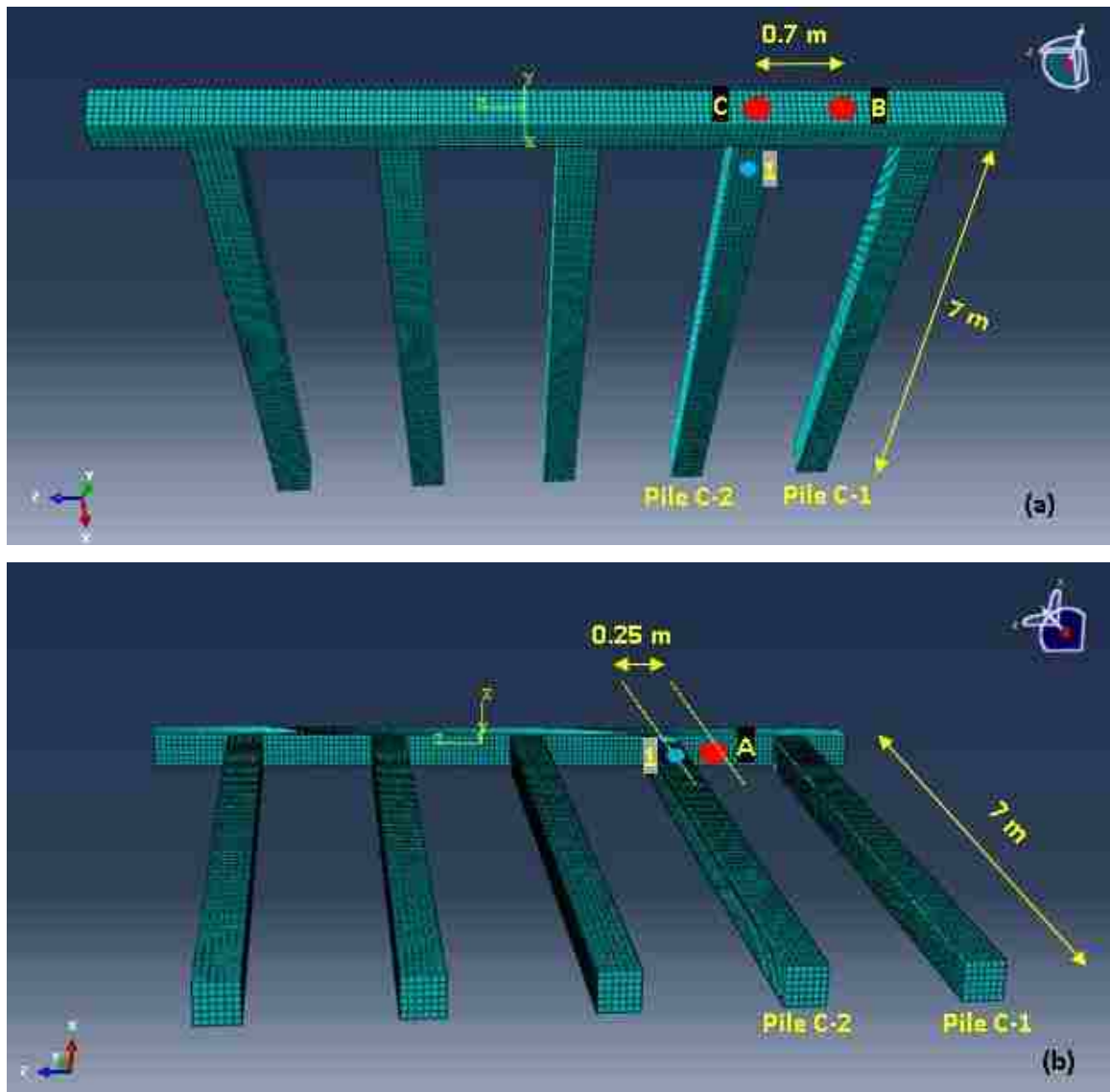
The actual waveform detected in field tests is subjected to damping inherent in the wood and surrounding material which absorbs the wave energy. To investigate the effect of material damping, the damping coefficients  $\alpha=0.1$  and  $\beta=0.0001$  corresponding to the Rayleigh damping equation ( $[C] = \alpha [M] + \beta [K]$ ) were considered in modeling.

Figure 198 shows the simulated FEM model. Downward strikes at points B and C and upward strike at point A were applied as the source. The velocity signals obtained from Node 1 (corresponding to accelerometer 1 in Figure 121) located 0.3 m below the pile top are investigated here. The signals obtained from numerical simulations are compared to filed results samples for each striking method in Figures 199 to 201. The results show that all strikes can produce interpretable results. The impulse and echoes were completely

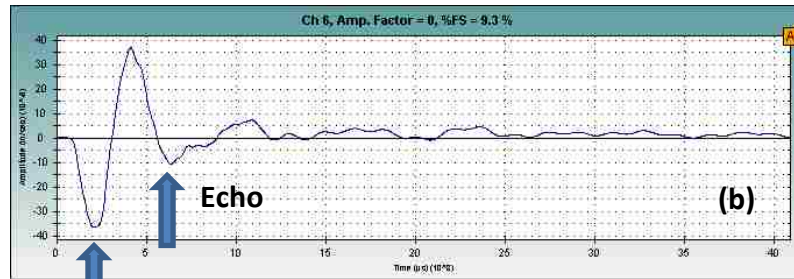
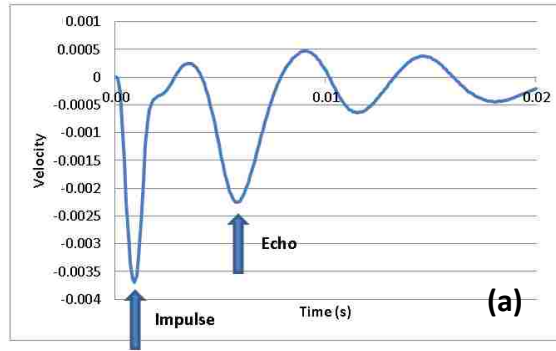


detectable on the graphs. The lengths corresponding to the time differences between the impulse and echo are very close to the actual length. The errors are less than %10. The results are summarized in Table 81.

The results also show that, among all these three striking methods, the signals' amplitudes for striking at point C (center) is maximum whereas they are minimum for point B (eccentric). This can be one of the main reasons for superiority of striking at C over striking at points A and B and superiority of A over B in the field tests results. The amplitudes of the impulses and echoes are indicated in Table 82 for all striking methods.

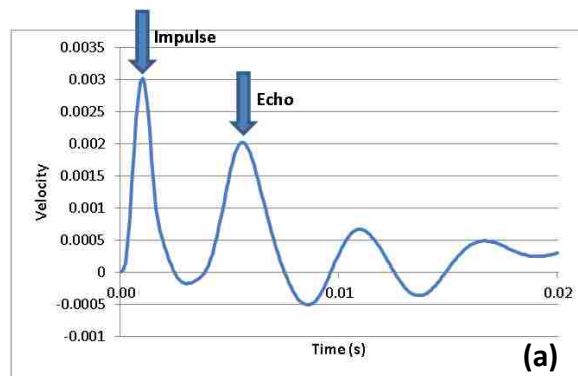


**Figure 198. FEM Model of Foundation Located at Bent C in Bridge No.1676 showing striking points (a) B, C and (b) A**



Impulse

Figure 199. Velocity Signal Obtained at Node 1 and Produced by Striking on Point C from (a) Numerical Simulation (b) Field



Impulse

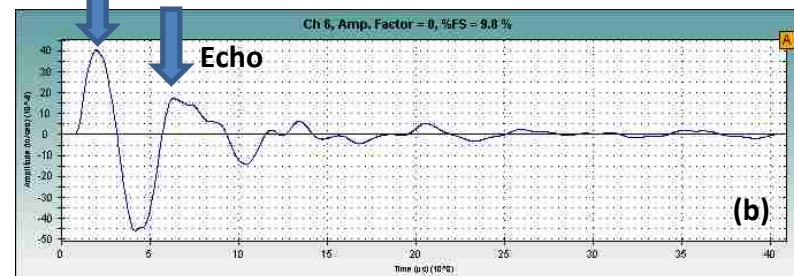
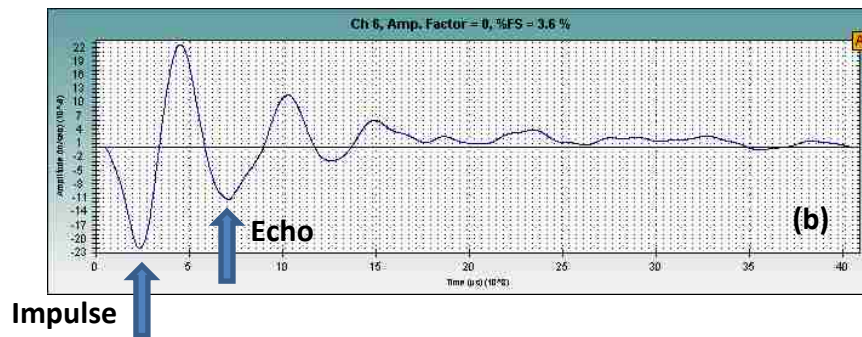
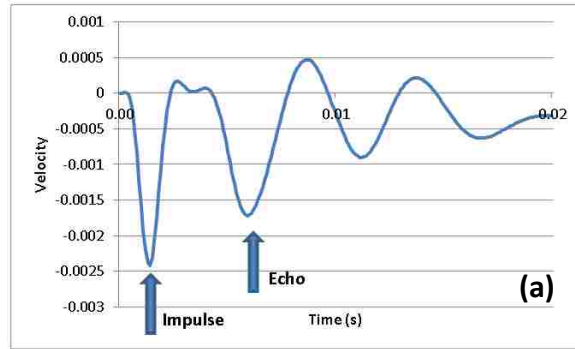


Figure 200. Velocity Signal Obtained at Node 1 And Produced by Upward Striking on Point A from (a) Numerical Simulation (b) Field



**Figure 201. Velocity Signal Obtained at Node 1 and Produced by Striking on Point B from (a) Numerical Simulation (b) Field**

**Table 81. Lengths Calculation Results for Different Striking Methods on Foundation of Bridge No.1676**

Striking Method	$\Delta t(s)$ from Numerical Simulation	$L_{tr}$ (m) from Numerical Simulation	$L_a$ (m)	Error (%)	$\Delta t(s)$ from Field	$L_{tr}$ (m) from Field
Striking at Point C	0.00485	7.31	6.70	9.1	0.00432	6.58
Striking at Point B	0.0045	6.86	6.70	2.36	0.00474	7.22
Striking at Point A	0.0046	7.01	6.70	4.63	0.00440	6.71

**Table 82. Amplitudes of the source signals for Different Striking Methods on Foundation of Bridge No.1676**

Striking Method	Impulse Amplitude	Echo Amplitude
Striking at Point C	-0.003694	-0.002231
Striking at Point B	-0.002421	-0.001712
Striking at Point A	0.002925	0.001943

#### 4.1.5 Waveform Analysis of Piles

A 6.7 m timber pile with a diameter of 0.3m was modeled in ABAQUS. The pile has a fixed support. The material properties are: elastic modulus = 6.19MPa, density = 800Kg/m<sup>3</sup>, Poisson's ratio = 0.3. The corresponding wave velocity is 2743 m/s .

Figure 202 shows the FEM model. Figure 203 shows the result of the acceleration at a node 0.3m far from the free end.

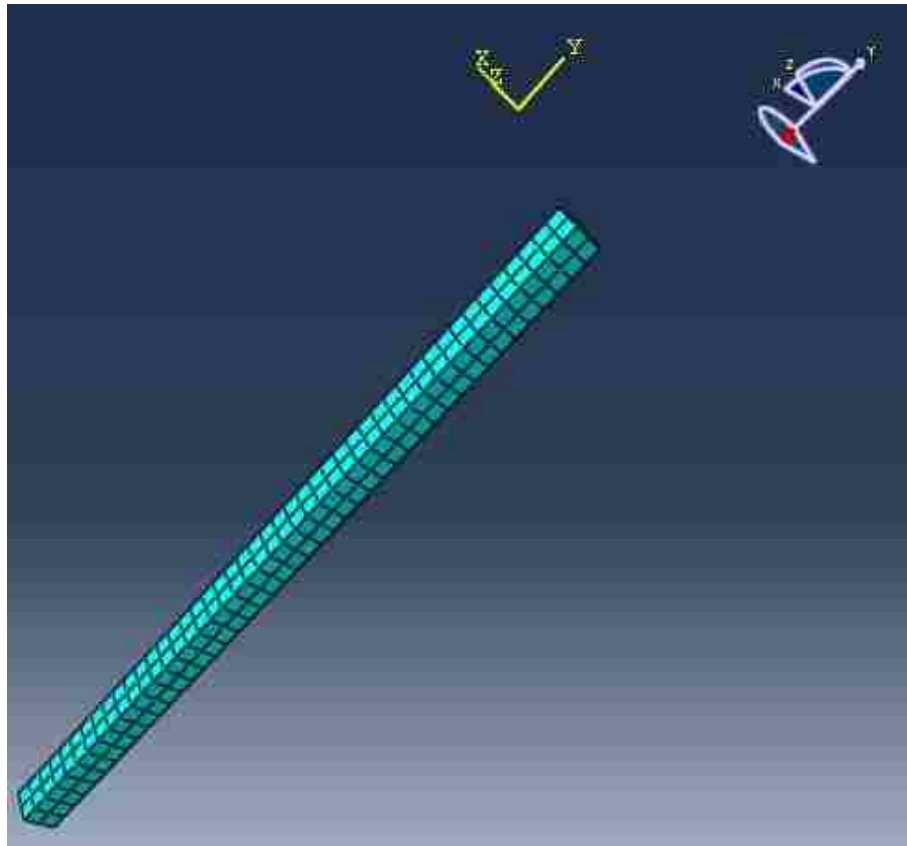


**Figure 202. FEM Mesh of Wood Column**

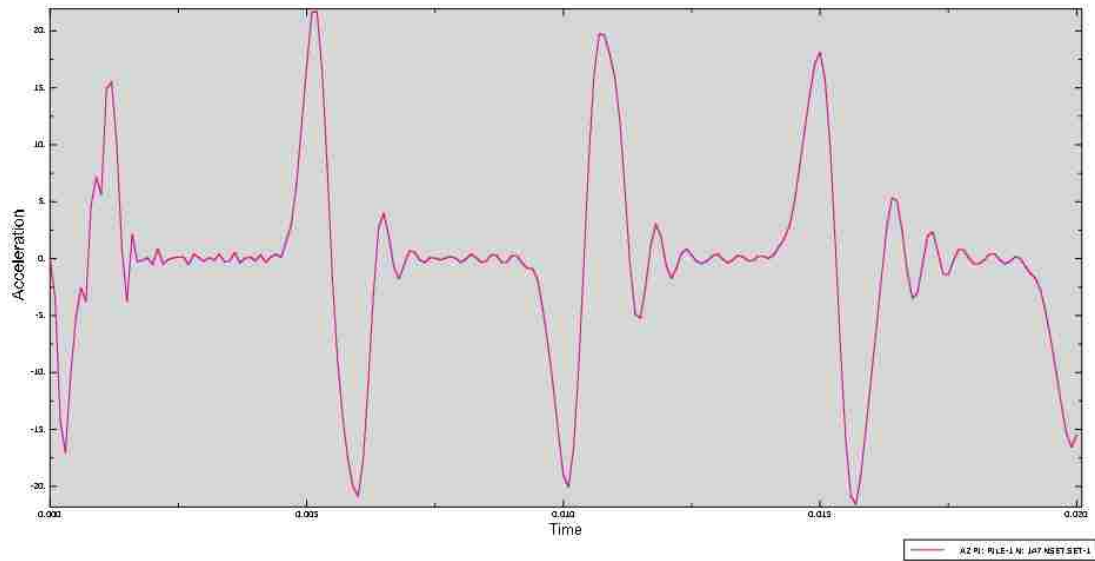


**Figure 203. Acceleration at a Node Close to the End of the Column**

Figure 203 shows that the waveform was inverted each time it hit the end. At a fixed boundary, a compression wave is reflected back as a compression wave (no phase change), while at the free end (left end near the node) it is converted to a tension wave. A tension wave is converted to a compression wave upon hitting the free end. Therefore, the sign of the incident wave changes as it reflected from the free end of the pile. On the other hand, the sign of the reflected wave is the same as the incident wave at the fixed end. This is why two valleys in the waveform acquired from field tests provide the complete travel time for reflection from the bottom of the pile.

In the next step the damping coefficients  $\alpha=0.2$  and  $\beta=0.0001$  corresponding to the Rayleigh damping equation were considered. In the presence of damping, the reflections arrive at the same time as shown in Figure 204, but the high-frequency content of the acceleration was removed and the amplitude decays over time similar to the field test results. The initial impulse (at time 0) is more evident. Compression force applied towards the right produces negative acceleration because the positive axis in our reference frame is pointing towards the left.

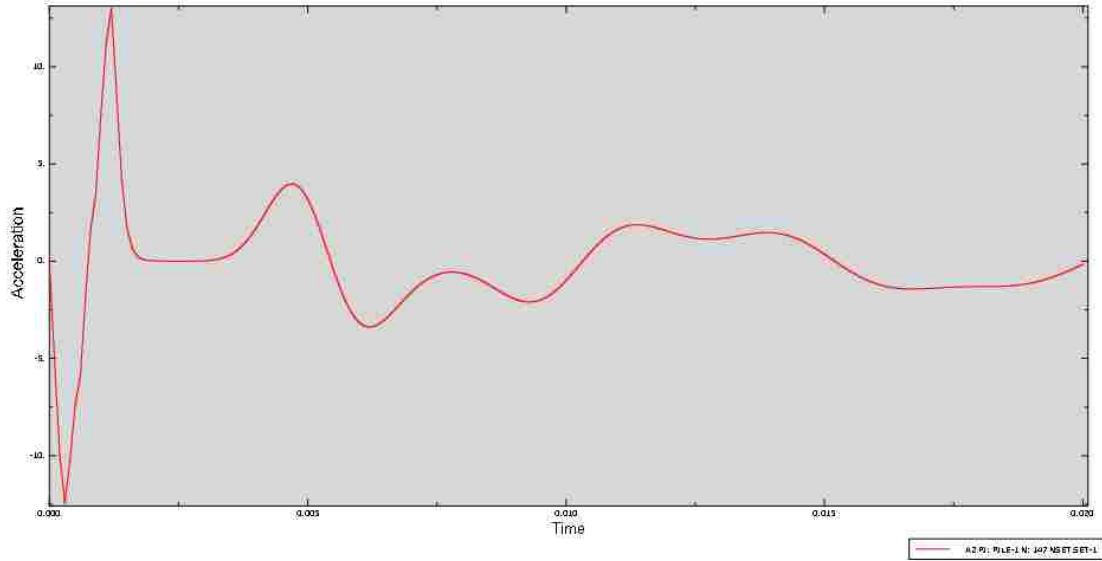


**Figure 204. Acceleration at a Node Close to the Free End (with Rayleigh Damping)**

Figure 205 shows a more complex waveform that was seen when the accelerometer was mounted too far from the free end (4.45m from free end). The reflections arriving from both ends made the analysis more difficult.

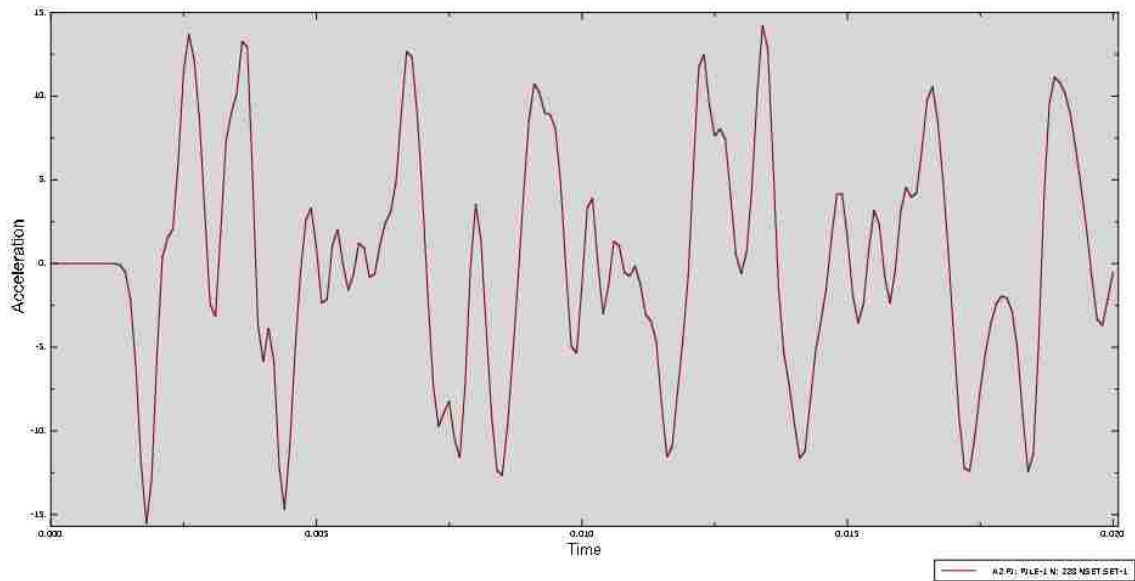


**Figure 205. Acceleration at a Node 1/3 Length of the Pile from the Left End**

## 4.2. Wave Propagation in Pier Walls

In this section, the wave propagation inside a 3-D pier wall was investigated. To do so, a concrete pier wall similar to the Pier 3 of Bridge No. 5899 was modeled in ABAQUS. The effects of hammer tip and the reflection from the deck on the received signals were examined.

The calculated height of Pier 3 was 23 ft (7m) from field SE tests results. The same height was used in the numerical model. The properties of the material and loading information are listed in Table 83. The assumed wave velocity (3261 m/s) is the same as that obtained in the field. The corresponding modulus of elasticity is calculated as:

$$E = \rho v^2 = 2400 \times 3261^2 = 25.52 \text{ GPa}$$

**Table 83. Input Parameters of the Finite Element Simulations.**

V (wave velocity)	3261 m/s
E (modulus of elasticity)	25.52 GPa
$\rho$ (density)	2400 kg/m <sup>3</sup>
$\nu$ (Poisson's ratio)	0.2
Impulse amplitude	1 MPa
Impulse shape	Parabola
Impulse duration	1.2 ms
Simulation time duration	20 ms
Elements type	C3D8R (8-node linear brick)
Approximate mesh dimensions	0.2 m

### 4.2.1 Wave Propagation in Pier Walls without Damping

No damping is considered in the numerical models and the effect of damping will be considered later.

#### 4.2.1.1 Effect of Pier Wall Width

Since the wave propagation in a pier wall may be different from that of a long slender pile, the results obtained from pier wall models with different widths were compared with the result of a long slender pile of the same height. The cross section and the side view of the selected pier wall are shown in Figure 206. Hereafter Nodes A and B assumed to be approximately coinciding with the Accelerometers 1 and 2 in the field tests respectively. The locations of Nodes A and B were two inches below the actual locations of Accelerometers 1 and 2 respectively, however the discrepancy is negligible compared with the height of the models.

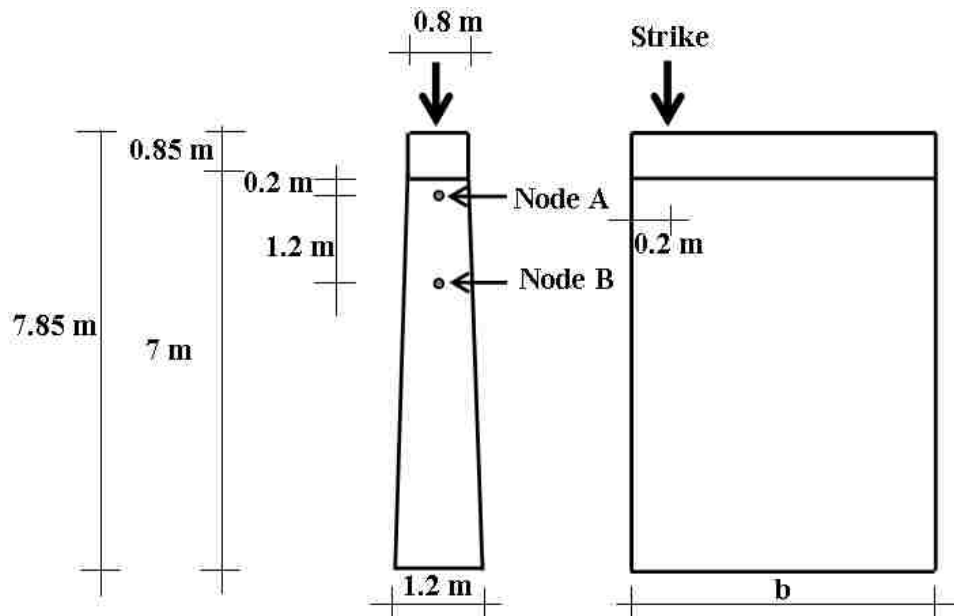


**Figure 206. Cross Section and Side View of the Pier Wall**

M1 is a finite element model of a square section pier (0.4 m x 0.4 m) with a length of 7.85 m. M2 to M6 are the models shown in Figure 206 of different widths (b). The width of each model is listed in Table 84. Model M6 has the same dimensions as the Pier 3 of Bridge No 5899.

**Table 84. Widths of the Pier in Models M2 to M6.**



Model	Width(m)
M2	0.4
M3	0.8
M4	1.7
M5	3.5
M6	5.2

A typical velocity graph obtained at Node A is shown in Figure 207. The unit of the velocity in this figure is m/s. Figure 208 shows the comparison of the velocity graphs of all models (M2 ~ M6). A total duration of 7 ms is shown here for clarity.

The degree of preciseness of determining  $\Delta t$  decreases with the increase of width  $b$ . The calculated length (6.2 m) is slightly less than the actual length in model M6 (6.8 m). The error is within the tolerance of SE tests (10%). The width of the pier slightly affects the estimation of the height of the pier in the numerical models.

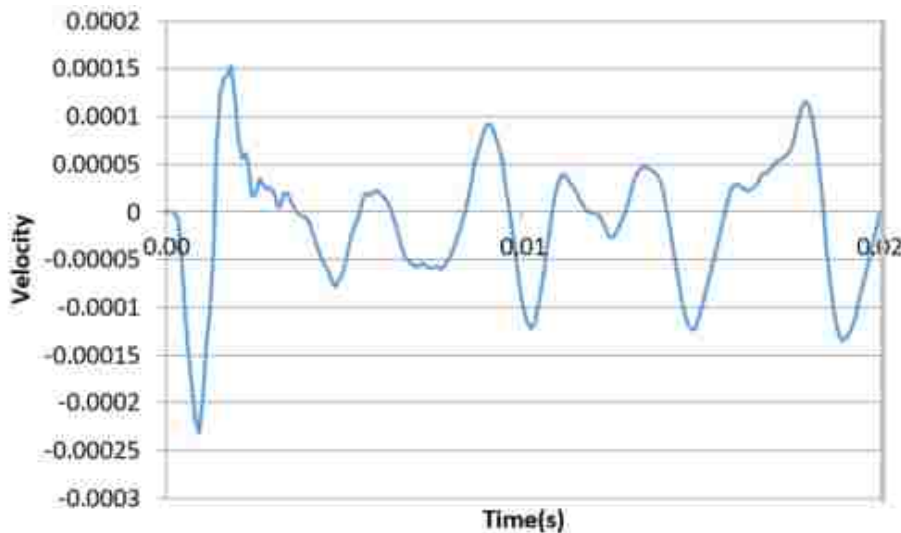


**Figure 207. Velocity Graphs Obtained at Node A (b = 5.2 m)**

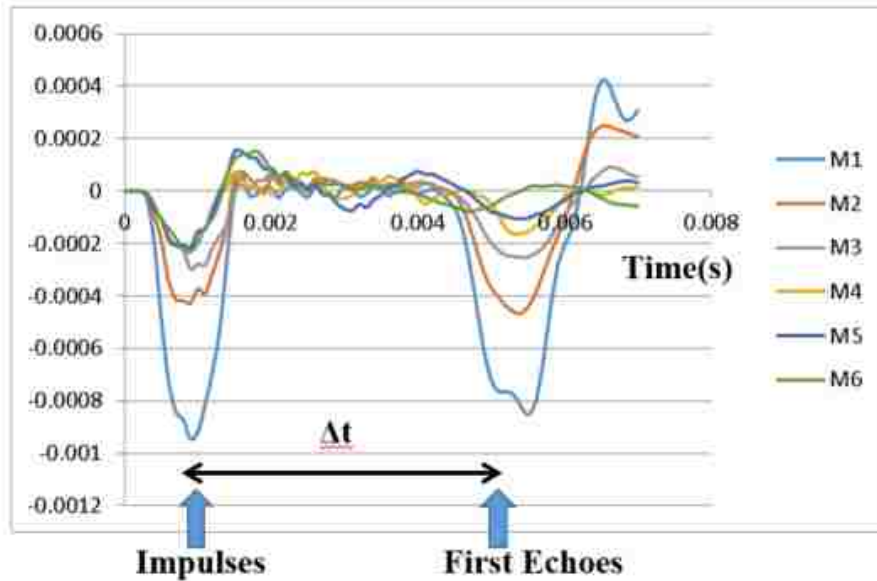


Figure 208. Impulses and the First Echoes of Models M1 to M6

#### 4.2.1.2 Effect of Hammer Tip

Different hammer tips (hard, medium-hard, and medium-soft) have been used on the pier in the field. It was decided to investigate the effect of hammer tip by using different impulse time durations. An FEM model of Pier 3 including the pier wall, the pile cap and a 2-ft deck was developed and the dimensions are shown in Figure 209.

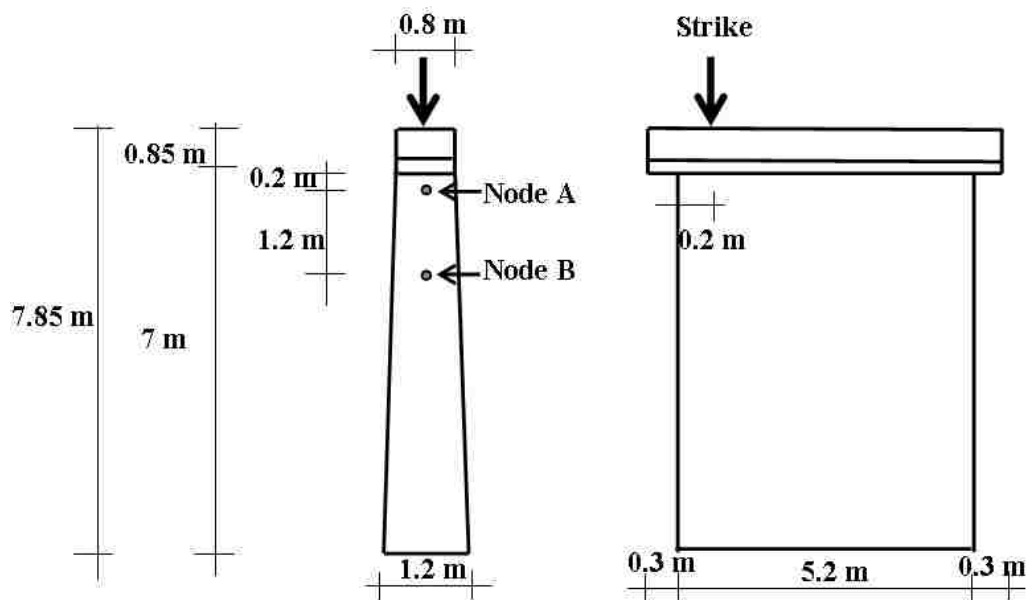


Figure 209. Dimensions of the Numerical Model and the Locations of the Source and Receiver

Three hammer tips and their corresponding impulse time durations are indicated in Table 85 for the three models (M7~M9). The velocity graphs of Models M7 to M9 at Nodes A and B are shown in Figures 210 and 211 respectively. The impulses and echoes can be identified for all models. The calculated heights based on the velocity graphs at Nodes A and B are indicated in Table 86.  $L_{tr}$  is the calculated length from  $\Delta t$  and  $L_a$  is the actual distance from the node to the pier bottom. The results are acceptable at Node A for different hammer tips. However, greater errors were found at Node B for medium-hard and medium-soft tips. The effect of hammer tip depends on the location of the sensors.

**Table 85. Impulse Time Durations and Corresponding Hammer Tips (M7~M9).**

Model	Hammer Tip Type	Impulse Time duration (ms)
M7	Hard	1.2
M8	Medium-hard	2.4
M9	Medium-soft	3.6

**Table 86. Calculated Nodes A and B Heights for Different Hammer Tips.**

Hammer Tip	Node A				Node B			
	$\Delta t$ (ms)	$L_{tr}$ (m)	$L_a$ (m)	Error (%)	$\Delta t$ (ms)	$L_{tr}$ (m)	$L_a$ (m)	Error (%)
Hard	4	6.52	6.85	-4.8	3.4	5.54	5.65	-1.9
Medium-hard	4.4	7.17	6.85	4.7	3.9	6.36	5.65	12.5
Medium-Soft	4.3	7.01	6.85	2.4	3.9	6.36	5.65	12.5

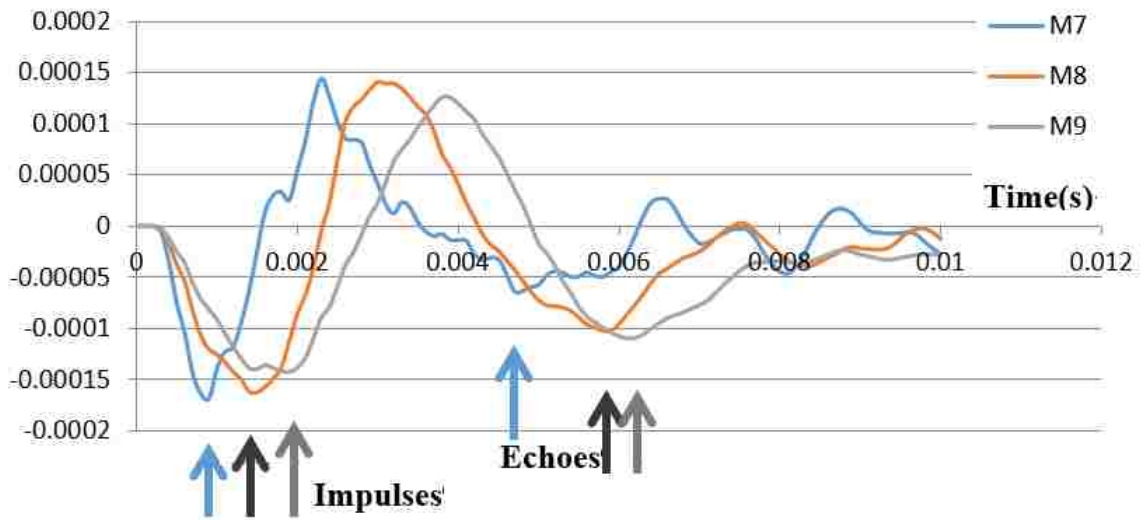


**Figure 210. Velocity Graphs of Models M7 to M9 Obtained at Node A**

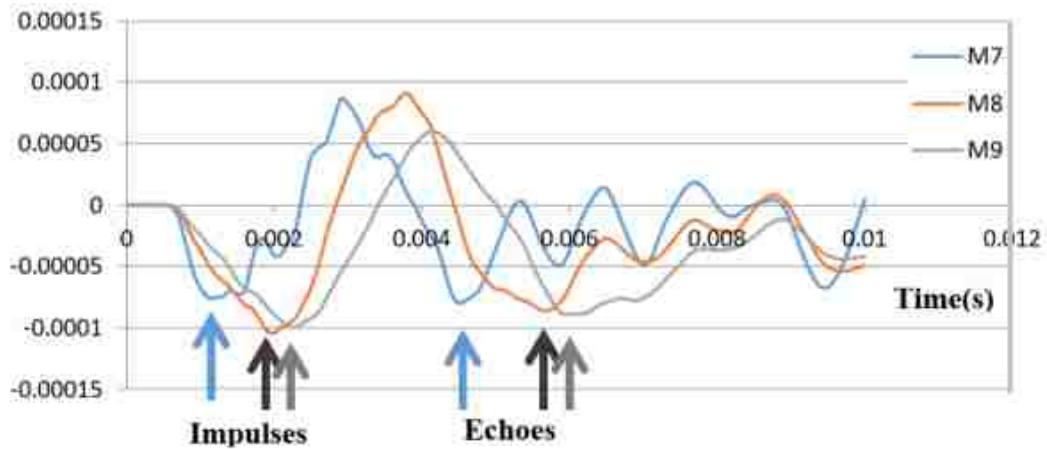


**Figure 211. Velocity Graphs of Models M7 to M9 Obtained at Node B**

#### **4.2.1.3 Effect of Deck Reflection**

The effect of reflection from the end of the deck was investigated by varying the deck dimension. The cross section and side view of the model are indicated in Figure 212.

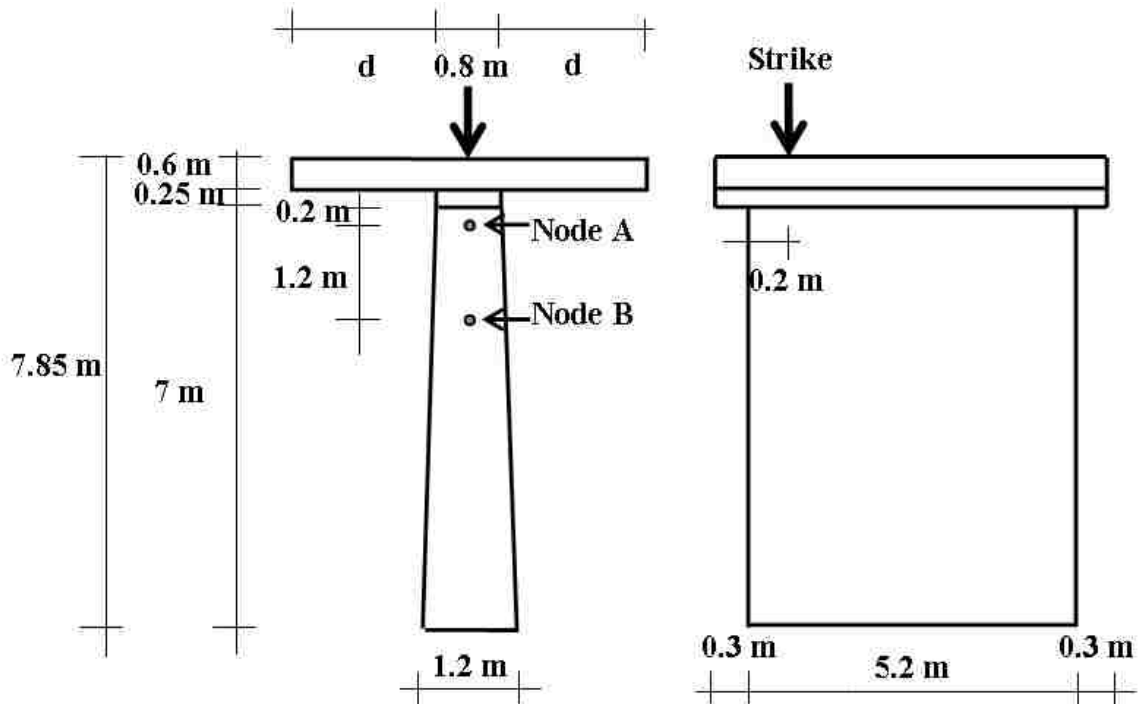


**Figure 212. Cross Section and Side View of a Model with Deck**

Finite element analyses on models with different deck widths ( $d$ ) were performed where  $d$  is listed in Table 87.

**Table 87. Deck Widths for FEM Models M10 to M12.**

Model	$d$ (m)
M10	13
M11	10
M12	7

A typical velocity graph obtained at Node A is shown in Figure 213. Figure 214 shows the velocity graphs of these three models. The impulses and echoes are the same for different widths of deck (see Points I and E on Figure 214).  $\Delta t = 4.1$  ms corresponds to a length of 6.69 m which is very close to the actual height of Node A (6.8m). Therefore, there is no deck effect.

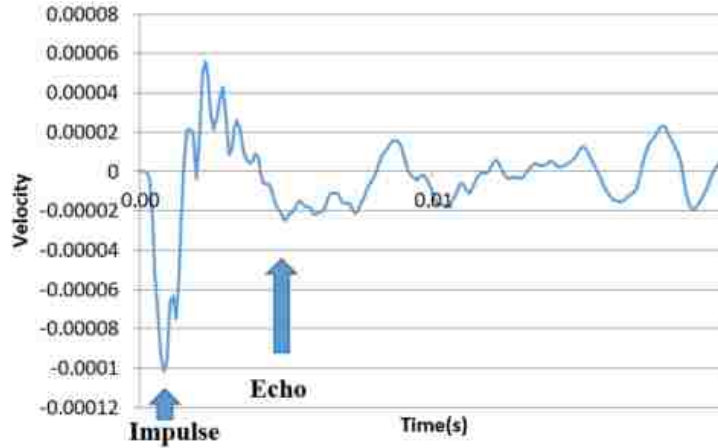


Figure 213. Velocity Graph Obtained in Node A ( $d = 10$  m)

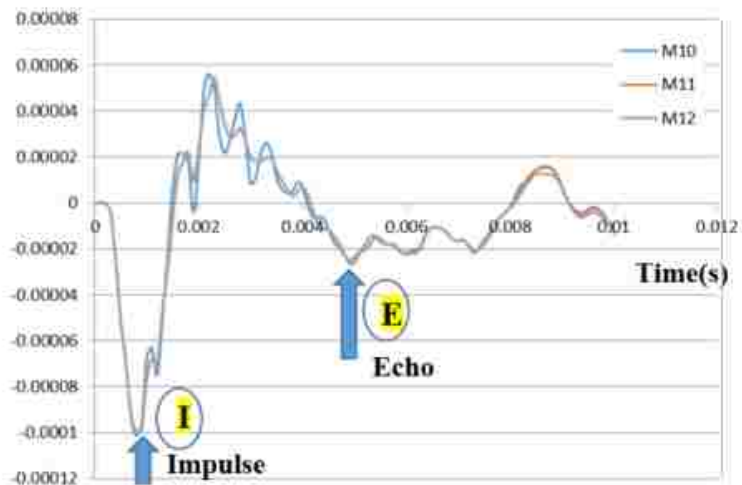
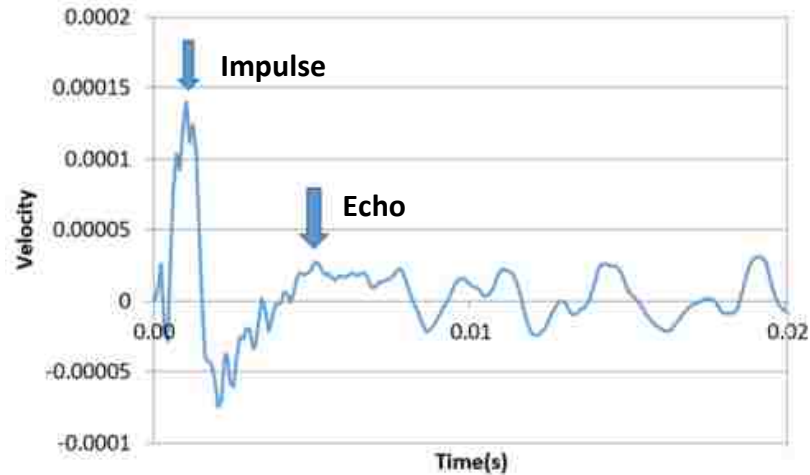


Figure 214. Velocity Graphs Obtained at Node A (M10 to M12)

#### 4.2.1.4 Effect of Upward Striking

Upward striking on the pile cap and on the bridge deck were simulated with the numerical model shown in Figure 212 ( $d = 7$  m). The velocity graphs obtained at Node A by striking on the pile cap and deck are shown in Figures 215 and 216, respectively. The impulses and echoes were identified with ease for upward striking at the pile cap and deck. The calculated heights are very close to the actual height and listed in Table 88. Therefore, both upward striking on the pile cap and on the bridge deck are acceptable alternative source to determine the height of the pier wall when the top of the deck is inaccessible.



**Figure 215. Velocity Graphs Obtained from Upward Striking at the Pile Cap**

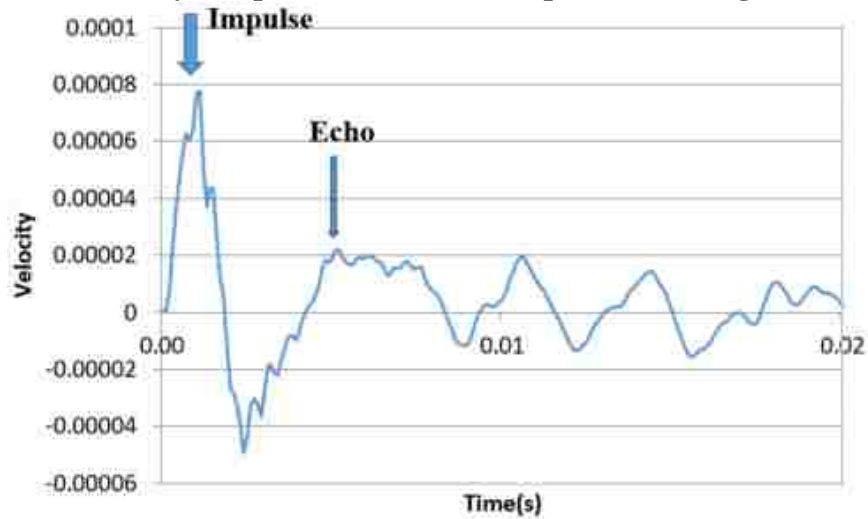


**Figure 216. Velocity Graphs Obtained from Upward Striking at the Bridge Deck**

**Table 88. Calculated Heights for Upward Striking.**

Striking Location	$\Delta t$ (ms)	$L_{tr}$ (m)	$L_a$ (m)	Error (%)
Pile cap	4	6.52	6.8	-4.1
Bridge deck	4	6.52	6.8	-4.1

#### 4.2.1.5 Summary of FEM Study of Pier Walls without Damping

The time difference between the impulse and echo did not change significantly with different widths of the pier wall. Similar numerical results were found for all hammer tips when the receiver was close to the top of the pier. For the deck width greater than 7 m, the

reflections from the end of the deck did not affect the signals. Since the calculated heights obtained from the upward striking were similar to the actual height, applying upward striking on the pile cap or on the bridge deck is good alternative to determine the height of the pier walls while the top of the deck is inaccessible.

#### **4.2.2 Wave Propagation in Pier Walls with Damping**

In section 4.2.1, a concrete pier wall similar to the Pier 3 of the Bridge No. 5899 was modeled using ABAQUS. The effects of pier width, hammer contact time, deck ends reflections and upward striking on the pier cap and bridge deck were investigated in the absence of energy dissipation. In this section, the effect of aforementioned factors was investigated again with material damping. To consider the effect of material damping, Rayleigh damping coefficients  $\alpha = 1.25$  and  $\beta = 0.00022$  were taken into account based on the pier wall resonant frequencies [41].

##### **4.2.2.1 Effect of Pier Wall Width**

To investigate the effect of damping on pier walls with different widths, three more models M13, M14 and M15 were added to the previous models M1 to M6. The width of models M13, M14 and M15 were 8, 10 and 15m respectively. The velocity graphs obtained at Node A for Models M2 and M15 for undamped and damped cases are depicted in Figures 217 and 218 respectively. In Model M2 (pier width = 0.4 m), the echo is clearly visible in both undamped and damped cases. The effect of damping is insignificant. Model M15 is an example of cases with the width greater than 5.2 m. In the undamped model, multiple echoes are shown in the vicinity of the expected echo. With the presence of damping, high frequency fluctuations around the echo have been eliminated and the echo point is detectable. The advantage of the presence of material damping in the data interpretation is evident.

The measured heights based on the velocity graphs at nodes A and B in Models M2 to M15 for both undamped and damped cases are shown in Tables 89 and 90 respectively. The actual height of the pier is also shown in these two tables. The echoes in the velocity graphs at Node B cannot be determined in undamped models when the width is greater



than 1.4 m. However, in all the models, the echoes become visible with material damping. The errors are greater at Node B than at Node A when the width is greater than 1.7 m.

The presence of high frequency vibrations near the echo makes interpretation difficult or impossible when there is no energy dissipation. FEM results showed that the presence of material damping divulges the echoes from the pier bottom by removing high frequency vibrations near the echo. Since the pier wall material possesses damping, the undamped cases will never happen in reality.

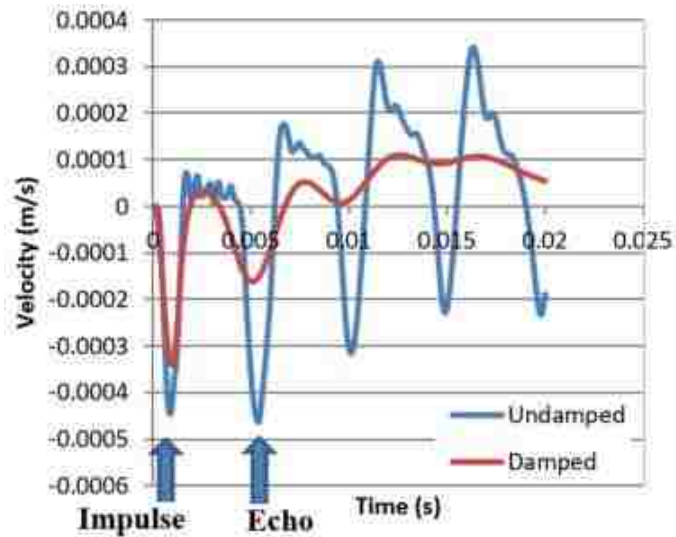


**Figure 217. Velocity Graph of Undamped and Damped Model M2 at Node A**

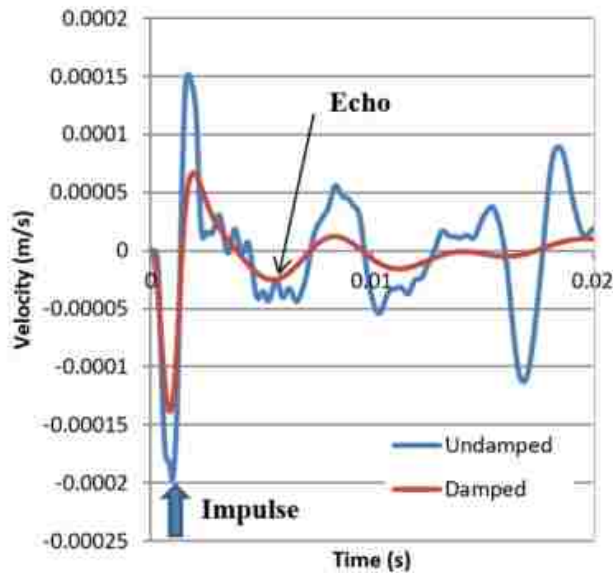


**Figure 218. Velocity Graph of Undamped and Damped Model M15 at Node A**

**Table 89. Measured and Actual Heights of Node A in Models with Various Widths.**

Model	Node A							
	Undamped				Damped			
	$\Delta t$ (sec)	$L_{tr}$ (m)	$L_a$ (m)	Error %	$\Delta t$ (sec)	$L_{tr}$ (m)	$L_a$ (m)	Error %
M2	0.0044	7.17	6.80	5.5	0.0039	6.36	6.80	-6.5
M3	0.0042	6.85	6.80	0.7	0.0039	6.36	6.80	-6.5
M4	0.0045	7.34	6.80	7.9	0.0043	7.01	6.80	3.1
M5	0.0045	7.34	6.80	7.9	0.0043	7.01	6.80	3.1
M6	0.0038	6.20	6.80	-8.9	0.004	6.52	6.80	-4.1
M13	Not Clear	-	6.80	-	0.0046	7.50	6.80	10.3
M14	Not Clear		6.80	-	0.0045	7.34	6.80	7.9
M15	Not Clear	-	6.80	-	0.004	6.52	6.80	-4.1

**Table 90. Measured and Actual Heights of Node B in Models with Various Widths.**

Model	Node B							
	Undamped				Damped			
	$\Delta t$ (sec)	$L_{tr}$ (m)	$L_a$ (m)	Error %	$\Delta t$ (sec)	$L_{tr}$ (m)	$L_a$ (m)	Error %
M2	0.0034	5.54	5.60	-1.0	0.0034	5.54	5.60	-1.0
M3	0.0035	5.71	5.60	1.9	0.0034	5.54	5.60	-1.0
M4	Not Clear	-	5.60	-	0.0038	6.20	5.60	10.6
M5	Not Clear	-	5.60	-	0.004	6.52	5.60	16.5
M6	Not Clear	-	5.60	-	0.0037	6.03	5.60	7.7
M13	Not Clear	-	5.60	-	0.0044	7.17	5.60	28.1
M14	Not Clear	-	5.60	-	0.0042	6.85	5.60	22.3
M15	Not Clear	-	5.60	-	0.0039	6.36	5.60	13.6

#### 4.2.2.2 Effect of Hammer Tip

The FEM model of a pier wall with a width of 5.2 m (see Figure 212) and material damping was analyzed with different hammer tips. The hammer tips and the corresponding impulse contact durations are shown in Table 91.

**Table 91. Hammer Tips and the Corresponding Impulse Contact Durations of Three Models.**

Model	Hammer Tip Type	Impulse Time Duration (ms)
M16	Hard	1.2
M17	Medium-hard	2.4
M18	Medium-soft	3.6

The impulses and echoes are recognizable for all three models. The calculated heights based on the  $\Delta t$  obtained at Nodes A and B are listed in Table 92. When the contact time increases, the error becomes greater at both Nodes A and B. In addition, the errors at Node B are greater than Node A. Therefore, it is recommended to use a hammer with hard tip and place the sensors as close as possible to the top of the pier wall to achieve more successful SE tests.

**Table 92. Calculated Heights of Nodes A and B for Damped Models.**

Model	Node A				Node B			
	$\Delta t$ (sec)	$L_{tr}$ (m)	$L_a$ (m)	Error %	$\Delta t$ (sec)	$L_{tr}$ (m)	$L_a$ (m)	Error %
M16	0.0041	6.69	6.80	-1.7	0.0038	6.20	5.60	10.6
M17	0.0043	7.01	6.80	3.1	0.004	6.52	5.60	16.5
M18	0.0048	7.83	6.80	15.1	0.0043	7.01	5.60	25.2

#### 4.2.2.3 Effect of Deck Reflection

The effect of the deck width was investigated by varying the deck dimension in the finite element models. The cross section and side view of the FEM model are depicted in Figure 219.

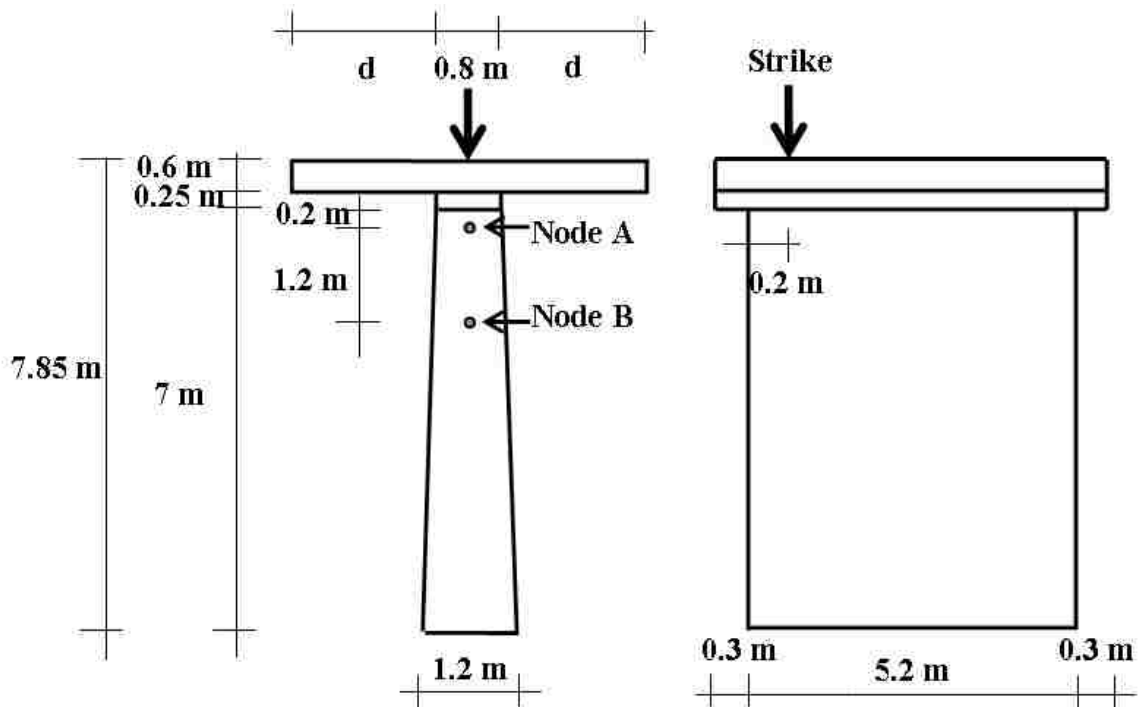


**Figure 219. Cross Section and Side View of the Models with Bridge Deck**

Finite element analyses on models with three different deck widths ( $d = 6, 8, 12$  m) were performed. The corresponding deck widths of these models are listed in Table 93.

**Table 93. FEM Models of Various Deck Widths.**

Model	d (m)
M19	6
M20	8
M21	12

The velocity graphs of above-mentioned undamped and damped models at Nodes A and B are plotted together in Figures 220 and 221 respectively. These graphs show that the impulse and echo are the same for models with the widths of 6, 8 and 12 m (see Points I and E on Figures 220 and 221). The calculated heights based on the  $\Delta t$  at Nodes A and B are shown in Table 94. Considering the echoes at Point E, the calculated lengths are very close to the actual lengths from the pier bottom to Nodes A and B in the undamped models. The error is less than 2%. However, the errors are large for the damped models.

Since the deck ends of Pier 3 in the field were located farther than 6 m, no deck effect is expected on the signals obtained from Accelerometers 1 and 2. However the errors become greater especially in Node B.

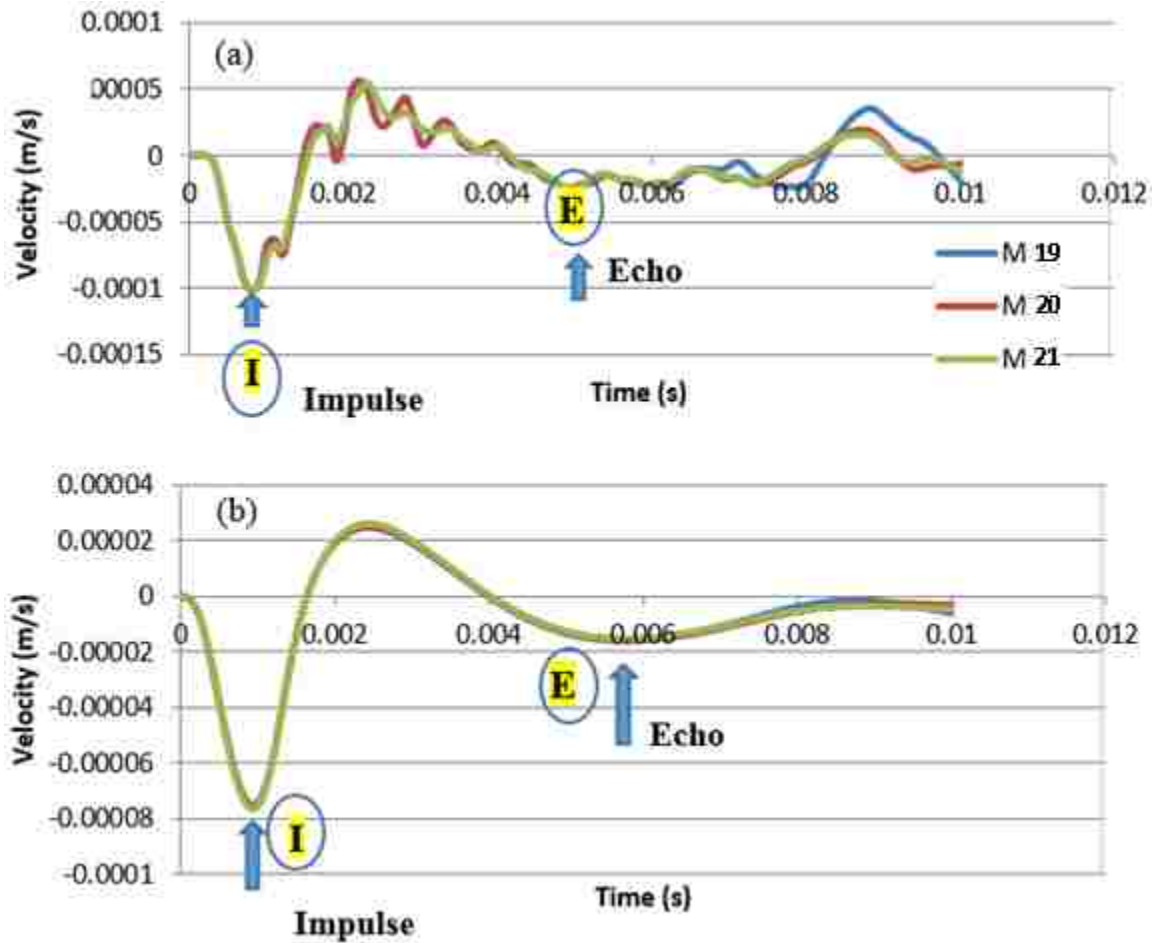


**Figure 220. Velocity Graphs Obtained at Node A (Models M19 to M21) (a) Undamped Models (b) Damped Models**

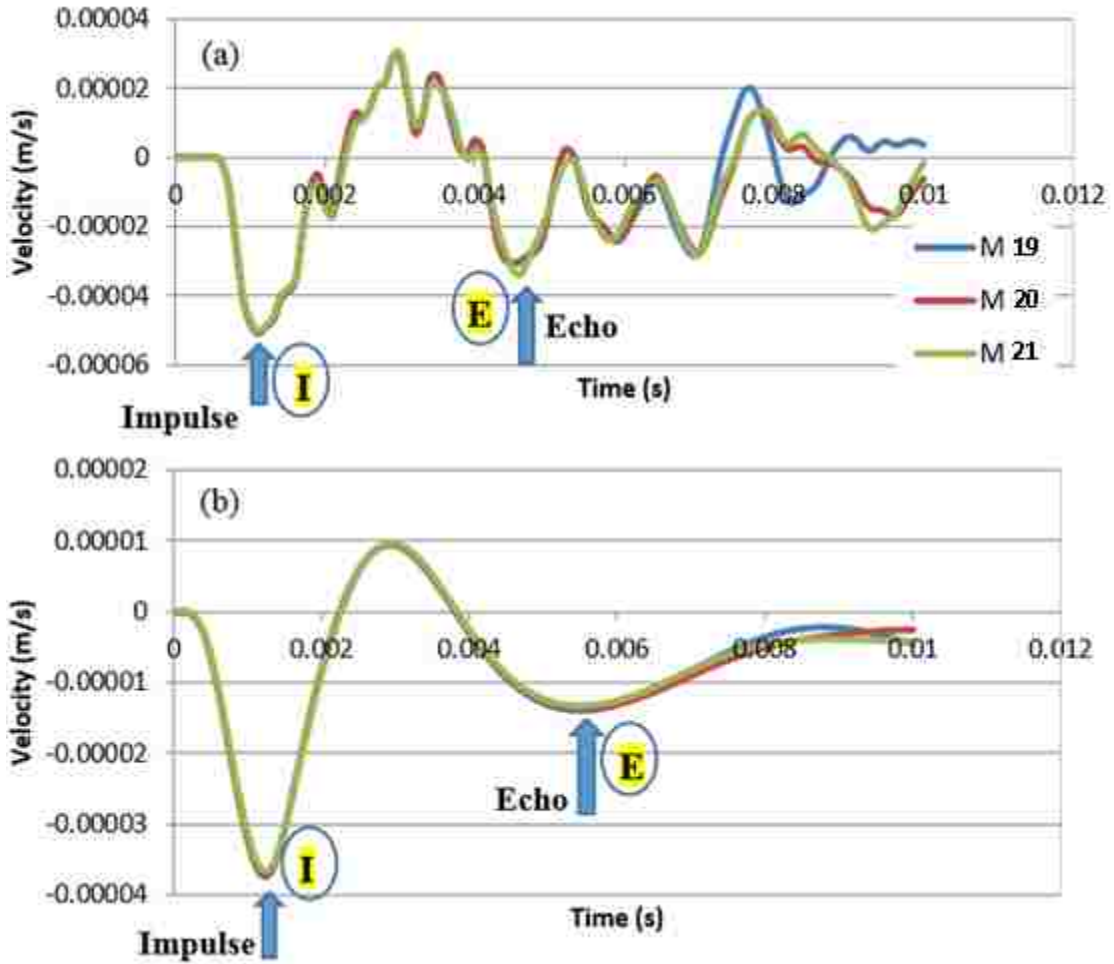


**Figure 221. Velocity Graphs Obtained at Node B (Models M19 to M21) (a) Undamped Models (b) Damped Models**

**Table 94. Calculated Heights Corresponding to Nodes A and B in Models M19 to M21.**

Node	Undamped				Damped			
	$\Delta t$ (sec)	$L_{tr}$ (m)	$L_a$ (m)	Error %	$\Delta t$ (sec)	$L_{tr}$ (m)	$L_a$ (m)	Error %
A	0.0041	6.69	6.80	-1.7	0.0047	7.66	6.80	12.7
B	0.0034	5.54	5.60	-1.0	0.0042	6.85	5.60	22.3

#### 4.2.2.4 Effect of Upward Striking

Upward striking on the pile cap and bridge deck were simulated in the numerical model shown in Figure 219 ( $d = 7\text{m}$ ). In Model M22 an upward strike on pier cap at Point C was applied, whereas the strike was applied at Point D in Model M23 (see Figure 133).

The velocity graphs of undamped and damped models obtained at Nodes A and B in Models M22 and M23 are shown in Figures 222 and 223, respectively. Although impulses and echoes can be identified for both upward striking methods, the first echoes are less distinguishable at Node A for the undamped model. This may be due to the reflections from the deck and pier cap that contaminate the result since Node A is closer to the deck. The echo becomes more distinct with the presence of damping. The calculated heights of Nodes A and B are listed in Tables 95 and 96 respectively. Similar to the previous findings, errors are greater when the sensor is farther away from the top of the pier.

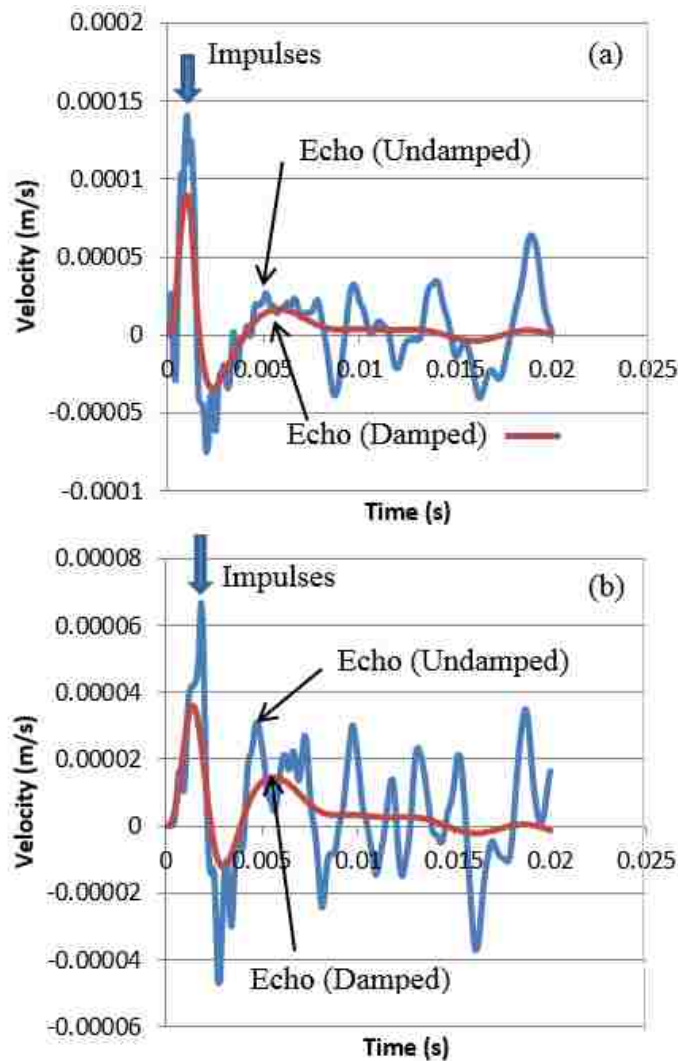


**Figure 222. Velocity Graphs of Undamped and Damped Models Obtained at (a) Node A and (b) Node B from Upward Striking on the Pier Cap (M22)**

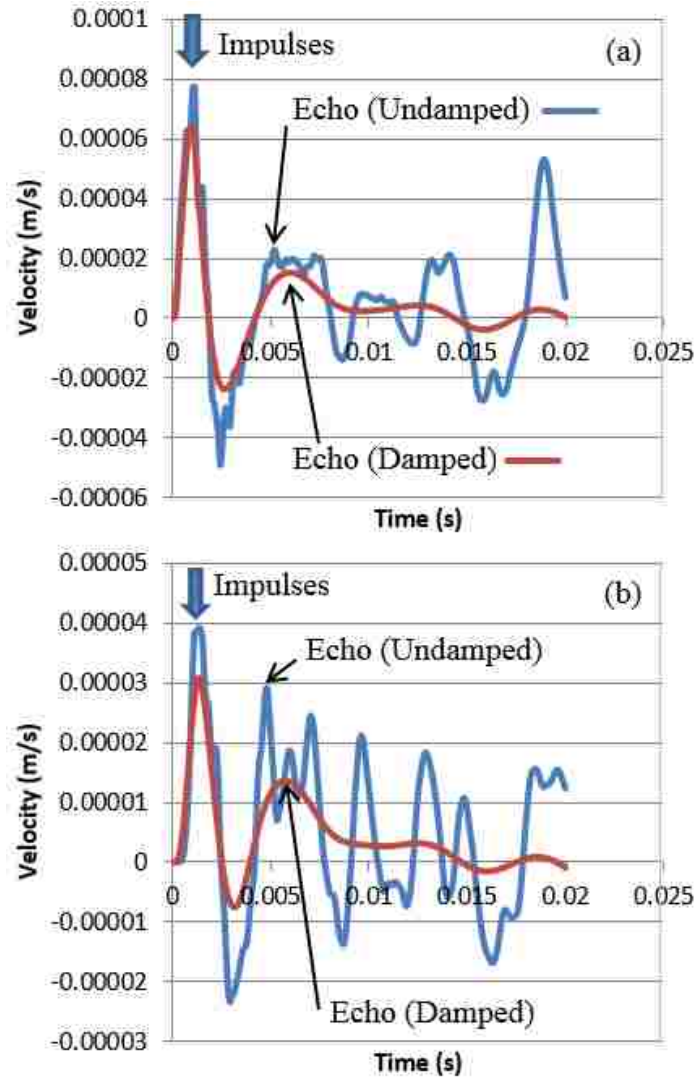


**Figure 223. Velocity Graphs of Undamped and Damped Models Obtained at (a) Node A and (b) Node B from Upward Striking on the Pier Cap (M23)**

**Table 95. Calculated Heights for Upward Striking at Node A in Models M22 and M23.**

Model	Node A							
	Undamped				Damped			
	$\Delta t$ (sec)	$L_{tr}$ (m)	$L_a$ (m)	Error %	$\Delta t$ (sec)	$L_{tr}$ (m)	$L_a$ (m)	Error %
M22	0.0041	6.69	6.80	-1.7	0.0046	7.50	6.80	10.3
M23	0.0042	6.85	6.80	0.7	0.0048	7.83	6.80	15.1



**Table 96. Calculated Heights for Upward Striking at Node B in Models M22 and M23.**

Model	Node B							
	Undamped				Damped			
	$\Delta t$ (sec)	$L_{tr}$ (m)	$L_a$ (m)	Error %	$\Delta t$ (sec)	$L_{tr}$ (m)	$L_a$ (m)	Error %
M22	0.0029	4.73	5.60	-15.6	0.004	6.52	5.60	16.5
M23	0.0035	5.71	5.60	1.9	0.0043	7.01	5.60	25.2

### 4.3 Complicated Foundations Comprising Pier Walls and Piles

Many bridges are supported by complicated foundations composed of a pier wall and piles or a buried pile cap and piles as shown in Figure 224. Since the piles are buried, the source and receiver of SE method can only be placed on the exposed pier wall or the superstructure. When the wave travels down the pier wall, two waves (a reflected and a transmitted wave) will be generated at the interface between the pier wall and pile due to the change of impedance. The transmitted wave travels down the pile and reflects back from the pile toe. That upward reflected wave will generate two waves at the interface again. The effect of the interface is similar to damping in terms of the reduction in the wave energy. Thus, it makes echo identification difficult unless the energy is large enough. It will be valuable to study numerically whether SE tests can be used to detect the pile length in such complicated foundations. This type of study was not found in the literature. The applicability of the SE method on this type of foundation is investigated by finite element analysis in this section.

Multiple FEM models were simulated to investigate the success of SE tests on aforementioned complicated foundations. The general specifications of the FEM models are indicated in Table 97.

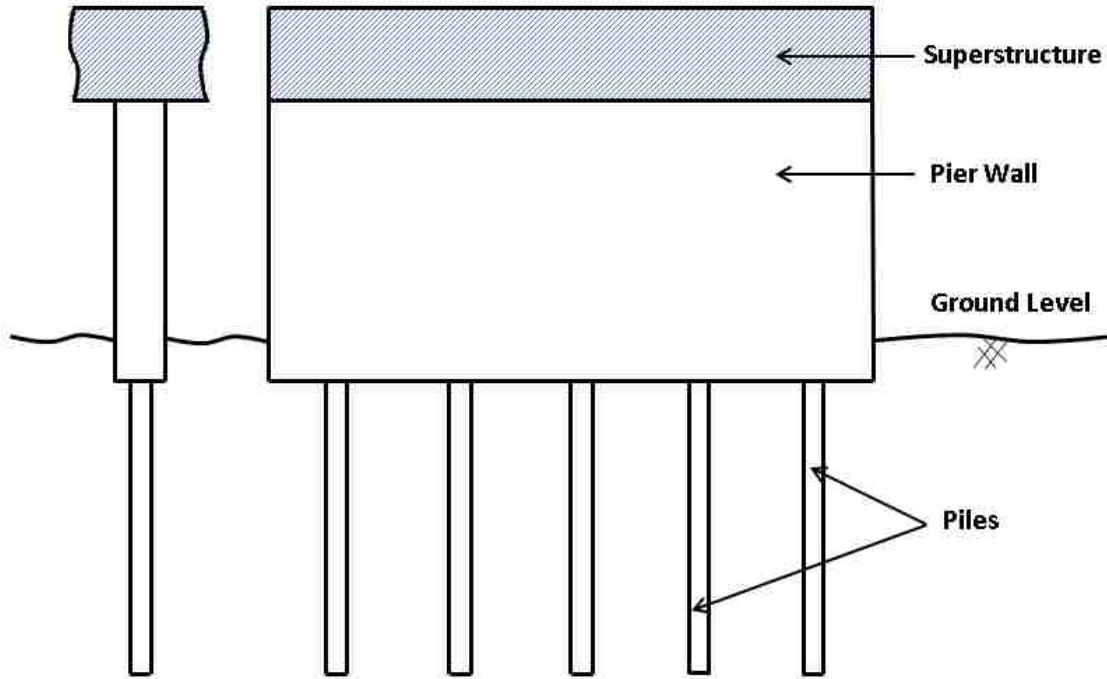


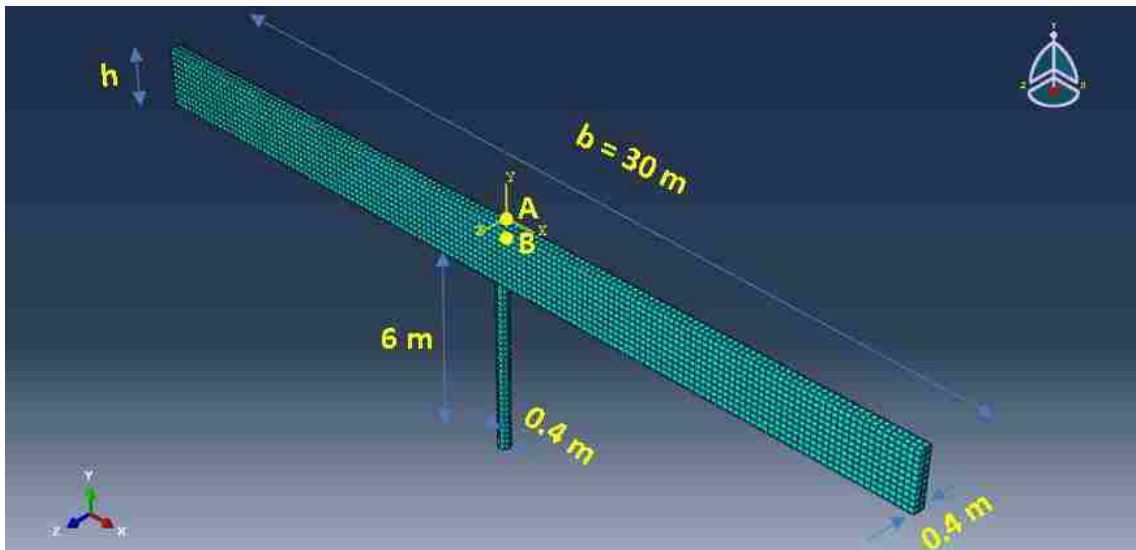
**Figure 224. Bridge Foundation Comprising a Pier Wall and Multiple Piles**

**Table 97. Specifications of Complicated Foundation FEM Models**

V (wave velocity)	3261 m/s
E (modulus of elasticity)	25.52 GPa
$\rho$ (density)	2400 kg/m <sup>3</sup>
$\nu$ (Poisson's ratio)	0.2
Impulse amplitude	1 MPa
Impulse shape	Parabola
Impulse duration	1.2 ms
Simulation time duration	15 ms
Elements type	C3D8R (8-node linear brick)
Approximate mesh dimensions	0.2 m
$\alpha$ (Rayleigh damping coefficient)	0.1
$\beta$ (Rayleigh damping coefficient)	0.0001

Figure 225 shows an FEM model of a pier wall supported by a pile of 6m length. The source is applied vertically at point A (center of the pier wall's top surface). The signals

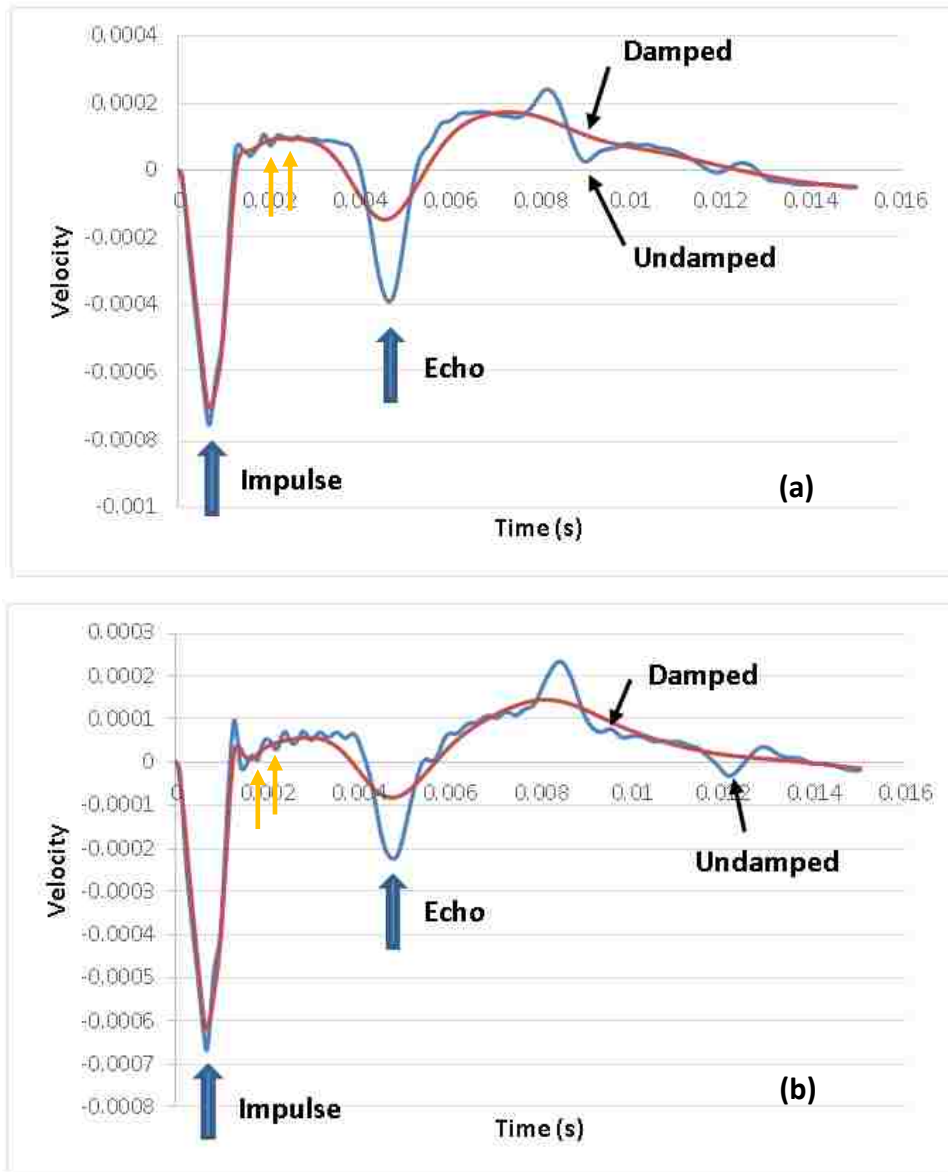
are recorded at Node B located 0.2m below the top surface of pier wall. In this model, it was decided to investigate if the pile toe reflection can be sensed by an accelerometer mounted on the side of the pier wall (node B). The width of the pier wall ( $b$ ) was selected big enough to prevent the interference of any reflections from the pier wall ends on the signals intended to capture pile toe echo. The height of the pier wall ( $h$ ) increased from 0.4m to 3 m to find the pier wall depth for which the pile toe can be identifiable.

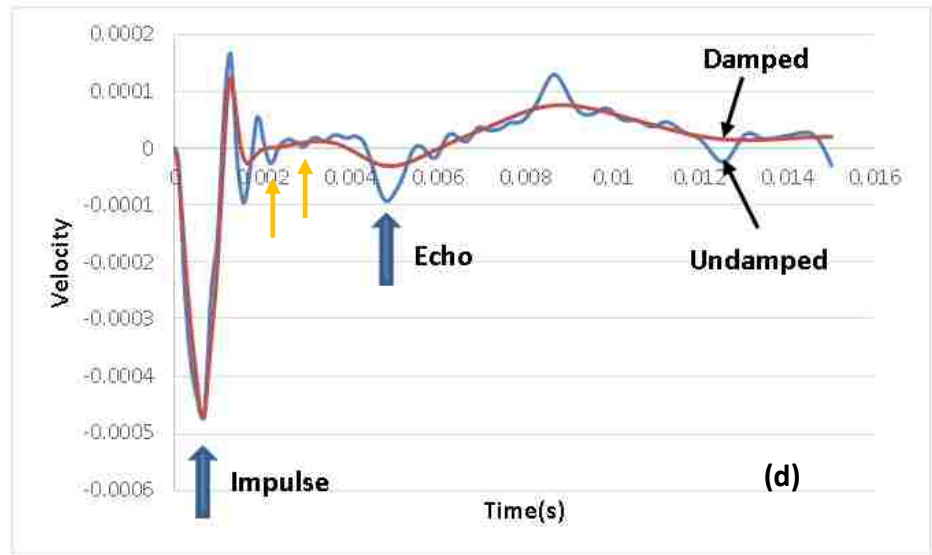
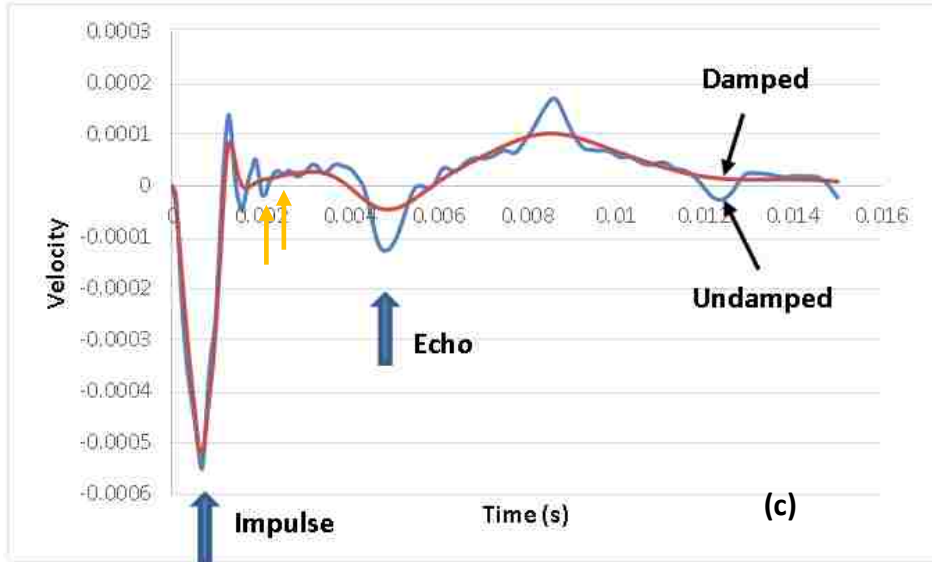


**Figure 225. An FEM model of a Pier Wall Supported by a Pile**

Figures 226 shows the velocity graph obtained at Node B for undamped and damped models for which the pier wall depths have increased from 0.4m to 1.4m. The undamped graphs show that, upon applying the source, consecutive reflections from the pier bottom will be sensed at Node B. The orange arrows indicate the reflections from the pier bottom. The blue arrow shows the reflection from the pile toe. The undamped models also show that the energy transmitted through the pile is great enough such that the echo from the pile toe can be detected in this configuration. The length calculations for models with different pier wall heights are indicated in Table 98. The errors of the calculated lengths are satisfactory and less than 6 percent. Although the pile toe echo is identifiable for all the heights between 0.4m to 1.4m, the amplitude of the echo is much smaller than the impulse especially when the pier height is between 1m to 1.4m. The damped models also show that the pile toe echo amplitude become much smaller when the pier depth

approaches 1.4m. It should be noted that in real cases the energy dissipation due to damping in surrounding soil make the pile toe echo even much smaller. Therefore, the success of the SE tests is questionable when the depth of the pier wall is not significantly smaller than 1.4m.





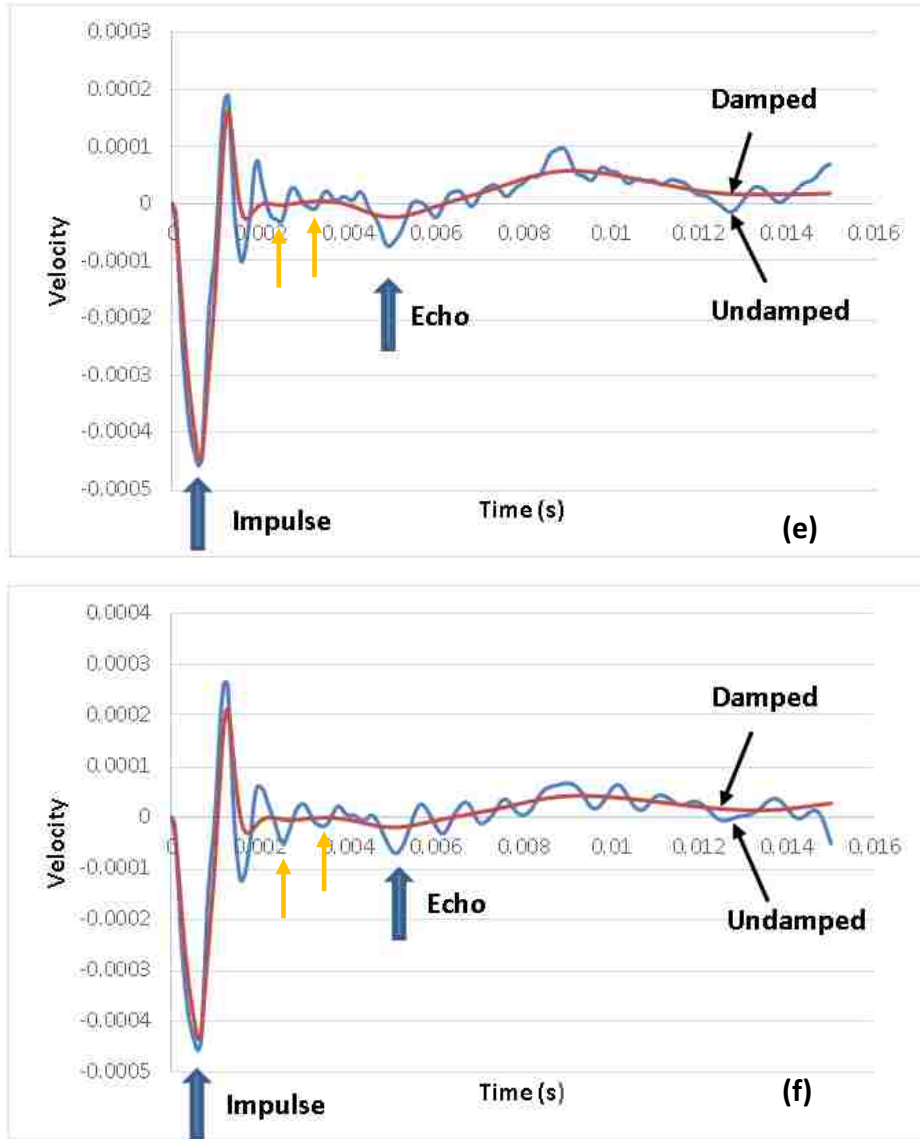
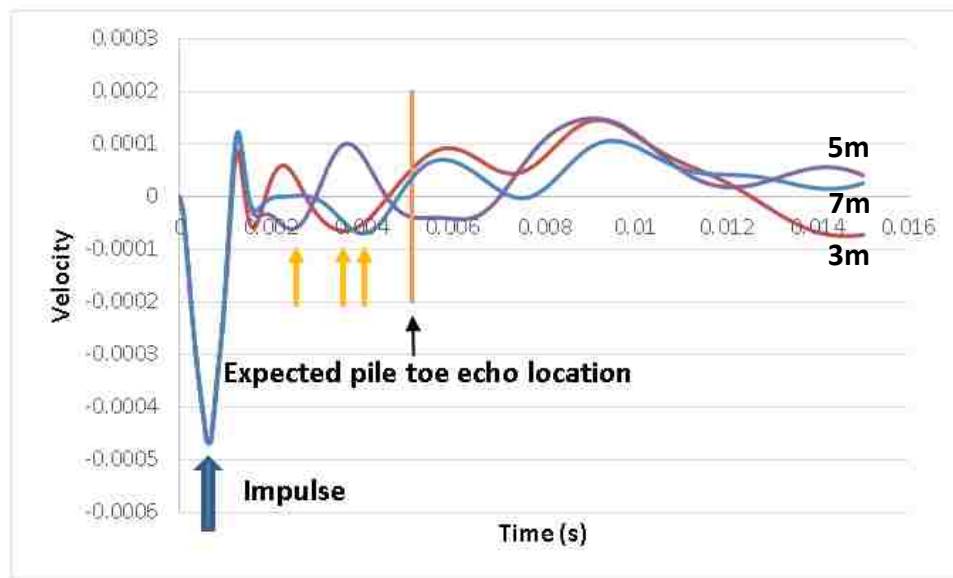


Figure 226. Velocity Signal Obtained at Node B for FEM Model with Height of (a) 0.4m, (b) 0.6m, (c) 0.8m, (d) 1m, (e) 1.2m, (f) 1.4m

Table 98. Length Calculation for Models with Different Pier Wall Height

Pier height (m)	$\Delta t$ (s)	$L_{tr}$ (m)	$L_a$ (m)	Error (%)
0.4	0.003975	6.48	6.2	4.51
0.6	0.004125	6.73	6.4	5.16
0.8	0.004195	6.84	6.6	3.63
1	0.0042	6.85	6.8	0.74
1.2	0.004275	6.97	7	-0.43
1.4	0.004482	7.3	7.2	1.39

More investigations on such complicated foundations also show that the success of the SE tests depends on the reflections from the pier wall boundaries. Figure 227 shows the velocity graphs obtained at Node B for damped models with pier wall widths (b) of 3, 5 and 7m. The height of the pier wall is 1m. The vertical green line shows the expected location of the pile toe echo (corresponding to the distance between node B and pile toe (6.8m)). The graphs show that the boundaries affect the reflected waves from pile toe. The black arrows show the identifiable echoes on the velocity signals which are not the same as the expected echoes from pile toe. The adverse effect of the reflections from the pier wall sides were obvious when the pier wall widths were smaller than 12m. However, the effect of boundaries disappeared when the width of the pier wall was more than 12m. The velocity graphs obtained at Node B for damped models with pier wall widths 12, 14, 16 and 30m are indicated in Figure 228. The graphs show that the pier sides are far enough such that they do not affect the reflections from the pile toe and all the models show echo points corresponding to pile toe.



**Figure 227. Velocity Graphs Obtained at Node B for Damped Models with Pier Wall Widths (B) of 3, 5 And 7m**

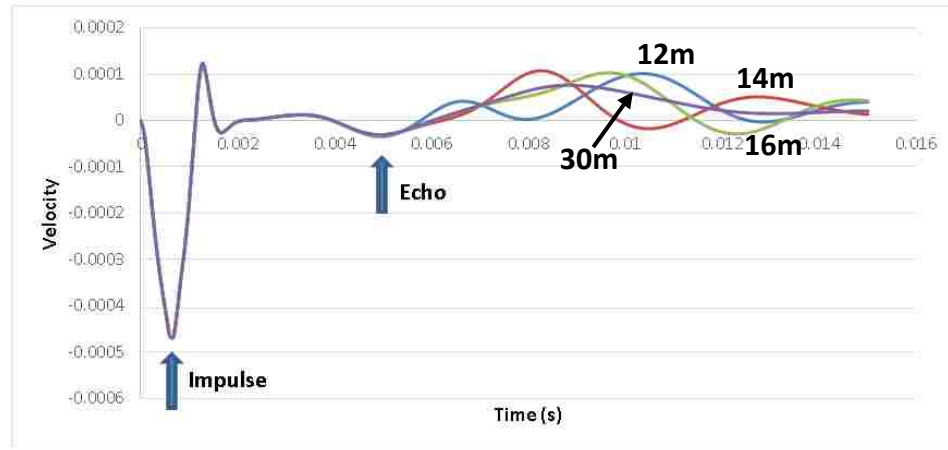


**Figure 228. Velocity Graphs Obtained at Node B for Damped Models with Pier Wall Widths (B) of 12, 14, 16 and 30m**

For piles which are not located at the middle, the same observations were identified in terms of the effect of boundaries on the pile toe's reflections. In the FEM model indicated in Figure 229 the pile is placed off-center in distances 3, 5 and 7 m from center ( $a = 3, 5, 7$ ) and the signals were recorded at Node B. Node B is located on the centerline of the pile, 0.2 m below pier wall top. Figure 230 shows the velocity graphs obtained at Node B for damped models with  $a = 3, 5, 7$ .

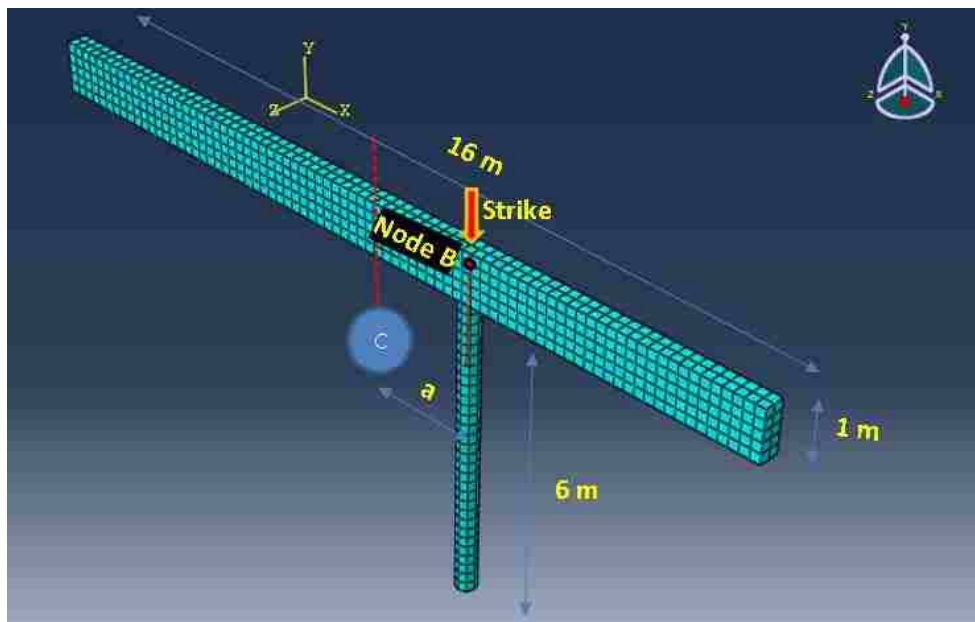


**Figure 229. FEM Model Utilized to Investigate the SE Tests in Pier Walls with Off-Center Piles**



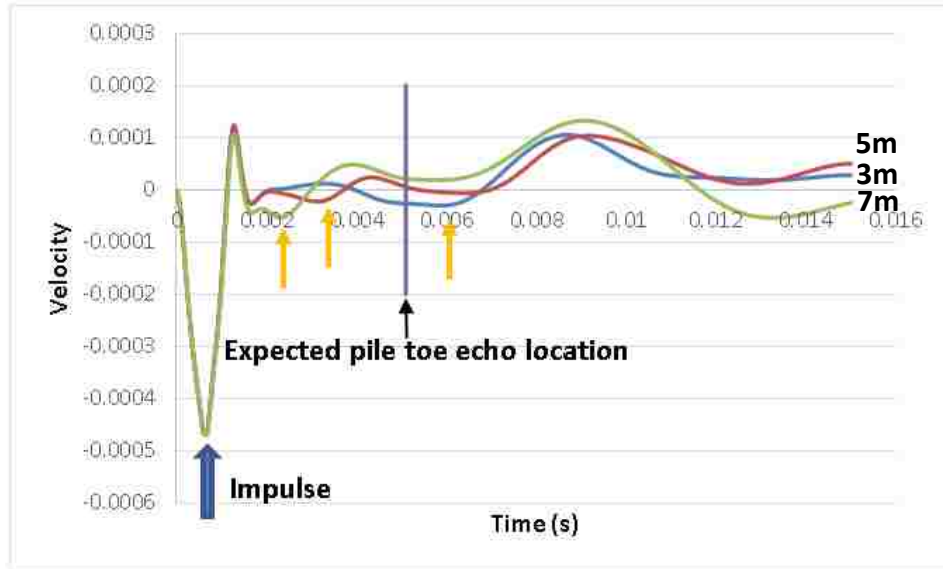
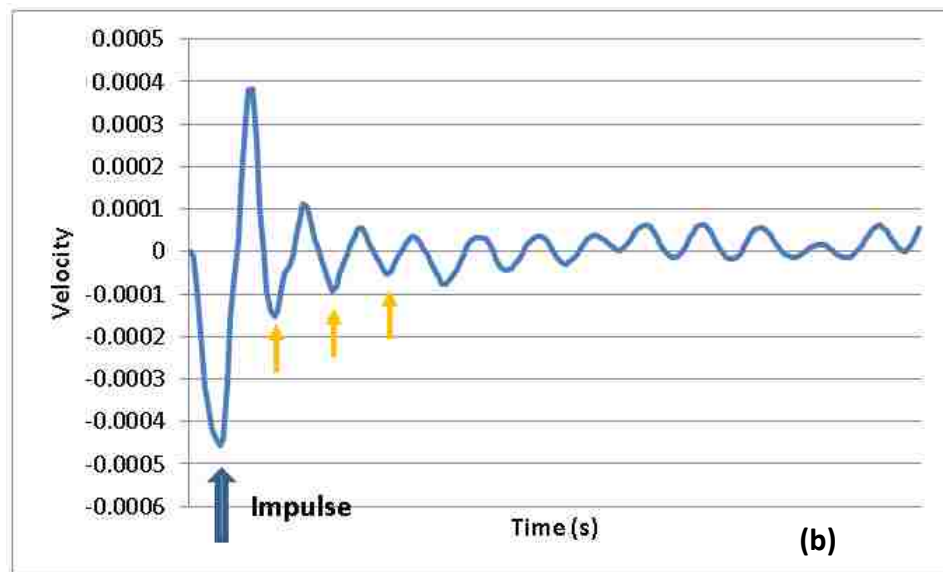
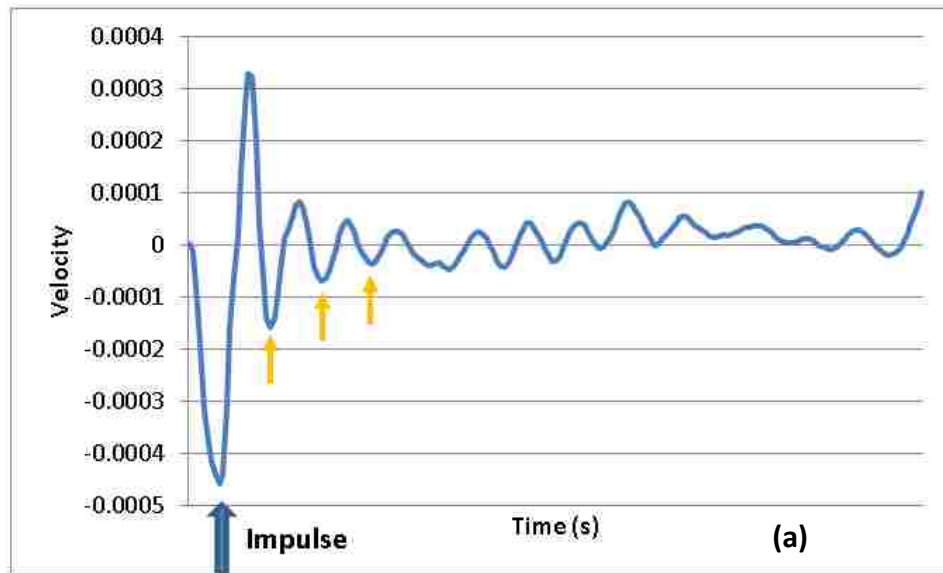


**Figure 230. Velocity signal obtained at Node B for FEM model with  $a = 3, 5$  and  $7$  m.**

Previously, Figure 228 showed that when the width of the pier wall was 16m and consequently the distance between the pile and pier wall side was 8m, the pile toe echo was identifiable. However, the graphs indicated in Figure 230 show that when the pile is placed far away from center with the same pier cap dimensions, the pile toe echo becomes concealed. The identified echoes on the signal curves are not related to the expected pile toe. Therefore, a 6m pile which was previously identifiable when it was placed below the pile cap center, will not be detectable anymore. When the pile is placed towards the ends, the pile toe echo may not be identifiable due to the adverse effect of the adjacent pier sides. Therefore, the success rate of the SE tests becomes worse. As a result, the investigated pile is detectable only when the distance between the pile and the closer end is approximately greater than the pile length plus the pier wall depth. The pile length cannot be determined when the pile is close to the pier wall side even the pile cap depth is much smaller than 1.4 and the surrounding soil is too soft (very small energy dissipation).

The results of foundations with higher pier walls show that when the pier height is more than 1.4 m, the pile toe reflection cannot be detected even with zero damping. The velocity graph obtained at Node B for models comprising a 6m pile and pier walls with different heights of 1.6m to 3m are shown in Figure 231. The graphs clearly show the consecutive reflections from the pier bottom (orange arrows) but not the reflection from

the pile toe. Therefore, there will be no success for SE tests if the height of the pier wall is more than 1.4m both with and without damping. Moreover, no success is observed when the recording node is placed near the pier wall and pile joint. Figure 232 shows the velocity signals obtained from nodes located 0.2, 0.4, 0.6, 0.8 and 1m above the pile and pier wall junction. All the signals obtained from different nodes are very similar and the pile toe is not detectible in none of the nodes.



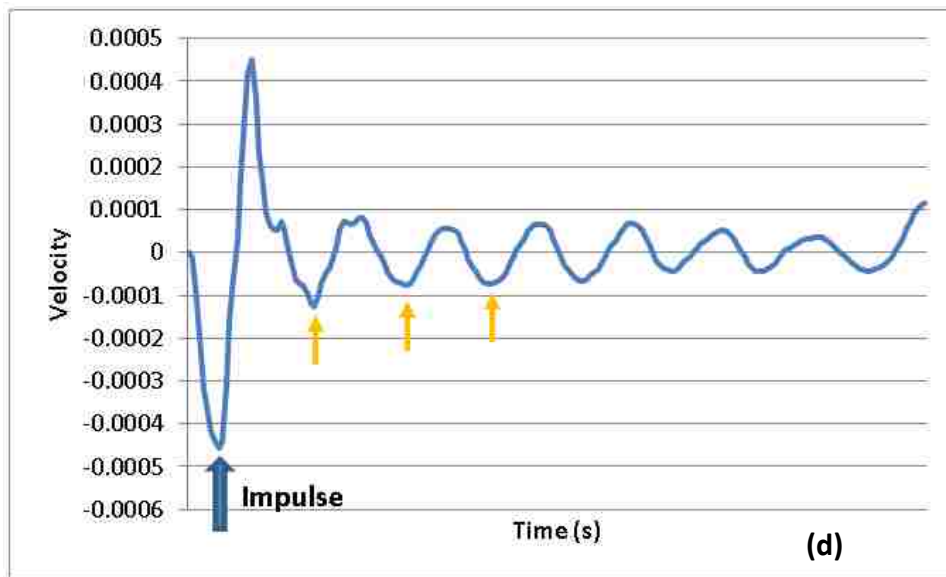
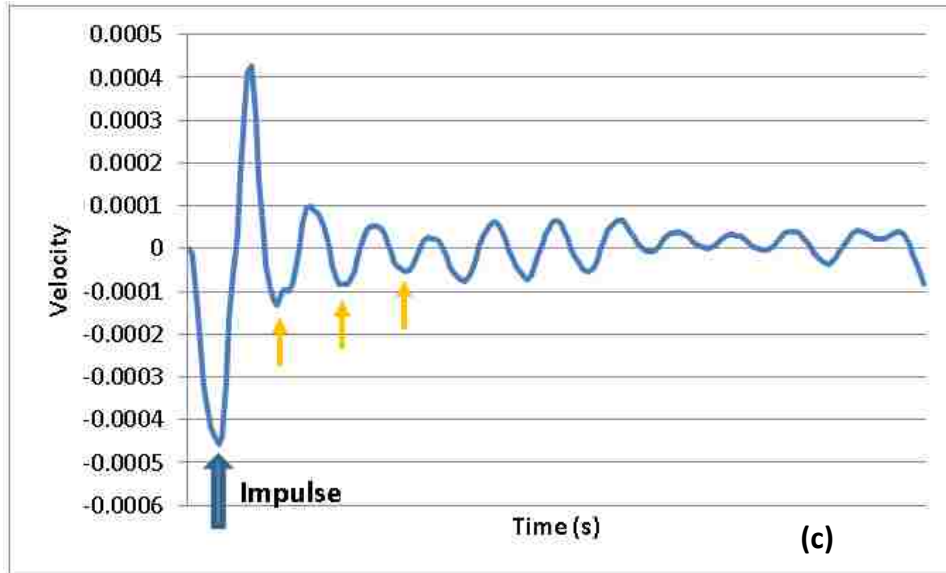


**Figure 231. Velocity Time-amplitude Signal Recorded at Node A for different Pier Heights (a) 1.6m, (b) 1.8m, (c) 2m, (d) 3m.**

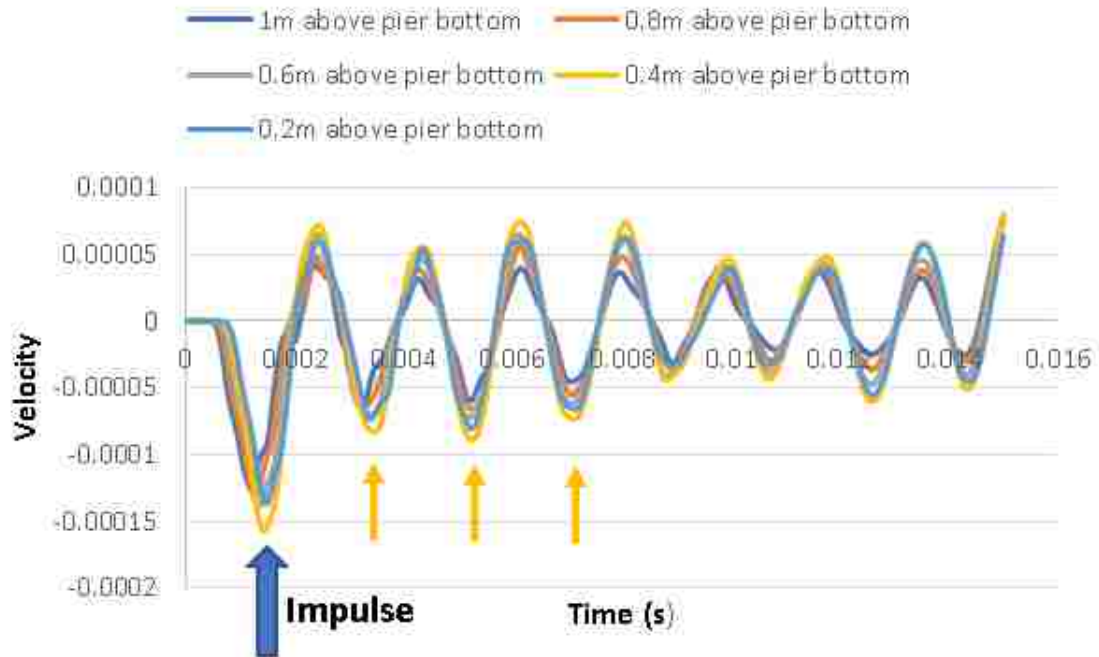


**Figure 232. Velocity signals obtained from nodes located 0.2, 0.4, 0.6, 0.8 and 1m above the pile and pier wall junction**

In summary, the abovementioned investigations revealed that if the height of the pier wall was less than 1.4m, the pile toe could be determined by the SE method. This observation is based on FEM models in the absence of damping from surrounding soil. In a real-world situation, the damping of the surrounding soil will reduce the amplitude of the reflected wave significantly. Therefore, the SE method may be able to detect the pile length beneath a pier wall with a thickness much less than 1.4m. In addition, the reflection from the pier wall boundaries worsen the success of the SE tests. The side of the pier wall should be far enough from the pile to obtain successful tests both for piles located below the center of the pier walls and off-center piles. These explain the unsuccessful SE tests reported by Olson (2) for the cases of shallow foundations with piles underneath.

## **4.5 Conclusions of Fem Simulations**

### **4.5.1 Wood Columns**

1D wave propagation in piles was modeled as the first step of the numerical investigation. Impulses of different shapes were imparted, and acceleration and velocity

were obtained at different nodes. The lengths of the piles were calculated based on the velocity-time histories. Foundation material (bedrock and soft soils) affects the polarity of the reflected waves from the pile toe.

The actual waveform detected from field tests depends on the intrinsic damping in the pile and the radial damping through the surrounding soils. The FEM results indicated that damping reduced the high-frequency content in the velocity-time history, and the amplitude decayed over time. This is consistent with the reality in the field.

The FEM analysis indicated a more complex waveform when the accelerometer was mounted farther from the top of the pile. This is due to the interference of the reflected waves from both ends. This also explains why inconsistent results happened more often at the accelerometer placed far away from the top of the pile.

In addition to the individual piles, the foundations composed of piles and pile caps were also modeled to investigate the signals obtained from such foundations. To do so, one of the foundations of investigated wood bridges was modeled. The FEM model provided means to compare signals obtained from different striking methods. The results show that both downward and upward striking on the pile cap can produce identifiable echoes related to the pile toe. However, among different viable striking methods, downward striking at center of the pile imparts more energy into the pile and consequently better results can be produced.

#### **4.5.2 Concrete Pier Walls**

A concrete pier wall similar to one of the investigated pier walls in the field, was modeled by 3D-FEM. The effects of pier width, hammer tip type, the reflections from the deck, and upward striking on the received signals were examined. The effect of the material damping on the signals was also investigated. The summary of the findings is presented here.

**Wave Propagation** The results obtained from 3D simulations showed that the 1D equation was applicable in the determination of the buried length of a pier wall. The time differences between the impulse and echo did not fluctuate significantly with the change of the width of the pier wall.

**Material Damping** The FEM results showed that the presence of material damping made the interpretation easier due to the removal of high frequency contents near the expected echo in the velocity graph. When there was no damping, multiple peaks and valleys occurred in the vicinity of the expected echo point, which made determining the echo very difficult. However, damping reduces the energy of the reflected wave, which may be detrimental in detecting the echo from the pile toe.

**Hammer Tip Type** Although good results were found for all hammer tips (rendering different impulse time durations in the simulations), accuracy decreased as contact time increased. Hard tip is recommended. This finding has also been confirmed from field observation.

**Deck Reflections** FEM analysis showed that the width of the deck may not affect the determination of height of the pier. Based on the FEM findings, there should not be any effect of deck reflections on the SE/IR test result since the widths of the decks of the investigated concrete foundation in the field were wide enough.

**Upward Striking on Pile Cap and Bridge Deck** The calculated pier wall height obtained from upward striking was similar to the height obtained from downward striking. When the top of the deck is inaccessible, upward striking on pile cap is a good alternative source application.

#### **4.5.3 Complicated Foundations Comprising Pier Walls and Piles**

The results of FEM analysis showed that, if the height of the pier wall was less than 1.4 m, the pile toe could be determined by the SE method in the absence of damping. However, in real bridge foundations, the damping of the surrounding soil will reduce the amplitude of the reflected wave significantly. Therefore, the SE method may be able to detect the pile length of a pier wall with a thickness much less than 1.4 m. The results also show that the reflections from pier wall ends make interpretation more difficult. The pile should have located far enough from the wall ends in order to have successful SE tests. These explains the unsuccessful SE tests reported in the literature for the cases of shallow foundations supported by piles.

## CHAPTER 5 CONCLUSIONS

Determining the geometry and specifically the depth of the unknown bridge foundations have been one of the great aims of state DOT in recent decades. The structural and scour safety of the bridge could be evaluated while enough information becomes available in terms of different specifications of the bridge foundations. Different destructive and nondestructive testing methods can be exploited to gather various information regarding the foundation geometry and material. Conventional destructive methods are expensive and limited in their applications. In contrast, Non-destructive tests (NDT) are usually appropriate means to obtain the unknown bridge foundation information. Various NDT techniques have been used and developed over the past two decades towards condition assessment of civil infrastructure. Among conventional Nondestructive methods, due to their advantages, the Induction Field and dynamic low-strain methods are among the most favorable methods to evaluate the structural integrity of concrete driven piles, cast-in-place piles, concrete filled steel pipe piles, steel H-piles and timber piles. In the current study, the IF, SE/IR and PS methods have been investigated and utilized on multiple bridge foundations to characterize the unknown bridge foundations including determining the length of piles and the height of pier walls. The investigated NDT methodology was validated by performing SE/IR and PS tests on two bridges with as-built drawings.

Before performing the field tests, preliminary tests were conducted in controlled environments to investigate various variables that may affect the selected nondestructive tests results. The preliminary tests gave rise to valuable knowledge in the testing procedures for conducting SE/IR, PS, and IF tests. The tests were conducted at the University of New Mexico (UNM) campus, and at a test site off campus.

The preliminary SE tests were performed on a concrete wall and three columns made of wood and concrete. The effect of various factors such as striking direction, accelerometer location, and hammer tip type were investigated. Based on the preliminary tests' observations, the following instructions were inferred for being implemented in the field:

- A vertical strike along with a vertically placed sensor is a proper way to conduct SE/IR tests.
- The results of SE/IR tests depend on the energy (strength) of the longitudinal wave, therefore, vertical striking on the top of the foundation is the best method to apply.
- When the top of the foundation is inaccessible, the accelerometers should be placed vertically on the side of the foundation no closer than 1-2 feet from the striking point.
- If high frequencies conceal either impulse or echo in the velocity graphs, using a softer hammer tip may eliminate the disturbing high frequencies and consequently eases the interpretation.
- Although the wave propagation inside a reinforced concrete wall was different from columns and piles, applying a vertical strike at the top of the wall produced successful SE tests. The tests were successful when the accelerometers were placed vertically on the top or on wooden blocks attached to the side of the wall.

The initial PS tests were conducted on a short reinforced concrete cylinder buried in ground at a test site off UNM campus. The preliminary PS test results indicated that the background noise affected the identification of the first arrival time of the wave. However, the effect of the existing noise seems to decrease with depth. This finding was considered as inconclusive due to the limited depth of the PVC pipes.

The preliminary IF tests were performed at two testbeds constructed to examine the capability of the equipment and to investigate various aspects of IF tests. The first testbed contained a metal I-beam placed horizontally in a wooden box full of soil. The box was filled with sand and clay and IF tests were conducted with the probe placed inside the PVC tubes at various locations. The soil type affected the results. Detecting the I-beam in sand was easier compared to clay although the beam was detected in both types of soil at a distance less than 18 in. The results also showed that the moisture content of soils had no effect on the IF tests.

Additional preliminary IF tests performed on the reinforced concrete cylinder located off campus which had been exploited to conduct PS tests. The results showed that the IF method could be used effectively to determine the depth of a reinforced concrete pier. An accuracy level of approximately 6 in was obtained. The tests were successful when



they were conducted at a borehole with a distance of 6 in and 12 in from the test pier. When the distance between the pier and the hole increased to 18 in or more, the results were less conclusive. It might be due to the location of the rebar that was 3 in from the pier surface. Therefore, the bore hole for IF tests must be drilled closer than 18 in (including a typical 2 in cover of concrete) to detect the reinforced concrete foundation.

After conducting preliminary NDT tests, SE/IR and PS field tests were performed with specific details to obtain the best possible results. Although the original plan of IF field tests included performing IF tests on a steel foundation, the intended IF tests were not conducted since the distance between the boreholes and the test piles were greater than 1.5 ft which was beyond the capability of the equipment. The bridges were selected in coordination with the NMDOT. The NDT field tests were performed on multiple bridge foundations composed of wood, steel and reinforced concrete. For each bridge, the foundation was investigated in detail to determine the foundation depth as well as to reveal any possible difficulties that might be encountered. The provided NDT test procedures allowed efficient collection of high quality data in the limited timeframe assigned for the field testing.

SE/IR tests were conducted on a railway bridge and six highway bridges with known and unknown foundations depths. The lengths of the piles and piers were determined using the velocity graphs obtained from the accelerometers based on time domain and frequency domain analyses. In some cases, IR analyses were carried out to support and confirm the SE interpretations. Depending on the conditions of the foundations and superstructures, most tests were successful. The SE/IR results showed that the obtained signal was affected by various factors such as striking method, sensor location, hammer tip type pile and superstructure conditions and environmental conditions.

*Method of Striking* Depending on the accessibility of the pile top and the condition of the superstructure, various source locations able to produce a longitudinal wave along the test object were examined. Vertical downward striking on either the pile top or a point inside the projected pile cross section on pile cap top surface transmits the most impulse energy directly to the pile, whereby the most consistent results were obtained. Consequently, these two methods are the best to conduct SE/IR tests. If direct striking at the top of the pile is not feasible, eccentric striking on the top of the pile cap or upward

striking on the bottom of the pile cap next to the pile are alternative options. If none of these striking methods can be used, impulse source can be generated by striking on a wooden block that is tightly attached onto the pile. Striking the existing bolts or members that brace the pile sometimes produce successful SE tests. It should be noted that each striking method will produce different levels of consistency depending on the strike quality, pile condition, and superstructure condition.

*Accelerometer Location* If possible, the receiver should be placed at the top of the pile. Otherwise, the location should be selected such that the arrival time of the reflected upward wave from the pile bottom differs significantly from the reflected downward wave from the pile top. In addition to this criterion, when the sensor is placed too close to the striking point, the noise of high frequency was observed that significantly affected the identification of the echo in the velocity graph. The field tests indicated that successful SE tests were obtained when the accelerometer was placed 1-2 ft from the impulse source. When the SE test was performed using two accelerometers, the inferred length of the pile was more consistent from the top accelerometer than the accelerometer mounted closer to the ground level, especially in the presence of running water. The accelerometer closer to the top of the pile is also better because of the less complication from the reflections of both pile ends.

*Hammer Tips* The hard tip produced more successful SE tests than the other three softer tips. However, the benefit of using softer hammer tips was found occasionally. The velocity graphs of hard tip sometimes contained multiple echoes. The input signal of the hard tip contains waves of higher frequencies. When such high frequencies appear in the vicinity of the expected echo, using softer tips may reveal the correct echo. When poor result of hard tip is observed, repeating the SE/IR test with a softer tip may overcome the difficulty. In addition to determining the success rate of the SE tests for different hammer tips, more investigation on the effect of the source signal amplitude was conducted for wood bridges. The results showed that the success rate of the SE tests is greater for sources with large amplitudes. It implies that stronger strikes can generate more interpretable results. As a result, for our utilized equipment, the tests should be performed with a moderately strong strike such that the amplitude of the produced signal exceeds 0.4 lbf to achieve satisfactory results for all types of the hammer tips.

*Environmental and Foundation Conditions* Environmental conditions may affect the SE/IR test results. In one of the investigated piles adjacent to water flow, the results of SE/IR tests were unsuccessful although various setups were attempted. It was expected that the noise due to the water flow (river current hit the pile) interfered with the SE tests. Other reasons might relate to the pile's condition such as rottenness or damage in the pile. The pile's condition has also a huge effect on the clarity of signals. In one case, where there was a huge longitudinal crack in the pile, it was difficult to identify the correct echo because of the multiple wave reflections from the crack. When such abnormalities exist in piles, the actual depth of the foundation may not be determined by the SE/IR method.

*Difficulties with Steel Piles* The SE/IR tests performed on a bridge supported by H-piles were not successful. High frequency vibrations were obvious in the velocity graphs that corresponded to the reflections from the boundaries of the steel cross section. When a strike is applied at the middle of the web, the wave travels both horizontally and vertically through the thin-walled members. The sensor receives the reflected waves from the free boundaries, which in turn interfere with the expected reflected longitudinal waves from the pile bottom. Apart from this difficulty, steel H-piles transmit a large portion of the wave energy into the surrounding soil due to their specific cross section shape. Less energy is transmitted to the pile bottom, which significantly decreases the amplitude of the echo from the pile toe.

*IR Analysis* The IR analysis (based on the frequency content of the entire waveform) was carried out as a complementary analysis for SE tests. In some cases, IR analysis yielded the correct pile length while the echoes of SE tests could not be identified. It is recommended to perform an IR analysis when the SE data do not reveal the foundation depth. The field results indicated that the pile length determined by IR analysis was slightly different from those of obtained from SE tests, however, the calculated pile lengths from IR analysis were more consistent than those obtained from the SE tests. This might be due to the occasional wave interference of various frequencies which might hinder pinpointing the echo from the pile toe in the velocity graphs.

PS tests were carried out on bridges supported by timber and steel piles. Both conventional and reverse PS tests were performed. For the steel piles the source was applied by vertical striking on an aluminum block attached to the H-pile web and horizontal

striking on the piles' sides. Vertical striking on the pile cap and horizontal striking on the pile were applied by both regular and sledge hammers for the bridge supported by timber piles. Reverse PS tests were also conducted on the bridge supported by timber piles. The conventional PS tests were successful but the reverse PS tests did not yield acceptable data due to the presence of ambient noise. The conclusions reported in this study are from the conventional PS tests only. During analyzing the PS tests results, the first arrival times were determined by inspecting the background noise level in the signals prior to arrival of any sound wave from the source. The first arrival time was determined as the time when the signal begins to increase and consistently distinguish itself from the background noise level. The PS tests showed that determining the arrival time of the first P-wave is a challenge depending on the level of ambient noise. The arrival time of the first P-wave was determined easily at greater depths since the ambient noise reduced with depth. The results also showed that both vertical and horizontal striking generated good signals although the signals provided by vertical striking were generally clearer than those of horizontal striking. In addition to the effect of noise and strike direction, the field study showed the effect of the distance between the borehole and the test pile. Good results were obtained when the distance between the source and receiver was less than or equal to 4 ft. PS tests did not work when the distance between the source and receiver was greater than 6 ft. Therefore, it is suggested that the borehole should be installed less than 6 ft from the test pile.

The numerical simulations provided means to compare the numerical results to the field tests results. The comparison resulted in better understanding and conducting the SE tests and interpreting the results. Finite Element simulations of 1D wave propagation in square-section wood piles and 3D wave propagation in concrete pier walls and complicated foundations were carried out. In the numerical simulations, major factors such as a foundation's bottom condition, foundation's material damping, hammer tip type, superstructure reflections, pier geometry and characteristics of striking, were studied using FEM models of piles, pier walls and complicated foundations comprising pier walls and piles.

1D wave propagation in piles was modeled as the first step of the numerical investigation. Various input impulse shapes were imparted, and acceleration and velocity

were obtained at different nodes. The lengths of the piles were calculated based on the velocity-time histories. Since the bedrock and soft soils underneath the pile toe affect the polarity of the reflected waves, the effect of the pile ends was also investigated. The actual waveform detected from field tests depends on the inherent damping in the pile and radial damping through the surrounding soils, therefore, material damping was considered in some models. The results indicated that damping reduced the high-frequency content in the velocity-time history, and amplitude decayed over time. In addition, the FEM analysis showed a more complex waveform when the accelerometer was mounted farther from the top. This is due to the wave interference of reflections from both ends. This explains why the sensor should not be placed too far from the pile top in the field.

In addition to the individual piles, foundations consist of piles and pile caps were also investigated. The selected FEM model had the same dimension as one of the investigated wood bridge foundations. Using this FEM model, signals obtained from different striking methods were compared and the best method was identified. The finding was in accordance with the field tests. The results showed that all considered striking methods including downward striking at the pile's center, downward eccentric and upward striking on the pile cap are capable of producing interpretable results. The impulse and echoes were completely detectable on the graphs. The resulted lengths corresponding to the time differences between the impulse and echo were very close to the actual length. The results also showed that, among all these three striking methods, the signals' amplitudes for striking at point center was maximum whereas the amplitudes are minimum for point eccentric strike. This observation can be one of the main reasons for superiority of striking at center over eccentric and upward striking on the pile cap.

In the next step, a concrete pier wall similar to one of the pier walls of an investigated concrete bridge was modeled. The effects of pier width, hammer tip type, the reflections from the deck and upward striking on the received signals were examined. The effect of material damping on the signals was also investigated in the study.

*Wave Propagation* The results obtained from 3D simulations show that the equation used for 1-dimensional problems can be used to determine the buried length of the pier wall. The time differences between the impulse and echo did not fluctuate significantly with the change of the width of the pier wall.

*Material Damping* The FEM results show that the presence of material damping facilitates interpretation due to the removal of high frequency contents near the expected echo in the velocity graphs. In the absence of damping, multiple peaks and valleys occur around the expected echo point, which makes determining the pier wall depth difficult. However, damping reduces the energy of the reflected wave, which may be detrimental for determining results in the field.

*Hammer Tip Type* Although good results were found for all hammer tips, accuracy decreases as contact time increases. It is recommended to use the harder tip and place the sensors as close as possible to the pier wall top but at least 1 to 2 ft from the source.

*Deck End Reflections* When the deck ends are far enough from the sensors locations, the reflected waves from the deck ends do not interfere with the pier bottom reflections. The results of the investigated pier wall show that the influence of the reflection from the end of the deck was insignificant when the deck ends were at least 6m from the pier wall.

*Upward Striking on Pile Cap and Bridge Deck* The calculated pier wall height using upward strikes is similar to the downward striking. Therefore, when the top of the deck is not accessible, good alternative source locations for strikes are to apply upward strikes on the pile cap or the bridge deck.

Finally, complicated foundations composed of pier wall and pile were simulated to reveal the capability of SE tests in detecting the pile length in such complicated foundations. To do so, FEM models with different dimensions were investigated. The results of FEM analysis showed that, if the height of the pier wall was less than 1.4 m, the pile toe could be determined by the SE method when there is no damping in the foundation-soil system. However, in real bridge foundations, the damping of the surrounding soil will reduce the amplitude of the reflected wave significantly. Therefore, the SE method may be able to detect the pile length of a pier wall with a thickness much less than 1.4 m. The results also show that the reflections from pier wall ends may fail the SE tests. The pile should be located far enough from the wall ends to have successful SE tests. The adverse effect of the pier ends may be even worse for piles which are not below the center of the pier wall. These explain the unsuccessful SE tests reported in the literature for the cases of shallow foundations supported by piles.

## **Future Work**

- Investigate the applicability of other NDT tests such as bending wave method on the simulated complicated foundations.
- Investigate the success of the SE/IR tests on complicated foundation with other types of geometry.
- Numerical simulation of the cracks in wood piles with different shapes and study their effects on the success rate of SE tests.

## **APPENDIX A NDT PROCEDURAL MANUAL**

### **INTRODUCTION**

The procedures manual presented herein was developed based on the findings from Project NM13STR-02 conducted by the University of New Mexico (UNM) for the New Mexico Department of Transportation (NMDOT). The overall goal is to provide guidance for performing future nondestructive testing (NDT) in New Mexico. One of the specific objectives of the project is to develop NDT procedures that can be employed to determine unknown foundation characteristics. One surface NDT method (Sonic Echo/Impulse Response (SE/IR)) and two borehole methods (Parallel Seismic (PS), and Induction Field (IF)) were selected based on capability, equipment cost, and operation cost. Also, all three NDT are proven technologies and the tests are very easy to operate. These three methods have been applied in the preliminary testing including columns of wood and reinforced concrete and a reinforced concrete wall. SE/IR and PS methods have been employed in field tests on bridges in New Mexico supported by timber piles, steel H-piles, and concrete piers. Finite element modeling of NDT tests performed on pier walls and columns have been carried out to shed light on the insight of SE/IR tests. The principles of these three NDT methods are explained here. Then the procedures of each method are presented following by the data interpretation of the results and good and poor examples. The calculation of the depth of the substructure is illustrated in examples of these three NDT methods.

Risk screening has been completed by NMDOT and Federal Highway Administration (FHWA) on bridges with unknown foundations. Based on the unknown bridge foundation database provided by the NMDOT Bridge Bureau, there are 266 bridges in New Mexico which do not have design and as-built plans completely identifying the type, depth, geometry, and materials of their foundations. NMDOT and FHWA prioritized these bridges by placing them into 3 categories (high risk, moderate risk, and low risk). They are categorized based on available information and visual assessments with the criteria defined by NMDOT. Table A1 presents the inventory of these bridges.



**Table A1. Inventory of Bridges with Unknown Foundations in New Mexico.**

	High Risk	Moderate Risk	Low Risk	Total
State	2	14	46	62
Local	20	22	162	204
Total	22	36	208	266

Since bridge substructures are made of concrete, timber, or steel, the selected NDT methods will work properly on these materials. The limitations and applications of the methods can be found in Table A2. All three NDT can be operated by one person in the field. However, it is more convenient to have two persons for SE tests and three persons for PS tests. Hands-on training on conducting these nondestructive tests is available at UNM at no cost for the next six months.

**Table A2. Relative Merits and Limitations of Sonic Echo/Impulse Response, Induction Field and Parallel Seismic Methods (42).**

Ability to Identify Foundation Parameter	Sonic Echo/Impulse Response	Induction Field	Parallel Seismic
Depth of Exposed Piles	Fair-Excellent	None-Excellent	Good-Excellent
Depth of Footing/Cap	Poor-Good	N/A	Good
Piles Exist under Cap	N/A	None-Excellent	Good
Depth of Pile below Cap	N/A	None-Excellent	Good -Excellent
Geometry of Substructure	N/A	N/A	Fair
Access Requirements:			
Bridge Substructure	Yes	Yes	Yes
Borehole	No	Yes	Yes
Effect of Soils on Response	Low-Medium	Medium-High	Medium
Limitations	Response complicated by bridge superstructure elements. Limit application to long piles Stiff soils and rocks limit wave penetration.	Only applicable to steel or reinforced substructure	Difficult to transmit large amount of seismic energy from pile caps to smaller (area) piles
Advantages	Lower cost equipment and inexpensive testing	Easy to test. Could work well to complement PS tests and help determine pile type.	Can detect foundation depths for largest class of bridges and subsurface conditions

## **BASIC PROCEDURES**

Selecting the suitable NDT method is commonly based on the substructure material (timber, concrete, and steel). The substructure material of each bridge with unknown foundations should be obtained first. Recent bridge inspection and scour evaluation reports should be collected and studied to identify bridge geometry, structure type, and construction materials. In addition, the average daily traffic is important to determine the time for conducting SE/IR and PS tests. The length of the span of the superstructure can be related to the design load on the pile cap. This information can be used to roughly determine the expected depth of foundation which is important for borehole nondestructive methods. A visit to the bridge site may be necessary to obtain relevant superstructure and substructure data or to verify or correct any questionable existing data. The following factors should be reviewed prior to the selection of the NDT method.

### **Bridge Deck**

A bridge deck may have several variables that affect the quality of the test result. The clearance below the bridge deck is very important for PS and IF methods. Special drilling equipment (Geoprobe 7822DT) shown in Figure A1 may be required for low clearance bridges. Connections between the superstructure and the substructure determine the extent of traffic noise that is transmitted through the structure itself to the foundation, affecting the SE/IR and PS tests. PS and IF methods require drilling a hole with a depth at least 15 ft beyond the expected depth within the certain distance from the foundation. The foundation design is based on the subsurface conditions and the anticipated structural loads which depend on the length and width of the span. Historical standard bridge designs in New Mexico can be consulted to estimate the expected pile depth. If the piles are in soils, presumed resistance of soils can be used to roughly estimate the pile length.



**Figure A1. Geoprobe 7822DT-Low Headroom Drill Rig**

### **Automotive Traffic**

Traffic on bridges may pose a substantial problem for SE/IR and PS methods. One factor to consider is the number of traffic lanes on the bridge relative to the volume of traffic and time of day. This relationship between traffic flow and existing lanes will greatly influence maintenance of traffic (MOT) plans and schedule. For SE/IR and PS methods, testing during non-peak hours (i.e. at night) may be preferable due to less noise and vibrations at night. If daytime lane closure is required on a highly traveled bridge, then some lane capacity analysis may be necessary to ensure minimal impact to traffic flow.

### **Season**

Seasonal weather fluctuations may affect the access of substructure. These impacts could be associated with variations in the water levels and flow velocities under a bridge. The running water may require the mobilization of a scaffold as shown in Figure A2.



**Figure A2. Mobile Scaffold (NMDOT District 4)**

### **Subsurface Conditions**

Highly variable soil strata may be reflected in the data resulting from NDT and should be considered while making estimates of the foundation depths. Many of the NDT methods utilize wave transmission principles based on wave velocities through soil strata. Wave velocities vary from one material to the next; therefore, some basic understanding of the subsurface conditions is helpful. The data interpretation from the NDT methods should be analyzed in conjunction with known or estimated rock depths as they apply to the area. Due to the common occurrence of deeper ground water table in New Mexico, the determination of the first arrival time in PS tests may not be as easy as those in other states. The subsurface conditions can assist engineers for better interpretation of SE/IR and PS results.

### **SELECT THE APPROPRIATE NDT METHOD**

Highway bridges are commonly supported on deep foundations. Shallow foundations are employed occasionally. The deep foundations are structural members that are made of timber, concrete, steel, composite (combination of two materials out of timber, steel, and concrete). Concrete-filled steel pipe piles are classified as composite piles. There are four common basic deep foundation construction methods. Deep foundations are based on one of the following techniques:

- Driven piles - Piles are driven into the ground by mechanical force. The prefabricated timber, steel, or concrete piles are driven into the ground by a hammer, pushed by shear brute force, or vibrated by a shaker.
- Driven cast-in-place piles – a hollow steel casing is driven into the ground first. The cavity is subsequently filled with concrete.
- Drilled shafts – a cylindrical hole of the required depth is excavated. Reinforcement cage is placed in the excavated hole and subsequently filled with concrete.
- Augercast (Continuous-flight auger) piles – a hollow stem auger is drilled into the ground. Concrete is pumped through the hollow stem of the auger while the auger is pulled up. Reinforcement, if necessary, is pushed into the concrete manually.

Three NDT methods (SE/IR, PS, and IF) can be used to determine the conditions of unknown bridge foundations. Equipment for conducting these three types of nondestructive tests purchased with project funds are available to NMDOT. The three NDT methods have different requirements regarding degrees of site access as shown in Table A2. SE/IR method generally requires access to the substructure of a bridge only. Borehole methods (PS and IF) require a soil boring that must be drilled as close as possible to the test pile before conducting any nondestructive tests.

When the foundations are buried beneath the pile cap, only PS method may be able to determine the depth of the foundation. Figure A3 can be employed to select the suitable NDT method based on the material of the exposed foundation. This flow chart was developed based on the success and failure of the NDT methods in the research project, cost, and the literature review. Option 1 is identified as the better available test method for each foundation material type.

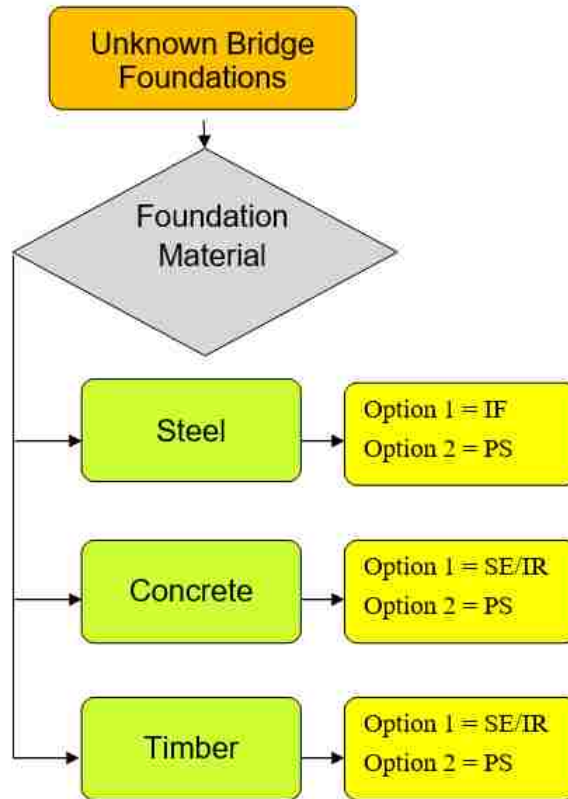


**Figure A3. Selection of Appropriate NDT Method**

### **Timber Piles**

For timber piles, SE/IR tests are recommended because of the cost. If SE/IR results are questionable or inconclusive, PS tests can be considered. IF tests are excluded since the method depends on the presence of metal within the foundation.

### **Concrete Piles**

For concrete piles, SE/IR tests are recommended. PS tests should be conducted only if SE/IR tests' results are questionable or inconclusive. If the borehole is drilled very close to the test pile (< 18 inches), optional IF tests can also be carried out before conducting PS tests. It is expected that the method works for concrete piles will also work for concrete-filled steel pipe piles.

### **Steel Piles**

For steel piles (H-piles, pipe piles with or without concrete filling), IF tests are recommended. Conduct PS tests only if a borehole cannot be drilled within 18 inches from the test pile. SE/IR tests are excluded since the method does not work on steel piles.

Engineers conduct SE/IR and PS tests by following the procedures developed from the System Reference Manual of SE/IR and PS by Olson. The steps to conduct IF tests are given in this document.

### SONIC ECHO/IMPULSE ECHO (SE/IR) METHOD

A small hammer equipped with an electronic trigger is utilized to generate the impact (source). The generated stress wave travels down the pile and reflects (or echoes) back at the interface of the pile toe and foundation soil. The wave is recorded through a sensor (accelerometer or geophone) either mounted on the top of the pile or mounted on the side of the foundation when the top of the foundation is inaccessible due to the presence of a pile cap. One sensor is generally adequate for SE/IR tests. Using two (or more) sensors provides the redundancy and improve the reliability, however, the exposed pile should be long enough to accommodate the additional accelerometers. Figure A4 shows an SE/IR setup that the source is applied by striking on the top of the pile and two sensors are mounted on the side of the pile.  $L_{ai}$  is the distance between the sensor  $i$  ( $= 1, 2$ ) and the top of the pile.

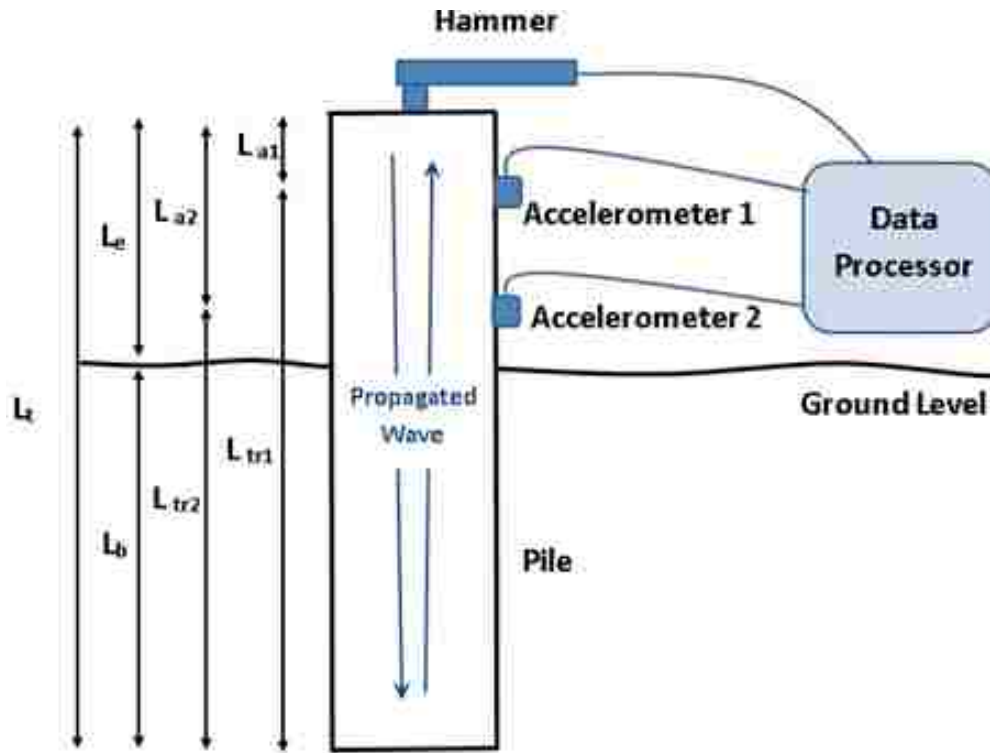


Figure A4. An SE/IR Test Setup



The size and weight of geophones make mounting them on the side of the pile difficult. Therefore, accelerometers are commonly employed as the sensors. Acceleration time history is collected by the sensor (Accelerometer 1 or 2). The acceleration time history is integrated to determine the velocity time history (velocity graph). The two schematic velocity graphs are plotted together in Figure A5. In this figure, the indicated impulse and echo points show the moments of the down-going and up-going waves passing through the sensor location respectively. The time difference between the impulse and echo denotes as  $\Delta t_i$  that is used to estimate the pile length in SE analysis. The pile length ( $L_t$ ) is calculated from the propagated wave velocity ( $v$ ), the distance between the sensor and the top of the pile ( $L_a$ ), and  $\Delta t$ . For Accelerometer 1, the pile length is:

$$L_t = L_{a1} + \frac{v \times \Delta t_1}{2} \quad (1)$$

The buried length of pile ( $L_b$ ) is:

$$L_b = L_t - L_e \quad (2)$$

Where  $L_e$  is the exposed pile length between the pile cap and ground surface.

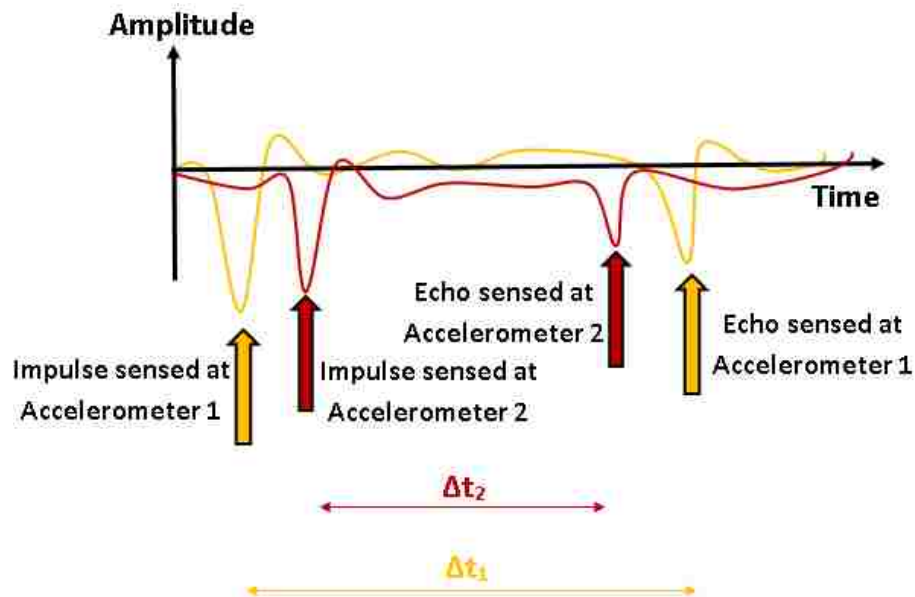


**Figure A5. Schematic Velocity Graphs at Accelerometers 1 and 2**

The acceleration time history obtained at the sensors together with the impulse signal of the source can also be investigated by IR analysis. The force time history and velocity graph are converted into a frequency domain using the Fast Fourier Transform. Mobility is defined as the ratio between the converted frequency-base velocity and the frequency-base force. The result is plotted as mobility versus frequency as shown in Figure A6. When the generated wave lengths are greater than the diameter of a prismatic pile, there are resonant frequencies that depend on the pile length and the propagated wave velocity as shown in Figure A6. The length of the pile can be estimated from the difference of successive resonant frequencies as:

$$L_t = \frac{v}{2 \times \Delta f} \quad (3)$$

Where  $\Delta f$  is the difference between consecutive resonant frequencies.

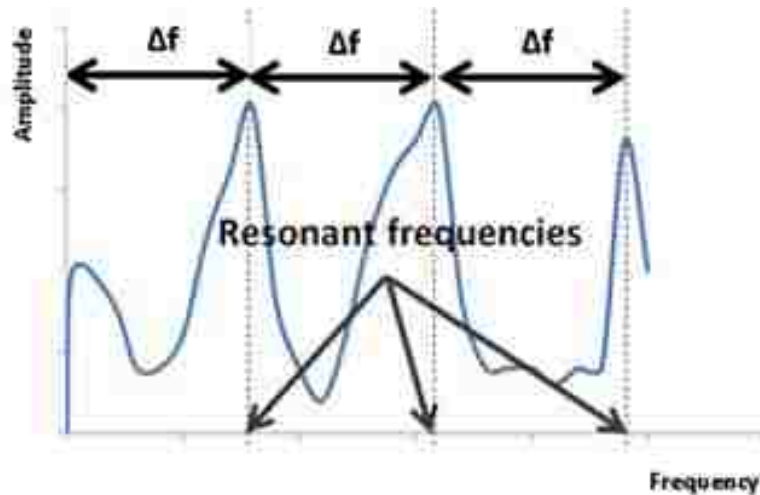


**Figure A6. Mobility Graph and Resonant Frequencies**

### SE/IR Test Procedure

The following steps are taken to conduct SE tests in the field. Detailed explanation of each step is given later.

1. Select the appropriate source application method.
2. Select the locations of sensors (accelerometers).

3. Assemble SE equipment.
4. Apply the source and acquire data.

After the data are collected in the field, the length of substructure can be derived using SE analysis and IR analysis later in the office.

It is crucial to identify the applicable methods of striking and sensor locations to capture intended echo from the foundation bottom. Striking should be applied at the top of the wing piles where the top of the pile is accessible. Due to the small sizes of timber piles, placing the accelerometer on the pile top may be unsuitable since the sensor will be too close to the source. When a superstructure presents above the foundation, the pile top becomes inaccessible. In such cases, other source application options must be used. The sensors should always be mounted on wooden blocks attached to the side of the pile by nails, screws, or superglue. The details of source application methods and sensors attachment are discussed here.

### **Appropriate Source Application Methods**

In SE tests, sonic waves are generated by striking a hammer on the surface of a substructure. Depending on the direction of the hammer strike, either longitudinal waves or shear waves can be generated through the pile. If a part of the top of a pile is accessible, generating longitudinal waves through the pile by striking on its top is preferred. If the pile top is inaccessible, other options such as striking a block attached to the side surface of the pile can be considered. Proper practical options of source location are described in the next sections for piles with or without accessible top.

#### *Piles with Accessible Top*

The source (vertical striking) should be applied at the top of the pile when the exposed top surface area is greater than the hammer as shown in Figure A7. The top of the pile is completely open for striking in Figure A7a while only a partial of the top surface is available for striking in Figure A7b.

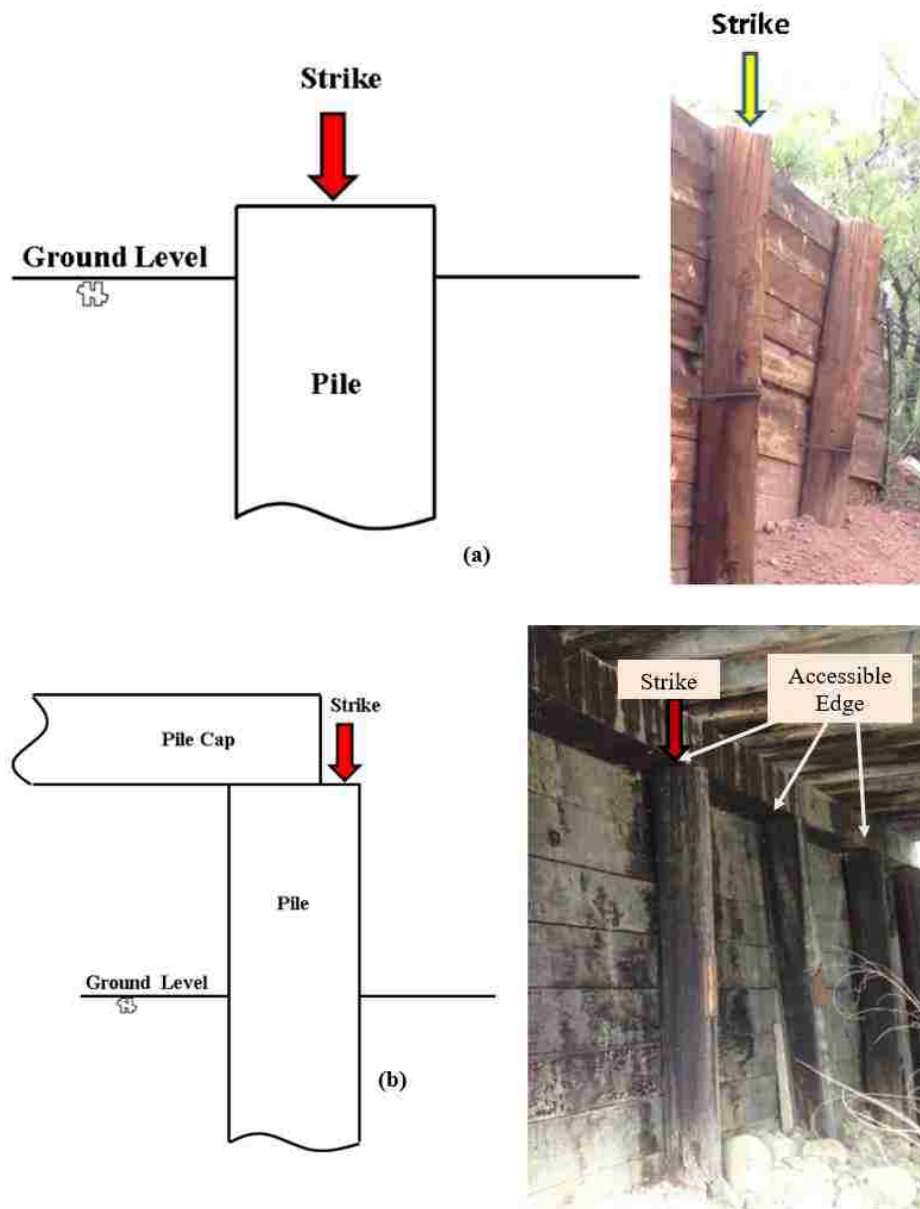


**Figure A7. Vertical Striking on Piles with Accessible Top**

*Piles without Accessible Top*

When the top of a pile is inaccessible, the longitudinal wave can be generated by other methods. Five options for applying the source are shown in Figures A8 to 12. Option 1 is identified as the best source application method and Option 5 is considered as the least favorable source application method. Option 1 is vertical striking on the pile cap above the pile as shown in Figure A8. If the pile cap above the pile is inaccessible, it is recommended

to conduct two SE tests: one test with Option 2 and the other test with Option 3. Conducting two SE tests improves the reliability with very little increase of time.

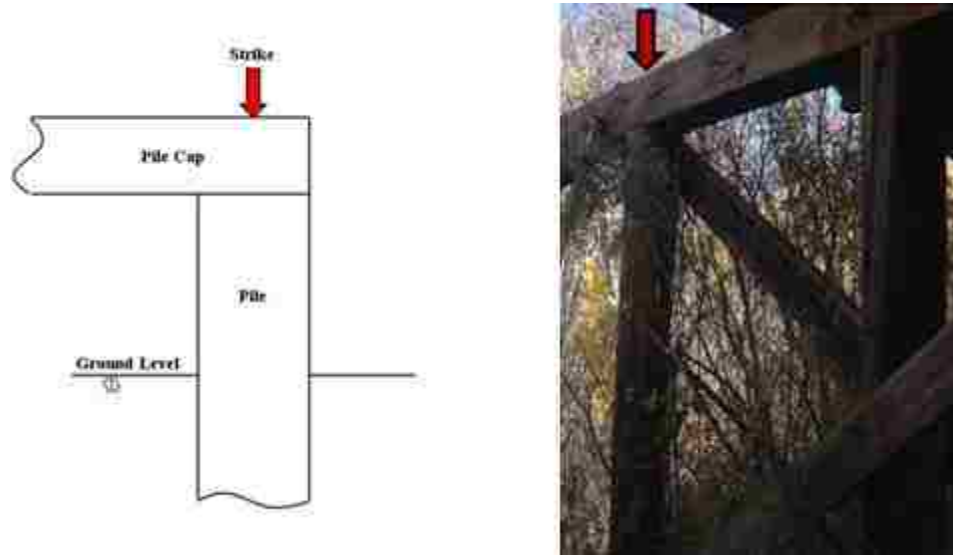


**Figure A8. Option 1: Vertical Striking on Top Surface of Pile Cap above the Pile**

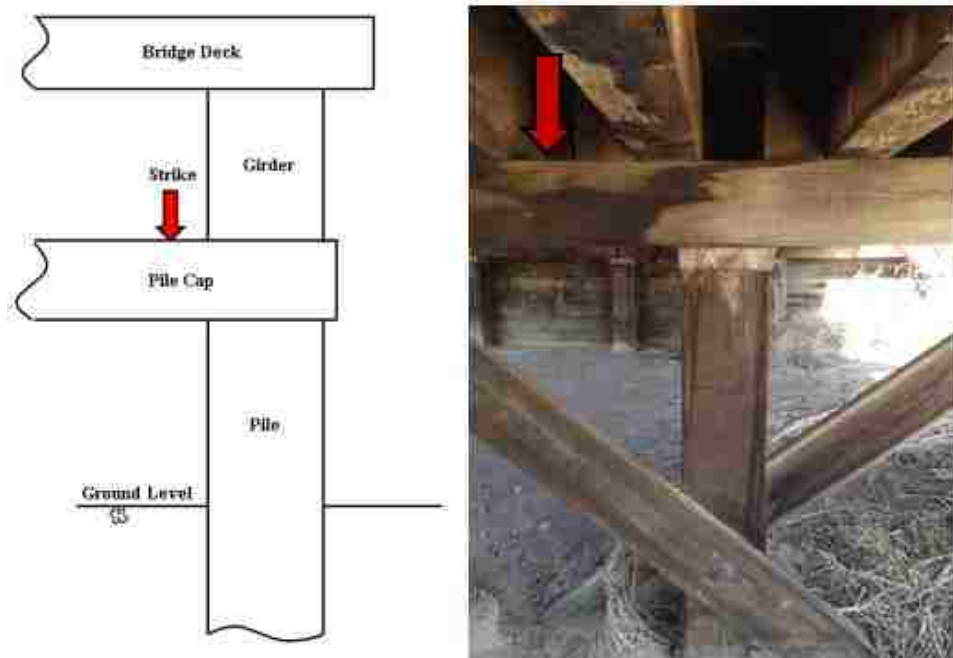


**Figure A9. Option 2: Eccentric Vertical Striking on Top Surface of Pile Cap**

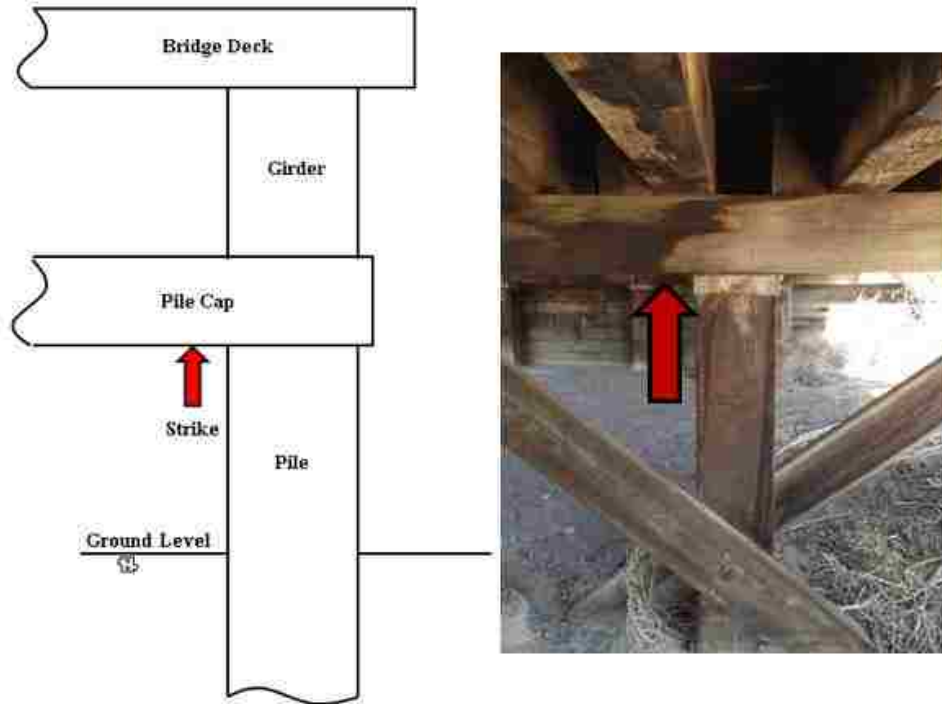


**Figure A10. Option 3: Upward Vertical Striking on Bottom Surface of Pile Cap**

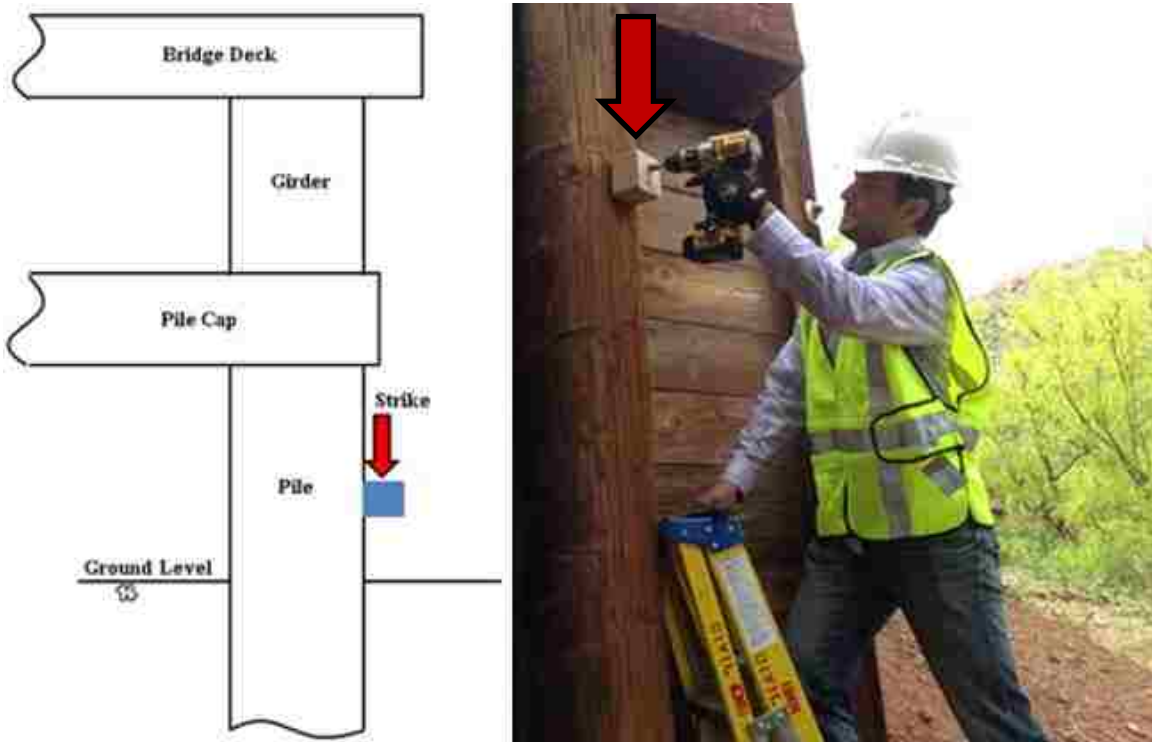


**Figure A11. Option 4: Vertical Striking on A Striking Block**

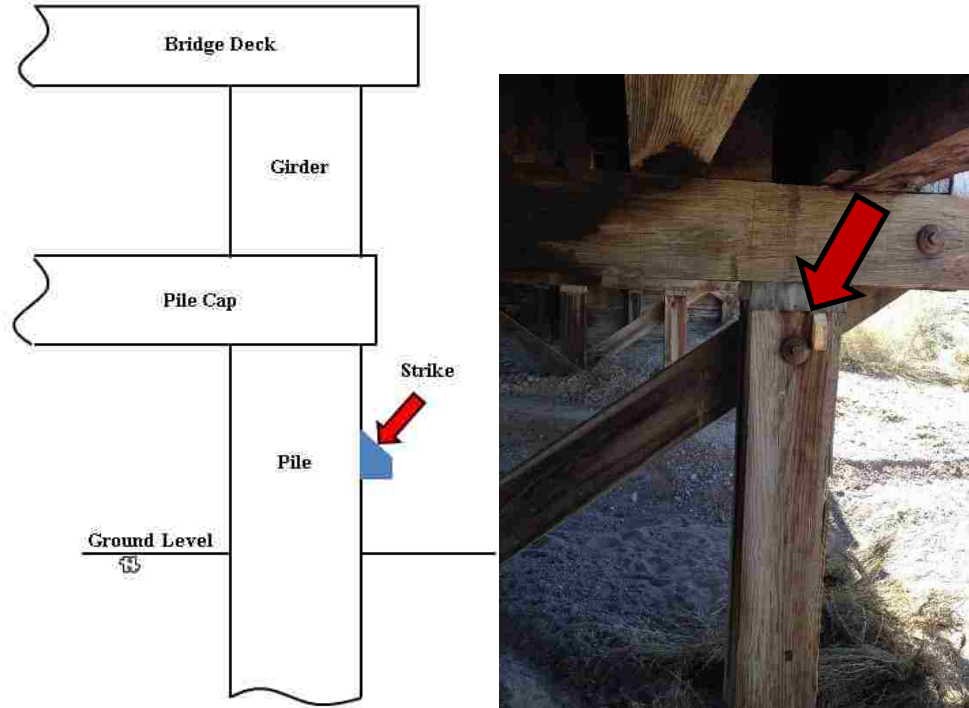


**Figure A12. Option 5: Inclined Striking on A Wedge Striking Block**

When a striking block is employed, the block should be properly secured by nails and screws to prevent any detachment during striking (see Figure A13). The dimensions of a striking block used in this project are shown in Figure A14. The only requirement of the dimensions of the striking block is that they must be greater than the size of the hammer. The striking block is located between the first accelerometer and the top of the pile. The hammer should not touch the pile during striking.



**Figure A13. Attaching the Striking Block on the Test Pile**

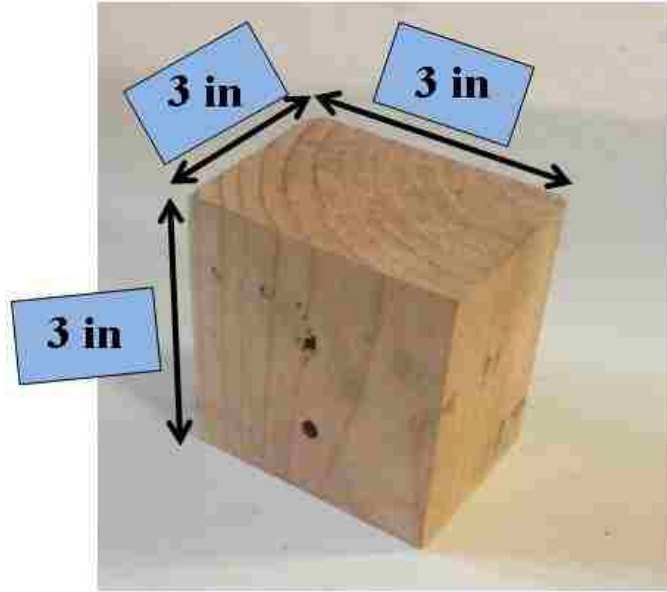


**Figure A14. Dimentions of the Striking Wood Block**



**Figure A15. Diagonals and a Bolt**



If Options 1 to 3 cannot be applied, good results have been obtained by striking on the existing bolt (see Figure A15).

In some old bridges, the quality of the connection between pile and pile cap may not be good enough to transmit wave energy properly down the pile. Options 4 and 5 may be better than Options 2 and 3.

### Placement of Sensors

If the top is accessible, the accelerometer should be placed on the top of the pile without the wooden block shown in Figure A16. The top surface must be flat, horizontal, and smooth. Otherwise, the accelerometer should be mounted on a wooden block attached to the side of the pile with nails, screws, or glue. The locations of the accelerometers will be discussed later. The dimensions of the wooden blocks used in the project are shown in Figure A16. The dimensions do not need to be precise if they are greater than the size of the accelerometer. An appropriate nut (No. 10) is glued onto the top surface of the block for attachment of an accelerometer.

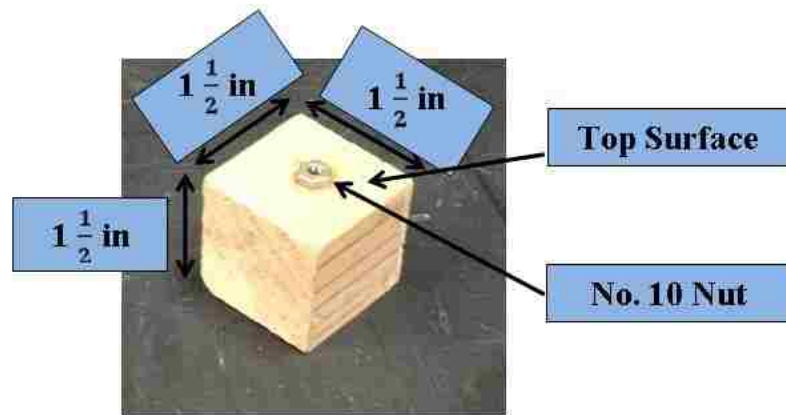


**Figure A16. Wooden Block for Attaching an Accelerometer**

### *Locations of Sensors*

When the top of the pile is accessible and the diameter of the pile is greater than 2 ft, the accelerometer is mounted vertically on the surface to capture longitudinal vibrations as shown in Figure A17. Vaseline is applied between the accelerometer and the top of the pile for better wave transfer from the pile to the sensor. An accelerometer can be mounted to the side of the pile by the wooden block (Figure A16) attached to the side of the pile

frequently by superglue as shown in Figure A18. The accelerometer is always placed vertically for our 1-axis accelerometers.

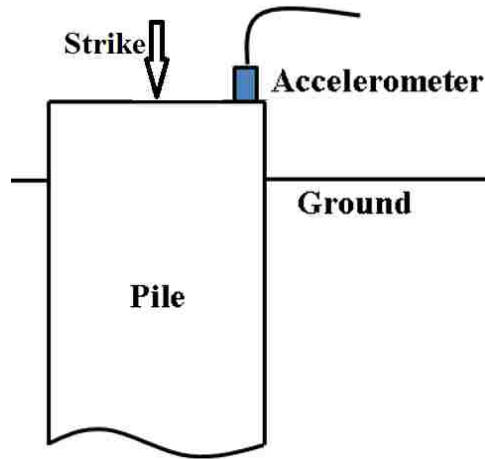


**Figure A17. Accelerometer Setup for Piles with Accessible Top**

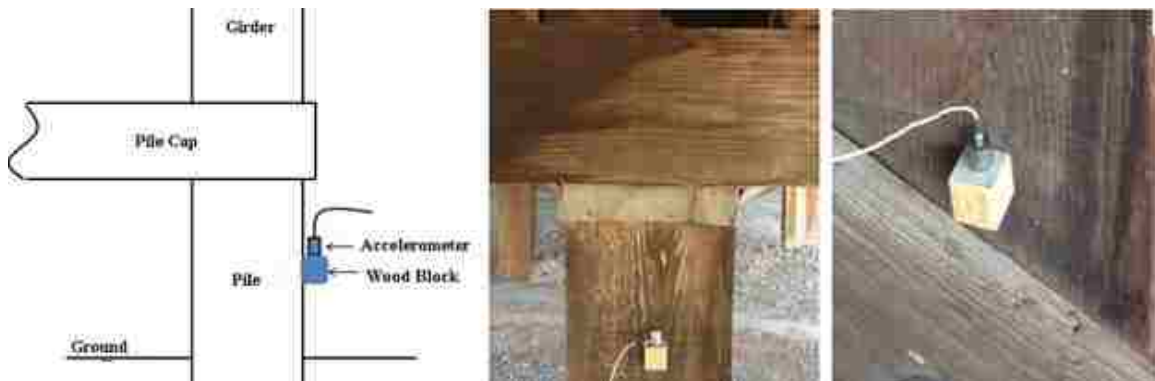


**Figure A18. Mounting Accelerometer on Piles without Accessible Top**

Good results have been obtained during this project when the accelerometer was placed 1-2 ft from the source. Therefore, it is recommended to place the first accelerometer 1-2 ft below the source (the striking point). The second accelerometer should be placed far away from the first accelerometer as possible (at least 2 ft). The locations of the sensors should be recorded for future data interpretation. Figure A19 shows the two accelerometers mounted on the side of the substructure. If two accelerometers are used two velocity graphs are obtained with a single hammer blow. Also, the propagated wave velocity can be estimated from the first arrival times at the two accelerometers. An example of the

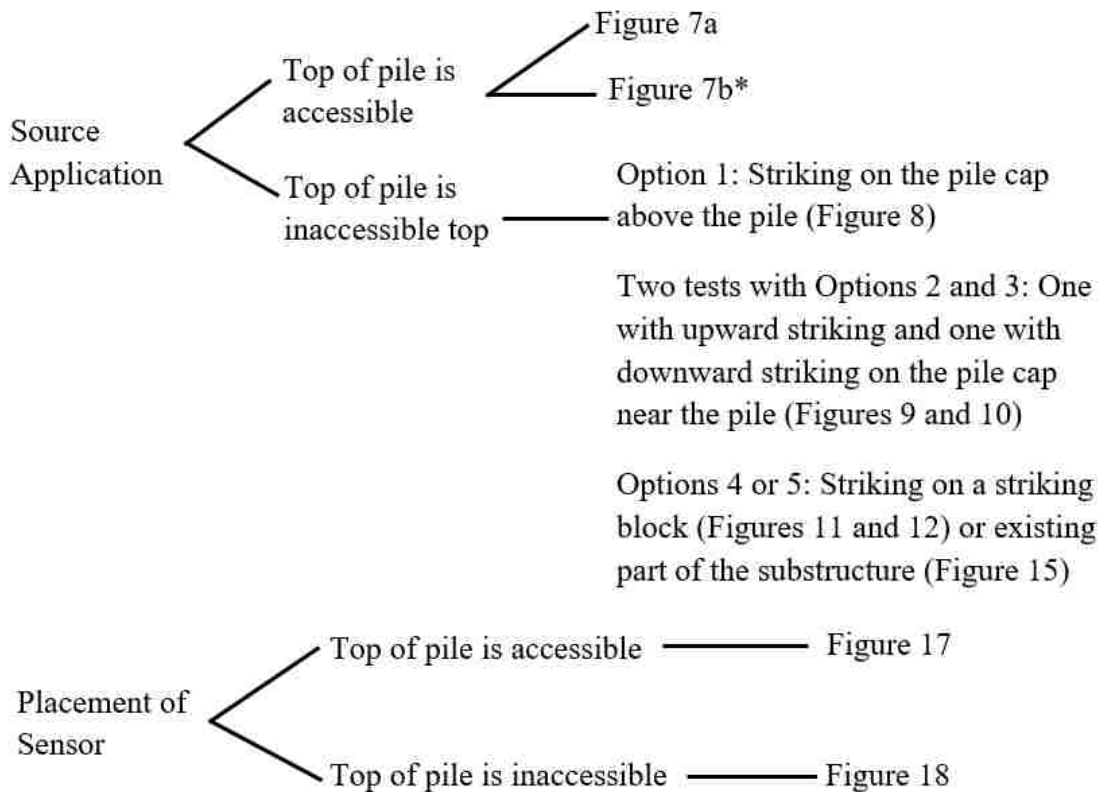
calculation of the propagated wave velocity will be presented later in this report. The project findings indicate that the calculated length based on the velocity graph from the first accelerometer was more consistent than that from the second accelerometer.



**Figure A19. Two Accelerometers Mounted on the Side of the Substructure**

## Summary of Source Application and Sensor Placement

Figure A20 shows the summary of source application and the placement of sensor.



\*For piles with partially accessible top, the accessible part of the pile top should be wide enough to allow producing a clean strike by the hammer

**Figure A20. Summary of Source Application and Placement of Sensor**

## Assemble Equipment

The equipment used for conducting SE/IR tests should be assembled as indicated in Figure A21.



**Figure A21. SE/IR Test Equipment**

In addition to the parts shown in Figure A21, the following items should also be brought to the site:

1. Duct tape and Electrical tape
2. Cordless power drill and drill bits
3. Tape Measure
4. 3/8-in screws (more than 3 in long) with washers
5. 2.5-in and 4-in nails
6. Professional Super Glue
7. Ladder (for access elevated surface)
8. Tools (hammers, screwdrivers, and wrenches)
9. Towel
10. Striking blocks and accelerometer mounting blocks

The equipment should be assembled on a flat surface close to the test pile. Figure A22 shows the SE/IR equipment on top of a table near the pier wall. There should not be any problem when the table is less than 45 ft from the substructure since the cables are 50 ft long.



**Figure A22. SE/IR Equipment Placement near a Test Pier Wall**

### **Acquire Data**

Once the equipment is assembled and the sensors are placed, an SE test is performed by striking at the selected location with the hammer shown in Figure A23a. Four different hammer tips shown in Figure A24b are available. Hard tip is used primarily unless poor results are observed which will be discussed later.

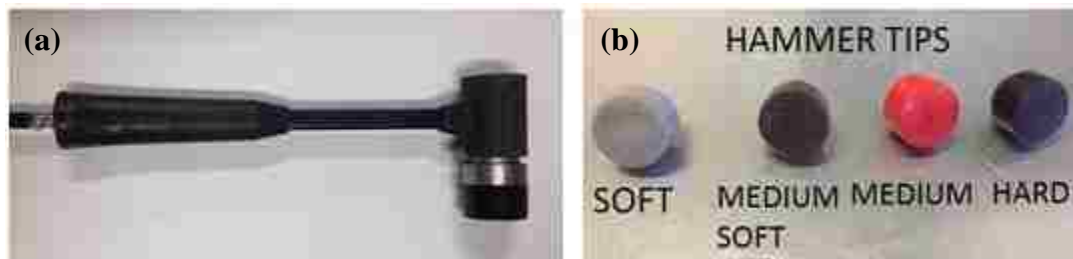


**Figure A23. A Hammer and Four Hammer Tips**

Before striking, execute the data acquiring software (WinTFS) per the User Manual to collect the acceleration time history. Input the calibration number for our 1-axis accelerometers (0.0025) and other default values. Upon striking, raw data collected by the accelerometer and the velocity graph will be displayed on the computer screen as shown in Figure A24. An impulse signal from the hammer strike is shown in Figure A25.

Due to the random nature of noise, repeating the tests may produce better velocity graphs.

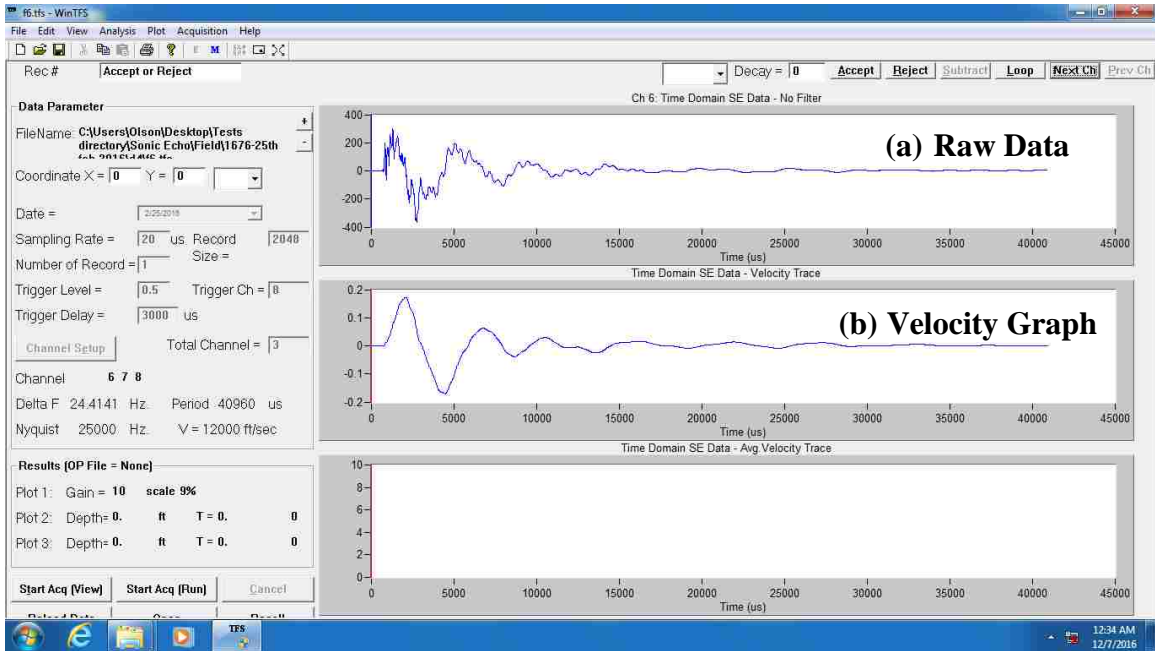


**Figure A24. Example of Acquired Acceleration and Velocity Time Histories**

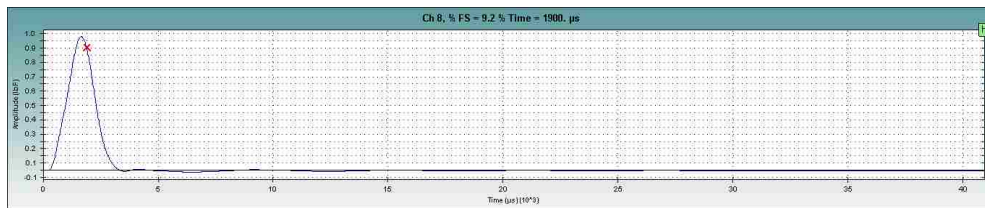


**Figure A25. Impulse Signal**

**Good and Poor SE Results** The most important result of an SE test is the velocity graph. The velocity graph of a good SE test should show a clear impulse and echo. The length of a pile is estimated based on the time difference between impulse and echo ( $\Delta t$ ) in SE analysis. A poor velocity graph is defined as:

- either the impulse or echo from the pile toe cannot be identified or echo from the pile toe cannot be identified
- the magnitude of the measured pile response does not decay with time.

Figure A26 shows two schematic good velocity graphs for downward and upward striking. Besides the echo from pile bottom, echoes from changes in impedance such as necks, bulges, layered soils, rock interface, internal cracks, and reflections from superstructure also appear in the velocity graphs. The impulse is the first lowest valley

(highest peak for upward striking) in the velocity graph. The second lowest valley (second highest peak for upward striking) can be considered as the echo. The impulse and echo should be on the same sides (above or below the horizontal axis) unless the pile is in hard rock.

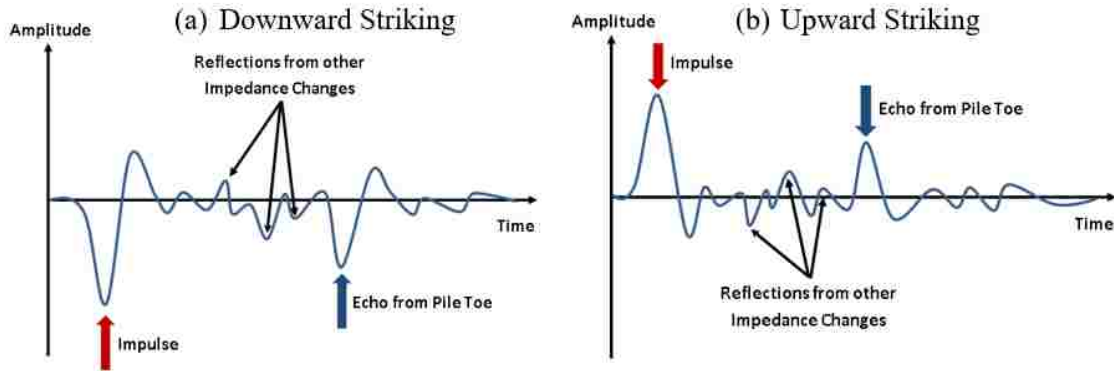


**Figure A26. Good Velocity Graphs of SE Tests**

Examples of good velocity graphs for piles of different lengths obtained in the field are shown in Figure A27. An example of good velocity graph for upward striking is shown in Figure A28.

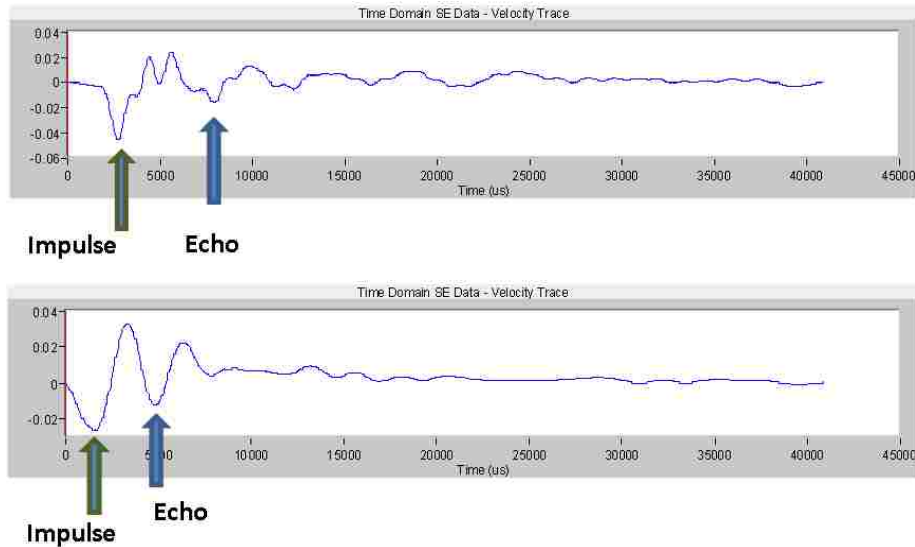


**Figure A27. Good Velocity Graphs Obtained in the Field**



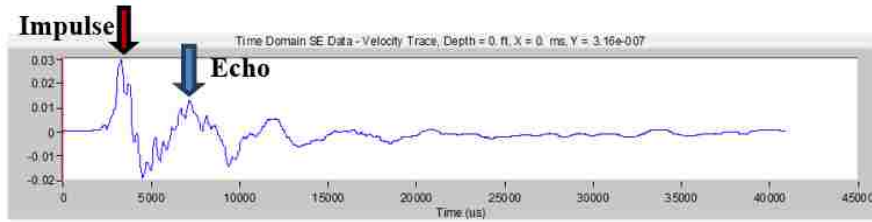


**Figure A28. Good Velocity Graph Obtained in the Field by Upward Striking**

Figure A29 shows three examples of poor velocity graphs that were identified in the project. The appearance of these velocity graphs is very different from those of good velocity graphs as shown in Figures A26 to 28. The measured pile response in Figure A29a and A-29c does not decay with time while the magnitude of the first valley is less than the magnitude of the second valley in Figure A29b. These measured pile responses are not related to the longitudinal wave produced from the hammer impact. They may be caused by the source application method, the poor coupling between the accelerometer and the pile, or noise. The solutions are shown in Table A3.

Ensure that there is no loose connection between the accelerometer and the wooden block (if used), no loose cable connection from the accelerometer to the Freedom PC. Repeating the test with the same source application method and sensor location may produce good velocity graphs. If not, repeating the test with a different source application method and/or different sensor location. If good velocity graphs cannot be obtained after applying all striking options, SE method is not applicable to the pile.

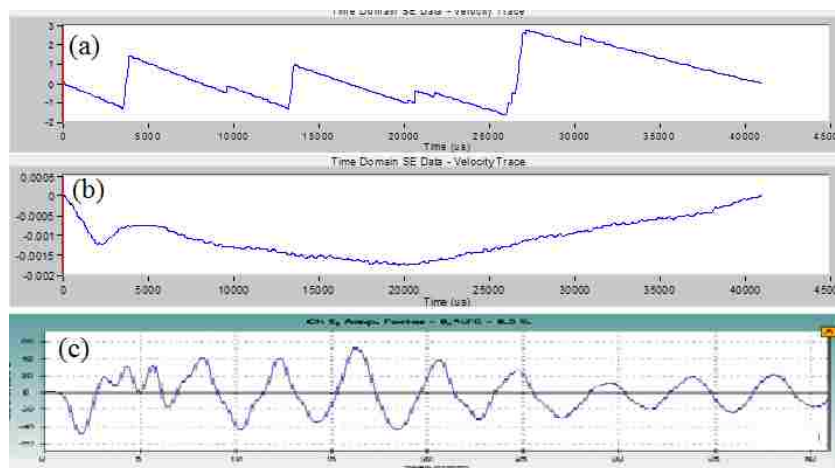


**Figure A29. Examples of Poor Velocity Graphs of SE Tests**

**Table A3. Troubleshooting Table for Poor Velocity Graphs Shown in Figure A29.**

Possible Reason	Solution
Loose cable connection	Reassemble the equipment
Accelerometer is loosely connected to the wooden block	Tighten the accelerometer in to the nut on the wooden block
Equipment malfunctions (cables, accelerometer)	Use another cable and accelerometer
Source application method	Select a different source application method
Vibration from other sources	Use another source application method Place the sensor at a different location Choose an environment with less noise (test at night)

Figure A30 shows a different type of poor velocity graph where the rough locations of impulse and echo are known (the ellipses in the graph). However, it is difficult to identify the correct impulse and echo times. Those closely spaced valleys are related to different wave trains. The cause is neither the sensor nor the cable connection. The magnitudes of these valleys may change by repeating the test. If the multiple valleys of similar magnitudes still appear in the velocity graph. The cause may be due to the frequency content of a hammer or reflections of superstructure. The solutions are listed in Table A4. Repeating the test with a softer tip should eliminate the multiple valleys of similar magnitudes. If not, repeating the test with a different sensor location.

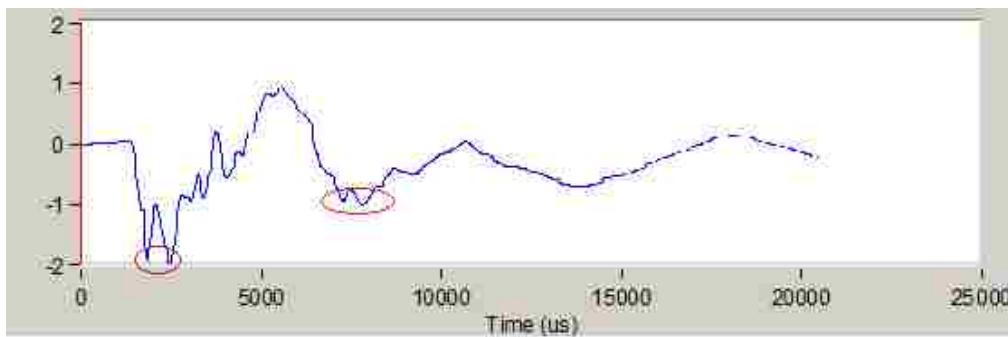


**Figure A30. Example of Poor Velocity Graph**

**Table A4. Troubleshooting Table for Poor Velocity Graphs Shown in Figure A30.**

Possible Reason	Solution
Source application method	Select a different source application method
Reflections of superstructure	Place the sensor at a different location
Frequency content of a hammer	Use another hammer tip

Poor velocity graphs may be due to poor impulse signals shown in Figure A31. A good impulse signal is previously shown in Figure A25. Figure A31a shows a signal for which the amplitude has exceeded the threshold. Repeating the test with a gentler blow should produce a good impulse signal. When multiple peaks appear in the impulse signal (see Figure A31b), repeating the strike with a sharper and quicker hammer blow may eliminate the multiple peaks. If a striking block is employed (see Figures A11 and A12), ensure the striking block is securely attached on the pile.

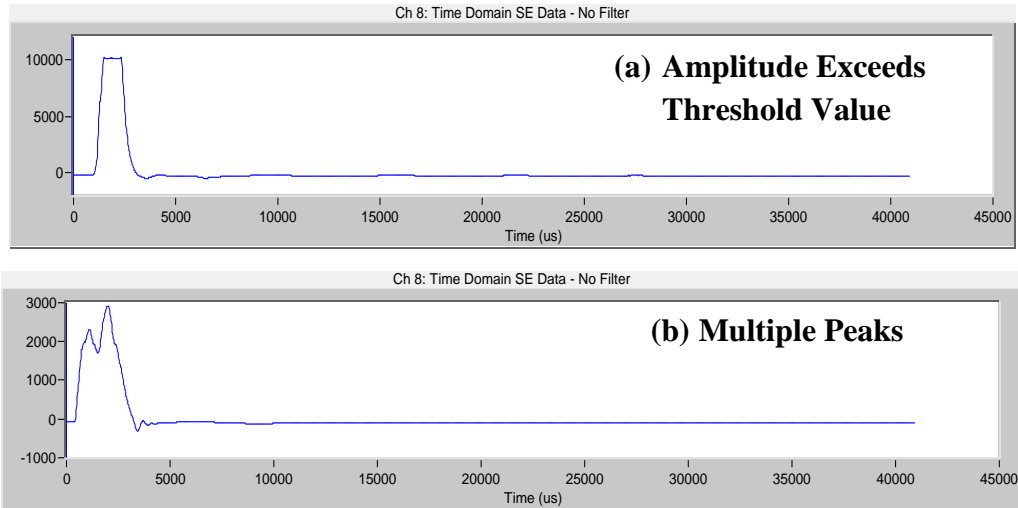


**Figure A31. Examples of Poor Impulse Signals**

If the impulse signal is good, repeating the test with different accelerometer location may produce better results.

If poor velocity graphs are still found after six trials, a different option for source application should be used. If good results are not obtained after applying all striking options, SE test cannot be applied to this pile.

A flowchart shown in Figure A32 was developed for conducting SE tests in the field. Once a good velocity graph from a sensor is obtained, other SE tests of the same source application and placement of sensors should be performed until two more good velocity graphs are obtained at the same sensor to ensure consistency. A good SE test is defined when three similar good velocity graphs are obtained at an accelerometer. Our research experience indicates that the two additional good velocity graphs happen often after the first good velocity graph has been attained. If three good velocity graphs cannot be obtained after 6 trials, start a new SE test with a different striking option and/or with different accelerometer location until all available striking options and possible sensor locations have been applied. The new sensor position should be 1 to 2 ft below the old position. If poor velocity graphs are found for all possible striking options and sensor placement, SE test cannot detect the length of the pile.

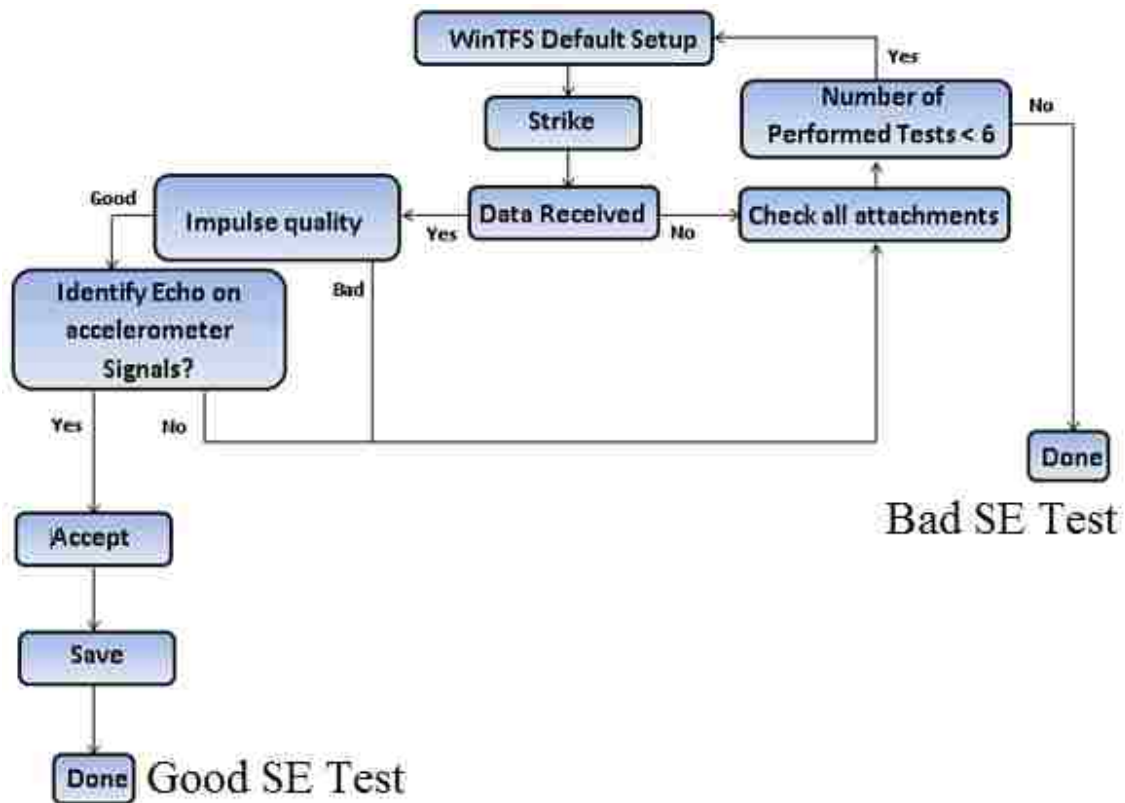


**Figure A32. Flowchart for Conducting SE Tests in the Field**

## Interpretation of Velocity Graphs

The length of the substructures is calculated from  $\Delta t$  (the time difference between the impulse and echo). The characteristics of echo related to various situations are presented here. Echoes from compression and tension waves are shown previously in Figures A27 and 28 respectively. Those graphs correspond to cases for which the pile toe is in soil. In such cases when the incident wave hits the interface of the pile and soil, the reflected wave has the same sign in the graph. When the pile toe is on rock that is stiffer than the material of substructure, the reflected wave has the opposite sign in the graph. The schematic echoes obtained from piles on soil and on rock are compared in Figure A33. It should be noted if the impedance change between the rock and pile's material is small, the pile toe reflection may be undistinguishable.

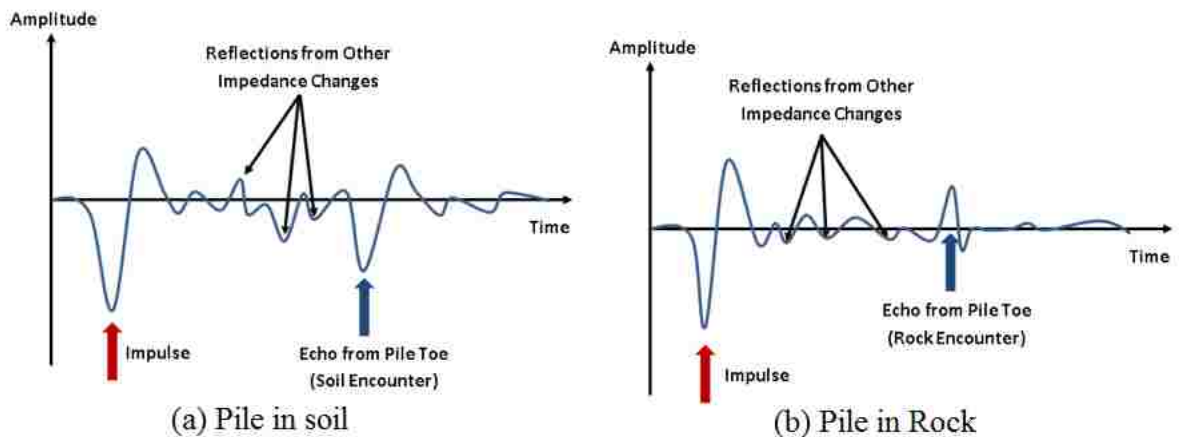


**Figure A33. Schematic Velocity Graphs for Piles in Soil and Rock**

When a notable crack in pile is located below the sensor, most of the energy may reflect and only small amount of energy transmits down. Therefore, the echo from the pile toe will be undetectable. In such cases, the velocity graph may only show consecutive reflections from the crack as indicated in Figure A34.

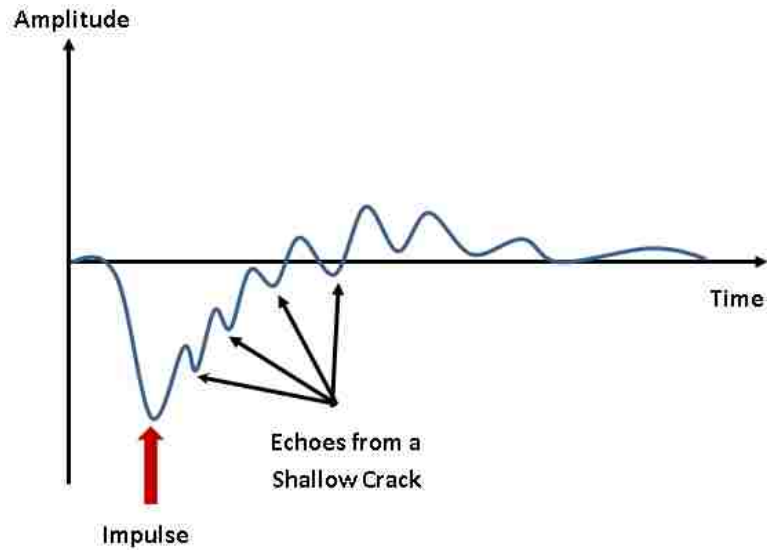


**Figure A34. Schematic Velocity Signal Showing Consecutive Reflections from an Internal Crack**

### **Determining Pile Length with SE Analysis**

The velocity graph of an SE/IR test can be analyzed in either time domain (SE analysis) or frequency domain (IR analysis). The velocity graph is used directly in SE analysis whereas the mobility graphs are generated in IR analysis by the software (WinTFS). It should be noted that, in both methods, the calculated pile lengths greater than 30 times of the pile diameter may be unreliable.

Figure A35 shows the velocity graphs of a real SE/IR test. Accelerometers 1 and 2 were located 1 and 3 ft below the top of a concrete wall respectively.

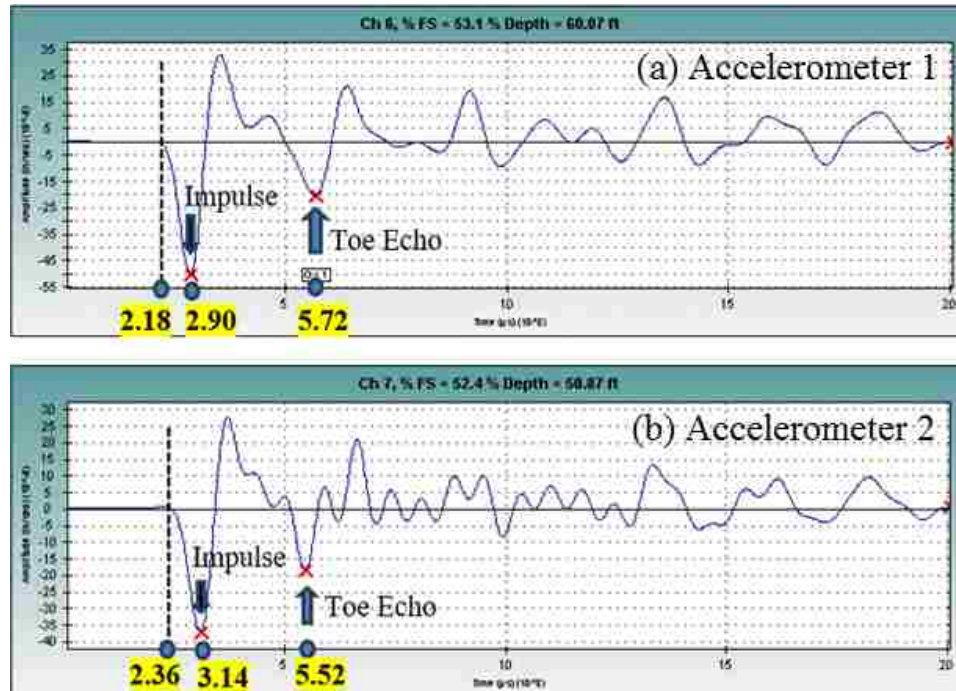


**Figure A35. Velocity Graphs Obtained from Two Accelerometers**

The wave velocity of the substructure material can be determined using two sensors in the field or assumed based on the material types. The longitudinal waves of wood and concrete range from 9,900 to 12,000 ft/s and 10,000 to 14,500 ft/s, respectively. The longitudinal wave velocity can be calculated from the time difference of the first wave arrivals at the two sensors. However, the accuracy of the wave velocity depends on the distance between the two sensors and the precision of the equipment.

In this example, the first arrival times at Accelerometers 1 and 2 are 2.18 and 2.36 ms respectively. Knowing the distance between the accelerometers (2 ft), the propagated wave velocity can be calculated as:

$$v = \frac{2}{(2.36 - 2.18) \times 10^{-3}} \approx 11100 \text{ ft/s}$$

From Figure A35a, the distance between Accelerometer 1 and the bottom of the concrete wall is:

$$L_{tr} = \frac{v \times \Delta t}{2} = \frac{11100 \times (5.72 - 2.9) \times 10^{-3}}{2} = 15.7 \text{ ft}$$

Given the sensor was located 1 ft from the top, the height of the concrete wall is:

$$L_t = L_{tr} + L_a = 15.7 + 1 = 16.7 \text{ ft}$$

From Figure A35b, the distance between Accelerometer 2 and the bottom of the concrete wall is:

$$L_{tr} = \frac{v \times \Delta t}{2} = \frac{11100 \times (5.52 - 3.14) \times 10^{-3}}{2} = 13.2 \text{ ft}$$

Given the sensor is located 3 ft from the top, the height of the concrete wall is:

$$L_t = L_{tr} + L_a = 13.2 + 3 = 16.2 \text{ ft}$$

Although the calculated heights are similar in this example, the research project result has shown that the length calculated from the sensor closer to the source is more consistent.

### **Determining Pile Length with IR Analysis**

If there is doubt about the SE results, IR analysis can be used to confirm the pile length. The findings of the project show that IR analysis yielded reasonable pile lengths in some cases. However, good velocity graphs do not guarantee good IR analysis leading to the determination of the pile length. The pile length estimated from poor velocity graphs is unreliable in general.

A mobility graph generated by the software is shown in Figure A36. Only one resonant frequency (red dot in the figure) is identified. This resonant frequency can be considered as  $\Delta f$  for estimating the pile length. The research findings showed that the reliability of the pile length calculated using the first resonant frequency is much lower than the pile length calculated using the difference between two resonant frequencies.



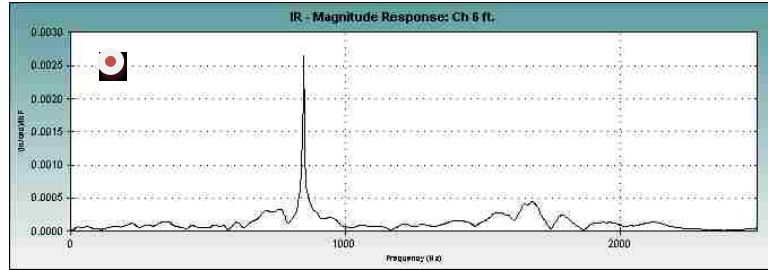


**Figure A36. Mobility Graph for IR Analysis**

The calculation of pile length using IR analysis is illustrated here. Figure A37 shows a mobility graph from a field SE/IR test. This mobility graph is better than Figure A36 since two resonant frequencies are identified in this figure. The difference between resonant frequencies is 331 Hz ( $\Delta f = 694 - 363$ ). With the assumed propagated wave velocity is 12,000 ft/s, the length of the pile is calculated as:

$$L_t = \frac{v}{2 \times \Delta f} = \frac{12000}{2 \times 331} = 18.1 \text{ ft}$$

If the first resonant frequency is used as  $\Delta f$  (363 Hz), the calculated pile length is 16.5 ft. Based on the research observation in this project, the actual pile length is closer than 18.1 than 16.5 ft.

In summary, IR analysis is not recommended as the primary tool to determine the pile length since the results are less reliable than those determined by SE analysis.

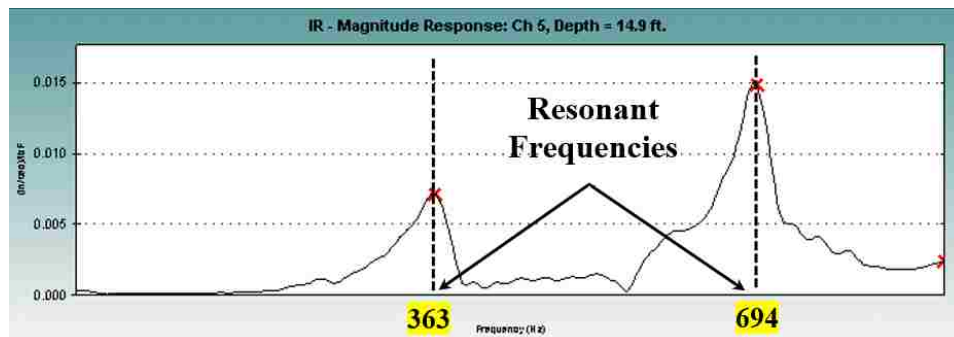


**Figure A37. Example of Mobility Graph Obtained from a Field Test**

## **PARALLEL SEISMIC METHOD**

### **Parallel Seismic Overview**

The PS method is a common low strain method that can be used to detect the length of piles. The method requires drilling a hole parallel to the test pile. The borehole is cased with a 2-in capped-end PVC tube and filled with clean water for better coupling with the sensor (hydrophone). The annular space between the PVC tube and the borehole is to be filled with compacted native soils.

In a PS test, an instrumented hammer produces an impulse that travels downward through the pile. As the stress wave travels down the pile, a portion of the wave is transmitted into the surrounding soil. The transmitted wave is recorded by a hydrophone that is inserted in a nearby borehole. The hydrophone is raised (or lowered) in uniform increments and the test is repeated at each increment. The first arrival time of the wave is defined at different depths. Figure A38 shows a typical setup and the velocity stacked plot from a PS test.

Since the wave velocity of the pile material is significantly higher than the wave velocities of soils, the arrival times differ between two consecutive depth increments, one tested when the hydrophone is parallel to the pile and the second when the hydrophone is below the pile. Two straight lines can be determined from these arrival times and the intersection of these two lines is then identified as the foundation depth. A benefit of the PS test is that the wave propagation through the soil provides information about the soil properties (such as stiffness) adjacent to the foundation. In addition, since each material has a specific wave velocity range, the measured slope of the lines above and underneath the pile toe can provide information about the type and quality of the pile's material.

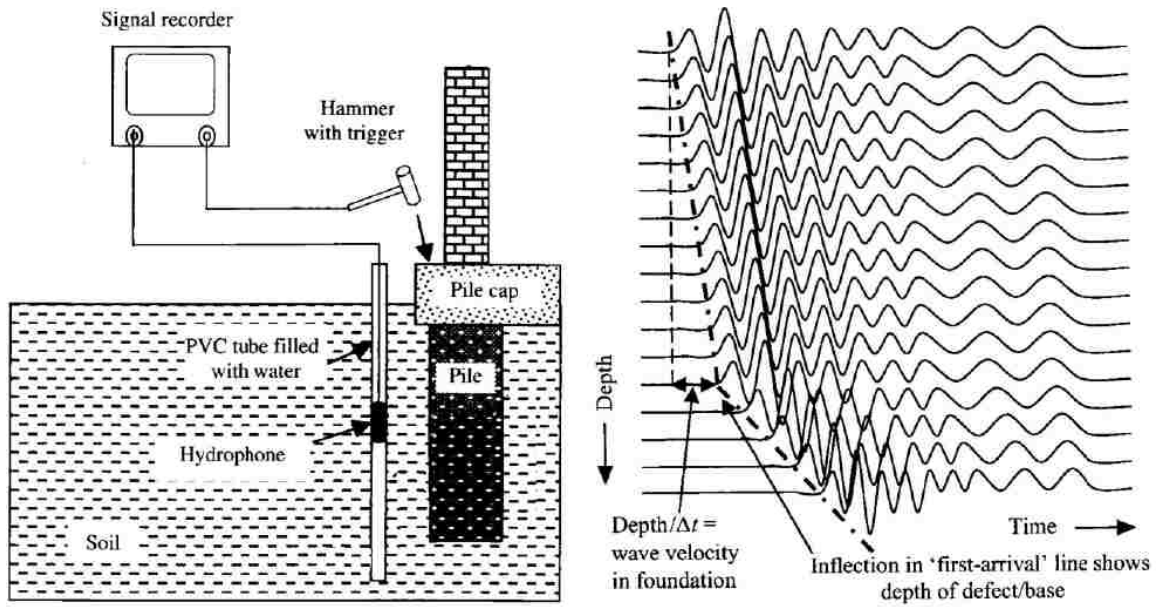


**Figure A38. Typical Setup and Test Data of Parallel Seismic Test (12)**

### PS Test Procedure

Before conducting a PS test, a borehole must be drilled next to the foundation. The following requirements are for preparing a borehole for PS tests:

- The borehole must align with the test pile.
- The depth of the borehole must be at least 15 ft below the expected pile toe level.
- The hole should be bored as close as possible to the test pile (no more than 6 ft away from the pile).
- A 2-in PVC tube is prepared based on the depth of borehole and the bottom of the tube is capped.
- The PVC tube is inserted into the hole and the annular space between borehole and tube is grouted or filled with compacted soil.
- The PVC tube is filled with water.

The PS test is carried out in three steps: setup the hardware, apply the source, and collect the data. The collected data will be processed at the office to determine the length of the pile.

**Hardware Assemblage** The PS equipment for conducting PS tests should be assembled as shown in Figure A39.

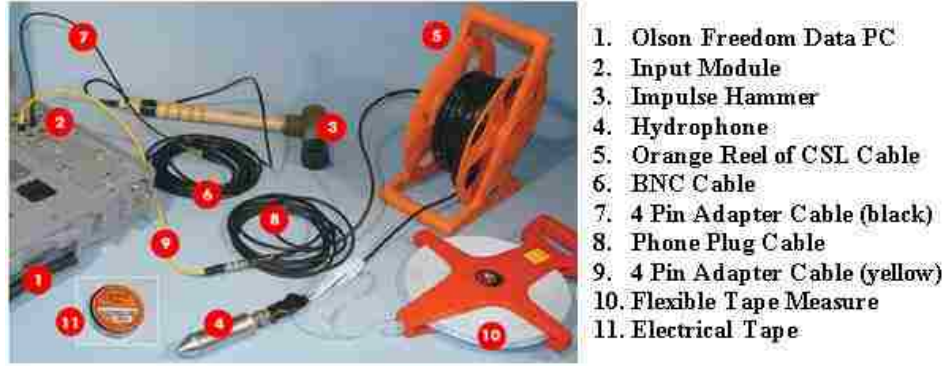


**Figure A39. PS Test Equipment**

### Source Application

The source is applied by a hammer (regular or sledge hammer) that strikes either vertically or horizontally. Although both vertical and horizontal striking produce acceptable data, the findings of the project revealed that the vertical striking excels horizontal striking. The source application methods (Figures A7 to 10) previously mentioned in the SE method can be used for conducting PS test. Horizontal striking will be used instead of Options 4 and 5 (Figures A11 and 12). The use of a striking block imposes uncertainty and additional cost.

If the horizontal striking is used, the direction of striking should follow Figure A40. As shown in Figure A40a, for square piles, the striking direction is along direction 1 if the bore hole is in Region A. If the borehole is in Region B, the strike should be along direction 2. For round piles, the direction of striking should be toward the borehole as shown in Figure A40b.

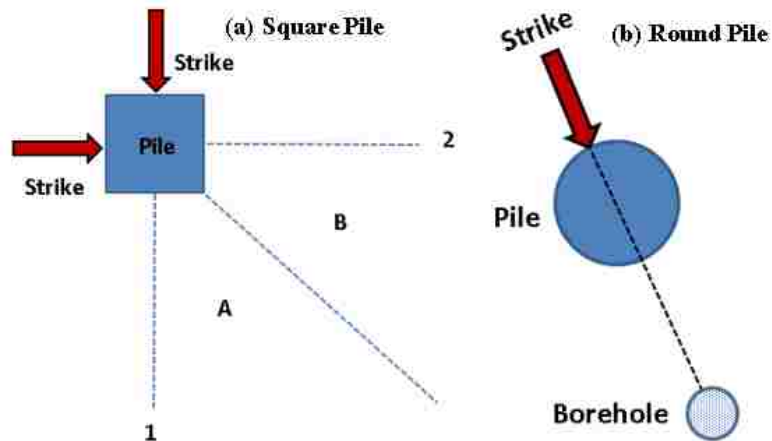


**Figure A40. Direction of Striking in PS Tests**

## PS Data Acquisition

Once the equipment is assembled, execute the “WinGEO-T” data acquisition software before applying the source. The hydrophone is then lowered towards the base of the tube in increments of 1 ft. At each depth, the substructure is struck with a hammer with hard tip. An example of the obtained signals including velocity graph and impulse signal are indicated in Figure A41.

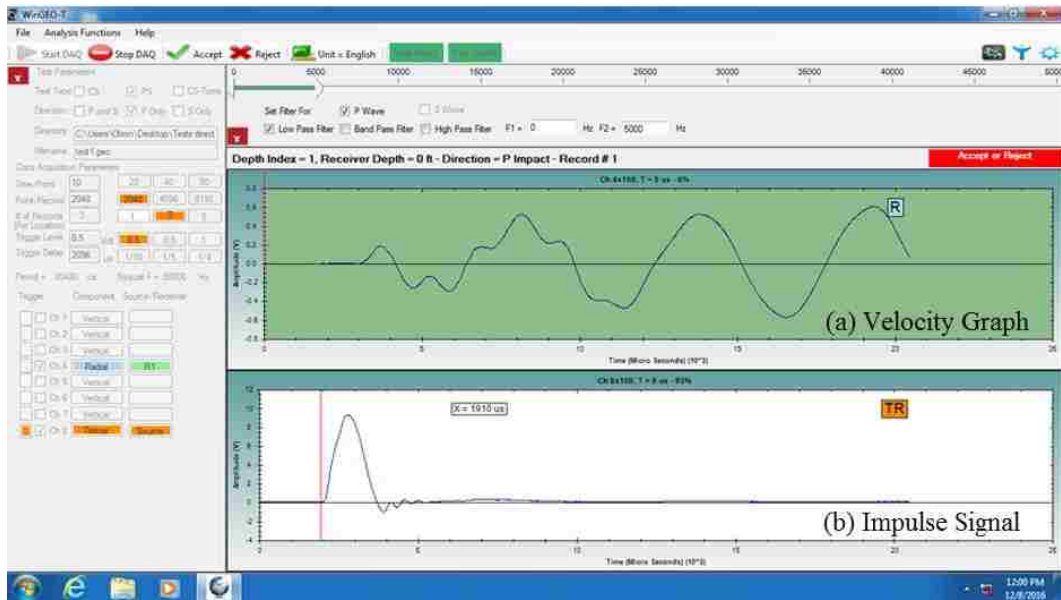


Figure A41. Example of Obtained Signals after a Hammer Strike

## PS Data Processing and Determining the Pile Depth

The velocity graphs recorded in each depth can be shown in a velocity stacked graph for easy comparison. Figure A42 shows a velocity stacked graph.

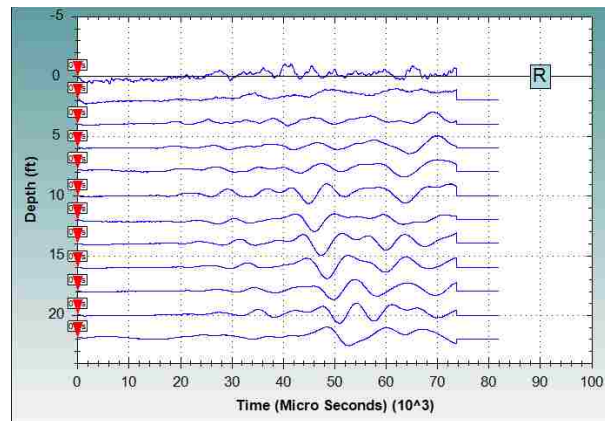
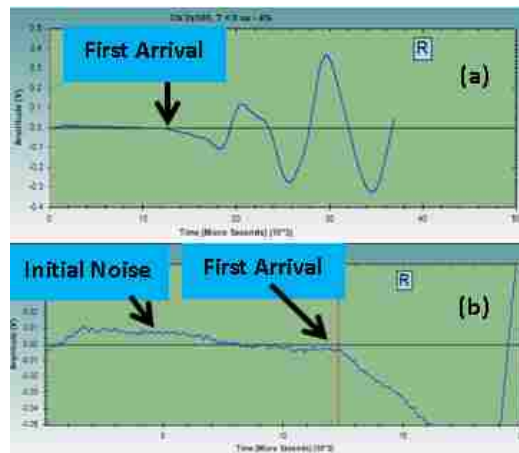


Figure A42. Example of a Velocity Stacked Graph

If obvious result is found as the one shown in Figure A38, the buried length of the pile is determined from the inflection point. Otherwise, the arrival time at each depth should then be picked from the velocity graph. First arrival times are determined by inspecting the background noise level in the signals that are evident prior to arrival of any sound wave from the source. The ‘First arrival’ is determined as the time when the signal begins to increase and consistently distinguish itself from the background noise level. The velocity graph may need to be enlarged to determine the First arrival. Figure A43b shows the initial noise and the first arrival. Determining the arrival time of the first P-wave precisely may be a challenge depending on the level of ambient noise. The project findings indicated that it was easy to determine the arrival times of the first P-wave at greater depths since the ambient noise reduced with depth.



**Figure A43. Example of (a) Original and (b) Enlarged Views of the Velocity Graph**

After determining the first arrival time at each depth, a plot of arrival time versus depth is created as shown in Figure A44. Two straight lines pass through the points aligned on approximately straight paths are defined. The intersection of these two lines (inflection point) indicates the location of the pile toe.

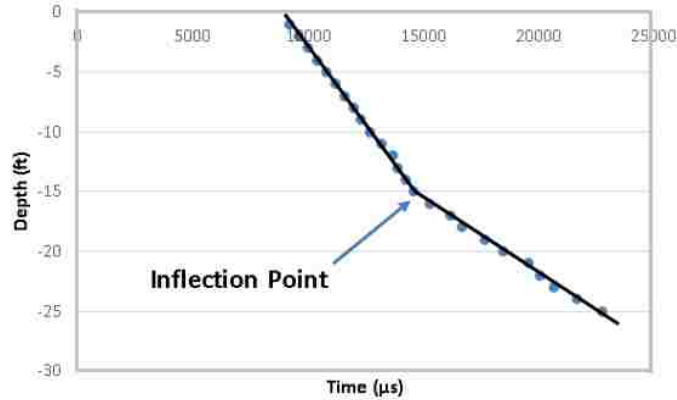


**Figure A44. Example of First Arrival Time Versus Depth and the Location of the Inflection Point**

The slopes of the lines above and below the inflection points also indicate the propagated wave velocity in the pile material and surrounding soil respectively. Since each material has a specific wave velocity range, the measured velocity of these lines can provide information about the type and quality of the pile’s material and surrounding soil. As an example, an unsuccessful PS test is shown in Figure A45. No inflection point could be identified. The borehole is not deep enough such that the pile length could not be identified. The solution is to drill a deeper borehole and repeat the PS test.

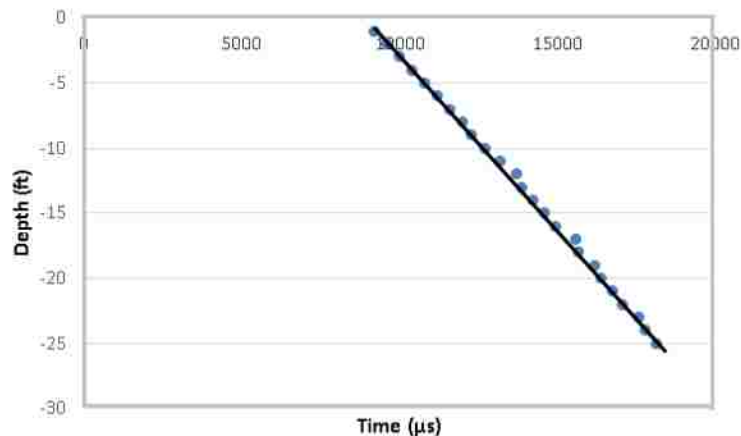


**Figure A45. Example of Unsuccessful PS Test**

Another example of unsuccessful PS test from our study is shown in Figure A46. It was difficult to determine the two straight lines from this noisy velocity stacked plot. Repeating the PS test at another time with less noise (at night) may solve the problem. If

the hammer does not produce adequately strong signals that are distinguishable from the background noise, a sledge hammer can be used.

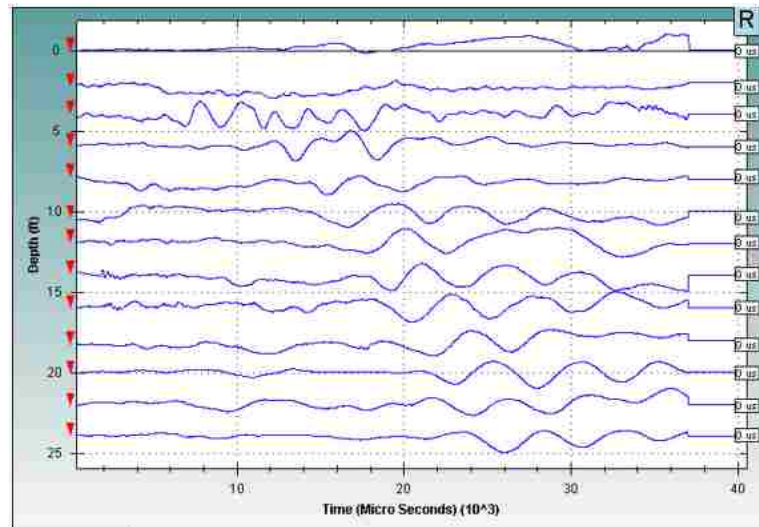


**Figure A46. Example of Noisy Velocity Stacked Plot**

## INDUCTION FIELD METHOD

Before conducting IF tests, a borehole must be excavated next to the foundation. The followings are the requirements to prepare the borehole:

- The borehole must be parallel to the test pile.
- The depth of the borehole must be at least 10 ft below the expected pile toe.
- The hole should be bored as close as possible to the test pile (no more than 1.5 ft away from the pile).
- A 2-in PVC tube is installed to keep the borehole from caving. Although endcap is not required but is highly recommended so that the hole can be used for PS test if necessary.
- The annular space between the borehole and the tube is filled with compacted soil.

An IF test is carried out in three steps: setup the hardware, collect the data, and process the data.



## Hardware Components

Figure A47 shows the correct assembly of the Length Inductive Test Equipment (LITE) used for conducting IF tests. The equipment includes battery, signal conditioning box, multimeter, and the Probe (induction sensor). The details of signal conditioning box are shown in Figure A48.

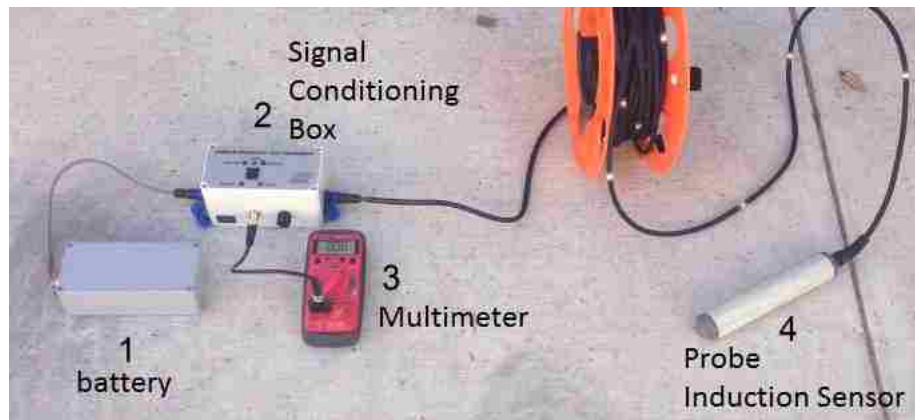


**Figure A47. Length Inductive Test Equipment (LITE) for IF tests**



**Figure A48. Details of Signal Conditioning Box**

## IF Data Acquisition

Calibrate the system before conducting IF tests. The calibration should follow these steps:

- 2) Assemble the components as shown in Figure A47.
- 2) Set the multimeter test dial to the “20V” in the DC voltage setting.

- 3) Set the reference point
  - Place the Probe at a location such that there is no metal object within 3 ft.
  - Push down the rocker switch until one of the three lights (negative/zero/positive) illuminates.
  - Turn the knob until the green light (middle one) is on and the voltage is approximately 2.5 V.
- 6) Push down the rocker until either NO METAL or METAL illuminates.
- 7) Bring the Probe in contact with a metal object, the multimeter should show a reading close to 5.04 V. If the readout is still less than 3V, the battery is low. A remote possibility is that either the multimeter or the Signal Conditioning Box is defective.

To conduct IF tests (after system calibration):

- 4) Insert the Probe into the PVC tube inside the previously installed borehole.
- 5) If the first reading remains 2.5 V, the distance between the hole and the metal in the pile is greater than 18 inches, or there is no metal in the substructure.
- 6) If the first reading is much greater than 3 V, lower the Probe in 1-ft increment and record the voltage at every foot till the bottom of the hole.

### **Data Processing**

The recorded voltage reading is plotted against depth as shown in Figure A49. The depth of the pile is located at where the voltage starts to drop. This figure is a schematic plot of a successful IF test where the voltage drops before the Probe touches the bottom of the hole.

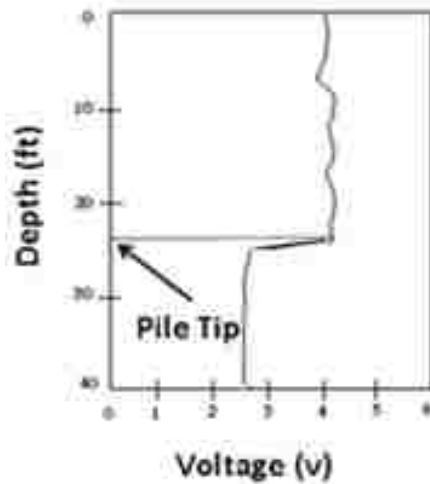


**Figure A49. Result of A Successful IF Test**

#### **Unsuccessful IF Tests**

- Voltage remains close to 2.5 V when the Probe is inside the PVC tube and at the ground level. The reason may be due to the borehole may be too far from the test pile or there is no steel reinforcement in the substructure. Obtain the voltage reading by placing the Probe next to the substructure. If the voltage is still 2.5 V, there is no steel reinforcement in the substructure. Use the existing borehole and conduct a PS test. If the voltage readout is close to 5 V, the solution is either to drill a hole closer to substructure and conduct the IF test or to conduct a PS test.
- If the voltage does not drop to 2.5 V when the Probe is at the bottom of the hole, the pile length is greater than the depth of the borehole. Drill a deeper borehole and repeat the IF test if the precise depth is needed.

## REFERENCES

1. Federal Highway Administration and Florida Department of Transportation (2010). “Unknown Foundation Bridges Pilot Study,” NCHRP Web-only document 107. [http://www.fdot.gov/maintenance/STR/IN/Unknown\\_Foundations\\_Pilot\\_Study\\_02-26-10.pdf](http://www.fdot.gov/maintenance/STR/IN/Unknown_Foundations_Pilot_Study_02-26-10.pdf)
2. Olson L. D. and Aouad, M. F. (2001). “Unknown Subsurface Bridge Foundation Testing,” NCHRP 21-5(2) Final Report, TRB, Washington DC.
3. Parker, G., Toro-Escobar, C. M. and Voigt, R. L. (1998). Countermeasures to protect bridge piers from scour, SAFL Project Report 433, 1998, Vols. 1 (27 p) and 2 (360 p).
4. Olson, L.D., Jalinoos, F., and Aouad, M.F. (1996). “NCHRP Research Results Digest 213: Nondestructive Testing of Unknown Subsurface Bridge Foundations, Results of NCHRP Project E 21-5”, Transportation Research Board, National Research Council, Washington, DC.
5. Stein, S. and Sedmera, K. (2006). “Risk-based management guidelines for scour at bridges with unknown foundation, NCHRP 24-25, Web-only Document-107. <http://www.trb.org/Publications/Blurbs/157792.aspx>.
6. Nichols, S. (2009) “Overview—Assessment of bridges with unknown foundations,” FHWA Unknown Foundation Webinar 1, (<http://www.fhwa.dot.gov/unknownfoundations>) (Jan. 13, 2010).
7. Rivers, B., and Nurmi, C. (2009). “Categorization, thresholds, and prioritization,” Assessment of Bridges with Unknown Foundations, FHWA Unknown Foundation Webinar 2, (<http://www.fhwa.dot.gov/unknownfoundations>) (Jan. 13, 2010).
8. Rivers, B. (2009). “Positive discovery and inference.” Assessment of Bridges with Unknown Foundations,” FHWA Unknown Foundation Webinar 3, <http://www.fhwa.dot.gov/unknownfoundations>) (Jan. 13, 2010).
9. Nurmi, C. (2009). “Plans of action and management systems for bridges coded ‘U’,” Assessment of Bridges with Unknown Foundations, FHWA Unknown Foundation Webinar 4, (<http://www.fhwa.dot.gov/unknownfoundations>) (Jan. 13, 2010).

10. Washer, G. A. (1997). "Developments for the Nondestructive evaluation of highways bridges in the United States," Proc. Non-Destructive Testing in Civil Engineering, (NDT-CE '97) Liverpool, UK, Vol. 2, 543-552
11. Aouad, M. F. and Olson, L.D., (1996). "Nondestructive Evaluation of Bridge Foundations," in "Structural Materials Technology and NDT Conference", ed. Stolarski and Hartbower, San Diego, CA, Technomic Publishing, ISBN# 1-56676-424-6, 293-298.
12. Hertlein, B. and Davis, A. (2006). Nondestructive Testing of Deep Foundations, John Wiley & Sons, p.265. <http://www.wiley.com/WileyCDA/WileyTitle/productCd-0470848502.html>
13. Davis, A.G. (1995). "Nondestructive Evaluation of Existing Deep Foundations," ASCE Journal of the Performance of Constructed Facilities, 9, 57-74.
14. Nash, D. (2010). "Unknown Foundations Investigations: The Experiences of the LA DOTD," 35<sup>th</sup> Southwest Geotechnical Engineers Conference, Baton Rouge, LA.
15. Chakraborty, S. and Brown, D. A. (1997) "Evaluation of Unknown Pile Length under Existing Bridges in Alabama," IR-97-05, p. 122.
16. Robinson, B. and Webster, S. (2008). "Successful Testing for Unknown Bridge Foundations," Fifth Highway Geophysics – NDE Conference, 101-110.
17. NCDOT Geotechnical Engineering Unit. (2010). "Unknown Bridge Foundation Process," Internal flowchart developed for NCDOT's Unknown Foundation Program. North Carolina Department of Transportation, Raleigh, NC.
18. Gucunski, N., Imani, A., Romero, F., Nazarian, S., Yuan, D., Wiggenhauser, H., Shokouhi, P., Taffe, A., and Kutrubes, D. (2013). Nondestructive Testing to Identify Concrete Bridge Deck Deterioration, National Academies Press, p. 85.
19. Hossain, M., Khan, M., Hossain, J., Kibria, G., and Taufiq, T. (2013). "Evaluation of Unknown Foundation Depth Using Different NDT Methods," Journal of Performance of Constructed Facilities, 27(2), 209-214.
20. Terracon (2011). <http://ds.terracon.com/2011/09/state-of-the-art-deep-foundation-testing/>
21. Finno, R.J. and Gassman, S.L., Osborn, P.W. (1997). "Non-Destructive Evaluation of a Deep Foundation Test Section at the Northwestern University National Geotechnical

- Experimentation Site A Report Submitted to the Federal Highway Administration, Northwestern University, Evanston, Illinois.
22. Yin, J., and Liu, M. (1999). "Assessment of Pile Integrity by Low-Strain Stress Wave Method", *HKIE Transactions*, 6:1, 42-49.
  23. Kim, D.S. and Kim H.W., (2003). "Effects of Surrounding Soil Stiffness and Shaft Length in the Impact-Echo Test of Drilled Shaft." *KSCE Journal of Civil Engineering*, 7(6), 755-762.
  24. Ni, S., Lehmann, L., Charng J., Lo, K. (2006). "Low-Strain Integrity Testing of Drilled Piles with High Slenderness Ratio", *Computers and geotechnics*, 33, 283-293.
  25. Ni, S.-H., Huang, Y.-H., Lo, K.-F., and Charng, J.-J. (2011). "Estimating the Flaw Size in Drilled Shafts Using an Impulse Response Method," *KSCE Journal of Civil Engineering*, 15(7):1197-1207.
  26. Rausche, F., Shen, R.K., and Likins, G. (1991). "A Comparison of pulse echo and transient response pile integrity test methods," *Transportation Research Board, Annual Meeting*, January 1991, Washington, D.C.
  27. Jozi, B., Dackermann, U., Braun R., Li, J., and Samali, B. (2014). "Application and Improvement of Conventional Stress -Wave- Based Non-Destructive Testing Methods for the Condition Assessment of In -Service Timber Utility Poles" 23<sup>rd</sup> Australasian Conference on the Mechanics of Structures and Materials (ACMSM23), Byron Bay, Australia, December 9-12.
  28. Ding, X.M., Liu, H.L., and Zhang, B. (2011). "High-frequency interference in low strain integrity testing of large-diameter pipe piles," *Sci. China Sci. Tech.* , 54(2), 420-430.
  29. Huang, Y., Ni, S., Lo, K., Charng, J. (2010) "Assessment of Identifiable Defect Size in a Drilled Shaft Using Sonic Echo Method: Numerical Simulation", *Computers and Geotechnics*, 37, 757-768.
  30. Yu, C., and Liao, S. (2006). "Theoretical Basis and Numerical Simulation of Impedance Log Test for Evaluating the Integrity of Columns and Piles", *Can. Geotech. J.*, 43, 1238-1248.

31. Davis, A., and Dunn, C., (1974). "From the Theory to Field Experience with the Non-Destructive Vibrations Testing of Piles", Proc. Instn. Civ. Engrs, Part 2, 57, December, 571-593.
32. Lo, K.F., S.H., Ni, S.H., Huang, Y.H., and Zhou X.M. (2009). "Measurement of Unknown Bridge Foundation Depth by Parallel Seismic Method." Experimental Techniques 33(1), 23-27.
33. Turner, M.J. (1997). Integrity Testing in Piling Practice, Ciria Report 144. London.
34. Liao, S.-T., Tong, J.-H, Chen, C.-H. and Wu, T.-T. (2006). "Numerical simulation and experimental study of Parallel Seismic test for piles," International Journal of Solids and Structures 43(7), 2279–2298.
35. Sack, D., Slaughter, S., and Olson, L. (2004). "Combined Measurement of Unknown Foundation Depths and Soil Properties with Nondestructive Evaluation Methods", DOI: <http://dx.doi.org/10.3141/1868-08>.
36. Olson, L. (2010). "Condition Assessment of Unknown Foundations", 35<sup>th</sup> SW Geotechnical Engineers Conference, April 26-29, Baton Rouge, LA.
37. Standard Test Method for Low Strain Impact Integrity Testing of Deep Foundations (2013), <https://www.astm.org/Standards/D5882.htm>
38. American Concrete Institution (2013), Report on Nondestructive Test Methods for Evaluation of Concrete in Structures
39. Eshaghi, S., Dashti, H., Shahverdi, M., (2012). "Evaluation of Internal Cracks and Collapse in Poplar Wood (*Populus nigra*) during a Conventional Drying Process with Ultrasonic Inspection", Not Sci. Biol., 4(2), 141-145.
40. [http://www.engineeringtoolbox.com/sound-speed-solids-d\\_713.html](http://www.engineeringtoolbox.com/sound-speed-solids-d_713.html)
41. Spears, R.E. and Jensen, S.R. (2009). "Approach for Selection of Rayleigh Damping Parameters Used for Time History Analysis," ASME Pressure Vessels and Piping Division Conference, July 26-30, Prague, Czech Republic.
42. Olson, L.D., Jalinoos, F., and Aouad, M.F. (1998). "Determination of Unknown Subsurface Bridge Foundations" A summary of the NCHRP 21-5 Interim Report.